POST-PEAK RESPONSE ANALYSIS USING THE FINITE ELEMENT METHOD

A THESIS

submitted in fulfilment of the requirements for the award of the degree of

DOCTOR OF PHILOSOPHY

in

EARTHQUAKE ENGINEERING

By

KHALID MOIN

DEPARTMENT OF EARTHQUAKE ENGINEERING
UNIVERSITY OF ROORKEE
ROORKEE–247 667 (INDIA)

JULY, 1996

Gratis

UNIVERSITY OF ROORKEE
Roorkee

CANDIDATE'S DECLARATION

I hereby certify that the work which is being presented in the thesis entitled ***Post-Peak Response Analysis Using the Finite Element Method*** in fulfilment of the requirement for the award of the Degree of Doctor of Philosophy and submitted in the Department of Earthquake Engineering of the University is an authentic record of my own work carried out during a period from July 1992 to July 1996 under the supervision of Dr. Pankaj.

The matter presented in this thesis has not been submitted by me for the award of another degree of this or any other University.

Khalid Moin
Signature of the Candidate

This is to certify that the above statement made by the candidate is correct to the best of my knowledge.

Date: 26 July 1996

Signature of Supervisor

The Ph.D. Viva-Voce examination of **Khalid Moin**, Research Scholar, has been held on 31.1.1997

Signature of Supervisor | Signature of H.O.D. | Signature of External Examiner

ABSTRACT

With increasing load, a structure undergoes increasing deformation. Beyond a critical or peak load level, structure's inability to take any more loads causes failure. Failure can be distributed or localized. In general, the failure of civil engineering structures is localized and is caused by a series of densely populated cracks which coalesce in an extremely small region. The numerical simulation of crack formation and propagation has been a subject of considerable research. Although, post-peak states are usually not tolerated in the design of structures, the knowledge of post-peak behaviour can be of great help in understanding the strengths and weaknesses of structures. Further, the understanding of the failure modes is important to avoid brittle failure. It is for this reason that the capabilities to predict post-peak deformation behaviour is essential in addition to finding the ultimate load carrying capacity.

The underlying aim of the thesis is to simulate post-peak behaviour of the structure using strain softening plasticity and the finite element method. In this regard the objectives of the thesis are outlined as follows.

- To review the literature related to computational plasticity with emphasis on strain softening and localization.
- To evolve benchmark tests in elastoplasticity particularly under strain softening conditions.
- To study the post-yield behaviour, conditions of localization and mesh sensitivity issues using numerical samples with various yield criteria.
- To develop algorithms for dynamic strain softening problems and to conduct studies on the possible use of strain softening under seismic forces.
- To study post-peak response of some realistic structures.

Some recent developments in computational elastoplasticity are discussed. Current literature in the area of strain softening plasticity and its use in simulating post-peak behaviour is reviewed. Issues related to the use of indirect displacement control and evolution of localization conditions are also reviewed.

Emphasis is laid on the Hoffman yield criterion which is pressure sensitive and valid for anisotropic elastoplasticity. The present study, however, is limited to the isotropic form of the Hoffman criterion. A return mapping algorithm using the backward Euler

scheme for this criterion is discussed. The evolution of this criterion for strain softening plasticity wherein both equivalent compressive and tensile strengths are assumed to reduce as compared to when only the tensile strength is assumed to decline is considered.

The possibility of using strain softening elastoplasticity for the prediction of post-peak seismic response is explored. Numerical implementation of strain softening has been known to cause problems of convergence, load step sensitivity and discretization sensitivity (or mesh sensitivity). Many of these difficulties have been surmounted for static analysis. Numerical problems associated with the use of strain softening in the solution of dynamic problems are highlighted and some methods of overcoming them discussed. Consideration is generally limited to one dimensional problems arising out of elastoplastic strain softening behaviour. The results indicate that dynamic response does not become unbounded due to strain softening. Strain softening, however, introduces a large zero frequency component as compared to strain hardening or perfect plasticity. The frequency content at frequencies other than zero is not significantly altered. These preliminary investigations indicate that strain softening in conjunction with an appropriate stress updating algorithm can be employed in the seismic analysis of structures.

The analysis of industrial structures and substructures is often conducted using elastoplastic constitutive laws, in conjunction with the finite element method. The finite element codes may be used as a "black box" by personnel who may be inadequately trained in the method. In order to train analysts and to check the validity of finite element codes, the benchmarks can be of paramount importance. Further, exact solutions in computational elastoplasticity cannot be used directly as these often pertain to solutions that are valid only for particular cases. However, these solutions can be used as benchmark tests to check the validity of finite element codes and accuracy of numerical solution procedures.

In the present study tests for three different yield criteria *viz.* von Mises, Mohr Coulomb and Hoffman are discussed. The perfectly plastic as well as strain hardening/softening cases are examined. The benchmark tests are based on prescribed displacement field format. Tests are evolved that can be used to verify the ability of finite element packages in accurately predicting first yield and flow in the post-elastic regime.

The exact integration of constitutive equations for an isotropic plastic von Mises material that incorporate linear hardening/softening for some specific cases are developed. Illustrative tests are included.

Exact solutions for Mohr Coulomb criterion that include linear strain hardening or softening plasticity and the presence of singular regions are also developed. A number of biaxial and triaxial illustrative tests are included.

The isotropic form of the Hoffman criterion is a cylindrical paraboloid in the principal stress space. As such it is not straightforward to evolve closed form solutions for this criterion. However, tests that can illustrate the stress changes in the principal stress space and can serve as tools for understanding, are studied. Simple tests under perfect plasticity and strain softening conditions are examined.

Post-peak response can be described as the response of a structure that is incapable of sustaining any additional loads. The post-peak behaviour is associated with progressive failure of the structure, which in turn can be modelled using softening plasticity. Strain softening implies declining equivalent yield strength parameter in the yield criterion. This does not, necessarily imply post-peak (declining) load-deflection response and the load might actually increase.

The behaviour of elastoplastic von Mises, Mohr Coulomb and Hoffman materials under simple load paths and considering perfect/strain softening plasticity are studied. In addition to the movement of the stress point in the principal stress space emphasis is laid on the load displacement behaviour. The study also examines the use of the accoustic tensor as a localization indicator.

Uniaxial compression tests on single elements used in the study indicate that for associated von Mises plasticity the localization conditions are not necessarily satisfied immediately after first yield, even under strain softening conditions. Critical values of the softening parameter are evaluated such that the localization condition is satisfied immediately after first yield. It is seen that if the softening parameter is of greater magnitude than the evaluated critical magnitude, then the localization direction is not unique. Increasing the softening parameter beyond a certain magnitude may lead to instability. It is seen that this limit is more stringent than the local uniqueness requirements. Single element compressive tests indicate that a descending or constant load displacement response is obtained only after the satisfaction of the localization condition.

Similar uniaxial tests indicate that it is far easier to satisfy the localization conditions with the Mohr Coulomb criterion. The satisfaction of the localization condition is accompanied by post-peak behaviour for simple uniaxial test. For these tests a flat or a

descending load displacement response is observed depending on the assumption of perfect or strain softening plasticity.

The study shows that post-peak behaviour using the Hoffman criterion is strongly influenced by the ratio of uniaxial tensile and compressive strengths. In case of softening plasticity the post-yield response is totally different when both equivalent tensile and compressive strengths are assumed to reduce as compared to when only the tensile strength is assumed to decline. Mesh sensitivity of the post-peak response is also studied for von Mises and Hoffman criterion. Good (mesh insensitive) results are obtained when nonlocal material laws are employed.

The algorithms and ideas developed are applied to some engineering problems. Post-peak response of simple systems such as a cantilever beam, plane strain tension specimen and a notched beam is studied. The failure patterns of a slope under varying post-yield conditions are examined. Strain softening plasticity is also applied to the seismic analysis of Koyna dam.

ACKNOWLEDGEMENT

I express my heartfelt gratitude and sincerest thanks to Dr. Pankaj, Reader, Earthquake Engineering Department, University of Roorkee, Roorkee for his valuable guidance, useful discussions and constant encouragement. He has been a source of inspiration and a close friend apart from being the supervisor.

I would like to thank Prof. S. Basu and Dr. A. Kumar for their support in the computational activities undertaken at shake table facility. I feel fortunate enough to have enjoyed their patronage during this study.

Useful discussions with Professors G.C. Nayak and D.K. Paul are gratefully acknowledged.

I feel indebted to Prof. S.K. Thakkar, Head, Earthquake Engineering Department for providing me the necessary facilities in the department.

My gratefulness to Prof. I.H. Khan, Head, Department of Civil Engineering, Jamia Millia Islamia for sponsoring me for Ph.D. programme under Q.I.P. and also for his constant inspiration for higher studies. The financial support provided by M.H.R.D., Government of India is duly acknowledged.

I express my deepest gratitude to my parents whose blessings helped me to reach this end.

The help and advice rendered by my friends and colleagues Messrs. Qasim Rafique, Mohammed Arif, Ziauddin Ahmad, Mohammed Shakil, Rajnish Shrivastava, Zulfiquar Ahmad, Abid Hasan, Mehdi Siavoshnia, Satish Bansal, Asim Zafar and Arshad Umar is also gratefully acknowledged.

Finally, thanks are due to my wife Juhee and my son Faraz and daughter Sheena for their sacrifices and patience, for they are the ones who shared the whole burden and paved the way.

Khalid Moin

CONTENTS

LIST OF NOTATIONS

$\mathbf{a}$	Flow vector directed normal to the yield surface $(=\frac{\partial F}{\partial \sigma})$
$\mathbf{a}_A, \mathbf{a}_B, \mathbf{a}_C$	Flow vector at point *A, B, C*
A	Hardening parameter
A_C	Hardening parameter corresponding to state at point *C*
A	Cross-sectional area
A_{cr}	Critical value of hardening parameter at which localization condition is satisfied
A_{cr90}	Critical value of hardening parameter at which localization condition is satisfied for range of angles (–90° to 90°)
$\mathbf{b}$	Flow vector with regard to plastic potential function Q $(=\frac{\partial Q}{\partial \sigma})$
β	Scalar load factor
β_j or β_p	Parameter deciding the type of algorithm employed
c	Cohesion
$\mathbf{C}$	Damping matrix
C_i	Material parameter $(i = 1,9)$
CS	Contact stress state
$\mathbf{D}$	Elasticity matrix
$\mathbf{D}^{cr}$	Tangent crack formulation matrix
$\mathbf{D}^{ct}$	Consistent tangent matrix
$\mathbf{D}^{ep}$	Elastoplastic matrix or tangential modulus matrix
$\mathbf{D}^{ep}_{ijkl}$	Elastoplastic matrix presented in tensorial form
Δ	Finite change
$\Delta(\cdot)_i$	Total increment between configuration *m* and *i*
$\delta(\cdot)_i$	Increments from state *i* to *j*
E	Young's modulus
E_T	Slope of the softening branch of stress strain curve
$\mathbf{E}^{ec}$	Tangent stiffness operator

$E_n^{\mathrm{I}}, E_t^{\mathrm{I}}, E_{nt}^{\mathrm{II}}$	Mode I stiffness moduli for (n, t) system respectively and shear stiffness for simultaneous cracking in the two orthogonal directions of principal orthotropy
e	Exponential
ε	Strain at a point
$\varepsilon_x, \varepsilon_y, \varepsilon_z$	Normal component of strain vector in x,y,z direction
ε^e	Elastic strain vector
ε^p	Plastic strain vector
ε_c	Constant responsible for the slope of the softening branch
ε_y	Yield strain
$\varepsilon_{11}, \varepsilon_{22}$	Principal strain
$\varepsilon_{c1}, \varepsilon_{c2}$	ε_c corresponding to localization band 1 and 2
$d\varepsilon$	Strain increment vector
$d\varepsilon^e$	Elastic strain vector
$d\varepsilon^p$	Plastic strain vector
$d\varepsilon_y^p$	Equivalent or uniaxial plastic strain
$d\varepsilon_{kl}$	Strain increment presented in tensorial form
$\Delta \mathbf{e}^{cr}$	Local crack strain in the local (n,t) coordinate system aligned with the crack orientation
$\Delta\varepsilon_i$	Incremental strain vector
η	Factor defining the type of algorithm employed lying between 0 and 1, ($\eta = 0$ explicit forward Euler algorithm, $\eta = 1$ backward Euler algorithm)
f	External load vector
F	Yield function
$\mathbf{F}$	Internal force vector
f_1, f_2	Equivalent nodal forces at nodes 1,2
f_c	Compressive yield strength
f_t	Tensile yield strength
f_{co}	Uniaxial compressive yield strength of virgin material
f_{to}	Uniaxial tensile yield strength of virgin material
$f(\sigma)$	Stress dependent component of yield function
$f(\sigma_c)$	Stress dependent component of yield function at point C

$f_2(Y(\kappa))$	Strength dependent component of yield function
F_c	Value of yield function at point C
F_O	Yield function at previous state
F_o	Step function load
F_{cn}	Yield function at a new state corresponding to point C
F_{co}	Yield function at previous state corresponding to point C
$F_I(t), F_D(t), F_E(t)$	Inertia forces, damping forces, elastic forces
ϕ	Angle of friction
G	Shear modulus
G_c	Energy required to fully open (to or beyond w_1) unit area of newly formed crack
g_k	Position vector
γ	Shear strain
h	Length of a single element in a discretised bar
H	Hardening modulus
I	Identity matrix
I_1	First stress invariant
I_{m-1}, I_d	Number of iteration that were required to achieve equilibrium in increment $m-1$ and the desired number of iteration
J_2	Second invariant of the deviatoric stress tensor
K	Stiffness of a SDF system
K	Stiffness matrix
K_T	Tangential stiffness
$\mathbf{K}^*$	Effective stiffness matrix
κ	Hardening/Softening parameter
$\kappa_A, \kappa_B, \kappa_C$	Hardening parameter corresponding to state at point A,B,C
l	Length of the bar
$d\lambda$	Proportionality constant termed as plastic multiplier
m	Mass of a SDF system
M	Mass matrix
$\boldsymbol{m}, \boldsymbol{n}$	Pair of unit vectors
$m+1$	Next converged state

ν	Poison's ratio
n	Ratio of uniaxial compressive and tensile strength ($=f_c / f_t$)
p	Order of polynomial
$\mathbf{P}$	Applied load vector of reference loads
$\mathbf{p}_\alpha$	Projection vector
$\mathbf{P}_\alpha$	Projection matrix
P_y	New load level
$P_{y\circ}$	Uniaxial yield strength of the virgin material
$\Delta\mathbf{P}$	Applied load increment vector corresponding to first iteration
$\delta\mathbf{P}$	Applied load increment vector corresponding to subsequent iterations
Q	Plastic potential function
q_i	Any scalar (i = 1,3)
R	Factor (between 0 and 1) that takes elastic stress increment only upto yield surface
$\mathbf{r}$	Vector representing difference between the current stresses and the backward Euler stresses
$\mathbf{r}_n, \mathbf{r}_\circ$	New and previous values of $\mathbf{r}$
${}^i\mathbf{R}$	Vector of residual forces at the end of iteration i
s_k	Unit vector in the direction of dg_k
ds	Length of the vector dg_k ($=\lvert dg_k \rvert$)
ΔS	Finite length called the arc-length
σ	Stress at a point
$\boldsymbol{\sigma}$	Stress vector
$\sigma_A, \sigma_B, \sigma_C$	Stress state at point A,B,C
$\sigma_x, \sigma_y, \sigma_z$	Normal component of stress vector in x,y,z direction
σ^e	Elastic stress
$\sigma_1, \sigma_2, \sigma_3$	Principal stresses (maximum, intermediate, minimum)
σ_{11}, σ_{22}	Principal stresses (maximum, minimum)
σ_n	Stress normal to the crack plane
σ_j^{el}	Elastic predictor stress
$\bar{\sigma}_{ii}^*$	Uniaxial compressive yield strengths

$\bar{\sigma}_{ii}$	Uniaxial tensile yield strengths
$\bar{\sigma}_{ij}\,(i \neq j)$	Uniaxial shear yield strengths
$d\boldsymbol{\sigma}$	Stress increment vector
$d\boldsymbol{\sigma}^e$	Elastic stress increment vector
$d\sigma_{ij}$	Stress increment presented with tensorial notation
$\Delta\boldsymbol{\sigma}^e$	Elastic predictor stress vector
$\Delta\sigma_x^e, \Delta\sigma_y^e, \Delta\sigma_z^e$	Normal component of $\Delta\boldsymbol{\sigma}^e$ in x,y,z direction
$(\,)_{ij}$	Superscript i represents direction of the plane on which stress acting and superscript j the direction of stress
${}^m(\,)$	Superscript m on left indicates current configuration
$(\,)^{cr}$	Superscript *cr* represents cracked component
$(\,)^{co}$	Superscript *co* represents continuum component
$(^+)$	Superscript $(^+)$ to the right Indicates one side of discontinuity
$(^-)$	Superscript $(^-)$ to the right indicates the other side of discontinuity
$[[.]]$	Shows the difference between the values on either side of discontinuity
t	Thickness of the localization band
$\mathbf{t}$	Incremental local traction
$\mathbf{T}$	Orthogonal transformation matrix
t_k	Unit vector tangential to surface S
Δt	Time step length
$\tau_{xy}, \tau_{yz}, \tau_{zx}$	Shear components of stress vectors in x,y,z direction (as per tensorial notations)
$\Delta\tau_{xy}, \Delta\tau_{yz}, \Delta\tau_{zx}$	Shear components of $\Delta\boldsymbol{\sigma}^e$ in x,y,z direction (as per tensorial notations)
u	Displacement of a node
U	Total elongation of the bar
$\mathbf{u}$	Total displacement vector
ΔE	Energy released on full rupture
v_i	Vector function
V_{t1}	Volume of localization band I $(= d_1 l_1 t = A_1 t)$
V_{t2}	Volume of localization band II $(= d_2 l_2 t = A_2 t)$

ω	Natural frequency of a SDF system ($=\sqrt{K/m}$)
dW^p	Plastic work
$x, \dot{x}, \ddot{x}$	Displacement, velocity and acceleration of a SDF system
$\mathbf{x}, \dot{\mathbf{x}}, \ddot{\mathbf{x}}$	Total nodal displacement, velocity and acceleration vector
x_1, x_2	Coordinate of one dimensional element
$\Delta\mathbf{x}_i$	Displacement vector (superscript on x denote iteration number)
Y	Normalized yield strength
Y_o	Uniaxial yield strength of the virgin material
ψ	Out of balance force or residual force
$\boldsymbol{\psi}$	Out of balance or residual force vector

LIST OF TABLES

LIST OF FIGURES

Chapter 1

General

1.1 Post-peak Analysis

With increasing load, a structure undergoes increasing deformation. Beyond a critical (or peak) load level, a structure's inability to take any more load causes failure. Failure is generally caused by a series of densely populated cracks which coalesce to form an extremely localized region of high strains or a crack. The numerical simulation of crack formation and propagation has been a subject of considerable research. Although, post-peak states are usually not tolerated in the design of structures, the knowledge of post-peak behaviour can be of great help in understanding the strengths and weaknesses of structures. A number of terms are used in the post-peak analysis of structures. Some of these are discussed in the following sections.

1.2 Localization

Localization is the formation of bands of intense straining. The post-peak behaviour of a structure is generally accompanied by these localization bands. Such bands have been seen in a wide variety of solids such as in ductile single crystal, in structural metals, in saturated clays, in quasi-brittle materials like rocks and concrete (Ortiz et al., 1987). According to Bazant (1976) the region of localization must condense to what might be considered as a surface. Schreyer and Chen (1986) pointed out that clearly defined surface is rarely observed in experiments and localization may consist of a band whose lateral dimensions will depend on material properties. It now appears that localization band width

would depend on the geometry of the structure, loading conditions and boundary conditions in addition to material properties. Mathematically localization has been described as a weak discontinuity that is responsible for discontinuous stress and strain fields (Willam et al., 1984).

The finite element method has been extensively used to numerically simulate post-peak analysis involving localization. The mathematical models used in conjunction with finite element method followed two distinct approaches. These are the *discrete crack* and the *smeared crack* approach. The basic essentials of these two approaches are discussed in the following section.

1.3 Crack Simulation

The ultimate result of progressive cracking, which dominates the nonlinear response of quasi-brittle materials such as concrete is a *localized failure*. This localized nature of failure inspired some researchers to develop the so-called discrete crack models (e.g. Ngo and Scordelis, 1967; Blaauwendraad and Grootenboer, 1981). In this approach the geometrical discontinuities due to cracking are incorporated within the idealisation of the structure and a crack is modelled as a geometrical discontinuity (Fig. 1.1).

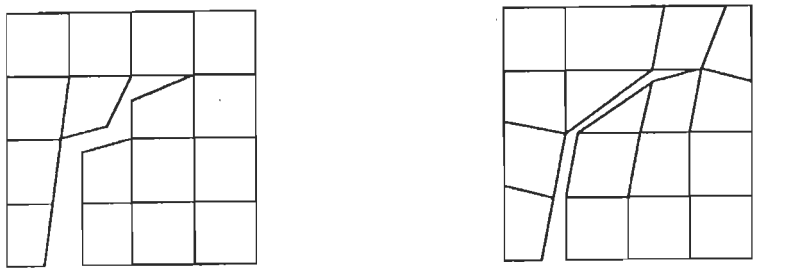

Without mesh refinement

With adaptive mesh refinement

Fig. 1.1 Finite element modelling with unknown crack path using discrete crack approach (redrawn from Cervera, 1986)

The approach is physically attractive as it reflects the highly localized nature of cracking. It represents the individual cracks as actual discontinuities in the finite element mesh. This approach models a crack by converting a nodal point into two nodal points with a crack in between. The constraints imposed by limitations of such a discrete crack

model fixes stringent limits on the formation of cracks at element boundaries. Furthermore, when a crack forms the mesh has to be redefined. Even though automatic procedures have been developed for such rearrangements, the discrete approach is not simple for large scale analysis of arbitrary structures. It has, however, been used successfully in some cases (Ram Kumar and Nayak, 1994). However, in many engineering problems crack positions are known a priori or a mechanism of discrete cracks can be imagined to occur in a fashion similar to yield line mechanism. For such cases the above mentioned drawbacks do not exist and a discrete crack analysis can be carried out. In the present study discrete crack approach is not used and would not, therefore, be considered any further.

Another method for incorporating cracking in finite element analysis is the "smeared crack" approach (Rashid, 1968; Suidan & Schonbrich, 1973; Bazant and Cedolin, 1979; Bazant and Gambarova, 1980; Bazant and Cedolin, 1983; Bazant and Oh, 1983; Bicanic et al., 1993). In this approach the cracking region is assumed to be finite. This approach, thus, models a crack as a continuum and will be discussed later in this study.

1.4 Strain Softening

Strain Softening can be defined as the decline of stress with increasing strain (Fig. 1.2). One common example occurs in the compressive loading of concrete cylinders. As the length of the specimen gradually decreases and compressive strains accumulate, the test specimen does not fail when maximum load is reached, but a subsequent decrease in the load can be observed under increasing deformation (Sandler, 1984). Extensive tests demonstrating strain softening in concrete were conducted by van Mier (1984) under a variety of loading conditions. In the earlier years, strain softening was considered a true material property and routinely incorporated into constitutive models. Softening is now conceived as a kind of structural property of a cracked continuum (Ottosen, 1986; Pramono, 1988; Bicanic and Pankaj, 1990). This can be explained by considering a concrete specimen subjected to uniaxial tensile loading (Fig. 1.3). The specimen is attached with three set of gauges as shown in Fig. 1.3. Up to a certain stress level the stress-strain curve is nearly linear and a similar behaviour is observed in the three regions A, B and C, then a deviation from linearity is observed (Hughes and Chapman, 1966; Gopalaratnam and Shah, 1985). As the strain increases a peak stress level is reached and a tensile macrocrack starts propagating in a very localized region. A clear strain softening will be observed in the region where crack has developed (covered by gauge A, Fig. 1.3).

However, in the area covered by gauge B, unloading will be observed due to the decreasing load-carrying capacity in the tensile crack zone. The overall deformation will show an average of A and B (van Mier 1984).

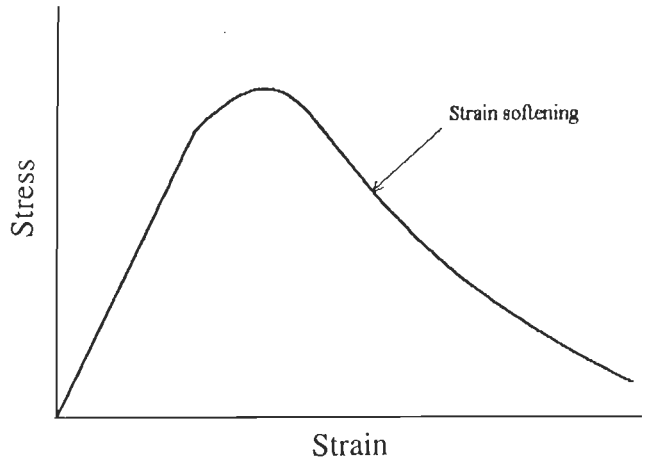

Fig. 1.2 One dimensional strain softening idealisation

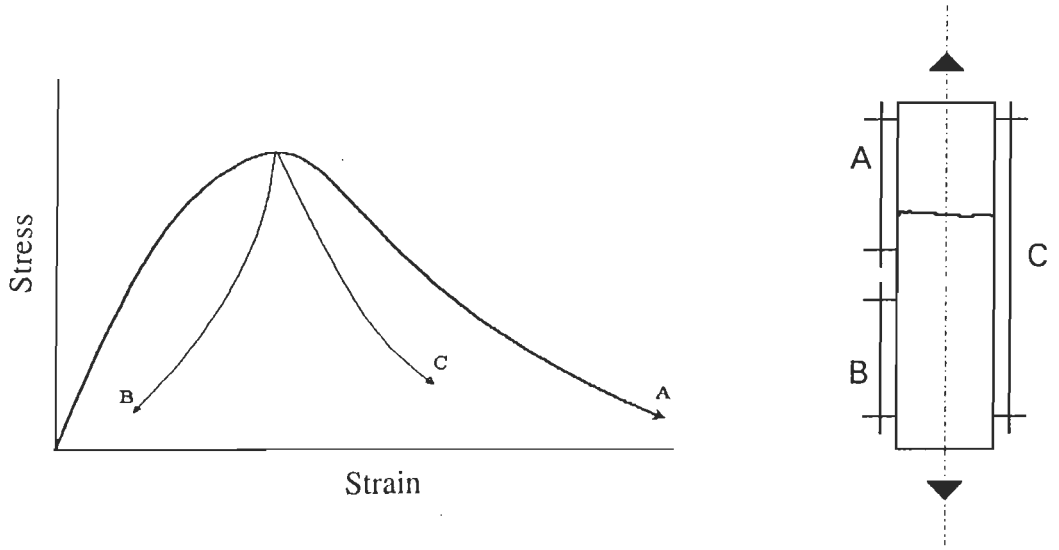

Fig. 1.3 Tensile stress strain behaviour of concrete (redrawn from van Mier, 1984)

Thus strain softening is a kind of average stress-strain behaviour of regions that unload and those that experience continued deformation. Clearly the slope of the softening

branch depends on the gauge length and region between which the stress-strain behaviour is being considered. In other words the softening modulus is not a local property like, say, the Young's modulus. A property such as Young's modulus is assumed to exist at every point of the continuum with no characteristic dimension attached. While strain softening modulus can only be defined with a characteristic dimension. It is thus termed as a structural or a non-local material property.

From the finite element simulation point of view, the traditional form of assuming the strain softening branch to be a material property led to results that depended on the analysts choice of the mesh (Bazant and Cedolin, 1979; Rots et al., 1985).

1.5 Scope and Layout of the Thesis

Nonlinear and post-peak analyses are essential in order to predict structural failure. From the design point of view understanding of the failure modes is important in order to avoid brittle failure. The post-peak deformations are much greater than its linear response limit. Post-peak behaviour is generally associated with progressive failure of structures. The basic aim of the present study is to examine the use of strain softening plasticity in its ability to predict post-peak response. The study uses the finite element method as a basic tool. The remainder of the thesis has been divided into eight Chapters (Chapter 2-9) and a brief layout is as follows:

- In Chapter 2 some recent developments in computational elastoplasticity are reviewed.
- In Chapter 3 various methodologies employed in the simulation of post-cracking behaviour are discussed. Attention is confined to the smeared crack approach. Rotating crack formulation of this approach used in conjunction with plasticity leads to the isotropic plasticity softening model. This has received special attention in this study. Treatment of localization as instability in softening plasticity, is discussed.
- Chapter 4 deals with the isotropic Hoffman yield criterion. The strain softening formulation of the isotropic Hoffman model is discussed when only uniaxial tensile strength declines and when both uniaxial compressive and tensile strengths are assumed to decline simultaneously. The integration of rate equations using backward Euler scheme is discussed and a computational algorithm to perform these integrations developed. An exact solution for the evolution of contact stresses that are required in semi implicit and explicit algorithms is derived.

- Chapter 5 discusses the application of strain softening problems with regard to static as well as dynamic cases. Two stress updating strategies are presented and the importance of updating stresses at the end of each converged step rather than at the end of each iteration is stressed upon. Possibility of using strain softening in dynamic problem is explored. The Chapter examines some generalized Newmark procedures and the stress updating algorithms in dynamic elastoplasticity, with special emphasis on strain softening.

- In Chapter 6 benchmark tests using von Mises, Mohr Coulomb, and isotropic Hoffman criterion are developed. The perfectly plastic as well strain hardening/softening cases are examined. The benchmark tests are based on prescribed displacement field format. Exact solutions that incorporate linear hardening/softening for some specific cases are developed for von Mises and Mohr Coulomb plasticity. A number of benchmark test problems are included. A number of illustrative biaxial and triaxial tests are included. Tests using Hoffman yield criterion, which can serve as tools for understanding are evolved under perfectly plastic and strain softening conditions.

- Chapter 7 considers the post-peak behaviour of a single element subjected to a mixture of displacement and boundary tractions. Localization indicators at various stages of loading are examined for von Mises, Mohr Coulomb and Hoffman criteria. Mesh sensitivity of the post-peak response is also studied for von Mises and Hoffman criteria.

- In Chapter 8 the ideas developed above are applied to some engineering problems. The post-peak responses of simple problems such as a cantilever, plane strain tension specimen, a notched shear beam (Ingraffea beam) are studied. The failure patterns of a slope under varying post-yield conditions are examined. Strain softening plasticity is also applied to the seismic analysis of Koyna dam.

- Chapter 9 briefly discusses the observations that emerge from this thesis. Some specific and some general suggestions for future research are outlined.

References

Bazant, Z.P. (1976) – Instability, ductility and size effect in strain softening concrete, *J. Eng. Mech., ASCE*, **102**(2), 331-344.

Bazant, Z.P. and Cedolin, L. (1979) – Blunt crack band propagation in finite element analysis, *J. Eng. Mech., ASCE*, **105**(2), 297-315.

Bazant, Z.P. and Cedolin, L. (1983) – Finite element modelling of crack band propagation, *J. Str. Div., ASCE*, **109**(1), 69-92.

Bazant, Z.P. and Gambarova (1980) – Rough cracks in reinforced concrete, *J. Str. Div., ASCE*, **106**(4), 819-842.

Bazant, Z.P. and Oh, B.H. (1983) – Crack band theory for fracture of concrete, *Materials and Structures, Research and Testing, (RILEM*, Paris), **16**, 155-177.

Bicanic, N., de Borst, R., Grestle, W., Murray, D.W., P-Cabot, G., Saouma, V., Willam, K.J. and Yamazaki, J. (1993) – Computational aspects of finite element analysis of reinforced concrete structures, *Structural Engineering and Structural Mechanics Research Series, Report No. CU/SR- 93/3*, University of Colorado at Boulder.

Bicanic, N. and Pankaj (1990) – On mesh design for concrete strain softening analysis, *Computer Aided Analysis and Design of Concrete Structures*, (Eds. Bicanic, N. and Mang, H.), Vol. 2, Pineridge Press, 959-974.

Blaauwendraad, J. and Grootenboer, H.J. (1981) – Essentials for discrete crack analysis, *IABSE, Colloquium on Advanced Mechanics of Reinforced Concrete*, Delft, 263-272.

Cervera, M. (1986) – Nonlinear analysis of reinforced concrete structures using three dimension and shell finite element models, *Ph.D. dissertation*, University College of Swansea, University of Wales.

Gopalaratnam, V.S. and Shah, S.P. (1985) – Softening response of plain concrete in direct tension, *J. Am. Concrete Inst.*, **82**, 310-323.

Hughes, B.P. and Chapman, G.P. (1966) – The complete stress strain curve for concrete in direct tension, *RILEM Bull.*, **30**, 95-97.

van Mier (1984) – Strain softening of concrete under multiaxial loading conditions, *Ph.D. dissertation*, Eindhoven University of Technology, The Netherlands.

Ngo, D. and Scordelis, A.C. (1967) – Finite element analysis of reinforced concrete beams, *J. American Conc. Inst.*, **64**(3), 152-163.

Ortiz, M., Leroy, Y. and Needleman, A. (1987) – A finite element method for localized failure analysis, *Computational Methods in Applied Mechanics and Engineering*, **61**, 189-214.

Ottosen, N.S. (1986) – Thermodynamical consequences of strain softening in tension, *J. Eng. Mech., ASCE*, **112**(11), 1152-1164.

Pramono, E. (1988) – Numerical simulation of distributed and localized failure in concrete, *Ph.D. Thesis*, University of Colarado, Boulder.

Ram, K. and Nayak, G.C. (1994) – Numerical modelling of tensile crack propagation in concrete dams, *J. Str. Div., ASCE*, **120**(4), 1053-1074.

Rashid, Y.R. (1968) – Analysis of prestressed concrete pressure vessels, *Nuclear Engineering and Design*, **7**(4), 334-344.

Rots, J.G., Nauta, P., Kusters, G.M.A. and Blaauwendraad, J. (1985) – Smeared crack approach and fracture localization in concrete, *HERON*, 30, 1-48.

Sandler, I.S. (1984) – Strain softening for static and dynamic problems, *Proceeding Symposium on Constitutive Equations: Micro, Macro and Computational Aspects*, (Ed. Willam, K. J.), 217-231.

Schreyer, H.L. and Chen, Z. (1986) – One dimensional softening with localization, *J. Appl. Mech., ASCE*, **53**, 791-797.

Suidan, M. and Schnobrich, W.C. (1973) – Finite element analysis of reinforced concrete, *J. Str. Div., ASCE*, **99**(10), 2109-2122.

Willam, K.J., Bicanic, N. and Sture, S. (1984) – Constitutive and computational aspects of strain softening and localization in solids, *ASME/WAM Meeting, New Orleans, Symposium on Constitutive Equations, Macro and Computational Aspects*, Vol. G00274 (Ed. Willam, K.), New York, 223-252.

Chapter 2

Review of Computational Plasticity

2.1 Introduction

Hill (1950); Prager (1959); and Hoffman and Sachs (1953) wrote excellent texts on the theory of plasticity. The use of plasticity with the finite element method came with the pioneering work of Yamada et al. (1968), Zienkiewicz et al. (1969), Nayak (1971) and Nayak and Zienkiewicz (1972).

Elastoplastic finite element analysis was popularised by the lucid text of Owen and Hinton (1980). Later Crisfield (1991) included the developments of the eighties in his very "user-friendly" book. This Chapter discusses plasticity basics and reviews some of the developments in the computational plasticity that have taken place in the recent years.

2.2 Basics of Plasticity

In this section the basic ideas behind the flow theory of plasticity are considered (e.g. Zienkiewicz and Taylor, 1991).

It is generally accepted (theoretically as well as experimentally) that the yielding will trigger if the stress σ satisfies the following requirement:

$$F(\sigma, \kappa) = 0 \tag{2.1}$$

where κ is hardening/softening parameter. The instantaneous value of κ will decide the position of the yield surface which can be visualised as a surface in stress space (Fig. 2.1).

It was first suggested by von Mises that basic behaviour defining the plastic strain increments is related to the yield surface. Let $d\varepsilon^p$ denote the increment of plastic strain then this increment can be represented as

$$d\varepsilon^p = d\lambda \frac{\partial F}{\partial \sigma}$$

$$= d\lambda \ \mathbf{a} \tag{2.2}$$

where **a** is known as the 'flow vector' or 'gradient vector'. In Eqn. 2.2, $d\lambda$ is defined as the proportionality constant, undetermined at this stage, also known as plastic multiplier. The rule (Eqn. 2.2) is known as normality principle because the requirement, that the plastic strain increment vector should be normal to the yield surface F is fulfilled by Eqn. 2.2. This requirement of normality can be removed by specifying separately a 'plastic potential'

$$Q = Q(\sigma, \kappa) \tag{2.3}$$

which defines the plastic strain increment in a similar fashion as Eqn. 2.2. This plastic strain increment is given by a flow rule

$$d\varepsilon^p = d\lambda \frac{\partial Q}{\partial \sigma} = d\lambda \ \mathbf{b} \tag{2.4}$$

The particular case $Q = F$ is known as *associated plasticity*. When this relation (Q=F) is not satisfied the plasticity in *non-associated*.

During an infinitesimal increment of stress, change of strains are assumed to be divisible into elastic and plastic parts as

$$d\varepsilon = d\varepsilon^e + d\varepsilon^p \tag{2.5}$$

The elastic strain increments and stress increments are related by a symmetric matrix of constants **D** as

$$d\sigma = \mathbf{D} d\varepsilon^e \tag{2.6}$$

Using Eqns. 2.4 and 2.6, Eqn 2.5 can be written as

$$d\varepsilon = \mathbf{D}^{-1} d\sigma + \frac{\partial Q}{\partial \sigma} \ d\lambda \tag{2.7}$$

The plastic increment of strain will occur only if the 'elastic' stress increment

$$d\sigma^e = \mathbf{D}\, d\varepsilon \tag{2.8}$$

tends to put the stress outside the yield surface, *i.e.*, this elastic increment is in the *plastic loading* direction. If, on the other hand, this stress change is such that *unloading* occurs then of course no plastic straining will be present. The test of the above relation is therefore crucial in differentiating between loading and unloading operations.

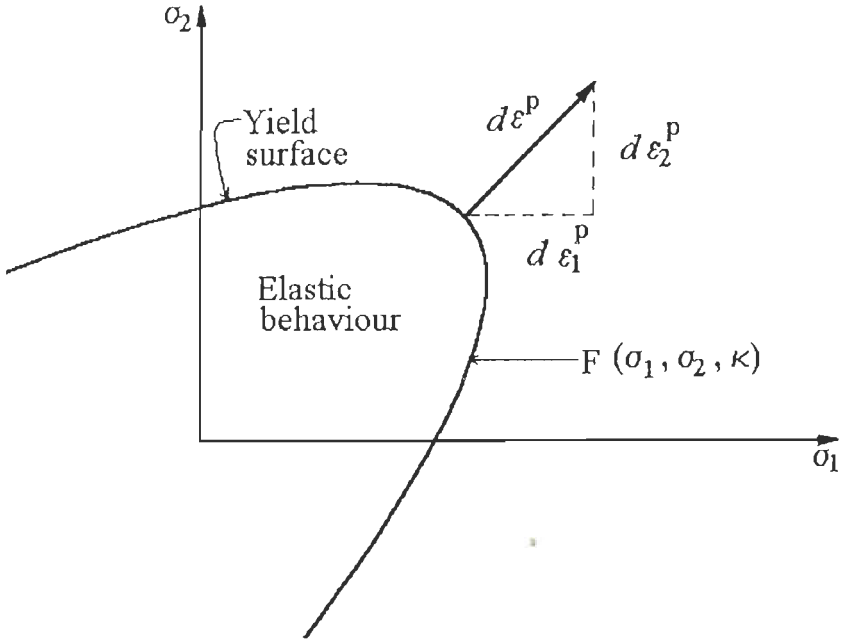

Fig. 2.1 Yield surface and normality criterion in two dimensional stress space

When plastic loading is occurring the stresses are on the yield surface given by Eqn. 2.1. Differentiating Eqn. 2.1 one obtains

$$dF = \frac{\partial F}{\partial \sigma_1} d\sigma_1 + \frac{\partial F}{\partial \sigma_2} d\sigma_2 + \ldots\ldots + \frac{\partial F}{\partial \kappa} d\kappa \tag{2.9}$$

For plastic flow the above derivative of F also vanishes, giving the 'consistency condition' as

$$dF = \left\{\frac{\partial F}{\partial \sigma}\right\}^T d\sigma - \mathrm{A}\, d\lambda = 0$$

$$dF = \mathbf{a}^T d\sigma - \mathrm{A}\, d\lambda \tag{2.10}$$

where A is the hardening parameter given by

$$\mathrm{A} = -\frac{1}{d\lambda}\,\frac{\partial F}{\partial \kappa}\,d\kappa \tag{2.11}$$

Using Eqns. 2.4-2.6 and Eqn. 2.10 the incremental stress-strain relation is obtained as

$$d\sigma = \left(\mathbf{D} - \frac{(\mathbf{Db})(\mathbf{Da})^T}{\mathrm{A} + \mathbf{a}^T\mathbf{Db}}\right) d\varepsilon = \mathbf{D}^{ep}\, d\varepsilon \tag{2.12}$$

where $\mathbf{D}^{ep}$ is the tangential modulus matrix. This matrix is symmetric when plasticity is associated. The stress increment can also be written as

$$d\sigma = \mathbf{D}(d\varepsilon - d\varepsilon^p) = \mathbf{D}(d\varepsilon - d\lambda\mathbf{b}) = \mathbf{D}(d\varepsilon - d\lambda\mathbf{a}) \tag{2.13}$$

with plastic multiplier

$$d\lambda = \frac{\mathbf{a}^T\mathbf{D}\;d\varepsilon}{\mathrm{A} + \mathbf{a}^T\mathbf{Da}} \tag{2.14}$$

While the above relations are "exact" for infinitesimal increments, for computational analysis the stress increments have to be obtained by integrating Eqn. 2.12 or 2.14.

2.3 Hardening Hypotheses

Plastic strain history along with hardening rules defines the subsequent yield surfaces. Two basic models exist (Crisfield, 1991): Isotropic hardening in which the yield surface expands (or contracts) uniformly about the stress space origin and Kinematic hardening in which the yield surface translates while preserving its original shape (Prager, 1955,1956; Ziegler, 1959). Many more hardening rules can be obtained by combination or generalisation of the above.

For isotropic hardening/softening the yield criterion can be written as

$$F(\sigma, Y) = f(\sigma) - f_2(Y(\kappa)) \tag{2.15}$$

where κ is a parameter depending on plastic strain history and Y is a uniaxial or equivalent yield stress. The parameter κ can be defined in either of the two ways as follows:

$$d\kappa = d\mathrm{W}^p = \left(d\varepsilon^p\right)^T \sigma \qquad \text{work hardening hypothesis} \tag{2.16}$$

$$d\kappa = d\varepsilon_y^p = \left(\frac{2}{3}(d\varepsilon^p)^T d\varepsilon^p\right)^{1/2} \quad \text{strain hardening hypothesis} \qquad (2.17)$$

Here dW^p is plastic work and $d\varepsilon_y^p$ is equivalent or uniaxial plastic strain.

For some cyclic loading problems, Bauschinger effect may become significant. For linear hardening considerations these effects can be illustrated for one dimensional case as shown in Fig. 2.2 (Crisfield, 1991). For such problems the yielding in tension lowers the compressive yield strength so that

$$\sigma - \alpha = \pm Y_o \qquad (2.18)$$

where α is defined as the 'kinematic shift' of the center of the yield surface. The actual hardening of the uniaxial stress σ takes place due to this shifting because Y_o (uniaxial yield strength) is assumed to be a fixed value. This phenomenon of kinematic hardening is not incorporated in this study.

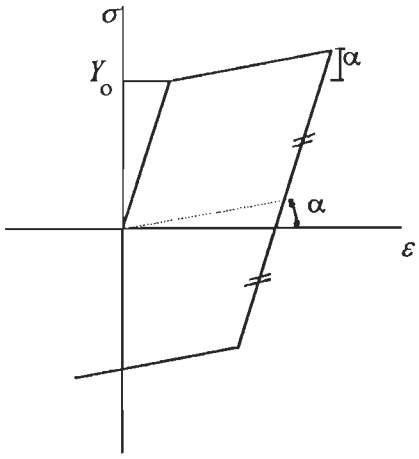

Fig. 2.2 One dimensional illustration of kinematic hardening

2.4 Backward Euler Integration

The process of evaluation of incremental stresses from incremental strains is not straightforward. This requires the integration of Eqn. 2.12, which involves material constitutive relations that are nonlinear.

Ortiz and Popov (1985) presented a generalised algorithm for the integration of the rate equations (Crisfield, 1991):

$$\sigma_C = \sigma_A + \mathbf{D}(\Delta\varepsilon - \Delta\varepsilon^p) = \sigma_B - \mathbf{D}(\Delta\varepsilon^p) \tag{2.19}$$

$$\Delta\varepsilon^p = \Delta\lambda[(1-\eta)\mathbf{a}_A + \eta\mathbf{a}_C] \tag{2.20}$$

$$\Delta\kappa = [(1-\eta)\kappa_A + \eta\kappa_C] \tag{2.21}$$

$$F_C = f_1(\sigma_C) - f_2(Y(\kappa_c)) = 0 \tag{2.22}$$

where, as shown in Fig. 2.3a, A is the starting point and point C is the destination on the yield surface. Y denotes uniaxial yield strength. Various algorithms are obtained by changing the factor η which can take values between 0 and 1. For $\eta = 0$ 'explicit' forward Euler algorithm is obtained. This algorithm does not ensure satisfaction of the yield condition defined by Eqn. 2.22. However, $\eta = 1$ leads to a 'backward-Euler' algorithm. The full 'backward-Euler' scheme involves a flow vector $\mathbf{a}_C$ that is normal to the yield surface at the final position C (Fig. 2.3b), for which the stresses, σ_C satisfy Eqn. 2.22. This algorithm has found widespread usage in recent years.

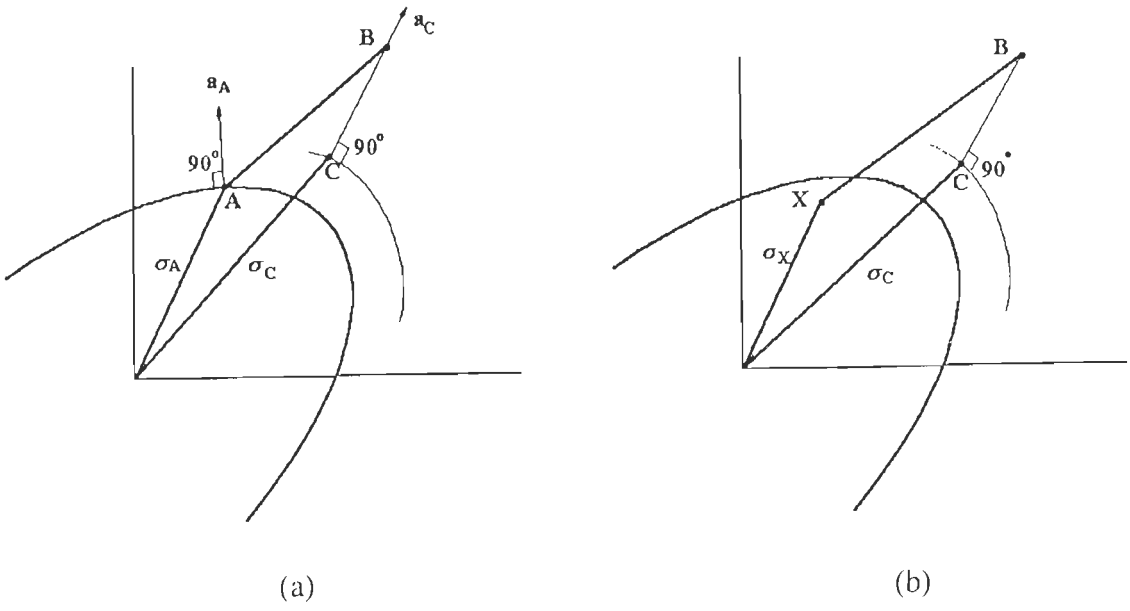

Fig. 2.3 Backward Euler returns from a stress state (a) on the yield surface (b) inside the yield surface

For backward-Euler algorithm ($\eta = 1$), Eqns. 2.19 and 2.20 yield

$$\sigma_C = \sigma_B - \Delta\lambda \ \mathbf{D}\mathbf{a}_C \tag{2.23}$$

clearly $\mathbf{a}_C$ cannot be obtained from the information at A or B (Fig. 2.3a). An iterative procedure at the Gauss point level is, therefore, required. A starting estimate for $\mathbf{a}_C$ can be the flow vector at B. Generally, this starting estimate will not satisfy the yield function and further iterations will be required. In order to derive such an iterative loop, a vector $\mathbf{r}$ can be assumed which represents the difference between the current stresses and the backward-Euler stresses *i.e.*

$$\mathbf{r} = \sigma - (\sigma_B - \Delta\lambda \, \mathbf{D}\mathbf{a}_C) \tag{2.24}$$

In order to satisfy the condition $F = 0$ *i.e.* reduce $\mathbf{r}$ to zero (with some tolerance), iterations are needed.

With the trial elastic stresses, σ_B being kept fixed, a truncated Taylor expansion can be applied to Eqn. 2.24 so as to produce new residual $\mathbf{r}_n$ where

$$\mathbf{r}_n = \mathbf{r}_\circ + d\sigma + d(\Delta\lambda)\mathbf{D}\mathbf{a} + \Delta\lambda \mathbf{D}\frac{\partial \mathbf{a}}{\partial \sigma} d\sigma \tag{2.25}$$

where $\mathrm{d}\sigma$ is the change in σ and $d(\Delta\lambda) = d\lambda$ is change in $\Delta\lambda$, setting $\mathbf{r}_n$ to zero gives

$$\mathrm{d}\sigma = -\left(\mathbf{I} + \Delta\lambda \, \mathbf{D}\frac{\partial \mathbf{a}}{\partial \sigma}\right)^{-1} (\mathbf{r}_\circ + d\lambda \, \mathbf{D}\mathbf{a}) = -\mathbf{Q}^{-1}\mathbf{r}_\circ - d\lambda \, \mathbf{Q}^{-1}\mathbf{D}\mathbf{a} \tag{2.26}$$

with

$$\mathbf{Q} = \left(\mathbf{I} + \Delta\lambda \, \mathbf{D}\frac{\partial \mathbf{a}}{\partial \sigma}\right)$$

Also, a truncated Taylor series on the yield function (Eqn. 2.22) gives

$$F_{Cn} = F_{CO} + \left.\frac{\partial F}{\partial \sigma}\right|_C d\sigma + \left.\frac{\partial F}{\partial Y}\right|_C dY = F_{CO} + \mathbf{a}_C^T \ d\sigma - \mathrm{A}_C \ d\lambda = 0 \tag{2.27}$$

Now dropping the superscript C, we can write

$$d\lambda = \frac{F_\mathrm{O} - \mathbf{a}^T\mathbf{Q}^{-1}\mathbf{r}_\circ}{\mathbf{a}^T\mathbf{Q}^{-1}\mathbf{D}\mathbf{a} + \mathrm{A}} \tag{2.28}$$

Use of Eqn 2.26 now yields the iterative stress change $d\sigma$.

2.5 Consistent Tangent Modular Matrix

The Newton Raphson method emerges as a slow procedure if the modular matrix $\mathbf{D}^{ep}$ (Eqn. 2.12) is used in conjunction with the backward-Euler integration scheme. The matrix $\mathbf{D}^{ep}$ is 'strictly' applicable only for infinitesimal increments. Simo and Taylor (1985) derived a tangent modular matrix that is 'consistent' with the backward-Euler integration algorithm. Hence the quadratic rate of convergence of Newton Raphson iterations is ensured.

After dropping the superscript C the backward-Euler return algorithm, Eqn. 2.23, at the post-return configuration (Fig. 2.3) can be written as (Crisfield, 1991)

$$\sigma = \sigma_B - \Delta\lambda\, \mathbf{D}\mathbf{a} \tag{2.29}$$

The suffix B in Eqn. 2.29 shows that σ_B are the elastic 'trial' stresses (Fig. 2.3b). Differentiation of Eqn. 2.29 results in

$$d\sigma = \mathbf{D}\, d\varepsilon - \Delta\lambda\, \mathbf{D}\frac{\partial \mathbf{a}}{\partial \sigma} d\sigma - d\lambda\, \mathbf{D}\mathbf{a} \tag{2.30}$$

On rearranging the terms of Eqn. 2.30, results in

$$\begin{aligned} \mathrm{d}\sigma &= \left(\mathbf{I} + \Delta\lambda\, \mathbf{D}\frac{\partial \mathbf{a}}{\partial \sigma}\right)^{-1} \mathbf{D}(d\varepsilon - d\lambda\, \mathbf{a}) \\ &= \mathbf{Q}^{-1}\mathbf{D}(d\varepsilon - d\lambda\, \mathbf{a}) \\ &= \mathbf{R}(d\varepsilon - d\lambda\, \mathbf{a}) \end{aligned} \tag{2.31}$$

where the $\mathbf{Q}$ matrix has already been defined in the previous section and

$$\mathbf{R} = \mathbf{Q}^{-1}\mathbf{D} \tag{2.32}$$

To remain on the yield surface, dF should be zero and hence using Eqns. 2.10 and 2.29

$$\begin{aligned} dF &= \mathbf{a}^T d\sigma - \mathrm{A} d\lambda \\ &= \mathbf{a}^T \mathbf{R}(d\varepsilon - d\lambda\, \mathbf{a}) - \mathrm{A}\, d\lambda = 0 \end{aligned} \tag{2.33}$$

The above equation yields

$$d\lambda = \frac{\mathbf{a}^T \mathbf{R}\, d\boldsymbol{\varepsilon}}{\mathrm{A} + \mathbf{a}^T \mathbf{R}\, \mathbf{a}} \tag{2.34}$$

which on substitution in Eqn. 2.31 results

$$d\boldsymbol{\sigma} = \mathbf{D}^{ct} d\boldsymbol{\varepsilon} = \left(\mathbf{R} - \frac{(\mathbf{Ra})(\mathbf{Ra})^T}{\mathrm{A} + \mathbf{a}^T \mathbf{R}\, \mathbf{a}} \right) d\boldsymbol{\varepsilon} \tag{2.35}$$

where $\mathbf{D}^{ct}$ is called the consistent tangent matrix. A comparison of $\mathbf{D}^{ct}$ and $\mathbf{D}^{ep}$ (Eqn. 2.12) shows that the former employs $\mathbf{R}$ where the latter uses $\mathbf{D}$. Obviously $\mathbf{D}$ is obtained from $\mathbf{R}$ with $\Delta\lambda = 0$. In this situation $\partial \mathbf{a} / \partial \boldsymbol{\sigma}$ is not required.

2.6 The Arc Length Method

The post-peak response of structures cannot be traced beyond peak or critical loads, under load control. As a result some form of indirect displacement control technique is essential. Among these, the arc length method (Wampner, 1971; Riks, 1979; Ramm, 1980; Crisfield, 1981,1982; de Borst, 1986; Crisfield, 1991; Foster, 1992; Lam and Morley, 1992; Pankaj and Shrikhande, 1993) emerged out as a powerful solution technique. The method has been used to solve problems of snap through, snap back and collapse (Crisfield, 1991). This formulation of arc length method is discussed below.

Notations adopted in the formulation are similar to that used by Ramm (1980) and shown in Fig. 2.4. A superscript on the left indicates current configuration *e.g.* ${}^m\mathbf{u}$, ${}^m\mathbf{P}$, ${}^m\mathbf{F}$ and ${}^m\psi$ are the total displacement vector, load vector, internal forces and out of balance forces at load step (or iteration number) m respectively. The process considers the proportional variation of load defined as

$${}^m\mathbf{P} = {}^m\beta\, \mathbf{P} \tag{2.36}$$

where ${}^m\beta$ is scalar load factor and $\mathbf{P}$ is a vector of reference loads. In order to obtain the next converged configuration m+1 from the current converged configuration, the iterations are needed. The notations used between the iterative cycle i and $i+1=j$ are shown in Fig. 2.7.

The total increment between configuration m and i are denoted by $\Delta(\cdot)_i$, *e.g.* $\Delta\mathbf{u}_i$, $\Delta\beta_i$, while the increments from i to j are denoted by $\delta(\cdot)_i$. Thus

$${}^i\beta = {}^m\beta + \Delta\beta_j = {}^i\beta + \delta\beta_j$$

and

$$^{j}\mathbf{u} = {}^{m}\mathbf{u} + \Delta\mathbf{u}_j = {}^{i}\mathbf{u} + \delta\mathbf{u}_j$$

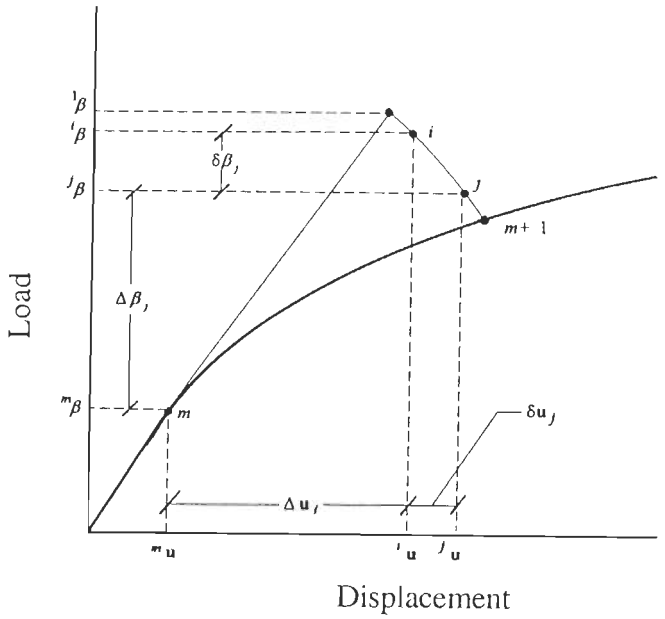

Fig. 2.4 Pictorial description of arc length method

In standard elastoplasticity, the governing equation is given by

$$^{i}\mathbf{K}\,\delta\mathbf{u}_j = \delta\beta_j\,\mathbf{P} + {}^{i}\mathbf{R} \tag{2.37}$$

where $^{i}\mathbf{K}$ is the stiffness matrix during the iteration i and $^{i}\mathbf{R}$ is the vector of residual forces at the end of iteration i.

For this procedure, Crisfield (1981) imposed a constraint, which forces the length of the displacement increment to remain equal to the arc length at each iteration, in the form

$$\Delta\mathbf{u}_i^T\Delta\mathbf{u}_i = \Delta S^2 \tag{2.38}$$

where ΔS is a finite length called the arc length. Using Eqn. 2.37, the change in displacement from iterative cycle i to j is given by

$$\begin{aligned}\delta\mathbf{u}_j &= {}^{i}\mathbf{K}^{-1}\,(^{i}\mathbf{R} + \delta\beta_j\,\mathbf{P}) \\ &= \delta\bar{\mathbf{u}}_j + \delta\beta_j\,\Delta\mathbf{u}_t\end{aligned} \tag{2.39}$$

where

$$\delta \bar{\mathbf{u}}_j = {}^i\mathbf{K}^{-1}\ {}^i\mathbf{R}$$

$$\Delta \mathbf{u}_t = {}^i\mathbf{K}^{-1}\ \mathbf{P}$$

Hence at each iteration, only $\delta \bar{\mathbf{u}}_j$ need be formed since $\Delta \mathbf{u}_t$ can be saved from the first iteration. The iterative displacement vector $\delta \mathbf{u}_j$ is only fully defined once $\delta\beta_j$ is known which can be determined using Eqns. 2.38 and 2.39 as

$$b_1\ \delta\beta_j^2 + b_2\ \delta\beta_j + b_3 = 0 \tag{2.40}$$

where

$$\begin{aligned} b_1 &= \Delta \mathbf{u}_t^T\ \Delta \mathbf{u}_t \\ b_2 &= 2\ \Delta \mathbf{u}_t^T\ (\delta \bar{\mathbf{u}}_j + \Delta \mathbf{u}_i) \\ b_3 &= (\delta \bar{\mathbf{u}}_j + \Delta \mathbf{u}_i)^T\ (\delta \bar{\mathbf{u}}_j + \Delta \mathbf{u}_i) - \Delta S^2 \end{aligned} \tag{2.41}$$

Eqn. 2.40 can now be solved for $\delta\beta_j$. The two roots of this quadratic equation will be designated as $\delta\beta_{j1}$ and $\delta\beta_{j2}$. To prevent "doubling back" on the original load-deflection path, the angle between the incremental displacement vector $\Delta \mathbf{u}_t$, before the current iteration, and $\Delta \mathbf{u}_j$, after the present iteration should be positive (Crisfield, 1981). There are two alternative values for $\Delta \mathbf{u}_j$ (called say $\Delta \mathbf{u}_{j1}$ and $\Delta \mathbf{u}_{j2}$) corresponding to the two solutions $\delta\beta_{j1}$ and $\delta\beta_{j2}$. Hence the two angles θ_1 and θ_2 are given by

$$\begin{aligned} \theta_1 &= \Delta \mathbf{u}_{j1}^T\ \Delta \mathbf{u}_i \\ \theta_2 &= \Delta \mathbf{u}_{j2}^T\ \Delta \mathbf{u}_i \end{aligned} \tag{2.42}$$

The appropriate root $\delta\beta_{j1}$ and $\delta\beta_{j2}$, is that which gives a positive angle. If both angles are positive then the appropriate root is that closest to the linear solution (Crisfield, 1981).

$$\delta\beta_j = -\left(\frac{b_3}{b_2}\right) \tag{2.43}$$

The first load increment is usually started using a unit increment. The length of the increment, ΔS is fixed as

$$\Delta \mathbf{u}_t^T\ \Delta \mathbf{u}_t = \Delta S^2 \tag{2.44}$$

If the required response is in the area of severe nonlinearity, the length may be varied, else it may be kept constant. The adjustment in the arc length may be carried out using (Crisfield, 1981)

$$\Delta S_m = \Delta S_{m-1}\left(\frac{I_d}{I_{m-1}}\right) \tag{2.45}$$

where I_{m-1} and I_d indicate number of iterations that were required to achieve equilibrium in increment $m-1$ and the desired number of iterations in the present increment respectively. For all increments other than first, the initial loading parameter $\delta\beta_1$ can be obtained as

$$\delta\beta_1 = \frac{\Delta S_j}{\Delta S_1} \tag{2.46}$$

If the determinant of the tangent stiffness matrix changes sign, the load increment sign has to be reversed, otherwise not.

References

de Borst, R. (1986) – Nonlinear analysis of frictional materials, *Ph.D. Dissertation*, Delft University of Technology.

Crisfield, M.A. (1981) – Fast incremental/iterative solution procedures that handles "snap-through", *Comp. Struct.*, **13**, 55-62.

Crisfield, M.A. (1982) – Local instabilities in nonlinear analysis of reinforced concrete beams and slabs, *Proc. Inst. of Engineers*, U.K., **73**, 135-145.

Crisfield, M.A. (1991) – Nonlinear finite element analysis of solids and structures; Vol. I, Essentials, John Wiley & Sons.

Foster, S. (1992) – An application of the arc-length method involving concrete cracking, *IJNME*, **33**(2), 269-285.

Hill, R. (1950) – The mathematical theory of plasticity, Oxford University Press.

Hoffman, O. and Sachs, G. (1953) – Introduction to the theory of plasticity for engineers, Mc-Graw Hill.

Lam, W.F. and Morley, C.T. (1992) – Arc-length methods for passing limit points in structural calculation, *J. Str. Eng.*, **118**(1), 169-185.

Nayak, G.C. (1971) – Plasticity and large deformation problems by the finite element method, *Ph.D. Thesis*, University College of Swansea, University of Wales.

Nayak, G.C. and Zienkiewicz, O.C. (1972) – Convenient forms of stress invariants for plasticity, *Journ. of Str. Div., ASCE*, **98**(4), 949-953.

Ortiz, M. and Popov, E.P. (1985) – Accuracy and stability of integration algorithms for elastoplastic constitutive relations, *IJNME*, **21**, 1561-1576.

Owen, D.R.J. and Hinton, E. (1980) – Finite elements in plasticity, Theory and Practice, Pineridge Press, U.K.

Pankaj and Shrikhande, M. (1993) – On the arc-length method in strain softening problems, *International Journal of Structures*, **13**(2), 93-107.

Prager, W. (1955) – The theory of plasticity: A survey of recent achievements, *Proc. Inst. Mech. Eng.*, **169**, 41-57.

Prager, W. (1956) – A new method of analysing stresses and strains in work hardening plastic solids, *J. Appl. mech.*, **78**, 493-496.

Prager, W. (1959) – An introduction to plasticity, *Addison-Wesley*, Amsterdam and London.

Ramm, E. (1980) – Strategies for tracing nonlinear response near limit points, *Proc. Europe-U.S. Workshop on Nonlinear Finite Element Analysis in Structural Mechanics* (Eds. Wunderlich, W., Stein, E. and Bathe, K.-J.), Springer-Verlag, 63-89.

Riks, E. (1979) – An incremental approach to snapping and buckling problems, *Int. J. of Solids and Struct.*, **15**, 524-551.

Simo, J.C. and Taylor, R.L. (1985) – Consistent tangent operators for rate independent elastoplasticity, *Copmut. Meth. Appl. Mech. Engng.*, **48**, 101-118.

Wampner, G.A. (1971) – Discrete approximations related to nonlinear theories of solids, *Int. J. of Solids and Struct.*, 7, 1581-1599.

Yamada, Y., Yoshimura, N. and Sakurai, T. (1968) – Plastic stress-strain matrix and its application for the solution of elastoplastic problems by finite element method. *Int. J. Mech. Sci.*, **10**, 343-354.

Ziegler, H. (1959) – A modification of Pragers hardening rules, *Q. Appl. Math.*, **17**, 55-65.

Zienkiewicz, O.C. and Taylor, R.L. (1991) – The finite element method, solids and fluid mechanics dynamics and nonlinearity, Fourth Edition, Vol. 2, Mc-Graw Hill International Editions.

Zienkiewicz, O.C., Valiappan, S. and King, I.P. (1969) – Elastoplastic solutions of engineering problems, initial stress, finite element approach, *IJNME*, Vol. I, 75-100.

Chapter 3

Simulating Post-Cracking Behaviour – A Review

3.1 Introduction

Simulation of cracking involves capturing of the degradation of a continuum to a discontinuum. It has often been argued whether a unique solution to these problems exists. A structure is subjected to deformations that are much greater than its linear response limit before it collapses. In fact, prior to structural collapse, microcracking in some zones leads to reduced stiffness (stiffness degradation) and stress carrying capacity (strain softening). For complex materials like reinforced concrete, failure may be caused due to several possible mechanisms, such as mortar cracking, reinforcement yield, bond slip, concrete crushing and interface sliding. Clearly to incorporate such a variety in numerical computations, is a difficult task. However, the understanding of the failure mode is important to avoid brittle failure. It is for this reason that the capability to predict the post-peak deformation behaviour is essential in addition to finding the ultimate load carrying capacity.

3.2 Failure Classification

Willam et al. (1994) classified failure modes according to the degree of discontinuity as follows:

(a) Distributed failure (spatially continuous): In this mode, the kinematic compatibility conditions of the intact continuum are not disturbed (Fig. 3.1a). The

tangential material operator matrix may become singular. However, no special finite element provisions are required to mathematically model such a failure.

(b) Localized failure (weak discontinuities): Such a failure causes discontinuities of strains and stress fields (Fig. 3.1b). It is now accepted that special provisions are required to be adhered to, in the finite element mesh, to be able to capture such a failure (Bicanic and Pankaj, 1990; Ortiz and Quigley, 1991; Steinmann and Willam, 1994).

(c) Discrete failure (strong discontinuities): Such a failure introduces not only discontinuous strains but also jumps in the displacement field (Fig. 3.1c). Strictly speaking such a failure can only be captured through discrete crack approaches discussed in Chapter 1. In fact fracture modes I, II and III of fracture mechanics imply such a failure. Clearly finite element analysis would require extensive re-zoning and re-alignment of the mesh.

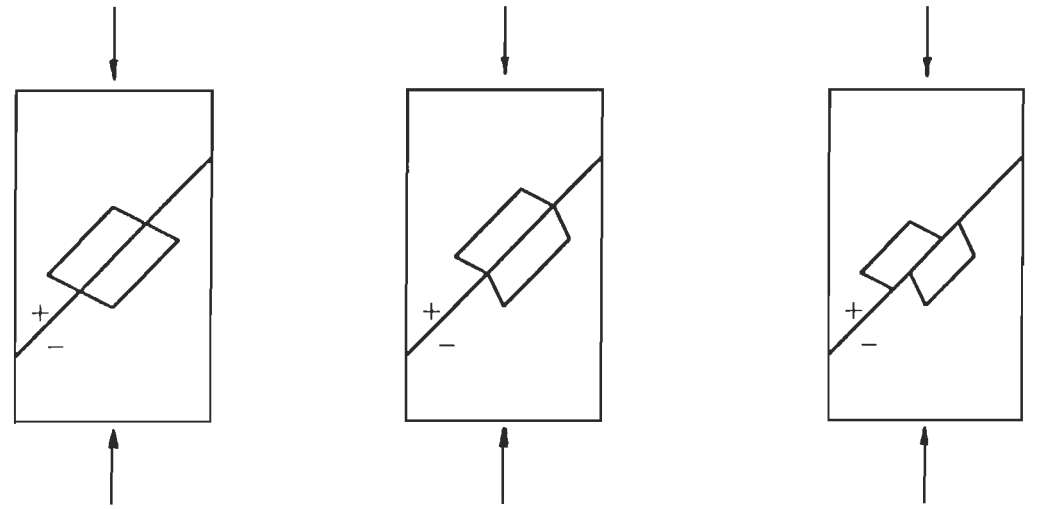

Fig. 3.1 Degradation of kinematic compatibility during progressive failure

In this study, attention will be confined to localized failure which can be modelled through the so called smeared crack approach. Clearly, thin bands of intense straining can be obtained if the finite element mesh is made extremely fine. Thus, it might be possible to simulate strong discontinuities by making an extremely fine finite element mesh.

3.3 Smeared Crack Approach

In the smeared crack approach, cracking is assumed to be caused by a set of densely populated or smeared cracks (Fig. 3.2). Computationally the smeared crack approach involves modification of the constitutive relations expressed in terms of stresses and strains in the region of interest. This approach has been used in many forms by several investigators (Bazant and Oh, 1983; Jiang, 1983; Nilson and Oldenburg, 1983; Glamberg, 1984; Rots et al., 1985; Petrangeli and Ozbolt, 1996). The finite element implementation of the smeared crack approach has followed two distinct methodologies *viz.* the fixed crack method (Rashid, 1968; Suidan and Schonbrich, 1973; Lin and Scordelis, 1975; Bazant and Oh, 1983; Liebengood et al., 1986) and the rotating crack method (Cope et al., 1980; Gupta and Akbar, 1984; Crisfield and Wills, 1987; Milford and Schonbrich, 1985). In the fixed crack method, it is assumed that the initially isotropic material becomes anisotropic at the onset of cracking with the principal axes of the material oriented along the direction of the crack. In the earlier work, only orthogonal cracks at the same point were permitted but subsequently attempts were made to allow multiple cracks at the same point (de Borst and Nauta, 1985). Since there was no control over the maximum tensile strength, the fixed crack method tended to overestimate the strength of the structures (Crisfield and Wills, 1987). In the rotating or swinging crack method the initially isotropic material remains isotropic and there is no permanent memory as in case of the fixed crack method. Thus any change in material properties at a point happens in all directions.

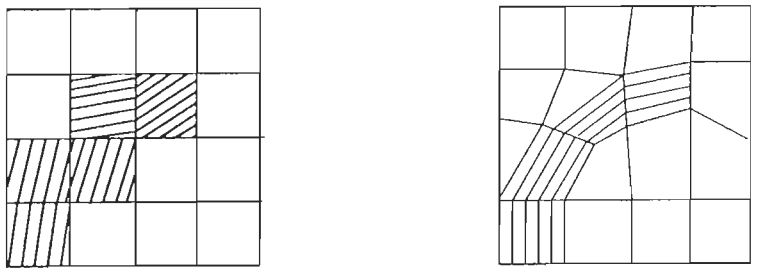

Without mesh refinement With adaptive mesh refinement

Fig. 3.2 Finite element modelling with unknown crack path using the smeared crack approach (redrawn from Cervera, 1986)

Each of the above methods have been employed using elasticity or plasticity based theories (Willam et al., 1987). Some attempts to mix these theories have also been made (de Borst and Nauta, 1985; de Borst, 1986). The basic features of the smeared crack approach are outlined in the following subsections.

3.3.1 Elasticity Based Approach

In this approach, the Rankine criterion of maximum principal stress governs the initial formation of cracks. Thus, converting the initially isotropic materials to an anisotropic form. The total strain increment $\Delta\boldsymbol{\varepsilon}$ of the cracked solid can be decomposed into the crack component $\Delta\boldsymbol{\varepsilon}^{cr}$ and the continuum component $\Delta\boldsymbol{\varepsilon}^{co}$ as (Guzina et al. 1995).

$$\Delta\boldsymbol{\varepsilon} = \Delta\boldsymbol{\varepsilon}^{cr} + \Delta\boldsymbol{\varepsilon}^{co} \tag{3.1}$$

The incremental strains in the above equation are in the global Cartesian coordinates. For a two-dimensional setting, $\Delta\boldsymbol{\varepsilon}^{cr}$ can be written in vector form as

$$\Delta\boldsymbol{\varepsilon}^{cr} = \left[\Delta\varepsilon_{xx}^{cr}, \Delta\varepsilon_{yy}^{cr}, \Delta\gamma_{xy}^{cr}\right]^{\mathrm{T}} \tag{3.2}$$

The local crack strain vector $\Delta\mathbf{e}^{cr}$ in the local (n, t) coordinate system which is aligned with the crack orientation, can be written as

$$\Delta\mathbf{e}^{cr} = \left[\Delta e_{nn}^{cr}, \Delta e_{tt}, \Delta\gamma_{nt}^{cr}\right]^{\mathrm{T}} \tag{3.3}$$

and the transformation between local and global crack strains is expressed as

$$\Delta\boldsymbol{\varepsilon}^{cr} = \mathbf{T}^{\mathrm{T}}\Delta\mathbf{e}^{cr} \tag{3.4}$$

where $\mathbf{T}$ denotes the orthogonal transformation matrix. Similarly, incremental local tractions in the (n, t) system

$$\Delta\mathbf{t}^{cr} = \left[\Delta t_{nn}^{cr}, \Delta t_{tt}^{cr}, \Delta t_{nt}^{cr}\right]^{\mathrm{T}} \tag{3.5}$$

can be related to the global stress increment $\Delta\boldsymbol{\sigma}$ as

$$\Delta\mathbf{t}^{cr} = \mathbf{T}^{\mathrm{T}}\Delta\boldsymbol{\sigma} \tag{3.6}$$

For simplicity, it is assumed that the continuum between the cracks remains linear elastic and isotropic, *i.e.*

$$\Delta\boldsymbol{\sigma} = \mathbf{D}\Delta\boldsymbol{\varepsilon}^{co} \tag{3.7}$$

where for plane stress

$$\mathbf{D} = \begin{bmatrix} \frac{E}{1-\nu^2} & \frac{\nu E}{1-\nu^2} & 0 \\ \frac{\nu E}{1-\nu^2} & \frac{E}{1-\nu^2} & 0 \\ 0 & 0 & G \end{bmatrix} \tag{3.8}$$

A softening relationship is adopted for the crack interface which relates surface tractions to the equivalent cracked strain through

$$\Delta \mathbf{t}^{cr} = \mathbf{D}^{cr} \Delta \mathbf{e}^{cr} \tag{3.9}$$

The smeared crack formulation is constituted by the properties of the tangent crack formulation $\mathbf{D}^{cr}$. The tangent crack operator $\mathbf{D}^{cr}$ is a 3×3 matrix for any two-dimensional case. In general it is assumed that there is no interaction between orthogonal cracks, except through the common shear modulus term (Willam et al, 1989). Normally, it is also assumed (Rots and Blaauwendraad, 1989) that the coupling among the direct and shear components in the crack tractions/strain expression may be neglected. Due to these assumptions, the crack tangent operator reduces to

$$\mathbf{D}^{cr} = \begin{bmatrix} E_n^{\mathrm{I}} & 0 & 0 \\ 0 & E_t^{\mathrm{I}} & 0 \\ 0 & 0 & E_{nt}^{\mathrm{II}} \end{bmatrix} \tag{3.10}$$

where E_n^{I} and E_t^{I} are the mode I stiffness moduli for (n, t) system respectively and E_{nt}^{II}, shear stiffness for simultaneous cracking in the two orthogonal directions of principal orthotropy.

The global stress increment, comprising an elastic-predictor and a crack-corrector component, can be expressed using Eqn. 3.1 as

$$\Delta \boldsymbol{\sigma} = \mathbf{D}(\Delta \boldsymbol{\varepsilon} - \mathbf{T} \Delta \mathbf{e}^{cr}) \tag{3.11}$$

This constitutive incremental stress-strain relationship, with the help of Eqn. 3.6 and Eqn. 3.9, results in

$$\Delta \boldsymbol{\sigma} = \left(\mathbf{D} - \mathbf{D}\mathbf{T}(\mathbf{D}^{cr} + \mathbf{T}^{\mathrm{T}}\mathbf{D}\mathbf{T})^{-1}\mathbf{T}^{\mathrm{T}}\mathbf{D}\right)\Delta \boldsymbol{\varepsilon} \tag{3.12}$$

In the above equation, the tangent stiffness has the same form as for incremental elastoplasticity. This equation is similar to the one developed by Rots and Blaauwendraad (1989) which denotes tangent stiffness operator by $\mathbf{E}^{ec}$. If the global coordinates align in the crack direction, then, the orthogonal transformation matrix $\mathbf{T} = \mathbf{I}$ (identity matrix), and for plane stress case $\mathbf{E}^{ec}$ reduces to

$$\mathbf{E}^{ec} = \begin{bmatrix} E_{nn}^{ec} & E_{nt}^{ec} & 0 \\ E_{tn}^{ec} & E_{tt}^{ec} & 0 \\ 0 & 0 & G_{nt}^{ec} \end{bmatrix} = E^{ec} \begin{bmatrix} E_n^{\mathrm{I}}(E + E_t^{\mathrm{I}}) & \nu E_n^{\mathrm{I}} E_t^{\mathrm{I}} & 0 \\ \nu E_n^{\mathrm{I}} E_t^{\mathrm{I}} & E_n^{\mathrm{I}}(E + E_t^{\mathrm{I}}) & 0 \\ 0 & 0 & \dfrac{G E_{nt}^{\mathrm{II}}}{E^{ec}(E_{nt}^{\mathrm{II}} + G)} \end{bmatrix} \tag{3.13}$$

with

$$E^{ec} = \frac{E}{E(E + E_n^{\mathrm{I}} + E_t^{\mathrm{I}}) + E_n^{\mathrm{I}} E_t^{\mathrm{I}}(1 - \nu^2)}$$

In the rotating crack approach, the moduli related to mode I-type cracking essentially coincide with those of the fixed crack approach. For the rotating crack approach, the shear term in Eqn. 3.13 (fixed crack approach) is different and can be expressed as

$$G_{nt}^{ec} = \frac{\sigma_{11} - \sigma_{22}}{2(\varepsilon_{11} - \varepsilon_{22})} \tag{3.14}$$

where σ_{11}, σ_{22} and $\varepsilon_{11}, \varepsilon_{22}$ denote principal stresses and strains respectively. In order to preserve the coaxiality between the stresses and strains when their principal axes rotate, this shear term is essential (Willam et al., 1989).

3.3.2 Plasticity Based Approach

If it is assumed that the material has experienced tensile cracking in a plane defined by normal n then in the crack plane, the subsequent yield condition would involve only normal and shear stresses. If Rankine criterion normal to the crack plane (without shear effect) is assumed, then the yield function can be written as

$$F = \sigma_n - Y = 0 \tag{3.15}$$

where σ_n is the stress normal to the crack plane and Y, the uniaxial or equivalent yield stress. In computational elastoplasticity, the relation between incremental stresses and strains is expressed as

$$\Delta\sigma = \mathbf{D}^{ep}\Delta\varepsilon \tag{3.16}$$

with the elastoplastic matrix

$$\mathbf{D}^{ep} = \mathbf{D} - \frac{(\mathbf{Da})(\mathbf{Da})^{\mathrm{T}}}{\mathrm{A} + \mathbf{a}^{\mathrm{T}}\mathbf{Da}} \tag{3.17}$$

In the fixed Cartesian frame the flow vector **a** can be expressed as (Pankaj, 1990)

$$\mathbf{a}^{\mathrm{T}} = (\cos^2\theta \quad \sin^2\theta \quad 2\sin\theta\cos\theta) \tag{3.18}$$

where θ denotes the angle form the global x-axis to the crack normal and the softening parameter A can be expressed as

$$\mathrm{A} = \frac{EE_T}{E - E_T} \tag{3.19}$$

where E and E_T are the Young's modulus and slope of the softening branch of the stress strain curve of the cracking material as shown in Fig. 3.3

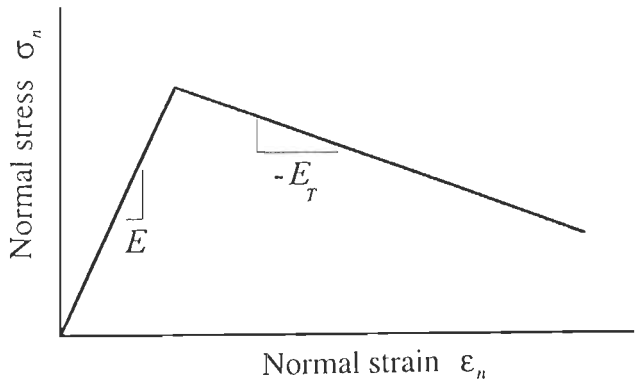

Fig. 3.3 Normal stress *vs.* normal strain

The elstoplastic tangent modulus matrix, after neglecting the Poisson's effect can be expressed for plane stress case as

$$\mathbf{D}^{ep} = E\begin{bmatrix} 1 & 0 & 0 \\ 0 & 1 & 0 \\ 0 & 0 & 0.5 \end{bmatrix} - (E - E_T)\begin{bmatrix} \cos^4\theta & \cos^2\theta\sin^2\theta & \sin\theta\cos^3\theta \\ \cos^2\theta\sin^2\theta & \sin^4\theta & \cos\theta\sin^3\theta \\ \sin\theta\cos^3\theta & \cos\theta\sin^3\theta & \sin^2\theta\cos^2\theta \end{bmatrix} \tag{3.20}$$

If the normal to the crack plane is aligned with global x-axis, then $\mathbf{D}^{ep}$ reduces to

$$\mathbf{D}^{ep} = \begin{bmatrix} E_T & 0 & 0 \\ 0 & E & 0 \\ 0 & 0 & 0.5E \end{bmatrix} \tag{3.21}$$

Plasticity based rotating crack approach is simply an isotropic softening model which can be depicted with the help of an yield criterion, for maximum tensile stress criterion (Rankine) without directionality, as

$$F = \sigma_1 - Y = 0 \tag{3.22}$$

with σ_1, the maximum principal stress.

Plasticity also gives a choice to use yield criterion other than the Rankine criterion to model cracking. With other yield criterion, the fixed and the rotating plasticity based approaches can be linked to anisotropic strain softening plasticity and isotropic strain softening plasticity respectively.

3.3.3 A Comparison of Various Approaches

The elasticity based fixed crack models have been widely used to model cracking within the smeared crack concept. These models can, however, significantly overestimate strength of the structures (Crisfield and Wills, 1987; Crisfield, 1988), since no control is imposed over the maximum tensile strength. In order to overcome such problems, models that permit multiple non-orthogonal cracks have been proposed (de Borst and Nauta, 1985). These allow formation of new cracks if the maximum principal stress indicates a crack where the change of the angle from the previous crack(s) is greater than a specified threshold angle. The choice of threshold angle is rather arbitrary. If the threshold angle is small, then a greater number of cracks can open. A constant monitoring is required for the crack state *i.e.* whether crack is open or closed. The state change of one crack promotes the state changes of others *i.e.* opening of one crack may cause closing of another (Rots, 1988). During such state changes, a decision as to which state change should be handled first needs to be made (Rots, 1988). This state change process also requires excessive bookkeeping.

The use of elasticity based rotating crack approach can overcome many of the above discussed problems (Cope et al., 1980; Gupta and Akbar, 1984; Crisfield and Wills, 1987; Crisfield, 1988). This approach however, overestimates strength for shear/compression failures. This probably is due to the basic nature of the failure criterion which is based on

the maximum principal stress/strain. Attempts to correct this overestimation of strengths have been made by assuming compression softening. This has been done both with elasticity based fixed crack approach (de Borst and Nauta, 1985; de Borst, 1986) and elasticity based rotating crack approach (Crisfield, 1988) augmented with a failure criterion.

The elasticity based approaches have the advantage that crack deformations are reversible on load reversal. Such an advantage, however, has a limited significance because of inability (physical) of the cracked material to fully gain its lost strength.

All the disadvantages of plasticity based fixed crack approach are similar to that of elasticity based approach with a major difference that the plastic deformations are irreversible. The plasticity based rotating crack approach utilising Rankine criterion would again require to be augmented with a failure criterion and some softening in tension-compression and compression-compression region to accurately predict limit loads. Therefore, a need for a single constitutive model that could be used to predict nonlinear behaviour of quasi-brittle materials, including cracking in both tension and compression, has emerged. Several such models have already been proposed (Pramono, 1988; Pramono and Willam, 1989; Pankaj, 1990; Bicanic et al., 1994), some in conjunction with the elasticity based approaches (de Borst and Nauta, 1985; de Borst, 1986).

3.4 Localization and Material Instability

It has been discussed earlier that localisation zones (zones of immense straining) and failures are common feature of many engineering materials like brittle rock masses, concrete and soil. In order to understand and explain such behaviour, modelling of the process of growth and interaction of microcracks that join together to form a macroscopic surface or region of rupture, is needed. However, in the present section an alternative hypothesis is considered in which localization can be understood as an instability in the macroscopic constitutive description of inelastic deformation of materials (Rice, 1973; Rudnicki and Rice, 1975). Instability is understood in the sense that the constitutive relations may allow the homogeneous deformations of an initially uniform material to lead to a bifurcation point, at which non-uniform deformations can be incipient in a planer band under conditions of continuing equilibrium and continuing homogeneous deformations outside the zone of localization.

Rudnicki and Rice (1975) initiated the method for finding the quantitative determination of critical conditions governing the onset of localisation followed by many researchers (Needleman and Tvergaard, 1983; Ortiz et al., 1987; Willam and Sobh, 1987; Leroy and Ortiz, 1989). It is now understood that these conditions are valid as long as structural homogeneity is preserved.

3.4.1 Condition of Localization

Making use of earlier related work (Rudnicki and Rice, 1975; Ortiz et al., 1987) and using indical notation for convenience, the condition of localisation can be derived as follows.

If g_k is a position vector defined, then for a vector function $v_i = v_i(g_k)$ one can write

$$dv_i = \frac{\partial v_i}{\partial g_k} dg_k \tag{3.23}$$

If the length of the vector dg_k is ds ($ds = |dg_k|$) and $s_k = dg_k / ds$ *i.e.* a unit vector in the direction of dg_k, then use of Eqn. 3.23, will give

$$\frac{dv_i}{ds} = \frac{\partial v_i}{\partial g_k} s_k \tag{3.24}$$

If v_i is considered to be constant on surface S, Eqn. 3.24 reduces to

$$\frac{dv_i}{ds} = \frac{\partial v_i}{\partial g_k} t_k = 0 \tag{3.25}$$

where t_k is the unit vector tangential to the surface S. This equation indicates that the vector $\partial v_1 / \partial g_k$ is orthogonal to arbitrary tangential vector t_k giving $\partial v_1 / \partial g_k = q_1 n_k$ where n_k is the unit vector normal to surface S and q_1 is a scalar. Similarly $\partial v_2 / \partial g_k = q_2 n_k$ and $\partial v_3 / \partial g_k = q_3 n_k$. In general, it can be expressed as

$$\partial v_i / \partial g_k = q_i n_k \tag{3.26}$$

If s_k of Eqn. 3.24 is replaced by n_k then $ds = dn$ and

$$\frac{dv_i}{dn} = \frac{\partial v_i}{\partial g_k} n_k = q_i n_k n_k = q_i \tag{3.27}$$

Now consider a homogeneously deformed material subjected to quasi-static increments of deformation $\dot{\varepsilon}$. Let $\boldsymbol{u}$ and $\nabla \boldsymbol{u}$ be the displacement field in the solid and displacement gradients respectively used to find if bifurcation can occur causing discontinuous deformation across a plane of orientation $\boldsymbol{n}$. At the onset of localisation $\boldsymbol{u}$ remains continuous but the displacement gradient exhibits a jump across the plane of discontinuity, *i.e.*

$$[[u_{i,j}]] = u_{i,j}^{+} - u_{i,j}^{-} \neq 0 \tag{3.28}$$

where the superscript $(^{+})$ indicates one side of discontinuity and superscript $(-)$ indicates the other. To show the difference between the values on either side of discontinuity, double brackets $[[\cdot]]$ are employed.

As $u_{i,j} = \partial u_i / dg_j$ one can write using Eqn. 3.26 and Eqn. 3.27

$$q_i = \frac{d[[u_i]]}{dn} \tag{3.29}$$

and

$$\frac{\partial [[u_i]]}{\partial g_j} = [[u_{i,j}]] = q_i n_j \tag{3.30}$$

At this stage consider a unit vector **m** along $\boldsymbol{q}$ *i.e.*

$$m_i = \frac{q_i}{q} \quad \text{where} \quad q = |\boldsymbol{q}| \tag{3.31}$$

The pair of the unit vector **n, m** completely define the nature of the discontinuity. For example when **m** is orthogonal to **n**, the material deforms in pure shear and when **m** is parallel to **n**, the band undergoes extension normal to the plane of discontinuity and may be interpreted as tensile or splitting failure. Between the above two extremes lies a mixed failure mode for which **m** and **n** are neither orthogonal nor parallel.

The strain jump can be obtained using Eqn. 3.30 as

$$\begin{aligned}[[\varepsilon_{i,j}]] &= \frac{1}{2}\left([[u_{i,j}]] + [[u_{j,i}]]\right) \\ &= \frac{1}{2}\left(q_i n_j + q_j n_i\right)\end{aligned} \tag{3.32}$$

To investigate the condition of localisation for elastoplastic material behaviour, the incremental stress strain relationships are rewritten in the following form

$$d\sigma_{ij} = \mathrm{D}^{ep}_{ijkl} d\varepsilon_{kl} \tag{3.33}$$

where $\mathbf{D}^{ep}$ is the tangent stiffness tensor for a material, for rate independent solids (elstoplastic solids) the localisation bifurcation analysis is carried out using the same branch of $\mathbf{D}^{ep}$ (in classical plasticity $\mathbf{D}^{ep}$ has loading and unloading branches) and so jump in Eqn. 3.33 leads to

$$[[d\sigma_{ij}]] = \mathrm{D}^{ep}_{ijkl} [[d\varepsilon_{kl}]] \tag{3.34}$$

Equilibrium across the discontinuity planes requires that the traction $\boldsymbol{t}$ be continuous *i.e.*

$$[[dt_j]] = [[n_i d\sigma_{ij}]] = n_i [[d\sigma_{ij}]] = 0 \tag{3.35}$$

which along with Eqn. 3.34 leads to

$$n_i \mathrm{D}^{ep}_{ijkl} [[d\varepsilon_{kl}]] = 0 \tag{3.36}$$

and which in turn using Eqn. 3.32 leads to the localisation condition

$$A_{jk}(\mathbf{n}) m_k = \left(n_i \mathrm{D}^{ep}_{ijkl} n_l\right) m_k = 0 \tag{3.37}$$

This condition has to be satisfied by **m** and **n** for the localisation mode to be possible. The onset of localisation occurs at the first point in the deformation history for which a non-trivial solution of Eqn. 3.37 exists. For a nontrivial solution of Eqn. 3.37 to exist, it is necessary

$$\det(A(\mathbf{n})) = 0 \tag{3.38}$$

So if a unit vector **n** satisfying Eqn. 3.38 can be found, it implies onset of localisation and gives its direction. From Eqn. 3.37 the vector **m** can then be found to fully define the localisation mode.

The unit vector **n** satisfying Eqn. 3.38 is known as 'acoustic tensor' (Willam and Sobh, 1987; Pramono, 1988). Once the condition of Eqn. 3.38 is established and the unit vector **n** satisfying this equation is evaluated, the onset of localisation and its direction can be predicted.

3.5 Need for Nonlocal Laws

Solutions that are not unique and depend on finite element mesh discretization are obtained if softening modulus is assumed to be a material property. This can be illustrated (Pankaj, 1990; Zienkiewicz and Taylor, 1991) with the aid of a simple bar of length l divided into elements of length h as shown in Fig. 3.4a.

The bar is subjected to a uniformly increasing extension u. In the virgin state, the material is assumed as elastic with a modulus E and uniaxial yield stress Y_o. After exceeding Y_o, the material is assumed to soften with a modulus E_T.

The stress-strain relationship can thus be written as (Fig. 3.4b)

$$\sigma = E\varepsilon \quad \text{for} \quad \varepsilon < Y_o / E = \varepsilon_y \tag{3.39}$$

In the post-yield region

$$\sigma = Y_o - E_T(\varepsilon - \varepsilon_y) \quad \text{for} \quad \varepsilon > \varepsilon_y \tag{3.40}$$

Unloading behaviour of the material from any plastic point can be represented as shown in Fig. 3.4b. The yielding of the system can take place in different possible ways. One possible solution is, of course, that in which all elements yield identically. The applied stress versus the elongation strain $\varepsilon = u/l$ curve is shown in Fig. 3.4c. For $h/l = 1$ assumption, the material behaviour curve obtained, is identical to the idealised stress strain curve of the material (Fig. 3.4c). However, the possibility exists that after reaching the maximum stress Y_o, only one element (probably with infinitesimally lower maximum yield stress) continues to behave plastically while all others unload elastically. The total elongation is now given by

$$U = (l-h)\frac{\sigma}{E} + h\left(\frac{Y_o - \sigma}{E_T} + \frac{Y_o}{E}\right) \tag{3.41}$$

which results in an overall strain as

$$\varepsilon = \frac{U}{l} = \sigma\left(\frac{l-h}{lE} - \frac{h}{lE_T}\right) + Y_o\left(\frac{h}{lE_T} + \frac{h}{lE}\right) \tag{3.42}$$

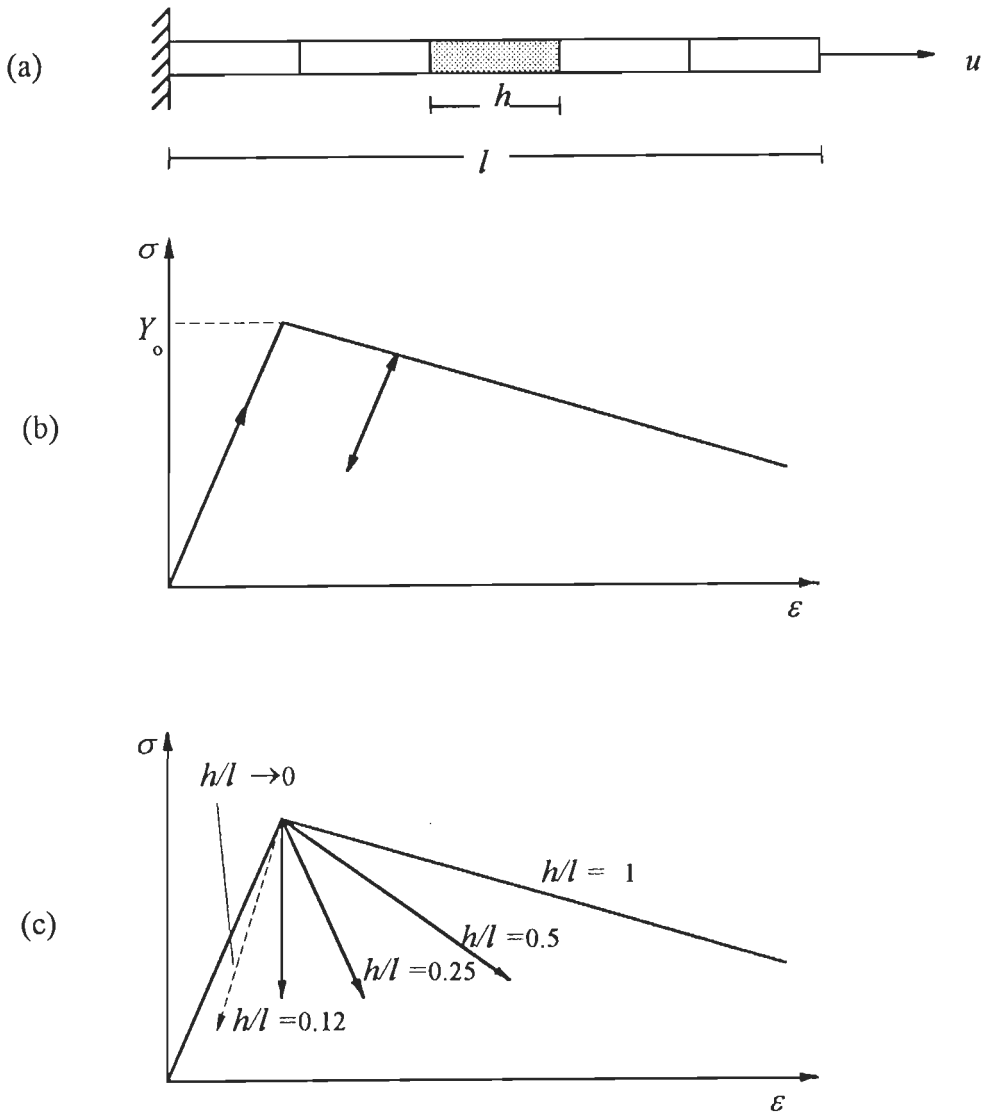

Fig. 3.4 Mesh size dependence in extension of homogeneous bar with a strain softening material (a) bar discretisation (Y_o perturbed in a single element). (b) idealised stress-strain behaviour of the material and (c) stress σ *vs.* average strain $\varepsilon = u/l$ assuming yielding in a single element of length h

As $h \to 0$, then $\varepsilon \to \sigma / E$. Clearly, a large number of solutions are possible for any element subdivision and in the present trivial example, a unique finite element solution is impossible (with localization to a singular element always occurring). Hence, in order to obtain similar results for different finite element discretisations, the softening modulus is made element size dependent (Pietruszczak and Mroz, 1981). Physical arguments for such an approach are available in the literature (Bicanic et al., 1985; Bazant and Lin, 1988; Bazant and P-Cabot, 1988; Mazars and Bazant (eds.), 1989).

3.5.1 Using the Concept of Fracture Energy

Hillerborg et al. (1976) proposed a two prameter fictitious crack model. Tensile strength and fracture energy are the two parameters which have been considered in the development of the model. If a specimen subjected to tension, enters into a post-yield region, then this model assumes elastic unloading in the entire length of the bar and an additional elongation in an infinitely thin cracked zone. In this infinitely thin cracked zone, constitutive relationship is defined in terms of normal stress and crack elongation. Stress transfer capability which the newly formed crack has, depends on the width of the crack in the stressed direction (Fig. 3.5) Once the crack width w attains a particular value w_1, the stress transfer capability reduces to zero. In order to overcome the stress in the crack opening process, energy is absorbed. This energy required for widening the crack from zero to w_1, (or beyond w_1) may be expressed as the energy required to fully open (to or beyond w_1) unit area of a newly formed crack

$$G_c = \int_0^{w_1} \sigma \, dw \tag{3.43}$$

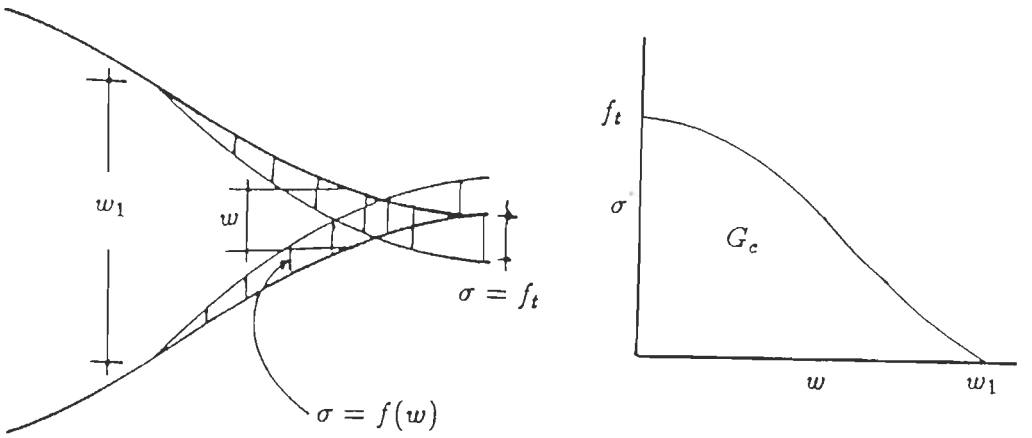

Fig. 3.5 Hillerborg's fictitious crack model

Within a smeared crack model, the above concept of fracture energy is utilised less rigorously and the accumulated fracture is distributed over a finite crack band width (Bicanic et al., 1986). This width in finite element analysis is related to mesh discretisation.

Material models which exhibit strain softening have an inherent dependence on the discretisation of the finite element mesh (Crisfield, 1982; Bazant and Oh, 1983; Rots, 1988). A length scale must therefore be included within the formulation to counteract this dependence. The fracture energy must be released over the effective crack width in order to curb such mesh sensitivity and thus produce mesh objective results. This implies that while the fracture energy is taken as a material property, the softening moduli depend on finite element mesh discretisation.

3.6 Strain Softening in Dynamic Problems

Strain softening was considered an unacceptable feature for a constitutive equation. Sandler (1984) considered a strain softening infinite bar under dynamic end loading and with a material which had a negative stress to strain ratio. He showed that in such a case, the response is immediately unbounded. Bazant and Belytschko (1985) argued that the tangent modulus becomes positive in rate independent plasticity on strain reversal.

It is now well accepted that softening can be incorporated in dynamic analysis without it leading to unbounded solution. While in this study, attention will be confined to strain rate independent material behaviour, strain softening has also been used with the strain rate dependent models with success (Sluys, 1992; Zoran. 1993).

References

Bazant, Z.P. and Belytschko, T. (1985) – Wave propagation in a strain softening Bar: exact solution, *J. Eng. Mech., ASCE*, **111**(3), 381-389.

Bazant, Z.P. and Lin, F.-B. (1988) – Non-local yield limit degradation, *IJNME*, **26**, 1805-1823.

Bazant, Z.P. and Oh, B.H. (1983) – Crack band theory for fracture of concrete, *Materials and Structures, Research and Testing, (RILEM*, Paris), **16**, 155-177.

Bazant, Z.P. and P-Cabot, G. (1988) – Nonlinear continuos damage, localization, instability and convergence, *J. App. Mech., ASCE*, **55**, 287-293.

Bicanic, N. and Pankaj (1990) – On mesh design for concrete strain softening analysis, *Computer Aided Analysis and Design of Concrete Structures*, (Eds. Bicanic, N. and Mang, H.), Vol. 2, Pineridge Press, 959-974.

Bicanic, N., Pearce, C.J. and Owen, D.R.J. (1994) – Failure predictions of concrete like materials using softening Hoffman plasticity model, *Computational Modelling of Concrete Structures*, (Eds. Mang, H., Bicanic, N. and de Borst, R.), Pineridge Press, 185-198.

Bicanic, N., Pramono, E., Sture, S. and Willam, K.J. (1985) – On numerical prediction of concrete fracture localizations, *Proc. NUMETA Conf.*, Balkema, 385-392.

Bicanic, N., Willam, K. and Sture, S. (1986) – Composite fracture model for strain softening and localized failure of concrete, *Computational Modelling of Reinforced Concrete Structures*, (Eds. Hinton, E. and Owen, D.R.J.), Pineridge Press, Swansea, 122-153.

de Borst, R. (1986) – Nonlinear analysis of frictional materials, *Ph.D. Dissertation*, Delft University of Technology, Delft, The Netherlands.

de Borst, R. and Nauta, P. (1985) – Nonorthogonal cracks in smeared finite element model, *Engng. Compt.*, **2**, 35-46.

Cervera, M. (1986) – Nonlinear analysis of reinforced concrete structures using three dimension and shell finite element models, *Ph.D. dissertation*, University College of Swansea, University of Wales.

Cope, R.J., Rao, P.V., Clark, L.A. and Norris, P. (1980) – Modelling of reinforced concrete behaviour for FE analysis of bridge slabs, *Numerical Methods for Nonlinear Problems*, Vol. 1, (Eds. Taylor, C. et al.) Pineridge Press, 457-470.

Crisfield, M.A. (1982) – Local instabilities in nonlinear analysis of reinforced concrete beams and slabs, *Proc. Inst. of Civil Engineers*, **2**(73),135-145.

Crisfield, M.A. (1988) – No-tension finite element analysis of reinforced concrete beams subjected to shear, *Workshop on Strain Localization and Size Effect Due to Cracking and Damage*, Cochan, France, Elsevier.

Crisfield, M.A. and Wills, J. (1987) – Numerical comparisons involving different concrete models, *IABSE Reports*, **54**, *Colloquium on Comp. Mech. Rein. Conc.*, Delft University Press, 177-187.

Glamberg, R. (1984) – Dynamic analysis of concrete structures, *Publication 84:1*, Chalmers University of Technology, Geoteborg, Sweden.

Gupta, A.K. and Akbar, H. (1984) – Cracking in reinforced analysis, *J. Str. Eng. ASCE*, **110**, 1735-1746.

Guzina, B.B., Rizzi, E., Willam, K. and Pak, R.Y.S. (1995) – Failure prediction of smeared crack formulations, *J. Eng. Mech., ASCE*, **121**(1), 150-161.

Hillerborg, A., Modeer, M. and Peterson, P.-E. (1976) – Analysis of crack formulation and crack growth in concrete by means of fracture mechanics and finite element, *Cem. Conc. Res.*, **6**, 773-782.

Jiang, J.J. (1983) – Finite element techniques for statical analysis of structures in reinforced concrete, *Ph.D. Thesis*, Chalmers University of Technology, Pub. 83:2.

Leibengood, L.D., Darwin, D. and Dodds, R.H. (1986) – Parameters affecting FE analysis of concrete structures, *J. Str. Eng., ASCE*, **112**, 326-341.

Leroy, Y and Ortiz, M. (1989) – Finite element analysis of strain localization in frictional material, *Int. J. Num. Anal. Meth. Geomech.*, **13**, 53-74.

Lin, C.-S. and Scordelis, A. (1975) – Nonlinear forms of R.C. shells of general form, *J. Str. Div., ASCE,* ST3.

Mazars, J. and Bazant, Z.P. (1989) – Cracking and damage, Elsevier Press, Dordrecht.

Milford, R.V. and Schonbrich, W.C. (1985) – Application of rotating crack model to R/C shells, *Comp. Struct.*, **20**, 225-239.

Needleman, A. and Tvergaard, V. (1983) – Finite element analysis of localization in plasticity, *Finite Elements: Special Problems in Solid Mechanics,* (Eds. Oden, J.T. and Carey, G.F.), Prentice Hall, Englewood Cliffs, NJ, 94-107.

Nilsson, L. and Oldenburg, M. (1983) – Nonlinear wave propagation in plastic fracture materials – A constitutive modelling and finite element analysis, *IUTAM Symposium on Nonlinear Deformation Waves*, (Eds. Nigul, U. and Engelbrecht, J.), Springer-Verlag.

Ortiz, M., Leroy, Y. and Needleman, A. (1987) – A finite element method for localized failure analysis, *Computational Methods in Applied Mechanics and Engineering*, **61**, 189-214.

Ortiz, M. and Quigley, J.J. (1991) – Adaptive mesh refinement in strain localization problems, *Comp. Meth. Appl. Mech. Eng.*, 781-804.

Pankaj (1990) – Finite element analysis in strain softening and localization problems, *Ph.D. Thesis*, University College of Swansea, University of Wales.

Petrangeli, M. and Ozbolt, J. (1996) – Smeared crack approaches – Material modelling, *Journal of Engineering Mechanics, ASCE*, **122**(6), 545-555.

Pietruszczak, S.T. and Mroz, Z. (1981) – Finite element analysis of strain softening materials, *IJNME*, **10**, 327-334.

Pramono, E. (1988) – Numerical simulation of distributed and localized failure in concrete, *Ph.D. Thesis*, University of Colarado, Boulder.

Pramono, E. and Willam, K. (1989) – Fracture energy based plasticity formulation of plain concrete, *J. Eng. Mech., ASCE*, **115**, 1183-1204.

Rashid, Y.R. (1968) – Analysis of prestressed concrete pressure vessels, *Nuclear Engineering and Design*, 7(4), 334-344.

Rice, J.R. (1973) – The initiation and growth of shear bands, *Proc. Symp. on Plasticity and Soil Mechanics, Cambridge, England*, (Ed. Palmer, A.C.), Dept. of Engng., University of Cambridge, England, 263-278.

Rots, J.G. (1988) – Computational modelling of concrete structures, *Ph.D. Thesis*, Civ. Engrng. Dept., Delft University of Technology, Delft, The Netherlands.

Rots, J.G. and Blaauwendraad, J. (1989) – Crack models for concrete: discrete or smeared? fixed, multidirectional or rotating?, *HERON*, **34**(1).

Rots, J.G., Nauta, P., Kusters, G.M.A. and Blaauwendraad, J. (1985) – Smeared crack approach and fracture localization, *HERON*, **30**, 1-48.

Rudnicki, J.W. and Rice, J.R. (1975) – Conditions for the localization of deformation of pressure-sensitive dilatent materials, *J. Mech. Phys. Solids*, **23**, 371-394.

Sandler, I.S. (1984) – Strain softening for static and dynamic problems, *Proceeding Symposium on Constitutive Equations, Micro, Macro and Computational Aspects*, (Edited by Willam, K. J.), 217-231.

Sluys, L.J. (1992) – Wave propagation, localization and dispersion in softening solids, *Ph.D. Thesis*, Delft University of Technology, Delft, The Netherlands.

Steinmann, P. and Willam, K. (1994) – Finite element analysis of elastoplastic discontinuities, *J. Eng. Mech., ASCE*, **120**(11), 2428-2442.

Suidan, M. and Schonbrich, W.C. (1973) – Finite element analysis of reinforced concrete, *J. Str. Div., ASCE*, **99**(10), 2109-2122.

Willam, K., Munz, T., Etse, G. and Menetrey, P. (1994) – Failure condition and localization in concrete, *Computational Modelling of Concrete Structures, EURO-C*, (Eds. Mang, H., Bicanic, N. and de Borst, R.), Vol. I, Pineridge Press, 263-281.

Willam, K., Pramono, E. and Sture, S. (1987) – Fundamental issues of smeared crack models, *Proc. Int. Conf. of Fract. of Conc. and rock*, Houston, Texas.

Willam, K., Pramono, E. and Sture, S. (1989) – Fundamental issues of smeared crack models, *Fracture of Concrete and Rock*, (Eds. Shah, S.P. and Swartz, S.E.), Springer-Verlag, New York, N.Y., 192-207.

Willam, K. and Sobh, N. (1987) – Bifurcation analysis of tangential material operators, *Numerical Methods in Engineering, Theory and Application*, (Eds. Middleton, J. and Pande, G.N.).

Zienkiewicz, O.C. and Taylor, R.L. (1991) – The finite element method, solids and fluid mechanics dynamics and nonlinearity, Fourth Edition, Vol. 2, Mc-Graw Hill International Editions.

Zoran, R. (1993) – Progressive fracture under dynamic loading conditions, *Ph.D. Thesis, C/Ph/174/93*, Department of Civil Engineering, University College of Swansea, University of Wales.

Chapter 4

Hoffman Yield Criterion

4.1 Introduction

Plasticity has seen the formulation of several constitutive models to represent material behaviour (Owen and Hinton, 1980; Fuschi et al., 1994; Viladkar et al., 1995). In the recent years, the finite element analysis of quasi-brittle composites has seen the reemergence of the Hoffman yield criterion (Schellekens and de Borst, 1990; Bicanic et al., 1994; Xikui et al., 1994). It is reported that the criterion is capable of describing the complex phenomenon that governs the failure of anisotropic composites. In this study attention is confined to isotropic form of the Hoffman criterion. In this form the criterion contains within it, the well known von Mises criterion. The attempt is to model failure by using strain softening in the post-yield phase. This chapter describes the criterion and its numerical implementation with strain softening.

4.2 Hoffman Yield Criterion

Hoffman (1967) modified the Hill (1947) criterion by including terms that are linear in the stress. Hoffman originally formulated his failure criterion for anisotropic materials, in the form:

$$C_1(\sigma_{22}-\sigma_{33})^2+C_2(\sigma_{33}-\sigma_{11})^2+C_3(\sigma_{11}-\sigma_{22})^2+C_4\sigma_{11}+C_5\sigma_{22}+C_6\sigma_{33}+ C_7\sigma_{23}^2+C_8\sigma_{31}^2+C_9\sigma_{12}^2=1 \quad (4.1)$$

where the constants C_i are nine independent material parameters. Six uniaxial tension and compression tests and three shear deformation tests are required for unique determination of these nine parameters.

The Eqn. 4.1 was reformulated in matrix-vector form by Schellekens and de Borst (1990) as

$$F = \frac{1}{2}\boldsymbol{\sigma}^T \mathbf{P}_\alpha \boldsymbol{\sigma} - \boldsymbol{\sigma}^T \mathbf{p}_\alpha - Y^2 = 0 \tag{4.2}$$

where for a three dimensional case

$$\boldsymbol{\sigma} = (\sigma_x \quad \sigma_y \quad \sigma_z \quad \tau_{xy} \quad \tau_{yz} \quad \tau_{zx})^T \tag{4.3}$$

$\mathbf{P}_\alpha$, the projection matrix is represented as

$$\mathbf{P}_\alpha = \begin{bmatrix} 2(\alpha_{31}+\alpha_{12}) & -2\alpha_{12} & -2\alpha_{31} & 0 & 0 & 0 \\ -2\alpha_{12} & 2(\alpha_{23}+\alpha_{12}) & -2\alpha_{23} & 0 & 0 & 0 \\ -2\alpha_{31} & -2\alpha_{23} & 2(\alpha_{31}+\alpha_{23}) & 0 & 0 & 0 \\ 0 & 0 & 0 & 6\alpha_{44} & 0 & 0 \\ 0 & 0 & 0 & 0 & 6\alpha_{55} & 0 \\ 0 & 0 & 0 & 0 & 0 & 6\alpha_{66} \end{bmatrix} \tag{4.4}$$

and $\mathbf{p}_\alpha$ the projection vector is denoted as

$$\mathbf{p}_\alpha = (\alpha_{11} \quad \alpha_{22} \quad \alpha_{33} \quad 0 \quad 0 \quad 0)^T \tag{4.5}$$

The material parameters α_{ij} are expressed as

$$\alpha_{12} = \frac{Y^2}{2}\left[\frac{1}{\bar{\sigma}_{11}^{\bullet}\bar{\sigma}_{11}} + \frac{1}{\bar{\sigma}_{22}^{\bullet}\bar{\sigma}_{22}} - \frac{1}{\bar{\sigma}_{33}^{\bullet}\bar{\sigma}_{33}}\right]; \qquad \alpha_{11} = Y^2\left[\frac{\bar{\sigma}_{11}^{\bullet} - \bar{\sigma}_{11}}{\bar{\sigma}_{11}^{\bullet}\bar{\sigma}_{11}}\right]; \qquad \alpha_{44} = \frac{Y^2}{3\bar{\sigma}_{23}^2}$$

$$\alpha_{13} = \frac{Y^2}{2}\left[\frac{1}{\bar{\sigma}_{11}^{\bullet}\bar{\sigma}_{11}} + \frac{1}{\bar{\sigma}_{33}^{\bullet}\bar{\sigma}_{33}} - \frac{1}{\bar{\sigma}_{22}^{\bullet}\bar{\sigma}_{22}}\right]; \qquad \alpha_{22} = Y^2\left[\frac{\bar{\sigma}_{22}^{\bullet} - \bar{\sigma}_{22}}{\bar{\sigma}_{22}^{\bullet}\bar{\sigma}_{22}}\right]; \qquad \alpha_{55} = \frac{Y^2}{3\bar{\sigma}_{31}^2}$$

$$\alpha_{23} = \frac{Y^2}{2}\left[\frac{1}{\bar{\sigma}_{22}^{\bullet}\bar{\sigma}_{22}} + \frac{1}{\bar{\sigma}_{33}^{\bullet}\bar{\sigma}_{33}} - \frac{1}{\bar{\sigma}_{11}^{\bullet}\bar{\sigma}_{11}}\right]; \qquad \alpha_{33} = Y^2\left[\frac{\bar{\sigma}_{33}^{\bullet} - \bar{\sigma}_{33}}{\bar{\sigma}_{33}^{\bullet}\bar{\sigma}_{33}}\right]; \qquad \alpha_{66} = \frac{Y^2}{3\bar{\sigma}_{12}^2}$$

where

Y is the normalised yield strength, $\bar{\sigma}_{ii}^{\bullet}$ are the uniaxial compressive yield strengths, $\bar{\sigma}_{ii}$ are the uniaxial tensile yield strengths and $\bar{\sigma}_{ij}$ $(i \neq j)$ are the uniaxial shear yield strengths.

For *isotropic materials* the nine yield strengths (of anisotropic material) are dependent on each other and reduce to only two independent ones (Bicanic et al., 1994). Now denoting $\overline{\sigma}_{ii}^{*}$ and $\overline{\sigma}_{ii}$ as

$$\overline{\sigma}_{ii}^{*} = f_c \qquad \overline{\sigma}_{ii} = f_t$$

The two parameters α_{ij} now reduce to

$$\alpha_{ij} = Y^2\left(\frac{f_c - f_t}{f_c f_t}\right) \qquad (i \le 3)$$

$$\alpha_{ij} = \frac{Y^2}{2}\left(\frac{1}{f_c f_t}\right) \qquad (i \ne j) \tag{4.6}$$

As a result of the isotropy constraint, the relation between uniaxial shear strength and the uniaxial compressive and tensile strength (f_c and f_t) is expressed through the relationship

$$\overline{\sigma}_{ij} = \sqrt{\frac{f_c f_t}{3}}$$

which leads to

$$\alpha_{ij} = \frac{Y^2}{f_c f_t} \quad (i \ge 4) \tag{4.7}$$

Finally the normalised yield strength, Y is fixed as

$$Y = (f_c f_t)^{1/2} \tag{4.8}$$

Making use of Eqn. 4.6 and 4.7, the material parameters are simplified to

$$\begin{aligned} \alpha_{ij} &= 1/2 && (i \ne j) \\ \alpha_{ij} &= f_c - f_t && (i \le 3) \\ \alpha_{ij} &= 1 && (i \ge 4) \end{aligned} \tag{4.9}$$

and hence, the corresponding projection matrix and projection vector can be expressed as

$$\mathbf{P}_\alpha = \begin{bmatrix} 2 & -1 & -1 & 0 & 0 & 0 \\ -1 & 2 & -1 & 0 & 0 & 0 \\ -1 & -1 & 2 & 0 & 0 & 0 \\ 0 & 0 & 0 & 6 & 0 & 0 \\ 0 & 0 & 0 & 0 & 6 & 0 \\ 0 & 0 & 0 & 0 & 0 & 6 \end{bmatrix}; \qquad \mathbf{p}_\alpha = \begin{bmatrix} f_c - f_t \\ f_c - f_t \\ f_c - f_t \\ 0 \\ 0 \\ 0 \end{bmatrix} \tag{4.10}$$

For the isotropic case Eqn. 4.2, in terms of σ_{ij}, f_c, f_t , can be alternatively written as

$$F = \{\sigma_x^2 + \sigma_y^2 + \sigma_z^2 - (\sigma_x\sigma_y + \sigma_y\sigma_z + \sigma_z\sigma_x) + 3(\tau_{xy}^2 + \tau_{yz}^2 + \tau_{zx}^2)\} + (f_c - f_t)(\sigma_x + \sigma_y + \sigma_z) - f_c f_t = 0 \quad (4.11)$$

It is more convenient to write the above equation in terms of the first stress invariant I_1 and the second deviatoric stress invariant J_2 as

$$F = 3J_2 + (f_c - f_t)I_1 - f_c f_t = 0 \quad (4.12)$$

Fig. 4.1 illustrates the Hoffman yield surface in the principal stress space. It can be seen that in the three dimensional principal stress space, the isotropic form of the Hoffman yield criterion is a cylindrical paraboloid. The criterion is pressure sensitive which is an important feature of quasi-brittle materials. The criterion does not have any singular regions as is the case with the Mohr Coulomb criterion, thus easing numerical implementation. Moreover, the criterion comprises of parabolic meridians which do not permit unrealistic increase in the size of the π-sections with increase in compressive hydrostatic stresses, as is the case for Mohr Coulomb and Drucker Prager criteria.

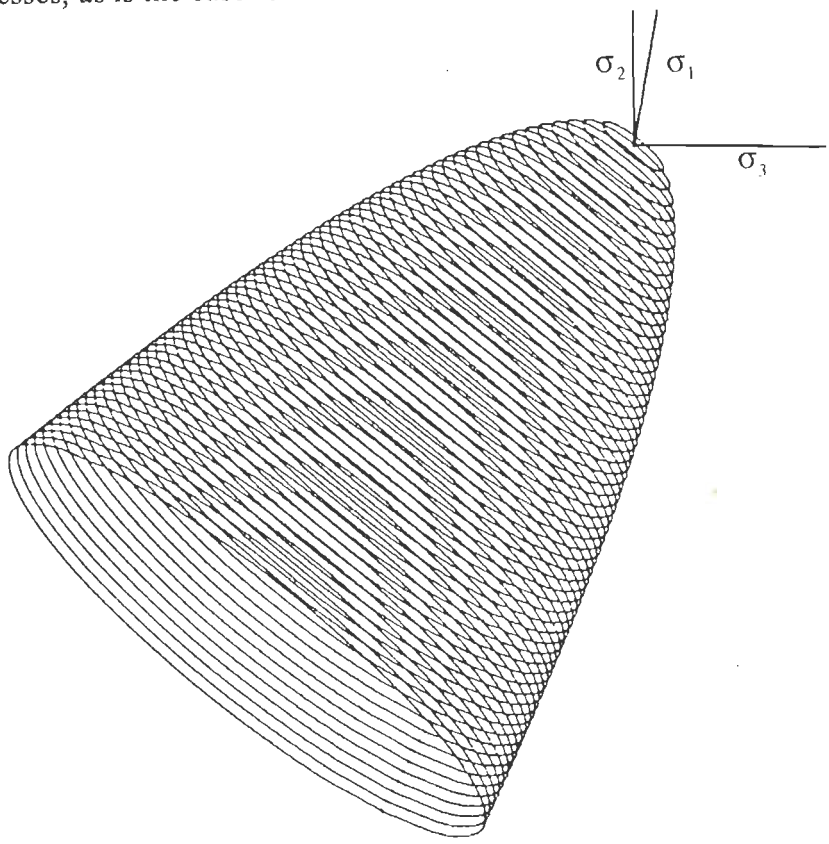

Fig. 4.1 Hoffman yield surface in principal stress space

4.3 Strain Softening Formulation

In this study, the softening response is assumed to have been initiated immediately after yielding. This is to maintain the mathematical transparency of the numerical computations so that the softening behaviour can be better understood. Clearly it is not difficult to incorporate hardening prior to softening if required. Strain softening evolution of the yield surface is assumed to occur in two ways (a) when f_t is assumed to decline (Eqn. 4.12) with increased plastic loading (Bicanic et al., 1994) and (b) when both f_c and f_t are assumed to decline simultaneously. In the former case the yield function can be written in terms of tensile yield strength $Y = f_t$ as

$$F = \{\sigma_x^2 + \sigma_y^2 + \sigma_z^2 - (\sigma_x\sigma_y + \sigma_y\sigma_z + \sigma_z\sigma_x) + 3(\tau_{xy}^2 + \tau_{yz}^2 + \tau_{zx}^2)\} + (f_c - Y)(\sigma_x + \sigma_y + \sigma_z) - f_c Y = 0$$

or

$$F = 3J_2 + (f_c - Y)I_1 - f_c Y = 0 \tag{4.13}$$

A typical evolution of the yield surface in the principal stress space with decline in Y (only f_t) is shown in Fig. 4.2. It can be seen that while the yield surface contracts in the tension-tension quadrant it expands towards the compressive end of the hydrostatic axis. This apparently implies a decrease of cohesion and an increase of frictional characteristics of the material. For the latter case where softening is considered to occur in both compression and tension, in order to simplify the problem, it is assumed that the ratio of the uniaxial compressive yield strength f_c and uniaxial tensile yield strength f_t is constant *i.e.* $f_c / f_t = n$ (constant). For this case the yield criterion can once again be written in terms of a single declining Y as

$$F = \{\sigma_x^2 + \sigma_y^2 + \sigma_z^2 - (\sigma_x\sigma_y + \sigma_y\sigma_z + \sigma_z\sigma_x) + 3(\tau_{xy}^2 + \tau_{yz}^2 + \tau_{zx}^2)\} + (n-1)Y(\sigma_x + \sigma_y + \sigma_z) - nY^2 = 0$$

or

$$F = 3J_2 + (n-1)I_1 Y - nY^2 = 0 \tag{4.14}$$

The evolution of the yield surface for this case is shown in Fig. 4.3. It is seen that the surface uniformly contracts in this case.

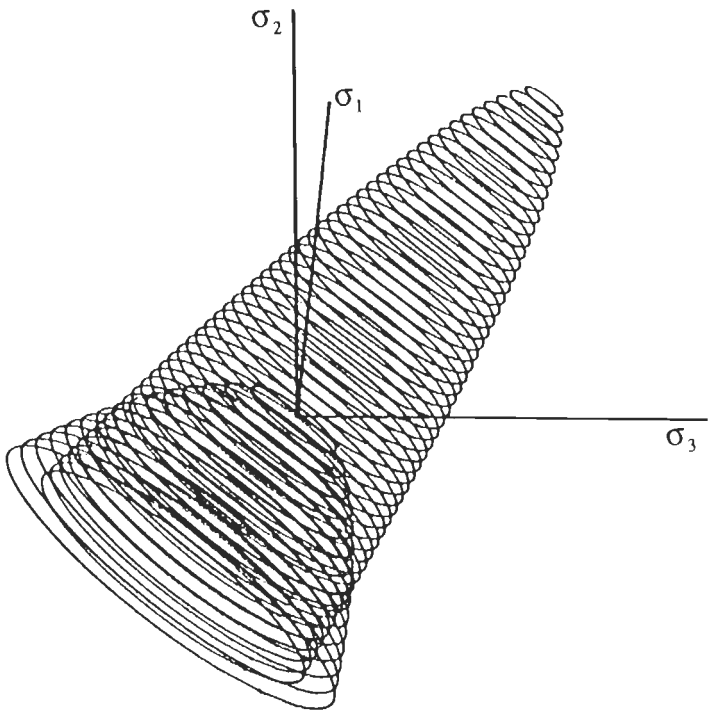

Fig. 4.2 Evolution of the Hoffman yield surface when only f_t reduces

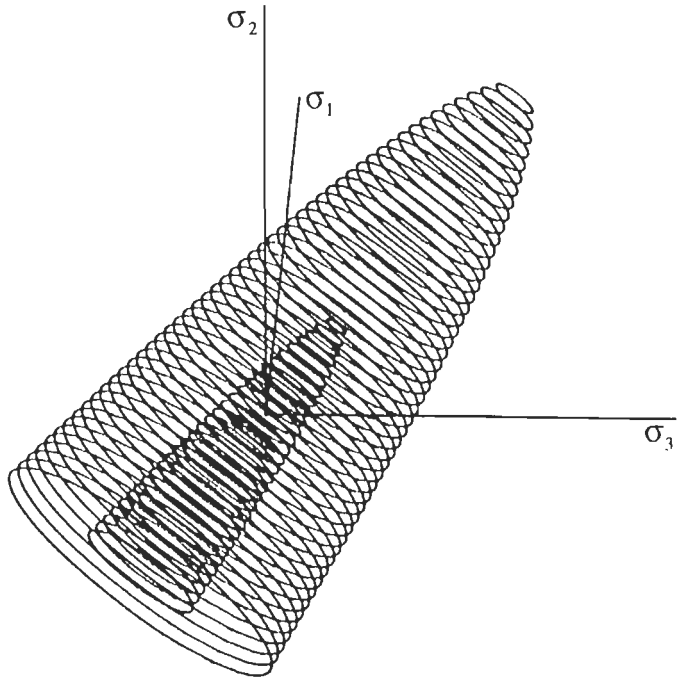

Fig. 4.3 Evolution of the Hoffman yield surface when both f_c and f_t reduce

An *exponential form* of strain softening is assumed for both cases wherein f_t or both f_c and f_t reduce as per the following equation

$$Y = Y_o \, e^{-\left(\varepsilon_y^p / \varepsilon_c\right)^2} \tag{4.15}$$

where Y and Y_o are the uniaxial yield stress in tension at the current and the virgin state of the material respectively. ε_y^p indicates the equivalent plastic strain while ε_c is a constant that is responsible for the slope of the softening branch. Clearly the value of ε_c will be mesh dependent and will depend on finite element discretisation.

It is, of course, easy to employ a *linear form* of softening given by

$$Y = Y_o + H\varepsilon_y^p \tag{4.16}$$

where H is the uniaxial hardening modulus which is positive for hardening and negative for softening.

If the magnitude of the compressive yield stress (f_c) and tensile yield stress (f_t) are identical, the pressure dependent component will reduce to zero (since $f_c - f_t = 0$) and Eqn. 4.12 reduces to

$$F = 3J_2 - Y^2$$

which is a squared form of the standard von Mises yield criterion. Thus von Mises criterion can be deduced from the isotropic Hoffman criterion.

4.4 Evaluation of Hardening Parameters

Hardening (or softening) parameters $d\varepsilon_y^p$ and A need to be evaluated for finding the current equivalent yield stress and for use in the formation of the elastoplastic modulus matrix.

For *strain hardening* hypothesis, the effective plastic strain $d\varepsilon_y^p$ can be written as

$$d\varepsilon_y^p = d\lambda \sqrt{\frac{2}{3}\left(\frac{\partial F}{\partial \sigma}\right)^T \left(\frac{\partial F}{\partial \sigma}\right)} \tag{4.17}$$

Use of Eqn. 4.13 (only f_t assumed to reduce) leads to

$$d\varepsilon_y^p = d\lambda\sqrt{2\left[6J_2 + (f_c - Y)^2\right]} \tag{4.18}$$

If, on the other hand, Eqn. 4.14 (both f_c and f_t assumed to reduce) is used, the effective plastic strain turns out to be

$$d\varepsilon_y^p = d\lambda\sqrt{2\left[6J_2 + [(n-1)Y]^2\right]} \tag{4.19}$$

The parameter A for strain hardening format can be written as (Pankaj, 1990)

$$\mathrm{A} = \mathrm{H}\frac{\partial F}{\partial Y}\sqrt{\frac{2}{3}\left(\frac{\partial F}{\partial \sigma}\right)^T\left(\frac{\partial F}{\partial \sigma}\right)} \tag{4.20}$$

This for Eqn. 4.13 leads to

$$\mathrm{A} = -\mathrm{H}(I_1 + f_c)\sqrt{2\left[6J_2 + (f_c - Y)^2\right]} \tag{4.21}$$

and for Eqn. 4.14 leads to

$$\mathrm{A} = -\mathrm{H}[2nY - (n-1)I_1)\sqrt{2\left[6J_2 + [(n-1)Y]^2\right]} \tag{4.22}$$

It is not difficult to evaluate these quantities for the work hardening format (de Groot and Kusters, 1980) wherein

$$d\varepsilon_y^p = -d\lambda\frac{\partial F}{\partial Y} \tag{4.23}$$

and

$$\mathrm{A} = \mathrm{H}\left(\frac{\partial F}{\partial Y}\right)^2 \tag{4.24}$$

Using these equations on Eqn. 4.13 leads to

$$d\varepsilon_y^p = d\lambda(I_1 + f_c) \tag{4.25}$$

and

$$\mathrm{A} = \mathrm{H}(I_1 + f_c)^2 \tag{4.26}$$

Similarly using them on Eqn. 4.14 leads to

$$d\varepsilon_y^p = d\lambda\,[2nY - (n-1)I_1] \tag{4.27}$$

and

$$A = H[2nY - (n-1)I_1]^2 \tag{4.28}$$

4.5 Evaluation of Contact Stresses

The evaluation of contact stress state plays an important role in the elastoplastic analysis as semi-implicit and explicit algorithms used in the integration of elastoplastic equations utilise the contact (or penetration) stress state as shown in Fig. 4.4 (Crisfield, 1991). The contact stress state defines the stress state at the onset of plastic loading.

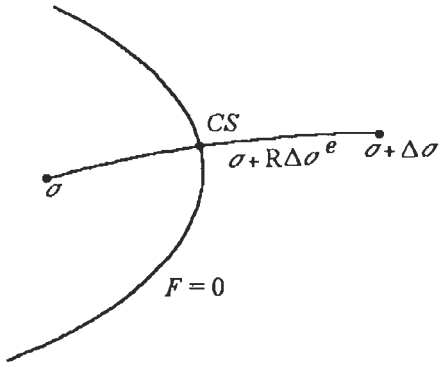

Fig. 4.4 Definition of the contact stress state

Iterative schemes are available for finding this transition from elastic to elastoplastic behaviour (Marques, 1984). It was subsequently shown that for some commonly used yield criteria, the contact stress state can be evaluated in closed form (Pankaj and Bicanic, 1989).

Here, the closed form evaluation of contact stresses for the Hoffman criterion is considered. Consider the Hoffman yield criterion which can be rewritten as

$$F(\sigma) = \{\sigma_x^2 + \sigma_y^2 + \sigma_z^2 - (\sigma_x\sigma_y + \sigma_y\sigma_z + \sigma_z\sigma_x) + 3(\tau_{xy}^2 + \tau_{yz}^2 + \tau_{zx}^2)\} + (f_c - f_t)(\sigma_x + \sigma_y + \sigma_z) - f_c f_t = 0 \tag{4.29}$$

Suppose for any point inside the Hoffman yield surface, the yield function is represented by

$$F(\sigma, f_c, f_t) < 0 \tag{4.30}$$

If the elastic increment step (elastic predictor) is in such a way that stress state jumps outside the yield surface then for this new state the yield function is expressed as

$$F(\sigma, f_c, f_t) > 0 \tag{4.31}$$

If R is a factor between 0 and 1, such that it takes the elastic stress increment only upto the yield surface *i.e.*

$$F(\sigma + R\Delta\sigma^e, f_c, f_t) = 0 \tag{4.32}$$

then the factor R corresponding to this state will give the exact stress state at the yield surface. If the state of stress in elastic domain is defined as

$$\sigma = \{\sigma_x \quad \sigma_y \quad \sigma_z \quad \tau_{xy} \quad \tau_{yz} \quad \tau_{zx}\}^T \tag{4.33}$$

and the incremental elastic predictor stress vector corresponding to an increment $\Delta\sigma^e$ is given by

$$\Delta\sigma^e = \{\Delta\sigma_x^e \quad \Delta\sigma_y^e \quad \Delta\sigma_z^e \quad \Delta\tau_{xy}^e \quad \Delta\tau_{yz}^e \quad \Delta\tau_{zx}^e\}^T \tag{4.34}$$

The contact stress state in expanded form can now be written as

$$\sigma + R\Delta\sigma^e = \begin{Bmatrix} \sigma_x + R\Delta\sigma_x^e \\ \sigma_y + R\Delta\sigma_y^e \\ \sigma_z + R\Delta\sigma_z^e \\ \tau_{xy} + R\Delta\tau_{xy}^e \\ \tau_{yz} + R\Delta\tau_{yz}^e \\ \tau_{zx} + R\Delta\tau_{zx}^e \end{Bmatrix} \tag{4.35}$$

Substituting in Eqn. 4.32 and using Eqn. 4.29, one obtains

$$a_1 R^2 + a_2 R + a_3 = 0 \tag{4.36}$$

where

$$a_1 = (\Delta\sigma_x^2)^e + (\Delta\sigma_y^2)^e + (\Delta\sigma_z^2)^e - \Delta\sigma_x^e\Delta\sigma_y^e - \Delta\sigma_y^e\Delta\sigma_z^e - \Delta\sigma_x^e\Delta\sigma_z^e + 3[(\Delta\tau_{xy}^2)^e + (\Delta\tau_{yz}^2)^e + (\Delta\tau_{zx}^2)^e]$$

$$a_2 = 2(\sigma_x \Delta\sigma_x^e + \sigma_y \Delta\sigma_y^e + \sigma_z \Delta\sigma_z^e) - (\sigma_x \Delta\sigma_y^e + \sigma_y \Delta\sigma_x^e + \sigma_y \Delta\sigma_z^e + \sigma_z \Delta\sigma_y^e + \sigma_z \Delta\sigma_x^e + \sigma_x \Delta\sigma_z^e) + 6(\tau_{xy} \Delta\tau_{xy}^e + \tau_{yz} \Delta\tau_{yz}^e + \tau_{zx} \Delta\tau_{zx}^e) + (f_c - f_t)(\Delta\sigma_x^e + \Delta\sigma_y^e + \Delta\sigma_z^e)$$

$$a_3 = \sigma_x^2 + \sigma_y^2 + \sigma_z^2 - \sigma_x\sigma_y - \sigma_y\sigma_z - \sigma_z\sigma_x + 3(\tau_{xy}^2 + \tau_{yz}^2 + \tau_{zx}^2) + (f_c - f_t)(\sigma_x + \sigma_y + \sigma_z) - f_c f_t$$

The correct value of R will clearly lie in the interval [0,1] and exact contact stress state can be obtained by solving the simple quadratic Eqn. 4.36 (Fig. 4.5).

4.6 Integration of Rate Equations

Integrating the rate equations using backward-Euler (fully implicit schemes) for Hoffman plasticity have been discussed in the work of Pearce (1993), Schellekens and de Borst (1989,1990) and Bicanic et al. (1994). In the present section some of these ideas are reconsidered.

The total strain increment can be decomposed into elastic and plastic parts for a particular step j as

$$\Delta\boldsymbol{\varepsilon}_j = \Delta\boldsymbol{\varepsilon}_j^e + \Delta\boldsymbol{\varepsilon}_j^p \tag{4.37}$$

The first term on right hand side is calculated from the linear elastic stress-strain relationship as

$$\Delta\boldsymbol{\varepsilon}_j^e = \mathbf{D}^{-1}\Delta\boldsymbol{\sigma}_j \tag{4.38}$$

where $\mathbf{D}$ is the constitutive matrix and $\Delta\boldsymbol{\sigma}_j$ is the stress increment. For associated flow rule, one can write

$$\Delta\boldsymbol{\varepsilon}_j^p = \Delta\lambda_j \frac{\partial F}{\partial \boldsymbol{\sigma}_j} \tag{4.39}$$

Using Eqns. 4.37-4.39 one can write

$$\Delta\boldsymbol{\varepsilon}_j = \mathbf{D}^{-1}\Delta\boldsymbol{\sigma}_j + \Delta\lambda_j \frac{\partial F}{\partial \boldsymbol{\sigma}_j} \tag{4.40}$$

Differentiating Eqn. 4.2 *w.r.t.* σ_j, the flow vector $\mathbf{a} = \partial F / \partial\boldsymbol{\sigma}_j$ can be evaluated as

$$\mathbf{a} = \frac{\partial F}{\partial \boldsymbol{\sigma}_j} = \mathbf{P}_a\boldsymbol{\sigma}_j + \mathbf{p}_a \tag{4.41}$$

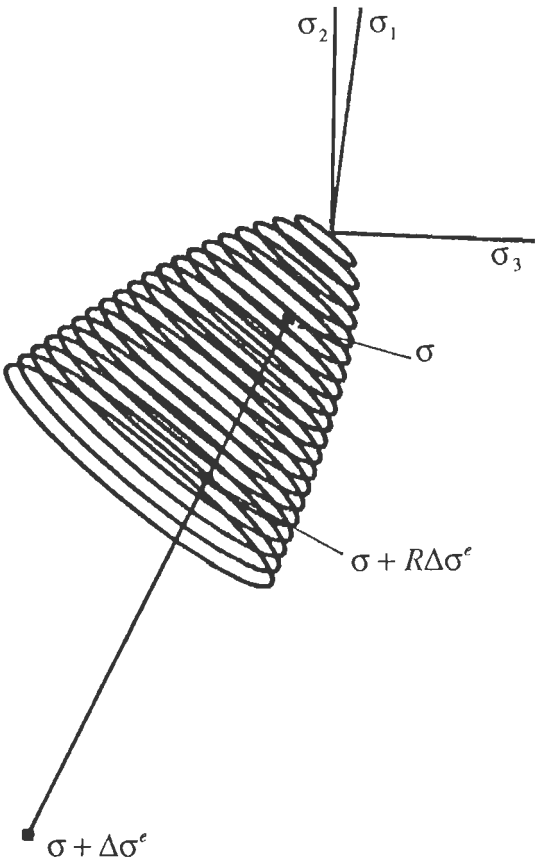

(a)

$R = 0.172497$

σ	$\Delta\sigma^e$
240.0	2400.0
80.0	800.0
80.0	800.0

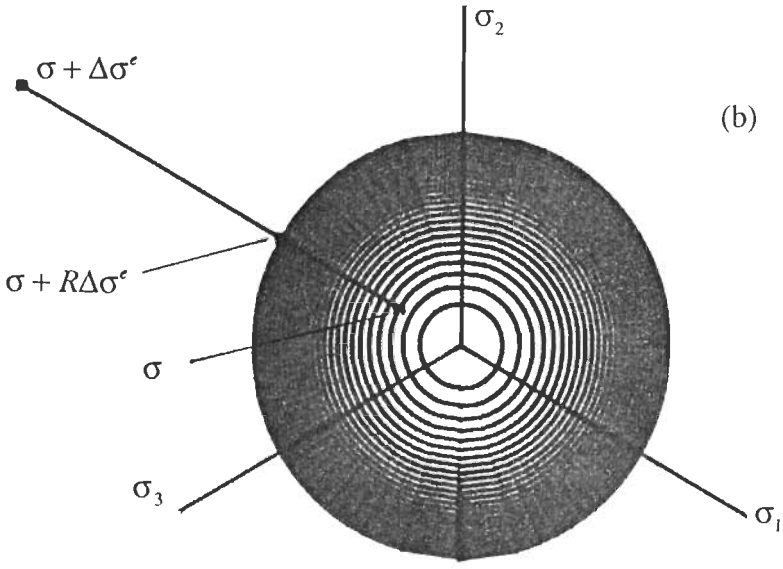

(b)

Fig. 4.5 Evaluation of the exact contact stress state (a) in principal stress space (b) π-plane representation

Putting the expression for the flow vector in Eqn. 4.40, one obtains

$$\Delta\boldsymbol{\varepsilon}_j = \mathbf{D}^{-1}\Delta\boldsymbol{\sigma}_j + \Delta\lambda_j(\mathbf{P}_\alpha\boldsymbol{\sigma}_j + \mathbf{p}_\alpha) \tag{4.42}$$

which on rearrangement results in

$$\mathbf{D}^{-1}\Delta\boldsymbol{\sigma}_j - \Delta\boldsymbol{\varepsilon}_j + \Delta\lambda_j(\mathbf{P}_\alpha\boldsymbol{\sigma}_j + \mathbf{p}_\alpha) = 0 \tag{4.43}$$

If the previously converged step is denoted by the subscript i, then

$$\mathbf{D}^{-1}\boldsymbol{\sigma}_i - \boldsymbol{\varepsilon}_i^e = 0 \tag{4.44}$$

Using Eqn. 4.44 in Eqn. 4.43 gives

$$\mathbf{D}^{-1}\Delta\boldsymbol{\sigma}_j - \Delta\boldsymbol{\varepsilon}_j + \Delta\lambda_j(\mathbf{P}_\alpha\boldsymbol{\sigma}_j + \mathbf{p}_\alpha) + \mathbf{D}^{-1}\boldsymbol{\sigma}_i - \boldsymbol{\varepsilon}_i^e = 0 \tag{4.45}$$

noting that

$$\boldsymbol{\sigma}_j = (\boldsymbol{\sigma}_i + \Delta\boldsymbol{\sigma}_j) \tag{4.46}$$

Eqn. 4.45 can be simplified and rearranged to give

$$(\mathbf{D}^{-1} + \Delta\lambda_j\mathbf{P}_\alpha)(\boldsymbol{\sigma}_i + \Delta\boldsymbol{\sigma}_j) - (\boldsymbol{\varepsilon}_i^e + \Delta\boldsymbol{\varepsilon}_j - \Delta\lambda_j\mathbf{p}_\alpha) = 0$$

or

$$(\mathbf{D}^{-1} + \Delta\lambda_j\mathbf{P}_\alpha)\boldsymbol{\sigma}_j = \boldsymbol{\varepsilon}_i^e + \Delta\boldsymbol{\varepsilon}_j - \Delta\lambda_j\mathbf{p}_\alpha \tag{4.47}$$

So the stress state can be expressed as

$$\boldsymbol{\sigma}_j = (\mathbf{D}^{-1} + \Delta\lambda_j\mathbf{P}_\alpha)^{-1}(\boldsymbol{\varepsilon}_i^e + \Delta\boldsymbol{\varepsilon}_j - \Delta\lambda_j\mathbf{p}_\alpha) \tag{4.48}$$

or

$$\boldsymbol{\sigma}_j = (\mathbf{I} + \Delta\lambda_j\mathbf{D}\mathbf{P}_\alpha)^{-1}\mathbf{D}(\boldsymbol{\varepsilon}_i^e + \Delta\boldsymbol{\varepsilon}_j - \Delta\lambda_j\mathbf{p}_\alpha) \tag{4.49}$$

From Eqn. 4.49, it is clear that the final state of stress is a function of plastic strain rate multiplier $\Delta\lambda_j$. To achieve a converged state of stress $\boldsymbol{\sigma}_j$, which satisfies the consistency condition, a backward-Euler return scheme (Bicanic et al., 1994) can be employed, where a truncated Taylor series expansion about position k is expressed as

$$F^{k+1} = F^k + \left.\frac{\partial F}{\partial \Delta\lambda_j}\right|_{\Delta\lambda_j^k} \left(\Delta\lambda_j^{k+1} - \Delta\lambda_j^k\right) \tag{4.50}$$

Linearisation of $F(\Delta\lambda_j)$ now requires that $F^{k+1} = 0$, leaving for the successive iterates

$$\Delta\lambda_j^{k+1} = \Delta\lambda_j^k - \left.\frac{F(\Delta\lambda_j)}{\frac{\partial F}{\partial \Delta\lambda_j}}\right|_{\Delta\lambda_j^k} \tag{4.51}$$

To evaluate $\frac{\partial F}{\partial \Delta\lambda}$, a methodology, which is, slightly different from that used by Bicanic et al. (1994) is adopted. Reconsider the Eqn. 4.14

$$F(J_2, I_1, Y) = 3J_2 + (n-1)I_1 Y - nY^2 = 0 \tag{4.52}$$

Making use of the chain rule $\frac{\partial F}{\partial \Delta\lambda}$ can be expressed as

$$\frac{\partial F}{\partial \Delta\lambda} = \frac{\partial F}{\partial J_2}\frac{\partial J_2}{\partial \boldsymbol{\sigma}}\frac{\partial \boldsymbol{\sigma}}{\partial \Delta\lambda} + \frac{\partial F}{\partial I_1}\frac{\partial I_1}{\partial \boldsymbol{\sigma}}\frac{\partial \boldsymbol{\sigma}}{\partial \Delta\lambda} + \frac{\partial F}{\partial Y}\frac{\partial Y}{\partial \Delta\lambda} \tag{4.53}$$

with

$$\begin{aligned} I_1 &= \sigma_x + \sigma_y + \sigma_z \\ J_2 &= (1/3)(\sigma_x^2 + \sigma_y^2 + \sigma_z^2) - (1/3)(\sigma_x\sigma_y + \sigma_y\sigma_z + \sigma_z\sigma_x) + \tau_{xy}^2 + \tau_{yz}^2 + \tau_{zx}^2 \end{aligned} \tag{4.54}$$

The different terms in Eqn. 4.53 are evaluated as

$$\begin{aligned} \frac{\partial F}{\partial J_2} &= 3.0 \\ \frac{\partial J_2}{\partial \boldsymbol{\sigma}} &= \left(\sigma_x - \frac{I_1}{3}, \sigma_y - \frac{I_1}{3}, \sigma_z - \frac{I_1}{3}, 2\tau_{xy}, 2\tau_{yz}, 2\tau_{zx}\right)^T \\ \frac{\partial F}{\partial I_1} &= (n-1)Y \\ \frac{\partial I_1}{\partial \boldsymbol{\sigma}} &= (1 \quad 1 \quad 1 \quad 0 \quad 0 \quad 0)^T \\ \frac{\partial F}{\partial Y} &= (n-1)I_1 - 2nY \end{aligned} \tag{4.55}$$

The evaluation of terms $\partial Y / \partial \Delta\lambda$ and $\partial \sigma / \partial \Delta\lambda$ is considered as follows:

Evaluation of $\frac{\partial Y}{\partial \Delta\lambda}$

Since the computation of $\frac{\partial F}{\partial \Delta\lambda}$ is influenced by the hardening hypothesis, hence this quantity has to be evaluated separately for *work hardening* format as well as for *strain hardening* format, considering either the linear strain hardening/softening or the exponential strain softening.

For *linear hardening/softening* case:

If the linear hardening is considered then the new stress level Y will be a function of hardening modulus H as

$$Y = Y_{\circ} + \mathrm{H}\varepsilon_y^p \tag{4.56}$$

where $Y_{\circ}$ is the initial yield stress level and ε_y^p is the effective plastic strain.

Differentiating Eqn. 4.56 with respect to $\Delta\lambda$ yields

$$\frac{\partial Y}{\partial \Delta\lambda} = \frac{\partial Y}{\partial \varepsilon_y^p}\frac{\partial \varepsilon_y^p}{\partial \Delta\lambda} = \mathrm{H}\frac{\partial \varepsilon_y^p}{\partial \Delta\lambda} \tag{4.57}$$

Use of Eqn. 4.27 for work hardening format gives

$$\frac{\partial Y}{\partial \Delta\lambda} = \mathrm{H}[2nY - (n-1)I_1] \tag{4.58}$$

Similarly for strain hardening format, use of Eqn. 4.19 leads to

$$\frac{\partial Y}{\partial \Delta\lambda} = \mathrm{H}\sqrt{2\left[6J_2 + [(n-1)Y]^2\right]} \tag{4.59}$$

For *exponential softening* case:

If the yield stress is assumed to decrease exponentially as discussed earlier as

$$Y = Y_{\circ}\, \mathrm{e}^{-\left(\varepsilon_y^p/\varepsilon_c\right)^2} \tag{4.60}$$

then differentiating and using Eqn. 4.27 for work hardening yields

$$\frac{\partial Y}{\partial \Delta\lambda} = \frac{\partial Y}{\partial \varepsilon_y^p}\frac{\partial \varepsilon_y^p}{\partial \Delta\lambda} = 2Y_\circ \frac{\varepsilon_y^p}{\varepsilon_c^2} \mathrm{e}^{-\left(\varepsilon_y^p/\varepsilon_c\right)^2} \left[2nY - (n-1)I_1\right] \tag{4.61}$$

For strain hardening format, use of Eqn. 4.19 leads to

$$\frac{\partial Y}{\partial \Delta\lambda} = -2\sqrt{2}\, Y_\circ \frac{\varepsilon_y^p}{\varepsilon_c^2} \sqrt{\left[6J_2 + [(n-1)Y]^2\right]}\ \mathrm{e}^{-\left(\varepsilon_y^p/\varepsilon_c\right)^2} \tag{4.62}$$

Evaluation of $\frac{\partial \sigma}{\partial \Delta\lambda}$

The term $\partial\sigma/\partial\Delta\lambda$, can be found using Eqn. 4.48. Once again attention is confined to the case when both f_c and f_t are assumed to decline while their ratio n remains constant. Noting that $\mathbf{p}_\alpha = \mathbf{p}_\alpha(Y)$ one can write

$$\begin{aligned}
\frac{\partial \boldsymbol{\sigma}_j}{\partial \Delta\lambda_j} &= -(\mathbf{D}^{-1} + \Delta\lambda_j \mathbf{P}_\alpha)^{-1}\left(\Delta\lambda_j \frac{\partial \mathbf{p}_\alpha}{\partial \Delta\lambda_j} + \mathbf{p}_\alpha\right) + (\boldsymbol{\varepsilon}_i^e + \Delta\boldsymbol{\varepsilon}_j - \Delta\lambda_j \mathbf{p}_\alpha)(-1)(\mathbf{P}_\alpha)(\mathbf{D}^{-1} + \Delta\lambda_j \mathbf{P}_\alpha)^{-2} \\
&= -(\mathbf{D}^{-1} + \Delta\lambda_j \mathbf{P}_\alpha)^{-1}\left[(\mathbf{D}^{-1} + \Delta\lambda_j \mathbf{P}_\alpha)^{-1}\mathbf{P}_\alpha(\boldsymbol{\varepsilon}_i^e + \Delta\boldsymbol{\varepsilon}_j - \Delta\lambda_j \mathbf{p}_\alpha) + \mathbf{p}_\alpha + \Delta\lambda_j \frac{\partial \mathbf{p}_\alpha}{\partial Y}\frac{\partial Y}{\partial \Delta\lambda_j}\right] \\
&= -(\mathbf{D}^{-1} + \Delta\lambda_j \mathbf{P}_\alpha)^{-1}\left[(\mathbf{D}^{-1} + \Delta\lambda_j \mathbf{P}_\alpha)^{-1}\mathbf{P}_\alpha(\mathbf{D}^{-1} + \Delta\lambda_j \mathbf{P}_\alpha)\boldsymbol{\sigma}_j + \mathbf{p}_\alpha + \Delta\lambda_j \frac{\partial \mathbf{p}_\alpha}{\partial Y}\frac{\partial Y}{\partial \Delta\lambda_j}\right]
\end{aligned} \tag{4.63}$$

The case of an isotropic material where $\mathbf{P}_\alpha$ and $(\mathbf{D} + \Delta\lambda_j \mathbf{P}_\alpha)^{-1}$ commute, leads to

$$\frac{\partial \boldsymbol{\sigma}_j}{\partial \Delta\lambda_j} = -(\mathbf{I} + \Delta\lambda_j \mathbf{D}\mathbf{P}_\alpha)^{-1}\mathbf{D}\left[\mathbf{P}_\alpha(\boldsymbol{\sigma}_j) + \mathbf{p}_\alpha + \Delta\lambda_j \frac{\partial \mathbf{p}_\alpha}{\partial Y}\frac{\partial Y}{\partial \Delta\lambda_j}\right] \tag{4.64}$$

Since the ratio of f_c and f_t remains constant one can write

$$\frac{\partial \mathbf{p}_\alpha}{\partial Y} = (n-1 \quad n-1 \quad n-1 \quad 0 \quad 0 \quad 0)^T \tag{4.65}$$

Thus all terms of Eqn. 4.53 are now known. It may be noted that the case when only f_t is assumed to decline as per Eqn. 4.13, then some of the terms derived would be different. However, no difficulty is encountered in deriving them. This is evaluated by iterative process and the iterative process continues until the condition $F = 0$ is satisfied. A computational algorithm that makes use of the above backward-Euler procedure is discussed in the following subsection for the plane strain case.

4.7 Computational Algorithm

The integration of rate equations discussed are presented in this subsection for plane strain conditions in an algorithmic form. The algorithm becomes operative only if $F(\sigma_j, Y) > 0$ at elastic predictor stress state σ_j.

Step 1 Set

$$\Delta\lambda_j = 0$$

$$\sigma_j = \sigma_j^{el} \qquad \text{(elastic predictor stress)}$$

$$\mathbf{P}_\alpha = \begin{pmatrix} 2 & -1 & 0 & -1 \\ -1 & 2 & 0 & -1 \\ 0 & 0 & 6 & 0 \\ -1 & -1 & 0 & 2 \end{pmatrix}$$ where the third row/column correspond to shear

$$\frac{\partial \mathbf{p}_\alpha}{\partial Y} = (n-1)\begin{Bmatrix} 1 \\ 1 \\ 0 \\ 1 \end{Bmatrix}$$

$$\frac{\partial F}{\partial J_2} = 3.0$$

$$\frac{\partial I_1}{\partial \sigma} = [1 \quad 1 \quad 0 \quad 1]^T$$

$$I_1 = (\sigma_x + \sigma_y + \sigma_z)_j$$

$$J_2 = [(1/3)(\sigma_x^2 + \sigma_y^2 + \sigma_z^2) - (1/3)(\sigma_x\sigma_y + \sigma_y\sigma_z + \sigma_z\sigma_x)]_j$$

Step 2 For the previously converged stress state *i*

Set

$$(Y)_j = (Y)_i$$

Step 3 Begin iterations and evaluate

$$\frac{\partial J_2}{\partial \sigma_j} = \begin{Bmatrix} \sigma_x - I_1/3 \\ \sigma_y - I_1/3 \\ 2\tau_{xy} \\ \sigma_z - I_1/3 \end{Bmatrix}$$

$$\frac{\partial F}{\partial I_1} = (n-1)Y$$

$$\frac{\partial F}{\partial Y} = (n-1)I_1 - 2nY$$

Step 4 Evaluate $\frac{\partial Y}{\partial \Delta\lambda}$ for one of the following

(a) For linear hardening/softening

(*i*) *work hardening format*

$$\frac{\partial Y}{\partial \Delta\lambda} = \mathrm{H}[2nY - (n\text{-}1)I_1]$$

(*ii*) *strain hardening format*

$$\frac{\partial Y}{\partial \Delta\lambda} = \mathrm{H}\sqrt{2\left[6J_2 + [(n-1)Y]^2\right]}$$

(b) For exponential softening

(*i*) *work hardening format*

$$\frac{\partial Y}{\partial \Delta\lambda} = 2Y_\circ \frac{\varepsilon_y^p}{\varepsilon_c^2} \mathrm{e}^{-\left(\varepsilon_y^p/\varepsilon_c\right)^2} [2nY - (n-1)I_1]$$

(*ii*) *strain hardening format*

$$\frac{\partial Y}{\partial \Delta\lambda} = -2\sqrt{2}\, Y_\circ \frac{\varepsilon_y^p}{\varepsilon_c^2} \mathrm{e}^{-\left(\varepsilon_y^p/\varepsilon_c\right)^2} \sqrt{\left[6J_2 + [(n-1)Y]^2\right]}$$

Step 5 Evaluate

$$\frac{\partial \boldsymbol{\sigma}_j}{\partial \Delta\lambda_j} = -(\mathbf{I} + \Delta\lambda_j \mathbf{D}\mathbf{P}_\alpha)^{-1}\mathbf{D}\left[\mathbf{P}_\alpha \boldsymbol{\sigma}_j + \mathbf{p}_\alpha + \Delta\lambda_j \frac{\partial \mathbf{p}_\alpha}{\partial Y}\frac{\partial Y}{\partial \Delta\lambda_j}\right]$$

where $\mathbf{I}$ is the identity matrix.

Step 6 Evaluate

$$\frac{\partial F}{\partial \Delta\lambda_j} = \frac{\partial F}{\partial J_2}\frac{\partial J_2}{\partial \boldsymbol{\sigma}_j}\frac{\partial \boldsymbol{\sigma}_j}{\partial \Delta\lambda_j} + \frac{\partial F}{\partial I_1}\frac{\partial I_1}{\partial \boldsymbol{\sigma}_j}\frac{\partial \boldsymbol{\sigma}_j}{\partial \Delta\lambda_j} + \frac{\partial F}{\partial Y}\frac{\partial Y}{\partial \Delta\lambda_j}$$

Step 7 Evaluate

$$\Delta\lambda_j^{k+1} = \Delta\lambda_j^k - \left.\frac{F(\Delta\lambda_j)}{\dfrac{\partial F}{\partial \Delta\lambda_j}}\right|_{\Delta\lambda_j^k}$$

and check if $\Delta\lambda_j^{k+1} < 0$.

Step 8 Evaluate

$$\sigma_j = (\mathbf{I} + \Delta\lambda_j \mathbf{D}\mathbf{P}_\alpha)^{-1}\left[\sigma_i + \mathbf{D}\Delta\varepsilon_j - \Delta\lambda_j \mathbf{D}\mathbf{p}_\alpha\right]$$

where σ_i is the previously converged stress state and $\Delta\varepsilon_j$ is the strain increment.

Step 9 For the new stress state compute

$$I_1 = (\sigma_x + \sigma_y + \sigma_z)_j$$

$$J_2 = [(1/3)(\sigma_x^2 + \sigma_y^2 + \sigma_z^2) - (1/3)(\sigma_x\sigma_y + \sigma_y\sigma_z + \sigma_z\sigma_x)]_j$$

Step 10 Evaluate $\Delta\varepsilon_y^p$ for one of the following cases

(a) Work hardening format

$$\Delta\varepsilon_y^p = d\lambda\,[2nY - (n-1)I_1]$$

(b) Strain hardening format

$$\Delta\varepsilon_y^p = \Delta\lambda_j \sqrt{2\left[6J_2 + [(n-1)Y]^2\right]}$$

Step 11 Increment effective plastic strain

$$\varepsilon_y^p \leftarrow \varepsilon_y^p + \Delta\varepsilon_y^p$$

Step 12 Evaluate the new uniaxial yield stress level

(a) For linear hardening/softening

$$Y = Y_\circ + \mathrm{H}\varepsilon_y^p$$

(b) For exponential softening

$$Y = Y_\circ\, \mathrm{e}^{-\left(\varepsilon_y^p/\varepsilon_c\right)^2}$$

Step 13 Check if $\left|F(\sigma_j, Y)\right| \le tolerance$. If the answer is negative go to Step 3 for the next iteration.

References

Bicanic, N., Pearce, C.J. and Owen, D.R.J. (1994) – Failure predictions of concrete like materials using softening Hoffman plasticity model, *Computational Modelling of Concrete Structures,* (Eds. Mang, H., Bicanic, N. and Borst, R.D.), Pineridge Press, 185-198.

Crisfield, M.A. (1991) – Nonlinear finite element analysis of solids and structures; Vol. I, Essentials, John Wiley & Sons.

Fuschi, P., Dutko, M., Peric, D. and Owen, D.R.J. (1994) – On numerical integration of five-parameter model for concrete, *Comp. Struct.*, **53**(4), 825-838.

de Groot, A.K. and Kusters, G.M.A. (1980) – General derivation of hardening formulas, *HERON*, **25**.

Hill, R. (1947) – A theory of the yielding and plastic flow of anisotropic materials, *Proc. R. Soc.*, **A193**, 281-297.

Hoffman, O. (1967) – The brittle strength of orthotropic materials, *J. of Comp. Mat.*, Vol. I, 200-206.

Marques, J.M.M.C. (1984) – Stress computation in elastoplasticity, *Engrg. Comput.* **1**, 42-51.

Owen, D.R.J. and Hinton, E. (1980) – Finite elements in plasticity: Theory and Practice, Pineridge Press, U.K.

Pankaj (1990) – Finite element analysis in strain softening and localization problems, *Ph.D. Thesis*, University College of Swansea, University of Wales.

Pankaj and Bicanic, N. (1989) – The exact evaluation of contact stress factor in elastoplasticity, *Engrg. Comput.*, **6**, 67-73.

Pearce, C.J. (1993) – Computational aspects of the Hoffman plasticity model for quasi-brittle solids, C/M/286/93, Dept. of Civil Eng., University College of Swansea, University of Wales.

Schellekens, J.C.J. and de Borst, R. (1989) – The use of the Hoffman yield criterion in finite element analysis of anisotropic composites, *Comp. Struct.*, **36**(6), 1087-1096.

Schellekens, J.C.J. and de Borst, R. (1990) – The use of the Hoffman yield criterion in finite element analysis of anisotropic composites, *Brussels Conf. on Composite materials: Design and Analysis*, 341-359.

Viladkar, M.N., Noorzaei, J. and Godbole, P.N. (1995) – Convenient forms of yield criteria in elasto-plastic analysis of geological materials, *Comp. Struct.*, **54**(2), 327-337.

Xikui, L., Duxbury, P.G. and Lyons, P. (1994) – Consideration for the application and numerical implementation of strain hardening with the Hoffman yield criterion, *Comp. Struct.*, **52**, 633-644.

Chapter 5

One Dimensional Strain Softening Problems

5.1 General

It is now well established that the strain softening and localization involves additional numerical difficulties as compared to non-strain softening or non-localization problems (such as perfectly plastic or strain hardening problems). In many softening and localization problems the tangential stiffness method or the Newton-Raphson update fails to converge due to non-positive definite stiffness matrix. As a result algorithms such as the initial stiffness method have to be used in order to ensure convergence. This can considerably reduce the speed of solution. It is possible to devise algorithms that can switch from tangential stiffness to initial stiffness at the onset of localization, which in turn may be detected using an Eigen value analysis (de Borst, 1986; Bicanic and Pankaj, 1990a).

The strategy adopted in the past for incremental/iterative stress updating (Owen and Hinton, 1980) led to accumulation of spurious plastic strains (Ramm and Matzenmiller, 1988; Bicanic and Pankaj, 1990b; Pankaj, 1990; Crisfield, 1991). This was earlier termed as path dependent behaviour (Mondker and Powell, 1975,1978; Marques, 1984) and later, perhaps more appropriately, load step sensitivity (Bicanic and Pankaj, 1990b; Pankaj, 1990) or problem of spurious plastic strain (Ramm and Matzenmiller, 1988; Crisfield, 1991). While the use of a wrong strategy can lead to spurious plastic strains in all plasticity problems the effect is more pronounced for softening problems.

Use of strain softening for one dimensional wave propagation problems has been dealt with in some detail by investigators (Bazant, 1976; Bazant and Belytschko, 1985; Belytschko et al., 1987), but its applications to structural dynamic problems are limited (Sandler, 1984; Moin and Pankaj, 1994; Pankaj, Moin and Barthwal, 1994; Pankaj and Moin, 1996). The present Chapter deals with using strain softening with one dimensional dynamic problems.

5.2 Problem of Spurious Plastic Strain

Over the past decade and a half there has been considerable deliberation over the strategy for updating stresses and strains in an incremental/iterative solution procedures. Two methodologies have emerged. In the first (Strategy A), stresses are updated at the end of each iteration based on the strain increment computed for that iteration. In the second (Strategy B), stress increment is computed for all strain increments accumulated upto that iteration and the stresses are updated only after the iteration process has converged. The former strategy was termed as a *path dependent* and the latter as *path independent* by Mondker and Powell (1975,1978). The same terminology was used by Marques (1984). Initially Mondker and Powell (1975,1978) felt that the former strategy was more consistent for Newton-Raphson iteration whereas the latter with the constant stiffness approach. Later it was shown that the former strategy led to illogical results in some cases (Bicanic and Pankaj, 1990b). The strategy caused accumulation of spurious plastic strain and spurious unloading (Ramm and Matzenmiller, 1988; Crisfield 1991) and load step sensitivity (Pankaj, 1990). The strategy worked as long as a single integration point was permitted to go in the post-elastic range in an incremental load step. To this end some investigators suggested that load step should be such that not more than one integration point enter the post-peak range within a single load step (Bazant and Chang, 1987).

Strategies A and B were named as the subincremental residual strategy and the total residual strategy respectively by Bicanic and Pankaj (1990b); and as procedure using iterative strains and procedure using incremental strains respectively by Crisfield (1991). Although some modifications to Strategy A have been suggested (Nyssen, 1981). Strategy B is now generally recommended (Crisfield, 1991; Zienkiewicz and Taylor, 1991).

5.2.1 Incremental Strain Procedure

The detailed steps of Strategy B that uses incremental strains are as follows:

***Step* 1:** Assemble the applied load increment vector $\Delta\mathbf{P}$. This is done once for every load increment (step) applied.

***Step* 2:** Assemble the stiffness matrix $\mathbf{K}$ or $\mathbf{K}_T$ (tangential stiffness matrix) if required.

***Step* 3:** Solve for incremental displacements. If this is the first iteration of a load step one solves for displacements $\Delta\mathbf{x}_1$ using

$$\mathbf{K}_T \, \Delta\mathbf{x}_1 = \Delta\mathbf{P}$$

where the subscript on $\mathbf{x}$ denotes the iteration number. In subsequent iterations in place of $\Delta\mathbf{P}$, $\delta\mathbf{P}_i$ is used, which is the residual force at the end of an iteration. From this $\delta\mathbf{x}_i$, the iterative displacement in iteration i is found using

$$\mathbf{K}_T \, \delta\mathbf{x}_i = \delta\mathbf{P}_i$$

These iterative displacement increments are added for calculation of the new stress state as

$$\Delta\mathbf{x}_i = \Delta\mathbf{x}_{i-1} + \delta\mathbf{x}_i$$

***Step* 4:** From incremental displacements $\Delta\mathbf{x}_i$ compute incremental strains $\Delta\boldsymbol{\varepsilon}_i$ in different elements.

***Step* 5:** Compute for each element (or integration point in general) stress change due to strain change assuming linear elastic behaviour as

$$\Delta\boldsymbol{\sigma}_i^e = E \;\; \Delta\boldsymbol{\varepsilon}_i$$

where the superscript e denotes that linear elastic assumption has been made.

***Step* 6:** The next step depends upon the state of stress at the end of the previously converged load step. With reference to Fig. 5.1 this implies whether the stress was at point *A*, *B* or *C* at the end of the last converged increment. Point *A* indicates that the plastic strain was zero and material was elastic. Point *B* indicates that the material was elastoplastic with positive plastic strain and new yield stress. Point *C* indicates that elastic unloading took place, the plastic strain was non zero and the material has a new yield

level. Points A and C indicate that the stress increase in this increment will be fully or partly elastic. For linear strain hardening and for all these cases the current yield level for each element can be evaluated as

$$Y = Y_o + H\varepsilon^p$$

where H is the linear strain hardening parameter; ε^p the plastic strain (at the previously converged state) and Y_o the uniaxial yield strength of the material.

Check if the point at last converged state was in the elastic range (points A or C) or was elastoplastic (point B) by comparing stresses at the end of the previous converged state σ with the yield stress value Y.

If $\sigma = Y$ *go to step 7, else go to step 10.*

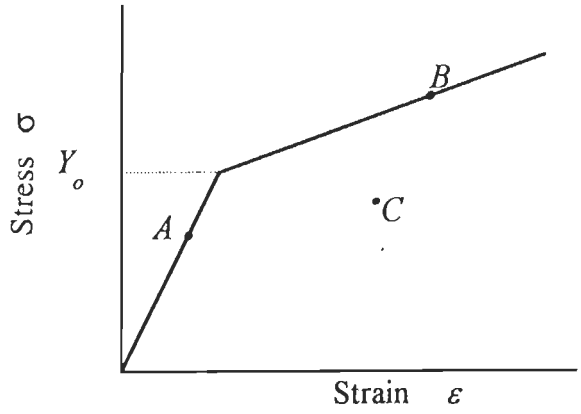

Fig. 5.1 Different possible stress states

***Step* 7:** The element had previously yielded *i.e.* was at point B. Check *if* $\sigma + \Delta\sigma_i^e > Y$ *If* the answer is NO *go to step* 8 *else to step* 9.

***Step* 8:** The element is now unloading. *Go to step* 15.

***Step* 9:** The element continues to undergo plastic deformation. Set R=1 and *go to step* 13 where the stress will be reduced to its appropriate value at point D (Fig. 5.2).

***Step* 10:** The material was at point A or C (Fig. 5.1). Check *if* $\sigma + \Delta\sigma_i^e > Y$ *If* the answer is NO *go to step* 11 *else go to step* 12.

***Step* 11:** The element is still elastic. *Go to step* 15.

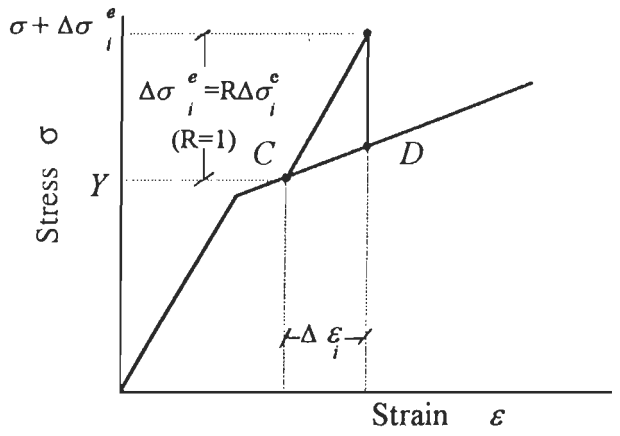

Fig. 5.2 Further yielding of an yielded element

***Step* 12:** The element was earlier elastic but has now yielded. The portion of stress greater than the yield value must be reduced to the elastoplastic line. Find factor R (Fig. 5.3) which divides the elastic (assumed) stress increment into two parts—(a) $(1-R)\Delta\sigma^e$ that will bring stresses to current yield level for which elastic stress strain law is applicable and (b) $R\Delta\sigma^e$ which is an elastic predictor that is required to be corrected to point *F*. The factor R is given by

$$R = \frac{EG}{EH} = \frac{\sigma + \Delta\sigma_i^e - Y}{\Delta\sigma_i^e}$$

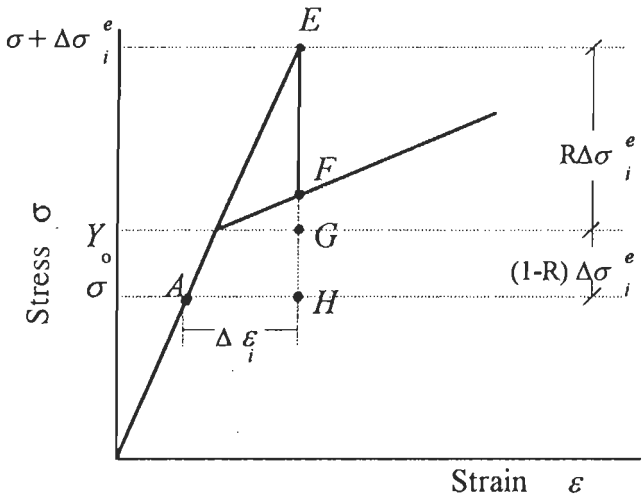

Fig. 5.3 Yielding of an elastic element

***Step* 13:** This step called the plastic corrector phase and is for elements that are undergoing elastoplastic deformation. The current increment of the stress can be found as

$$\Delta\sigma_i = (1-\mathrm{R})\Delta\sigma_i^e + E\left(1-\frac{E}{E+\mathrm{H}}\right)\mathrm{R}\Delta\varepsilon_i$$

where the first term accounts for the elastic portion of the stress increment. The new stress from this iteration i is given by

$$\sigma_i = \sigma + \Delta\sigma_i$$

***Step* 14:** The plastic strain increment $\Delta\varepsilon_i^p$ is found using

$$\Delta\varepsilon_i^p = \frac{\mathrm{R}\Delta\varepsilon_i}{1+\frac{\mathrm{H}}{E}}$$

and the total plastic strain is

$$\varepsilon_i^p = \varepsilon^p + \Delta\varepsilon_i^p$$

Go to step 16.

***Step* 15:** The element is undergoing elastic unloading. The stress is given by

$$\sigma_i = \sigma + \Delta\sigma_i^e$$

***Step* 16:** Calculate the equivalent nodal forces from the element stresses according to

$$\mathrm{f}_1 = -\mathrm{f}_2 = \begin{bmatrix} -\sigma_i A_x & \text{for} & \mathrm{x}_2 > \mathrm{x}_1 \\ \sigma_i A_x & \text{for} & \mathrm{x}_1 > \mathrm{x}_2 \end{bmatrix}$$

where A_x is the cross-sectional area and x_1 and x_2 are the coordinates of the one dimensional elements.

***Step* 17:** Assemble the equivalent nodal forces and applied load contributions for each element to give the total nodal values. If the iteration process has converged the difference between these would be zero (or small). One method of checking is based on the norm of these differences while another method is to check the norm of incremental displacements. If convergence has occurred *go to step* 1 *i.e.* the next load step. If it has not then residual forces exist *i.e.* force compatibility at nodes is not satisfied. In this case the residual force vector $\delta\mathbf{P}_i$ is assembled and a new iteration started from step 2.

5.2.2 Iterative Strain Procedure

The earlier used Strategy A which has been described by Owen and Hinton (1980), the iterative displacement increments $\delta \mathbf{x}_i$ calculated in step 3 are not accumulated to form incremental displacements for a load step. These iterative displacements and their corresponding iterative strains $\delta \boldsymbol{\varepsilon}_i$ are used in all subsequent computations. Thus the previous converged state is forgotten and the state (stresses, strains, displacements etc.) determination based on an iteration to iteration basis. So the yield stress level keeps changing in each iteration and so does the plastic strain.

5.2.3 Illustrative Problem

A simple problem is presented in this subsection to compare the procedures discussed and show how spurious unloading can take place if Strategy B is not employed.

A two bar discretization as shown in Fig. 5.4 is considered. To illustrate the key features of the two procedures for softening plasticity, a displacement of such a magnitude is prescribed at the free end of the bar so that the elastic predictor stresses in both the elements exceed the uniaxial yield stress Y_o.

Physically it appears to be logical that a prescribed displacement of the kind applied would cause element 2 to undergo softening (on account of its smaller area), while element 1 will elastically unload. The step by step numerical results obtained from the two procedures discussed earlier are tabulated in Tables 5.1 and 5.2. It can be seen from Table 5.1 (incremental strain procedure or Strategy B) that, although element 1 appears to have yielded during the iterative process it ultimately returns to the elastic branch (Fig. 5.5a). On the other hand element 1 elastically unloads only after accumulating permanent plastic strains if the iterative strain procedure (Strategy A) (Table 5.2 and Fig. 5.5b) is employed. Clearly this procedure would have yielded the same result as the previous procedure if the prescribed displacements were to be applied in small steps such that only one element were permitted to yield in a single load step. Thus this procedure leads to a problem of load step sensitivity and causes spurious plastic strains and unloading.

From this simple strain softening problem it appears that the simulation of the localized behaviour would also be aided by the incremental strain procedure.

(a)

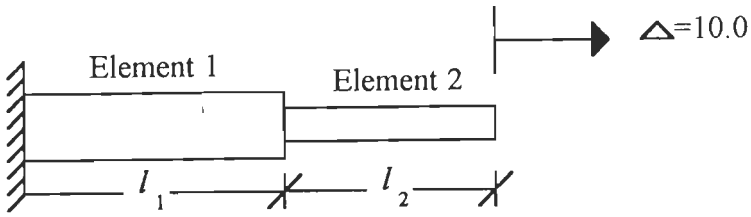

$l_1=1.0$ $l_2=1.0$

$A_1=1.2$ $A_2=1.2$

$E_1=1.0$ $E_2=1.0$

$Y_o=4.0$

(b)

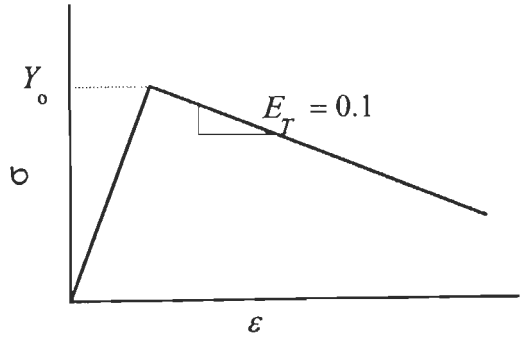

Fig. 5.4 (a) Two bar discretization with prescribed end displacement
(b) Constitutive behaviour of the two bars

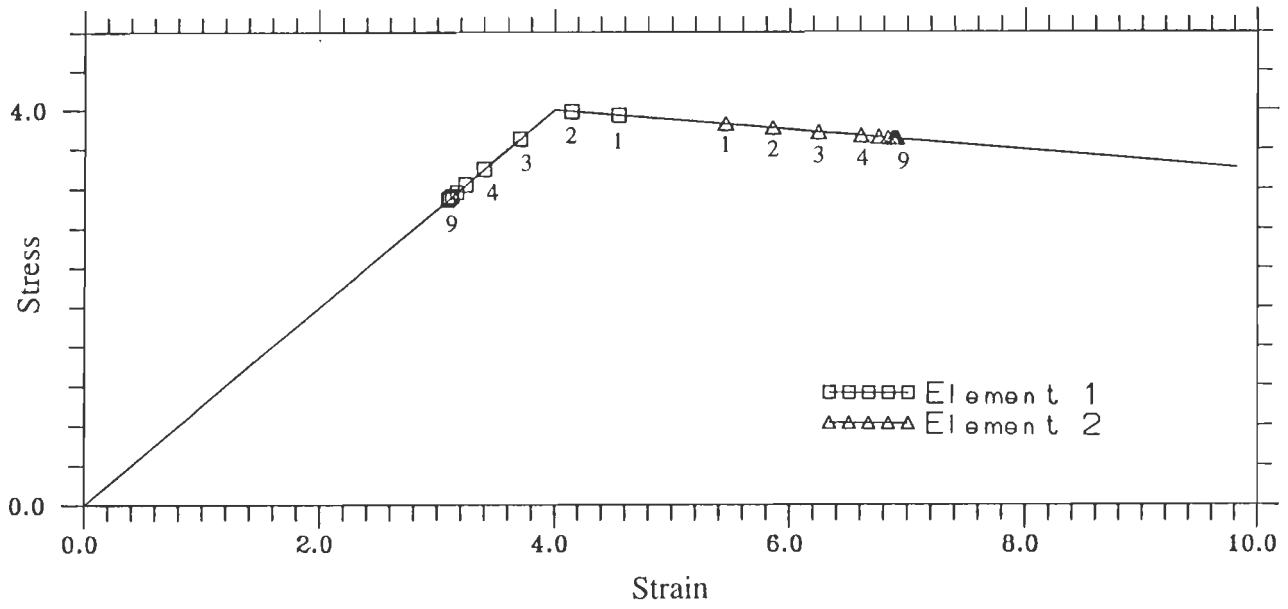

(a)

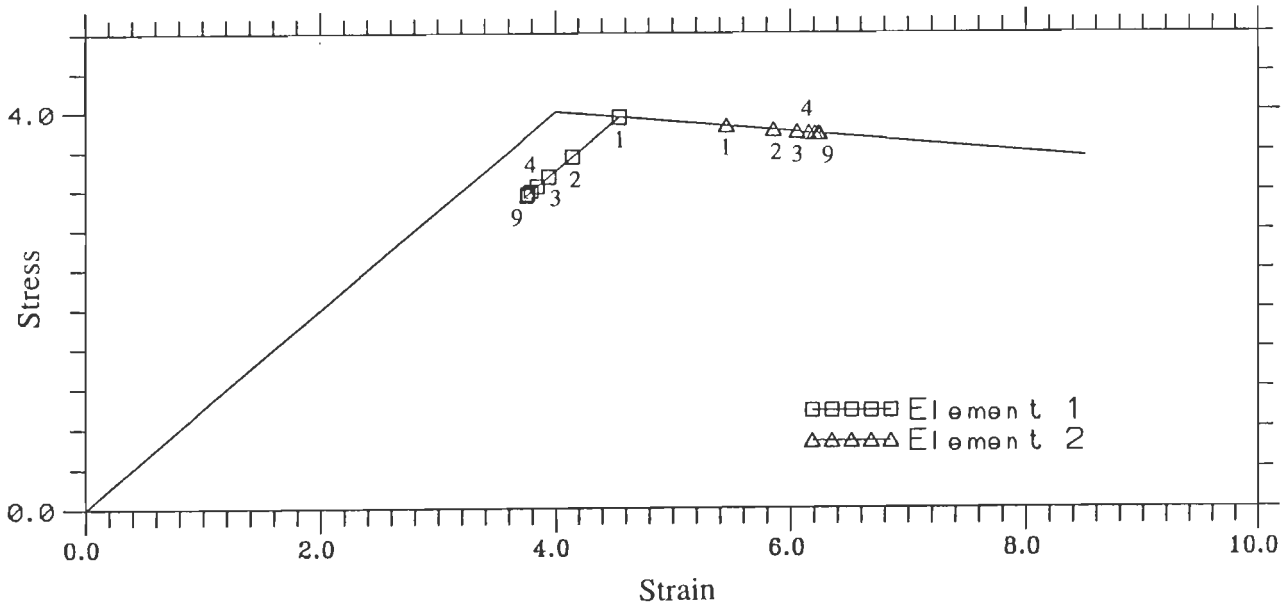

(b)

Fig. 5.5 Stress-strain state during the iterative process (a) Strategy B (b) Strategy A (Permanent plastic strain accumulated)

Table 5.1: Results of the Two Bar Problem Using Total Residual Strategy

	Displacement δx_i (or Δx_i) I	Total Displacement Δx_i II	Strain Increment $\Delta \varepsilon_i$ III	Elastic Stress Increment $\Delta \sigma_i^e$ IV	Yield Stress Y V	Stress Predictor $\sigma+\Delta\sigma_i^e$ VI	Corrected Stress σ_i VII	Plastic Strain ε_i^p VIII	Residual Loads δP_i IX
Element I	4.54545	4.54545	4.54545	4.54545	4.0	4.54545	3.94545	0.60000	–0.88000
ElementII	10.00000	10.00000	5.45455	5.45455	4.0	5.45455	3.85455	1.60000	0
Element I	–0.40000	4.14545	4.14545	4.14545	4.0	4.14545	3.98545	0.16000	–0.96799
ElementII	0	10.00000	5.85455	5.85455	4.0	5.85455	3.81455	2.04000	0
Element I	–0.44000	3.70545	3.70545	3.70545	4.0	3.70545	3.70545	0	–0.67599
ElementII	0	10.00000	6.24546	6.24546	4.0	6.24546	3.77055	2.52400	0
Element I	–0.30727	3.39818	3.39818	3.39818	4.0	3.39818	3.39818	0	–0.33799
ElementII	0	10.00000	6.60182	6.60182	4.0	6.60182	3.73982	2.86200	0
Element I	–0.15364	3.24454	3.24454	3.24454	4.0	3.24454	3.24454	0	–0.16900
ElementII	0	10.00000	6.75545	6.75545	4.0	6.75545	3.72445	3.03100	0
Element I	–0.07682	3.16772	3.16772	3.16772	4.0	3.16772	3.16772	0	–0.08449
ElementII	0	10.00000	6.83227	6.83227	4.0	6.83227	3.71677	3.11550	0
Element I	–0.03840	3.12932	3.12932	3.12932	4.0	3.12932	3.12932	0	–0.04225
ElementII	0	10.00000	6.87068	6.87068	4.0	6.87068	3.71293	3.15770	0
Element I	–0.01920	3.11011	3.11011	3.11011	4.0	3.11011	3.11011	0	–0.02112
ElementII	0	10.00000	6.88988	6.88988	4.0	6.88988	3.71101	3.17887	0
Element I	–0.00002	3.09091	3.09090	3.09091	4.0	3.09091	3.09091	0	0
ElementII	0	10.00000	6.90907	6.90907	4.0	6.90907	3.70909	3.19998	0

Table 5.2: Results of the Two Bar Problem Using Subincremental Residual Strategy

	Displacement δx_i I	Strain Increment $\delta \varepsilon_i$ II	Elastic Stress Increment $\delta \sigma_i^e$ III	Toatl Stress (Elastic Pre.) $\sigma_i + \delta \sigma_i^e$ IV	Yield Stress Y_i V	Corrected Stress σ_i VI	Plastic Strain ε_i^p VII	Residual Loads δP_i VIII
Element I	4.54545	4.54545	4.54545	4.54545	4.00000	3.94545	0.60000	–0.88000
Element II	10.00000	5.45455	5.45455	5.45455	4.00000	3.85455	1.60000	0.00000
Element I	–0.40000	–0.40000	–0.40000	3.54545	3.94545	3.54545	0.60000	–0.44000
Element II	0.00000	0.40000	0.40000	4.25455	3.85455	3.81455	2.04000	0.00000
Element I	–0.20000	–0.20000	–0.20000	3.34545	3.94545	3.34545	0.60000	–0.21999
Element II	0.00000	0.20000	0.20000	4.01455	3.81455	3.79455	2.26000	0.00000
Element I	–0.09999	–0.09999	–0.09999	3.24545	3.94545	3.24545	0.60000	–0.10999
Element II	0.00000	0.09999	0.09999	3.89454	3.79455	3.78455	2.23700	0.00000
Element I	–0.04999	–0.04999	–0.04999	3.19545	3.94545	3.19545	0.60000	–0.05499
Element II	0.00000	0.04999	0.04999	3.83454	3.78455	3.77955	2.42500	0.00000
Element I	–0.02499	–0.02499	–0.02499	3.17045	3.94545	3.17045	0.60000	–0.02750
Element II	0.00000	0.02499	0.02499	3.82954	3.77955	3.77705	2.45250	0.00000
Element I	–0.01250	–0.01250	–0.01250	3.15795	3.94545	3.15795	0.60000	–0.01375
Element II	0.00000	0.01250	0.01250	3.78955	3.77705	3.77580	2.46625	0.00000
Element I	–0.00620	–0.00625	–0.00625	3.15170	3.94545	3.15170	0.60000	–0.00687
Element II	0.00000	0.00625	0.00625	3.78830	3.77580	3.77517	2.47312	0.00000
Element I	-0.53×10^{-4}	-0.53×10^{-4}	-0.53×10^{-4}	3.14548	3.94545	3.14548	0.60000	0.00000
Element II	0.00000	0.53×10^{-4}	0.53×10^{-4}	3.77460	3.77455	3.77455	2.47997	0.00000

5.3 Elastoplastic One Dimensional Dynamic Problems

If in the static equilibrium equation 'acceleration dependent' inertia forces and 'velocity dependent' damping forces are included then the resulting equations of the equilibrium governing the linear dynamic response of a system of finite elements is given by

$$\mathbf{M}\ddot{\mathbf{x}} + \mathbf{C}\dot{\mathbf{x}} + \mathbf{K}\mathbf{x} = \mathbf{f} \tag{5.1}$$

where **M**, **C** and **K** are the mass, damping and stiffness matrices; **f** is the external load vector; and $\mathbf{x}, \dot{\mathbf{x}}, \ddot{\mathbf{x}}$ are the nodal displacements, velocity and acceleration vectors of the finite element assemblage. It should be noted (Bathe, 1982) that the Eqn. 5.1 has been derived from the considerations of equilibrium at time t; *i.e.* Eqn. 5.1 may be written as

$$\mathbf{F}_I(t) + \mathbf{F}_D(t) + \mathbf{F}_E(t) = \mathbf{f}(t) \tag{5.2}$$

where $\mathbf{F}_I(t)$ are the inertia forces, $\mathbf{F}_I(t) = \mathbf{M}\ddot{\mathbf{x}}$, $\mathbf{F}_D(t)$ are the damping forces, $\mathbf{F}_D(t) = \mathbf{C}\dot{\mathbf{x}}$ and $\mathbf{F}_E(t)$ are the elastic forces, $\mathbf{F}_E(t) = \mathbf{K}\mathbf{x}$, all of these being time dependent. Therefore in dynamic analysis, in principle, static equilibrium at time t, which includes the effect of acceleration dependent inertial forces and velocity dependent damping forces are considered. In this study consideration will be confined to nonlinearity arising out of elastoplastic material behaviour (nonlinear K). The mass and damping matrices will be assumed to be constant.

For nonlinear systems the most commonly used technique for solution of dynamic equations of motion is direct integration in the time domain. In direct integration method Eqn. 5.1 or Eqn. 5.2 is integrated without any previous transformation, using a numerical step by step procedure. These schemes are based on two ideas (Bathe and Wilson, 1976) as

- Eqn. 5.1 or Eqn. 5.2 is satisfied for only discrete stations (Newmark, 1959; Belytschko, 1978) or in other sense for each time interval (Zienkiewicz et al., 1980; Zienkiewicz et al., 1984).

- A variation of displacement, velocity and acceleration is assumed within each time interval. It is the form of this assumption (on the variation of displacements, velocities and accelerations within the time step) that determines the accuracy, stability and efficiency of each scheme.

Here consideration is limited to GN procedures (Katona and Zienkiewicz, 1985) and its efficacy with respect to simple elastoplastic problems with special attention on strain softening and localization. Ideas developed for the solution of static problems discussed earlier can be included for the solution of nonlinear equations of motion.

5.3.1 Generalized Newmark (GN) Procedure

This procedure applies Taylor series approach to derive a general form of single step algorithms that can be considered to be a generalization of Newmark method (Zienkiewicz and Wood, 1986). It results in a scheme which is not self starting. In the derivation one considers the satisfaction of the governing Eqn. 5.1 only at the end points of the interval Δt and writes (Katona and Zienkiewicz, 1985)

$$\mathbf{M}\ddot{\mathbf{x}}_{n+1} + \mathbf{C}\dot{\mathbf{x}}_{n+1} + \mathbf{K}\mathbf{x}_{n+1} = \mathbf{f}_{n+1} \tag{5.3}$$

with appropriate approximations for the values of $\mathbf{x}_{n+1}, \dot{\mathbf{x}}_{n+1}$ and $\ddot{\mathbf{x}}_{n+1}$. If one considers the Taylor series expansion the derivatives can be written as

$$\mathbf{x}_{n+1} = \mathbf{x}_n + \Delta t\dot{\mathbf{x}}_n + \cdots\cdots + \frac{\Delta t}{p!}\overset{p}{\mathbf{x}}_n + \beta_p \frac{\Delta t^p}{p!}(\overset{p}{\mathbf{x}}_{n+1} - \overset{p}{\mathbf{x}}_n)$$

$$= \tilde{\mathbf{x}}_{n+1} + \beta_p \frac{\Delta t^p}{p!}\overset{p}{\mathbf{x}}_{n+1}$$

$$\dot{\mathbf{x}}_{n+1} = \dot{\mathbf{x}}_n + \Delta t\ddot{\mathbf{x}}_n + \cdots\cdots + \frac{\Delta t^{p-1}}{(p-1)!}\overset{p}{\mathbf{x}}_n + \beta_{p-1}\frac{\Delta t^{p-1}}{(p-1)!}(\overset{p}{\mathbf{x}}_{n+1} - \overset{p}{\mathbf{x}}_n)$$

$$= \dot{\tilde{\mathbf{x}}}_{n+1} + \beta_{p-1}\frac{\Delta t^{p-1}}{(p-1)!}\overset{p}{\mathbf{x}}_{n+1}$$

$$\vdots \qquad \vdots \qquad \vdots$$

$$\overset{p-1}{\mathbf{x}}_{n+1} = \overset{p-1}{\mathbf{x}}_n + \Delta t\overset{p}{\mathbf{x}}_n + \beta_1\Delta t(\overset{p}{\mathbf{x}}_{n+1} - \overset{p}{\mathbf{x}}_n)$$

$$= \overset{p-1}{\tilde{\mathbf{x}}}_{n+1} + \beta_1\Delta t\overset{p}{\mathbf{x}}_{n+1} \tag{5.4}$$

where

$$\overset{p}{\mathbf{x}}_n = \frac{d^p \mathbf{x}_n}{dt^p}$$

In Eqn. 5.4 for a polynomial of degree p, a Taylor series remainder term has effectively been allowed in each of the expansions for the functions and its derivatives with parameter β_j, j=1,2,3,...,p which can be chosen to give good approximation properties to the algorithm.

Insertion of the first three equations of Eqn. 5.4 into Eqn. 5.3 gives a single equation from which $\overset{p}{\mathbf{x}}_{n+1}$ can be found. When this is determined $\mathbf{x}_{n+1}$ to $\overset{p-1}{\mathbf{x}}_{n+1}$ can be evaluated using

$$\overset{p}{\mathbf{x}}_{n+1} = \left(\mathbf{M}\Delta t^{p-2} \frac{\beta_{p-2}}{(p-2)!} + \mathbf{C}\Delta t^{p-1} \frac{\beta_{p-1}}{(p-1)!} + \mathbf{K}\Delta t^{p} \frac{\beta_p}{p!} \right)^{-1}$$

$$\times \left(\mathbf{f}_{n+1} - \mathbf{M}\ddot{\tilde{\mathbf{x}}}_{n+1} - \mathbf{C}\dot{\tilde{\mathbf{x}}}_{n+1} - \mathbf{K}\tilde{\mathbf{x}}_{n+1} \right) \qquad (5.5)$$

It can be easily shown that the commonly used Newmark method (Katona and Zienkiewicz, 1985) can be derived from the above generalized procedure. The above algorithm applies to both implicit and explicit schemes. In terms of generalized Newmark method an explicit scheme is simply defined by $\beta_p = 0$ for any order of p (Katona and Zienkiewicz, 1985). Conversely an implicit scheme is defined by $\beta_p \neq 0$, irrespective of the remaining integration parameters.

5.3.2 Algorithm for GN22 and GN32

A detailed implementation algorithm (Pankaj, Moin and Barthwal, 1994) for GN22 and GN32 is now discussed. The algorithm is in predictor corrector form which is particularly advantageous in nonlinear analysis. The changes required for nonlinear analysis are discussed in the following subsection.

(1) **Begin predictor corrector phase**

Set iteration counter i = 0

if p=2 *then*

$$\mathbf{x}^i_{n+1} = \mathbf{x}_n + \Delta t\, \dot{\mathbf{x}}_n (1-\beta_2)\left(\frac{\Delta t^2}{2}\right)\ddot{\mathbf{x}}_n$$

$$\dot{\mathbf{x}}_{n+1}^{i} = \dot{\mathbf{x}}_n + (1-\beta_1)\Delta t\ddot{\mathbf{x}}_n$$
$$\tilde{\mathbf{x}}_{n+1} = \mathbf{x}_{n+1}^{i}$$
$$\dot{\tilde{\mathbf{x}}}_{n+1} = \dot{\mathbf{x}}_{n+1}^{i}$$
$$\ddot{\mathbf{x}}_{n+1}^{i} = (\mathbf{x}_{n+1}^{i} - \tilde{\mathbf{x}}_{n+1})\left(\frac{2}{\beta_2 \Delta t^2}\right) = 0$$

else

$$\mathbf{x}_{n+1}^{i} = \mathbf{x}_n + \Delta t\,\dot{\mathbf{x}}_n + \left(\frac{\Delta t^2}{2}\right)\ddot{\mathbf{x}}_n + (1-\beta_3)\left(\frac{\Delta t^3}{6}\right)\overset{3}{\mathbf{x}}_n$$
$$\dot{\mathbf{x}}_{n+1}^{i} = \dot{\mathbf{x}}_n + \Delta t\,\ddot{\mathbf{x}}_n + (1-\beta_2)\left(\frac{\Delta t^2}{2}\right)\overset{3}{\mathbf{x}}_n$$
$$\tilde{\mathbf{x}}_{n+1} = \mathbf{x}_{n+1}^{i}$$
$$\dot{\mathbf{x}}_{n+1} = \dot{\mathbf{x}}_{n+1}^{i}$$
$$\ddot{\tilde{\mathbf{x}}}_{n+1} = \ddot{\mathbf{x}}_{n+1}^{i}$$
$$\overset{3}{\mathbf{x}}_{n+1}^{i} = (\mathbf{x}_{n+1}^{i} - \tilde{\mathbf{x}}_{n+1})\left(\frac{6}{\beta_3 \Delta t^3}\right)$$

endif

(2) **Form effective stiffness matrix $\mathbf{K}^*$**

if p=2 then

$$\mathbf{K}^* = \mathbf{M}\left(\frac{2}{\beta_2 \Delta t^2}\right) + \mathbf{C}\left(\frac{2\beta_1}{\Delta t \beta_2}\right) + \mathbf{K}$$

else

$$\mathbf{K}^* = \mathbf{M}\left(\frac{6\beta_1}{\Delta t^2 \beta_3}\right) + \mathbf{C}\left(\frac{3\beta_2}{\Delta t \beta_3}\right) + \mathbf{K}$$

endif

(3) **Evaluate residual forces**

$$\psi_i = \mathbf{f}_{n+1} - \mathbf{M}\ddot{\mathbf{x}}_{n+1}^{i} - \mathbf{C}\dot{\mathbf{x}}_{n+1}^{i} - \mathbf{K}\mathbf{x}_{n+1}^{i}$$

(4) **Solve for incremental displacements $\Delta\mathbf{x}^i$**

$$\mathbf{K}^*\Delta\mathbf{x}^i = \psi_i$$

(5) **Begin the corrector phase**

$$\mathbf{x}_{n+1}^{i+1} = \mathbf{x}_{n+1}^{i} + \Delta\mathbf{x}^i$$

if p=2 *then*

$$\ddot{\mathbf{x}}_{n+1}^{i+1} = (\mathbf{x}_{n+1}^{i+1} - \tilde{\mathbf{x}}_{n+1})\left(\frac{2}{\beta_2 \Delta t^2}\right)$$

$$\dot{\mathbf{x}}_{n+1}^{i+1} = \dot{\tilde{\mathbf{x}}}_{n+1} + \beta_1 \Delta t \ddot{\mathbf{x}}_{n+1}^{i+1}$$

else

$$\overset{3}{\mathbf{x}}_{n+1}^{i+1} = (\mathbf{x}_{n+1}^{i+1} - \tilde{\mathbf{x}}_{n+1})\left(\frac{6}{\beta_3 \Delta t^3}\right)$$

$$\dot{\mathbf{x}}_{n+1}^{i+1} = \dot{\tilde{\mathbf{x}}}_{n+1} + \beta_2 \left(\frac{\Delta t^2}{2}\right) \overset{3}{\mathbf{x}}_{n+1}^{i+1}$$

$$\ddot{\mathbf{x}}_{n+1}^{i+1} = \left(\ddot{\tilde{\mathbf{x}}}_{n+1} + \beta_1 \Delta t \overset{3}{\mathbf{x}}_{n+1}^{i+1}\right)$$

endif

(6) *if* (Δx^i and/or ψ > specified tolerance) *then*

i=i+1

go to (3)

else

go to (7)

endif

(7) *if* p=2 *then*

$$\mathbf{x}_{n+1} = \mathbf{x}_{n+1}^{i+1}$$

$$\dot{\mathbf{x}}_{n+1} = \dot{\mathbf{x}}_{n+1}^{i+1}$$

else

$$\mathbf{x}_{n+1} = \mathbf{x}_{n+1}^{i+1}$$

$$\dot{\mathbf{x}}_{n+1} = \dot{\mathbf{x}}_{n+1}^{i+1}$$

$$\ddot{\mathbf{x}}_{n+1} = \ddot{\mathbf{x}}_{n+1}^{i+1}$$

endif

(8) Set n=n+1 and begin next step

In the above algorithm the primary variable solved for is displacement rather than acceleration as would be the case if one were to use Eqn. 5.5. This is advantageous for elastoplastic problems where the tangent stiffness matrix is displacement (or strain) dependent. However, the disadvantage is that explicit scheme cannot be employed as this

would require β_2=0 or β_3=0 for GN22 and GN32 respectively and would generate indeterminate values in steps 2 and 5 of the algorithm.

5.3.3 Modification for Nonlinear Analysis

As the nonlinear problems discussed are confined to those arising out of elastoplastic material behaviour, the nonlinearity is confined to a nonlinear stiffness matrix which in turn depends on displacements. So mere replacement of **K** by elastoplastic stiffness matrix $\mathbf{K}^{ep}$ modifies the above algorithms for such an analysis (Owen and Hinton, 1980). When the initial stiffness approach is used one can continue to use **K** as far as the formation of the effective stiffness matrix $\mathbf{K}^*$ is concerned, while taking into account the effect of elastoplastic stiffness in the evaluation of residual force vector. If the stiffness matrix is reformulated in every iteration (N-R iteration) convergence may be achieved faster *i.e.* in fewer iterations. However additional computational effort is required in the formation of stiffness matrix and its triangularisation in every iteration. Further N-R procedure suffers from a drawback that **K** may become singular for elasto-perfectly plastic or elasto-strain softening materials.

5.3.4 Convergence Criteria

The convergence criteria were based on the norm of incremental displacements and the norm of residual forces. Thus the solution is said to have converged if

$$\left|\frac{\left((\mathbf{x}_n^{i+1})^T\mathbf{x}_n^{i+1}-(\mathbf{x}_n^{i})^T\mathbf{x}_n^{i}\right)}{((\mathbf{x}_n^{1})^T\mathbf{x}_n^{1})}\right| \le toler\ 1 \tag{5.6}$$

and

$$\left|\frac{\left((\psi_n^{i+1})^T\psi_n^{i+1}-(\psi_n^{i})^T\psi_n^{i}\right)}{((\psi_n^{1})^T\psi_n^{1})}\right| \le toler\ 2 \tag{5.7}$$

toler 1 and *toler* 2 are the specified tolerances and were kept at 0.001. Superscripts denote iteration number.

5.4 Strain Softening SDF System — An Exact Solution

An exact solution for a strain softening dynamic problem is worked out (Moin and Pankaj, 1994). This solution will be used as a benchmark in subsequent subsections.

A bar element with a concentrated mass at one end as shown in Fig. 5.6a assumed to be undergoing axial vibration is considered to constitute an undamped single degree freedom system. A step function load as shown in Fig. 5.6b is assumed to act on the mass of the system. The idealized elasto-strain softening plastic load displacement curve is shown in Fig. 5.6c.

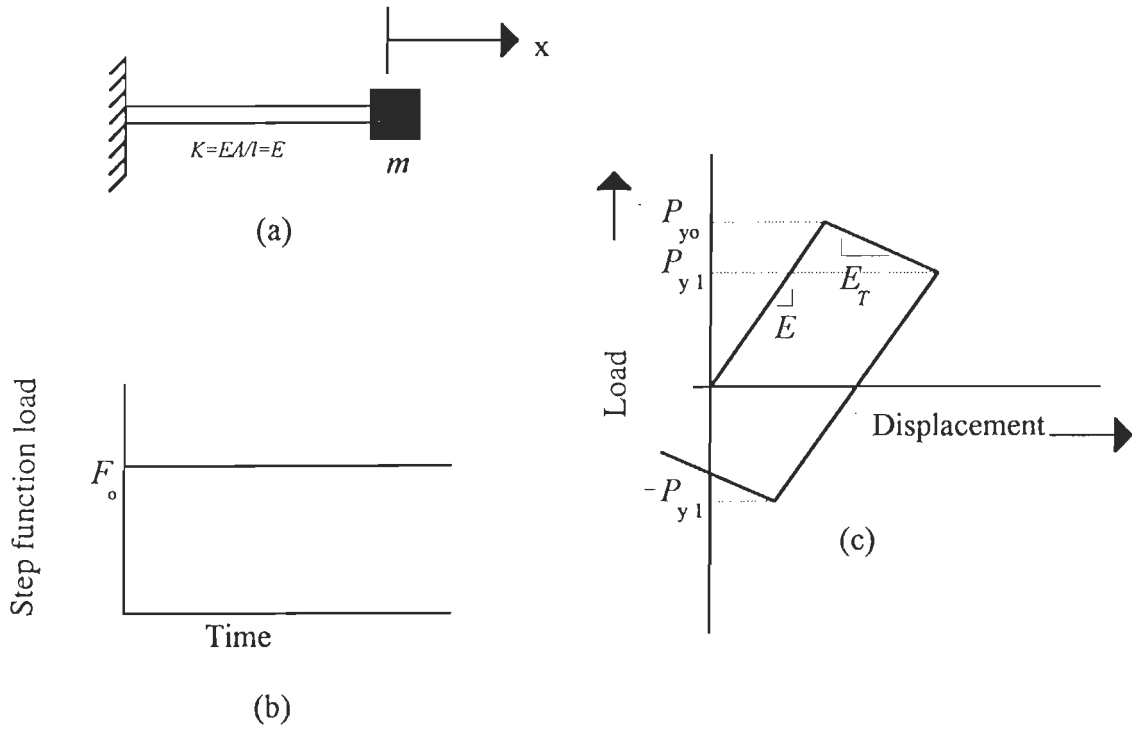

Fig. 5.6 (a) Undamped SDF system
(b) Step function load and
(c) Idealized load displacement behaviour of the bar

For the sake of simplicity stiffness K is considered to be synonymous with modulus E and tangential stiffness K_T with tangential modulus E_T. For bar element acting as spring in the axial direction, the above simplification would imply that the element has unit length and unit area.

The dynamic response of the system shown in Fig. 5.6a under the given loading, changes from elastic to post-peak elastoplastic softening and then back to elastic. The behaviour is thus divided into three sub-domains as shown in Fig. 5.7. The solution in these three sub domains is as follows:

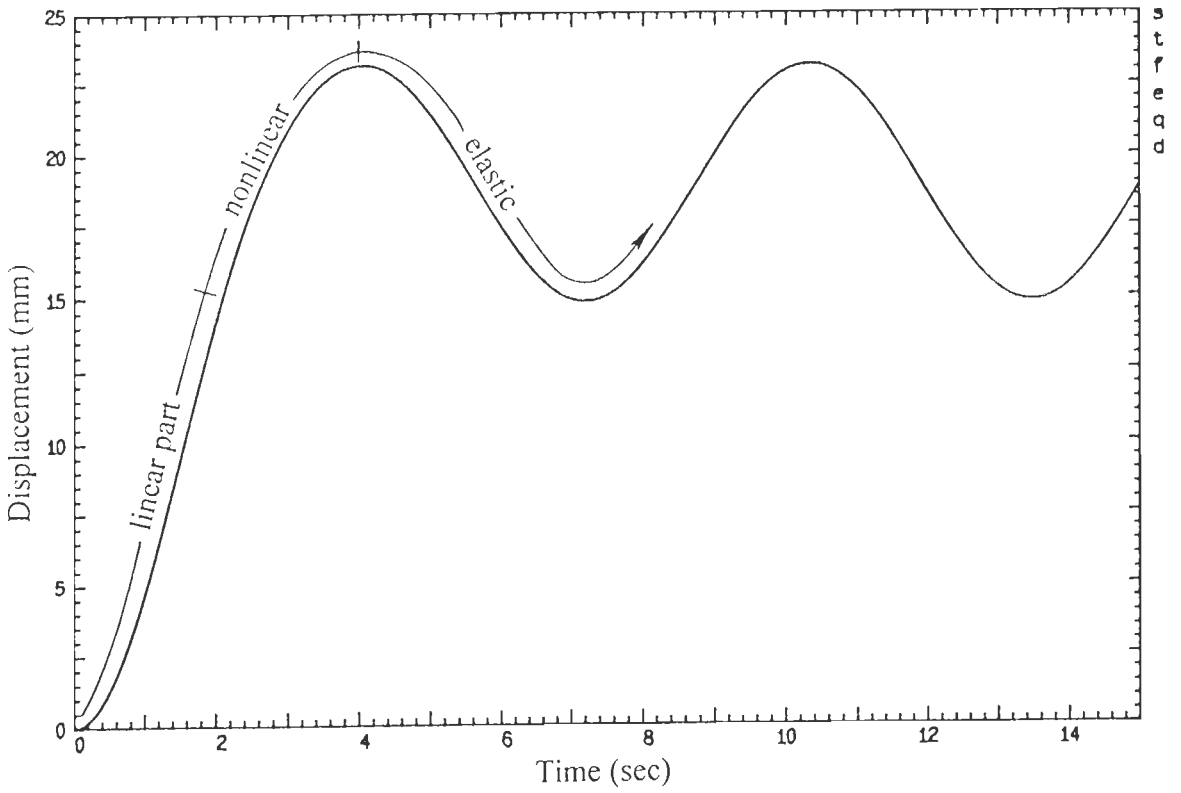

Fig. 5.7 Displacement response of a strain softening undamped SDF system under step function load

Linear Part: When the step function load acts on the system at rest, the system behaves as an elastic system and the equation of motion is

$$m\ddot{x} + Kx = F_o \tag{5.8}$$

which can be solved for initial conditions, $x_{t=0} = 0$ and $\dot{x}_{t=0} = 0$. The solution is

$$x(t) = \frac{F_o}{K}[1 - \cos\omega t] \tag{5.9}$$

where $\omega = \sqrt{K/m}$ is the natural frequency of the SDF system. The maximum displacement response is $2F_o/K$. This will cause a force of $2F_o$ in the spring. Clearly if the yield limit is more than $2F_o$ the system would remain elastic. However when this is not so, the spring would become nonlinear at some time $t = t_1$. At this instant of time

$$x(t_1) = \frac{F_o}{K}(1 - \cos\omega t_1) \tag{5.10a}$$

$$\dot{x}(t_1) = \frac{F_o}{K}\omega(\sin\omega t_1) \tag{5.10b}$$

$$\ddot{x}(t_1) = \frac{F_o}{K}\omega^2(\cos\omega t_1) \tag{5.10c}$$

Nonlinear Part: The equation of motion in the strain softening region can be expressed as

$$m\ddot{x} + P_y = F_o \tag{5.11}$$

where P_y is the new load level with $|P_y| \le P_{yo}$ (Fig. 5.6c), P_{yo} is the yield strength of the virgin material. For linear softening plasticity, the magnitude of P_y would go on declining with increase in displacement as shown in Fig. 5.6c and is given by

$$P_y = P_{yo} - \left(x - \frac{P_{yo}}{E}\right)E_T \tag{5.12}$$

where E and E_T are slopes of elastic and softening branches respectively. It may be noted that E_T is taken to be positive.

Putting P_y from Eqn. 5.12 into Eqn. 5.11 the equation

$$m\ddot{x} + \left\{P_{yo} - \left(x - \frac{P_{yo}}{E}\right)E_T\right\} = F_o \tag{5.13}$$

is obtained whose solution is

$$x(t') = B_1 e^{t'\sqrt{C_1/m}} + B_2 e^{-t'\sqrt{C_1/m}} - \frac{C_2}{C_1} \tag{5.14}$$

with $C_1 = E_T$, $C_2 = F_\circ - P_{y\circ}\left(1+\frac{E_T}{E}\right)$ and $t' = t - t_1$. The constants B_1 and B_2 are found from initial conditions (Eqn. 5.10) as

$$B_1 = \left[\frac{F_\circ}{K}(1-\cos\omega t_1)\right] + \frac{C_2}{C_1} - B_2$$

$$B_2 = 0.5\sqrt{\frac{m}{C_1}}\left[\frac{F_\circ}{K}(1-\cos\omega t_1)\sqrt{\frac{C_1}{m}} + \frac{C_2}{\sqrt{C_1 m}} - \left(\frac{F_\circ}{K}\right)\sin\omega t_1\right]$$

by differentiating Eqn. 5.14 and equating it to zero, the time at which maximum displacement is reached can be found as

$$t_1' = 0.5\sqrt{\frac{m}{C_1}}\ln\frac{B_2}{B_1} \tag{5.15}$$

at this instant of time the velocity becomes zero and then the displacement changes sign. Clearly the system becomes elastic again (elastic unloading).

Similarly for an elasto-perfectly plastic system $E_T = 0$ the solution in the nonlinear phase is

$$x = \frac{F_\circ - P_{y\circ}}{m} - \frac{t'^2}{2} + \frac{F_\circ}{E}(1+\omega t'\sin\omega t_1 - \cos\omega t_1) \tag{5.16}$$

and the time at which the system reverts to the elastic unloading phase is obtained as

$$t_1' = \frac{F_\circ}{\omega}\frac{\sin\omega t_1}{P_{y\circ} - F_\circ} \tag{5.17}$$

Elastic Unloading: The equation of motion upon elastic unloading is

$$m\ddot{x} + Ex' = F_\circ \tag{5.18}$$

where x' is the elastic displacement given by

$$x' = x - \left[x(t_1') - \frac{P_y}{E}\right] \tag{5.19}$$

using Eqn. 5.12 the solution is obtained as

$$x(t'') = B_3\cos\omega t'' + \frac{F_\circ'}{K_1} \tag{5.20}$$

where

$$t'' = t' - t_1',$$
$$K_1 = E - E_T,$$
$$F_o' = F_o + \left(Ex(t_1') - P_{yo} - P_{yo}\frac{E_T}{E} \right) \quad \text{and}$$
$$B_3 = B_1 e^{it_1'\sqrt{C_1/m}} + B_2 e^{-it_1'\sqrt{C_1/m}} - \frac{C_2}{C_1} - \frac{F_o'}{K_1}$$

it can be seen that future response of the SDF system (*i.e.* at $t'' > 0$) will be governed by the above equation and the system will not enter the nonlinear regime again.

In a similar manner, once again, for elasto-perfectly plastic system in this phase

$$x = \left[\frac{F_o - P_{yo}}{m} - \frac{t_1'^2}{2} + \frac{F_o}{E}(1 + \omega t_1' \sin \omega t_1 - \cos \omega t_1) \right] \cos pt'' + \frac{F_o'}{E} \qquad (5.21)$$

In this case too the system will not reenter the nonlinear regime.

This simple problem illustrates that *strain softening does not necessarily lead to unbounded displacement response in dynamics*. Moreover, the system vibrates with frequency ω, which it would have done even if it were purely elastic.

5.5 Spurious Plastic Strain in Dynamics

It was seen earlier that for static problems a proper stress updating strategy is needed to take care of large load/displacement steps else spurious plastic strain accumulates. Similar stress updating procedures are used in the solution of dynamic problems as well. Here the conventionally used iterative strain procedure for dynamic analysis (Owen and Hinton, 1980) is compared with the incremental strain procedure for a dynamic problem. It is seen that presence of acceleration dependent inertia forces and velocity dependent damping forces do not impose any additional complexity when the incremental strain procedure is employed.

The system shown in Fig. 5.6a with mass m, Young's modulus E, cross-sectional area A and length l all equal to unity was considered. A softening modulus E_T was assumed 10% of the Young's modulus. The yield strength of the bar $P_{yo} = 15.0$ was assumed. A step function loading as shown in Fig. 5.6b was assumed to act on the mass of the system with $F_o = 10.0$. If the system were to remain elastic then the maximum

displacement would be $2F_o/K$ (Eqn. 5.9). This will cause an axial force of $2F_o$ in the bar. Clearly, therefore, the system cannot remain elastic for the chosen parameters.

The response of the system was computed using the exact and numerical procedures discussed earlier. The numerical solution was obtained by using the GN22 algorithm in its unconditionally stable form. In subsequent sections it will be seen that this algorithm is superior to some of the GN32 procedures. The GN22 algorithm used employed the incremental strain procedure as well as the iterative strain procedure for updating strains and stresses. The displacement response comparison is shown in Figs. 5.8-5.10. It can be seen that for the smallest time step ($\Delta t = 0.01$sec) the numerical procedures match well with the exact solution. As the step becomes larger (Figs. 5.9-5.10) the exact solution and the numerical solutions are seen to be different form each other. In each case the results from the incremental strain procedure being closer to the exact solution. The accumulation of plastic strain with time is shown in Fig. 5.11. Once again it is seen that greater spurious plastic strain results when the iterative strain procedure is adopted.

It is clear that a single degree freedom system considered would yield the same results with both incremental and iterative strain procedures for static problems. In fact in the case of static problems the difference in the results from the two procedures emerges due to inter element stress adjustments. At the first sight it is surprising to see a difference of such magnitude for a single degree of freedom system in case of dynamic problems. This, apparently, is due to the inter dependence of displacement, velocity and acceleration vectors. Thus the need to use incremental strain procedure for dynamic analysis can not be overemphasized.

5.6 A Comparison of Some Generalized Newmark Algorithms

Once again the problem of step function loading (Fig. 5.6b) acting on the system shown in Fig. 5.6a was considered. The following parameters were assumed:

$$K = 4100\ N/mm,\quad m = 100Kg,\quad P_{y_o} = 3280\ N \quad and \quad F_o = 2000\ N$$

Both GN22 and GN32 algorithms are used in conjunction with the initial stiffness method and the Incremental strain procedure. For GN32 procedure the value of the parameters β_q is so chosen that the algorithms are *single step equivalents* of well known Houbolt and Wilson θ methods. Relationship of generalized Newmark method with these methods has been established by Katona and Zienkiewicz (1985). The Houbolt method is

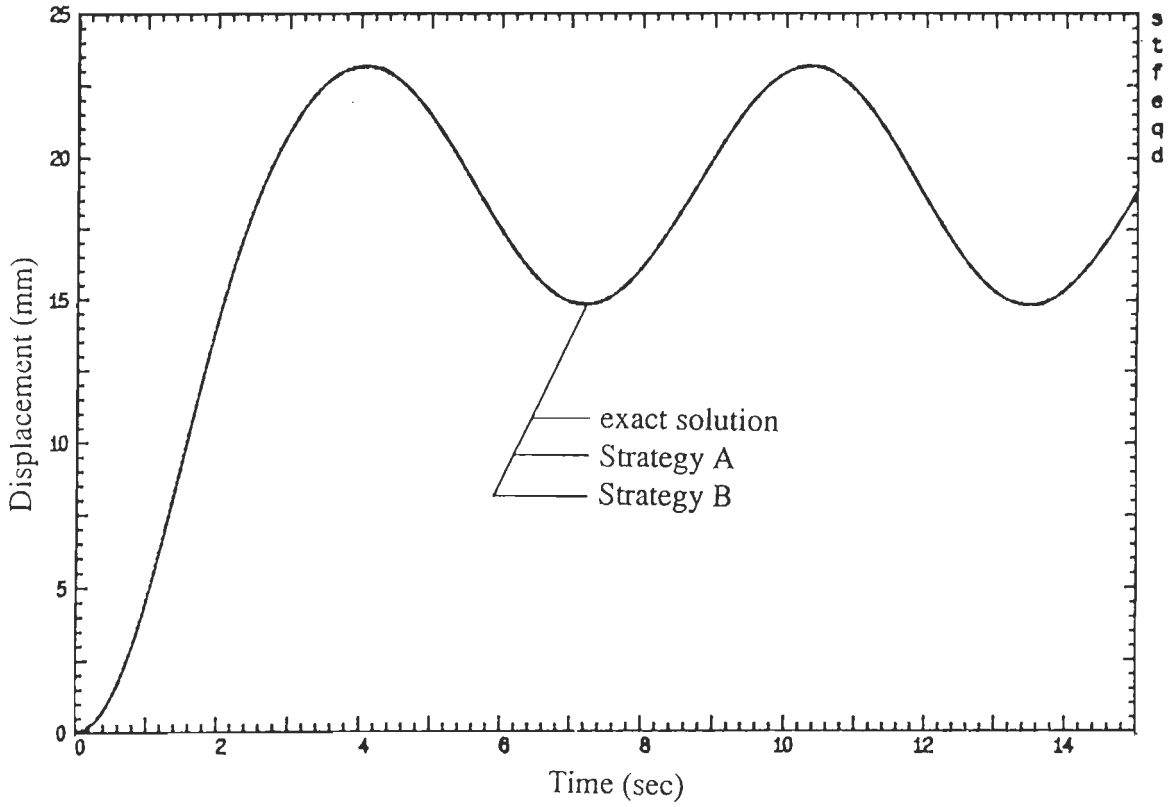

Fig. 5.8 Comparison of exact elasto-strain softening displacement response of an undamped SDF system with numerically computed response using GN22 algorithm ($\Delta t = 0.01$ sec)

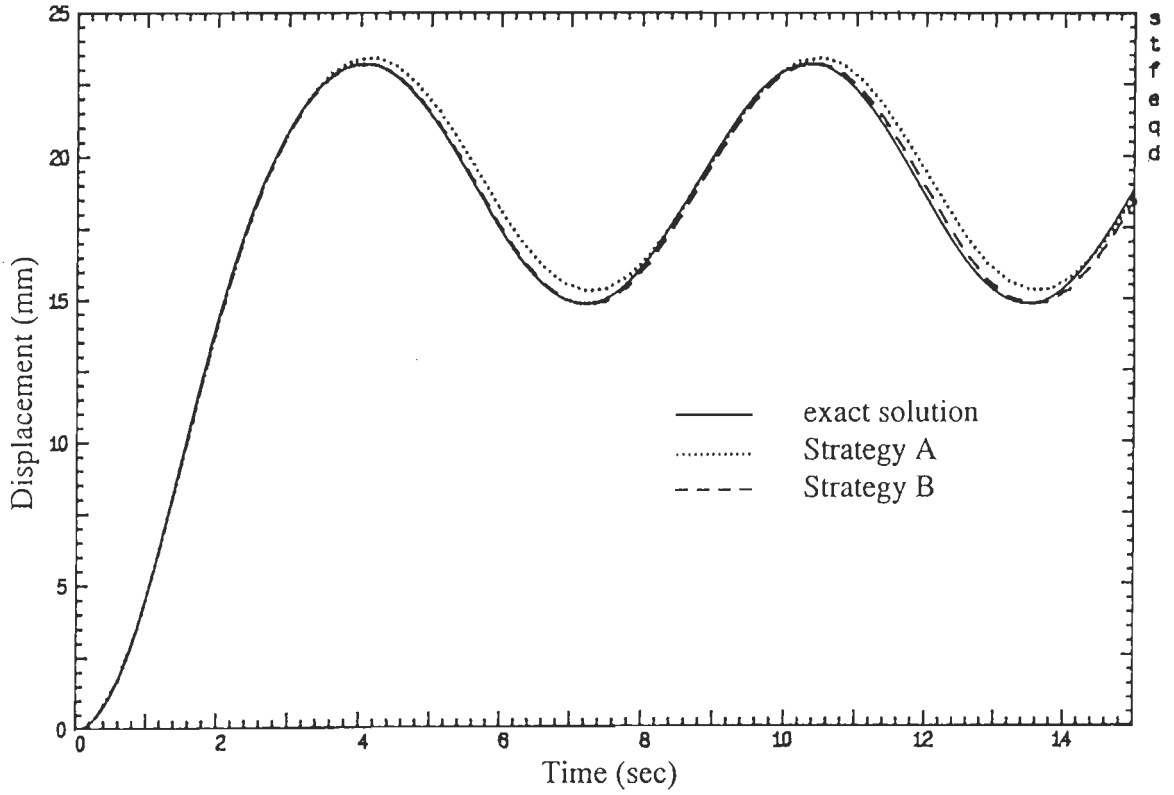

Fig. 5.9 Comparison of exact elasto-strain softening displacement response of an undamped SDF system with numerically computed response using GN22 algorithm ($\Delta t = 0.3$ sec)

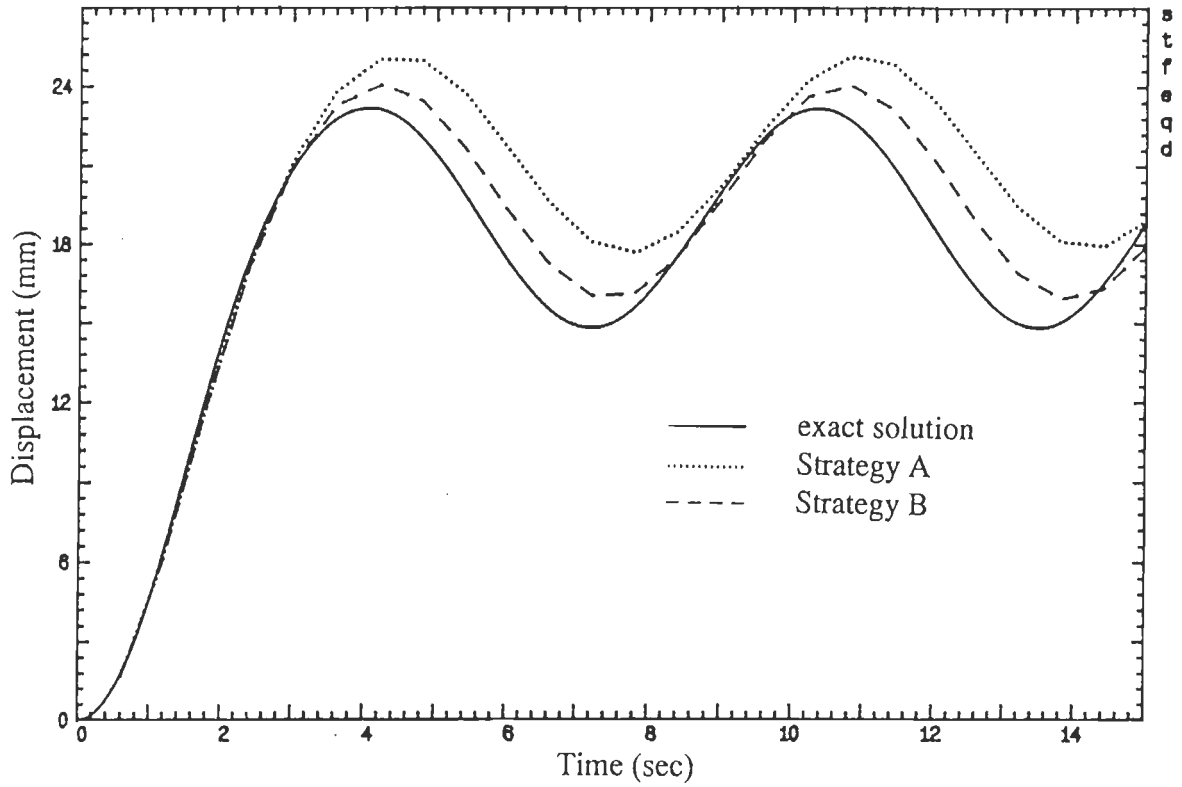

Fig. 5.10 Comparison of exact elasto-strain softening displacement response of an undamped SDF system with numerically computed response using GN22 algorithm ($\Delta t = 0.6$ sec)

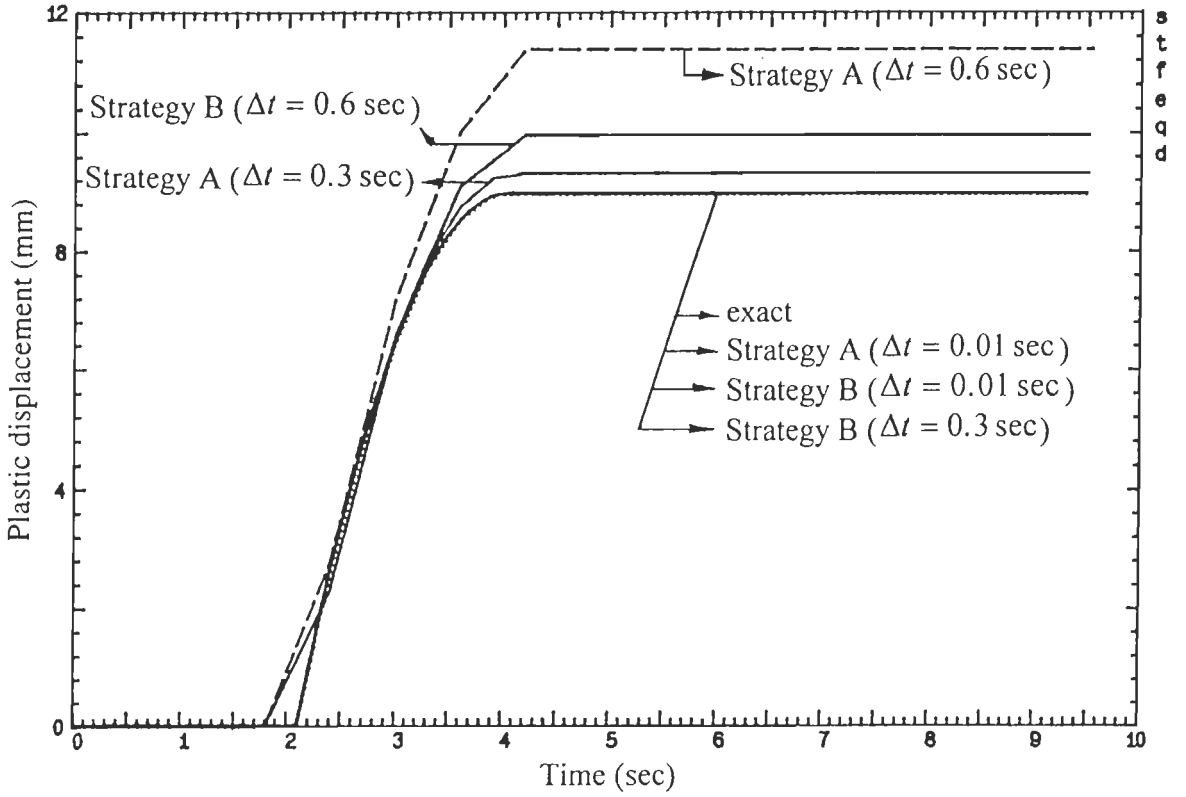

Fig. 5.11 Increase of plastic strain with time using GN22 algorithm and different time steps

essentially a multistep method. GN32 becomes equivalent to the Houbolt method when $\beta_1 = \theta_1 = 2$, $\beta_2 = \theta_2 = 11/3$, $\beta_3 = \theta_3 = 6$ and to Wilson θ method when $\beta_1 = \theta_1 = \theta_w$, $\beta_2 = \theta_2 = \theta_w^2$, $\beta_3 = \theta_3 = \theta_w^3$ (Katona and Zienkiewicz, 1985). The Wilson θ method is unconditionally stable when $\theta_w \geq 1.366$ (Bathe, 1982). The unconditionally stable form of GN22 with $\beta_1 = \beta_2 = 0.5$ was used.

The single step equivalents of GN32 have not been sufficiently tested. The reason, perhaps, is that GN32 is difficult to use when the initial conditions are other than zero. This is due to the fact that the method requires initial value of the third derivative of displacement for which no expression is available.

The first series of analysis was conducted assuming elastic-perfectly plastic constitutive behaviour with an yield force $P_{y_0} = 3280\text{N}$. For such a system an exact (closed form) displacement response was found and plotted along with GN22 and GN32 (Wilson θ and Houbolt cases). For each case a time step Δt=0.05 sec was employed. The displacement response is shown in Fig. 5.12. It can be seen that GN22 is closest to the exact solution, while Houbolt equivalent of the GN32 is the farthest.

A second series of analyses were conducted in which the same single degree of freedom system with strain softening post-elastic behaviour ($E_T = 410$ N / mm) was considered. Again the results of GN22, GN32 Wilson θ and GN32 Houbolt cases were compared with the exact (closed form) displacement response (Fig. 5.13). Once again it was observed that the GN22 is closest to the exact response while Houbolt equivalent of GN32 is the farthest. A analysis for a larger period of time (Fig. 5.14) illustrates considerable amplitude decay for the Houbolt equivalent of GN32, a little less for the Wilson θ equivalent and none for the unconditionally stable form of GN22. These simple examples indicate the superiority of the unconditionally stable form of the GN22 algorithms.

5.7 Dynamic Response Due to Different Post-Peak Constitutive Behaviour

The problem considered in section 5.6 was analysed with different post-elastic constitutive behaviour as shown in Fig. 5.15. An E_T of the same magnitude 410 N / mm was employed for both strain hardening and strain softening cases (Fig. 5.15b–5.15c) with different signs. The displacement response is shown in Fig. 5.16.

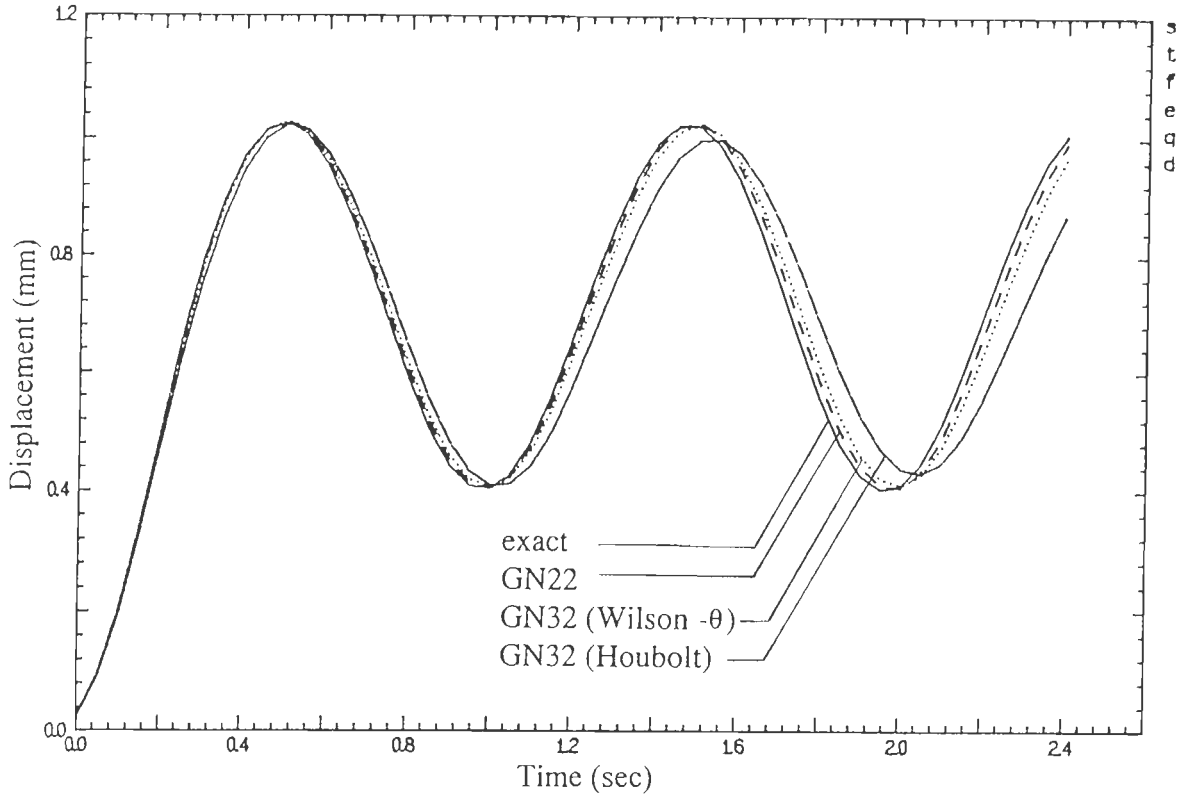

Fig. 5.12 Response of a SDF elastic-perfectly plastic system to step function loading using different algorithms

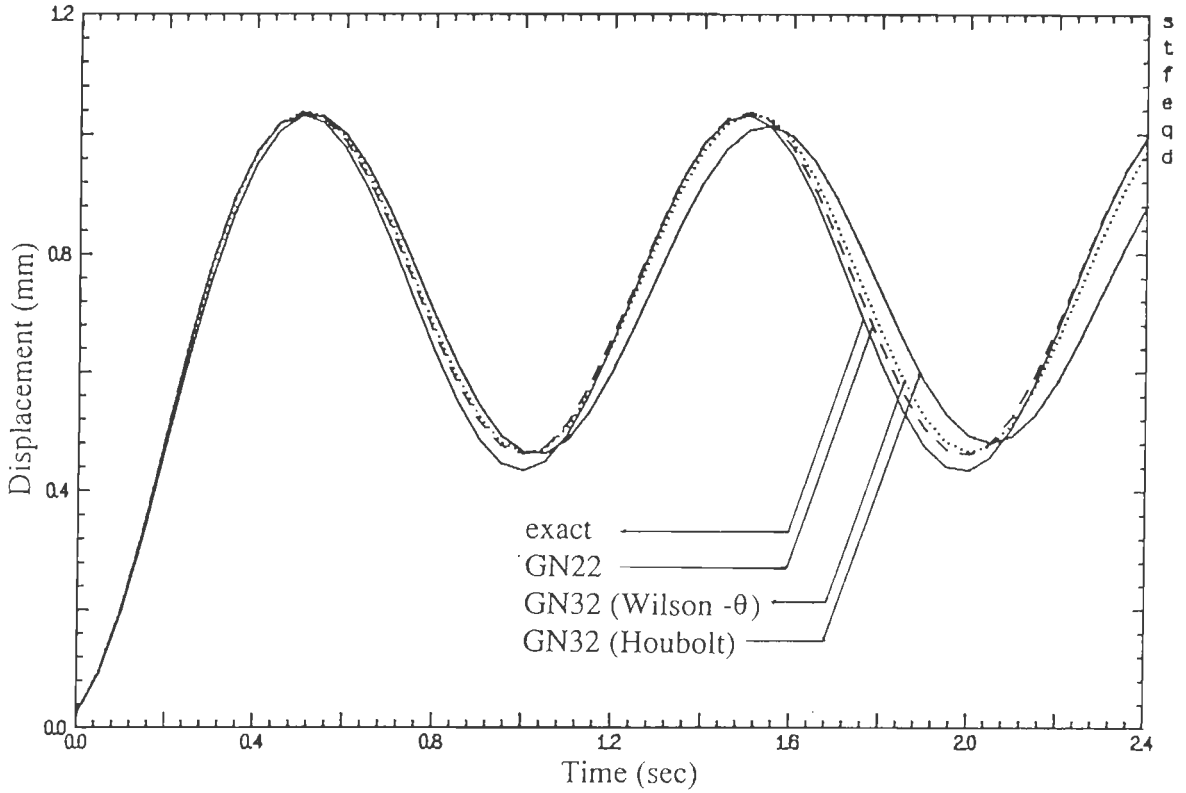

Fig. 5.13 Response of a SDF elastic-strain softening system to step function loading using different algorithms

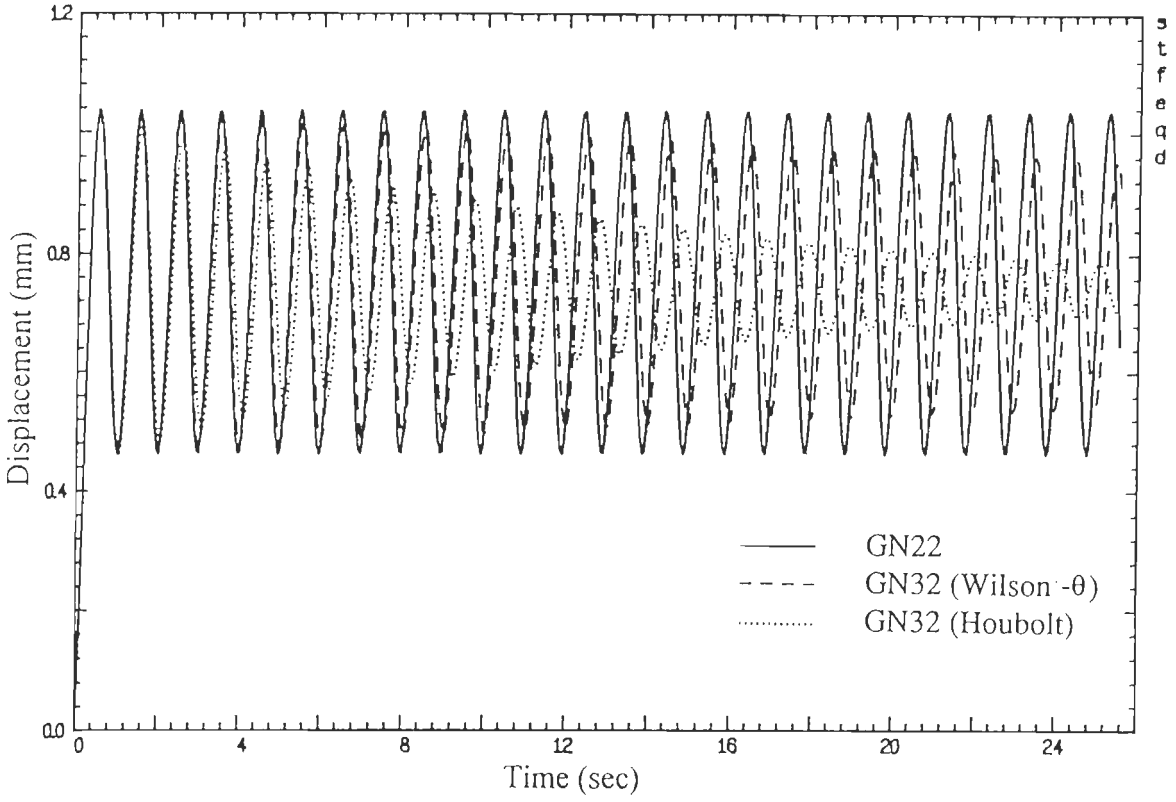

Fig. 5.14 Extended response of a SDF system with elastic strain softening characteristics to step function loading using different algorithms

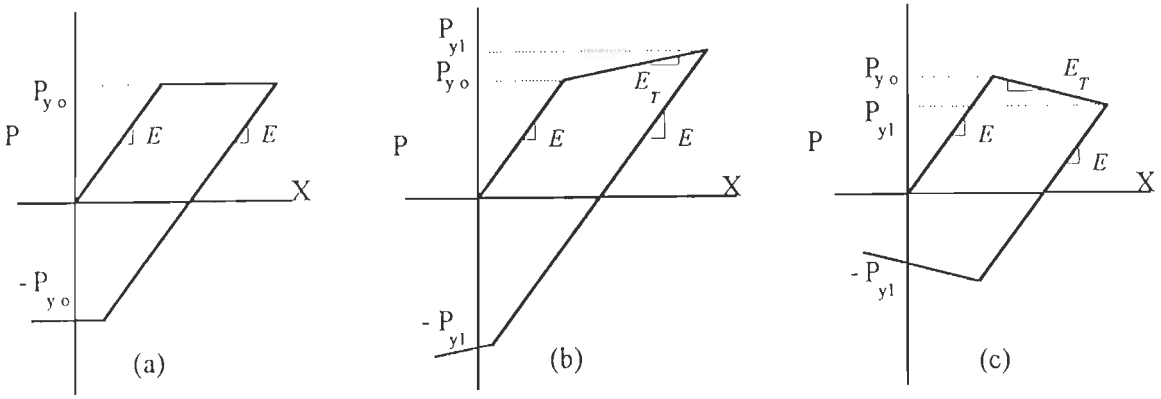

Fig. 5.15 (a) Elastic-perfectly plastic (b) Elastic-strain hardening plastic (c) Elastic-strain softening plastic

It can be seen that irreversible plastic displacement increases as the spring characteristics are changed from elastic to strain hardening to perfectly plastic to strain softening. It would appear that the period of oscillation would increase in the same sequence (Zienkiewicz and Wood, 1986). A Fourier analysis of the frequency content, however, reveals that there is no change in the predominant frequency of the vibration as the spring characteristics change (Fig. 5.17). In each case there is a zero frequency component (ZFC) which is due to the mass not vibrating about the zero displacement position. This component is highest for the strain softening case and zero for elastic case. This analysis shows that strain softening can be used for dynamic analysis as well (Moin and Pankaj, 1994). Moreover, the system continues to vibrate and does not cause an unbounded response.

In order to study the behaviour of different time stepping algorithms under different post-elastic constitutive behaviour the analysis was conducted for an extended period of time. The results are shown in Figs. 5.18-5.20. Amplitude decay is observed for all cases of Wilson θ and Houbolt equivalents.

5.8 Seismic Response of Nonlinear SDF System

The base of a single degree of freedom (SDF) system of Fig. 5.6a with $K = 4100\ N/mm$ and $m = 100Kg$ was subjected to an actual earthquake acceleration history. The corrected accelerogram of the Uttarkashi earthquake of October 20, 1991 obtained at 30.738N and 78.792E (Earthquake Engineering Studies, 1993) was used for the purpose. A constant viscous damping of 5% of the critical was considered and the bar was assumed to be (a) Elastic, (b) Perfectly plastic and (c) Strain softening. For the strain softening case $E_T = 410\ N/mm$ was assumed. The response was computed using GN22 algorithm with Δt=0.02 sec. In the first instance the yield force value $P_{yo} = 2.05 \times 10^5\ N$ was assumed. The displacement response is shown in Fig. 5.21. It can be seen that for nonlinear cases the mass does not vibrate about the zero displacement position. The Fourier analysis (Fig. 5.22) of the response indicates that in general, the predominant frequency content does not change with the change in post-elastic constitutive behaviour although some low frequency components appear to have been added to the response. Due to the mass finding new mean position to vibrate about, a zero frequency component is included in the response (Fig. 5.22). These changes of the mean position take place with the building up of the plastic displacements, which happens in a short time (Fig. 5.23) and

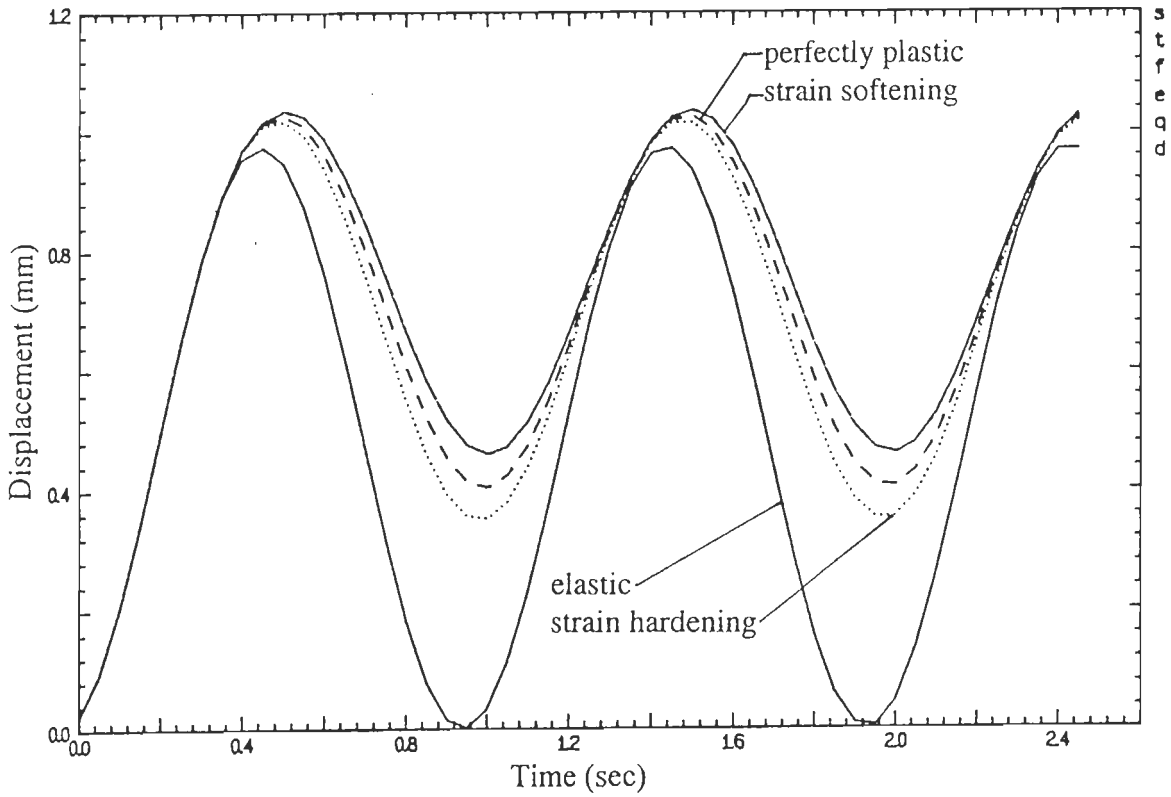

Fig. 5.16 Response of a SDF system with different post-yield characteristics to step function loading using GN22 algorithm

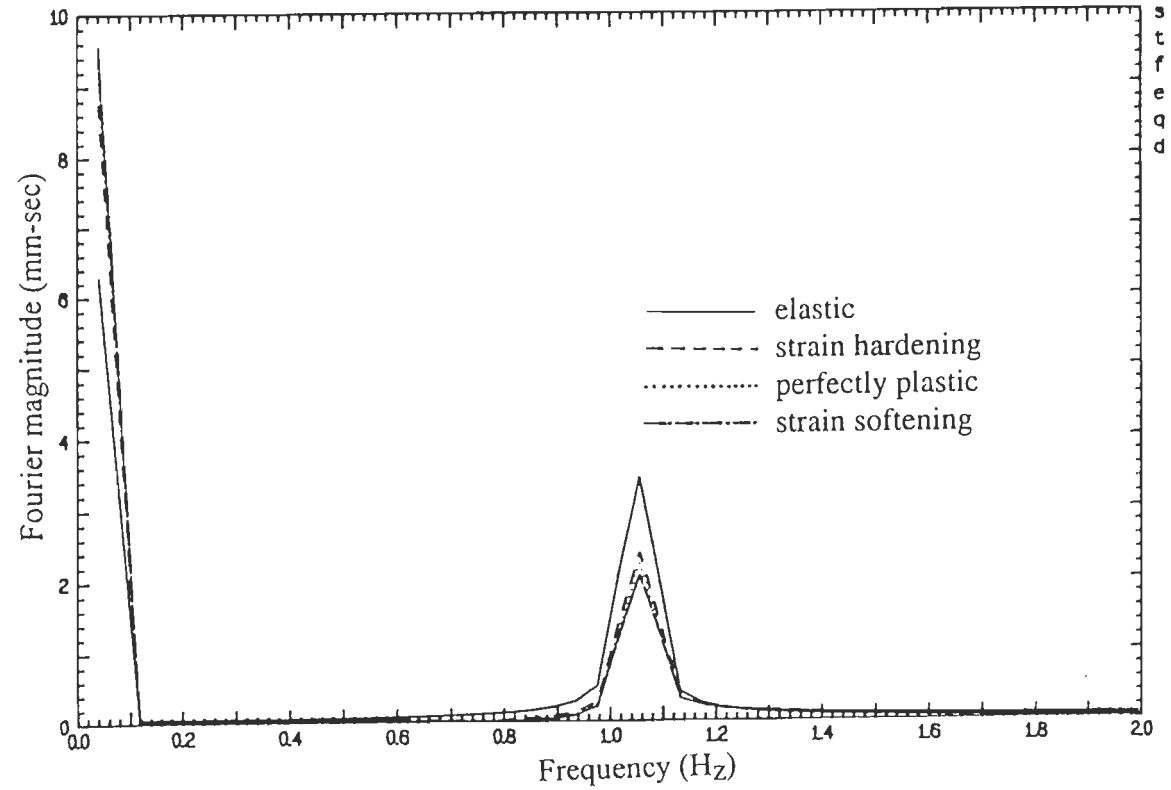

Fig. 5.17 Fourier magnitude of displacement response of a SDF system with different post-yield characteristics under step function loading

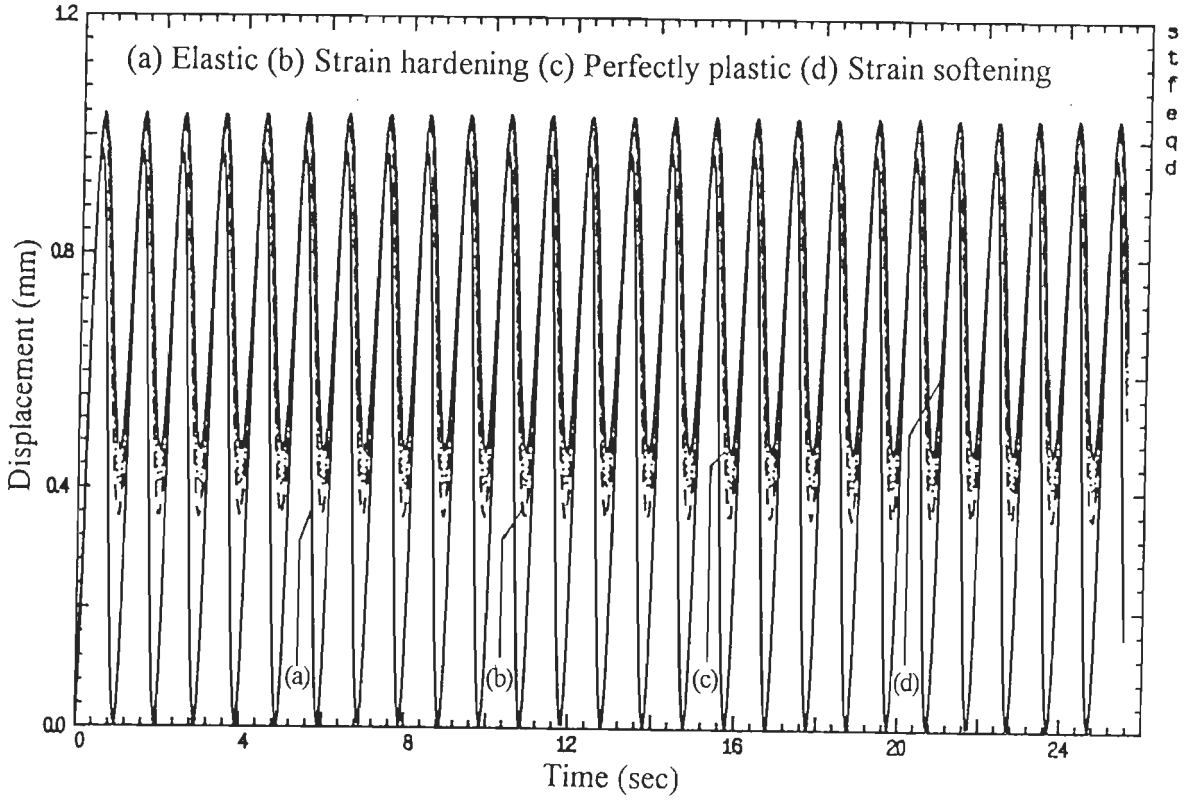

Fig. 5.18 Extended displacement-time response of a SDF system with different post-yield characteristics to step function loading using GN22 algorithm

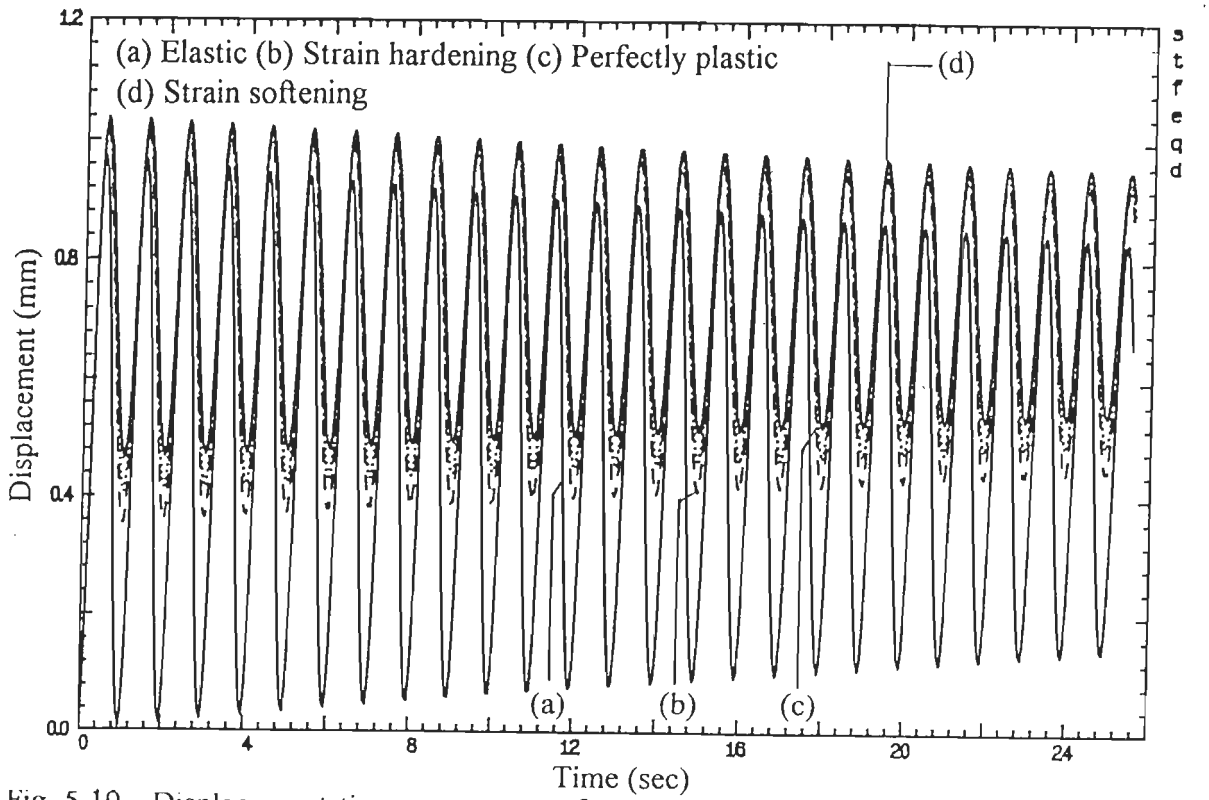

Fig. 5.19 Displacement-time response of a SDF system with different post-yield characteristics to step function loading using GN32 (Wilson–θ) algorithm

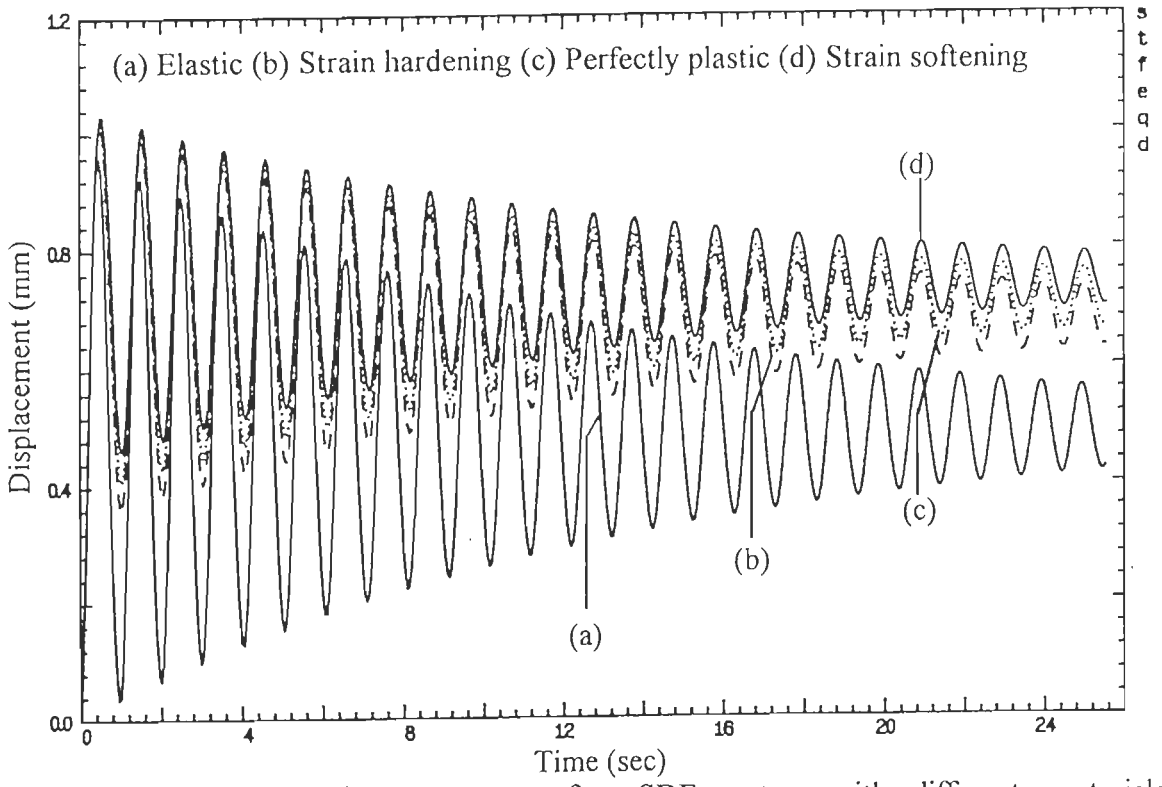

Fig. 5.20 Displacement-time response of a SDF system with different post-yield characteristics to step function loading using GN32 (Houbolt) algorithm

remains constant thereafter. The maximum plastic displacement for this example was found to be 22.43 mm and 25.03 mm for perfectly plastic and softening cases respectively.

The second analysis was conducted after reducing the yield force P_{yo} to $1.23 \times 10^5 N$. The displacement response is shown in Fig. 5.24 and the Fourier magnitude plot of the response is illustrated in Fig. 5.25. Once again it can be seen that for elastoplastic cases a zero frequency component is incorporated in the response. The ZFC in this case (Fig. 5.25) is smaller as compared to the earlier case with higher yield level (Fig. 5.22) although the plastic displacement levels (Fig. 5.26) are much higher (48.56 mm and 54.94 mm for perfectly plastic case and elastic strain softening case respectively). The reason for the lower ZFC is, that in this case the plastic displacement increments take place during both compression and tension of the bar thus reducing the ZFC.

It is seen from the above discussion that elastoplasticity does not alter the predominant frequency response of the system. It, however, introduces a zero frequency and some low frequency components in the response. It is also seen that strain softening plasticity can be used with dynamic problems.

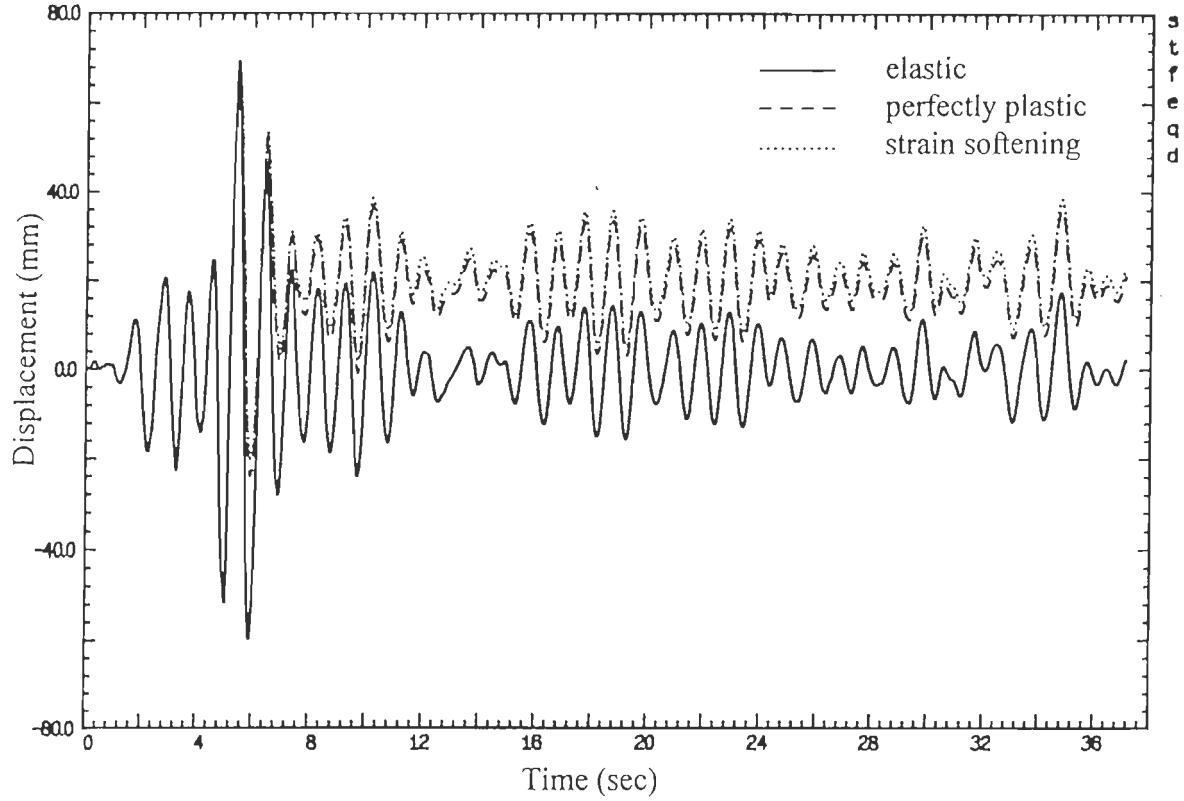

Fig. 5.21 Displacement time response of a SDF system with different characteristics to Uttarkashi earthquake excitation ($P_{y_0} = 2.05 \times 10^5 N$)

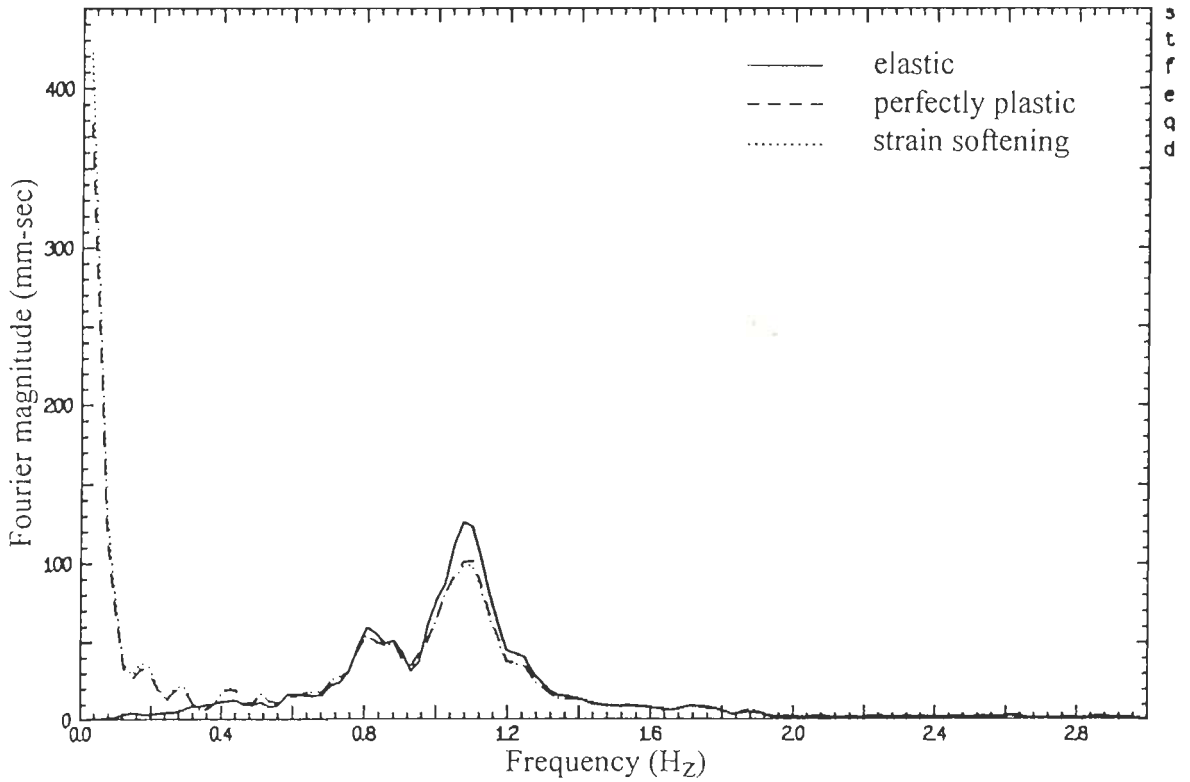

Fig. 5.22 Fourier magnitude plot of the displacement response ($P_{y_0} = 2.05 \times 10^5 N$)

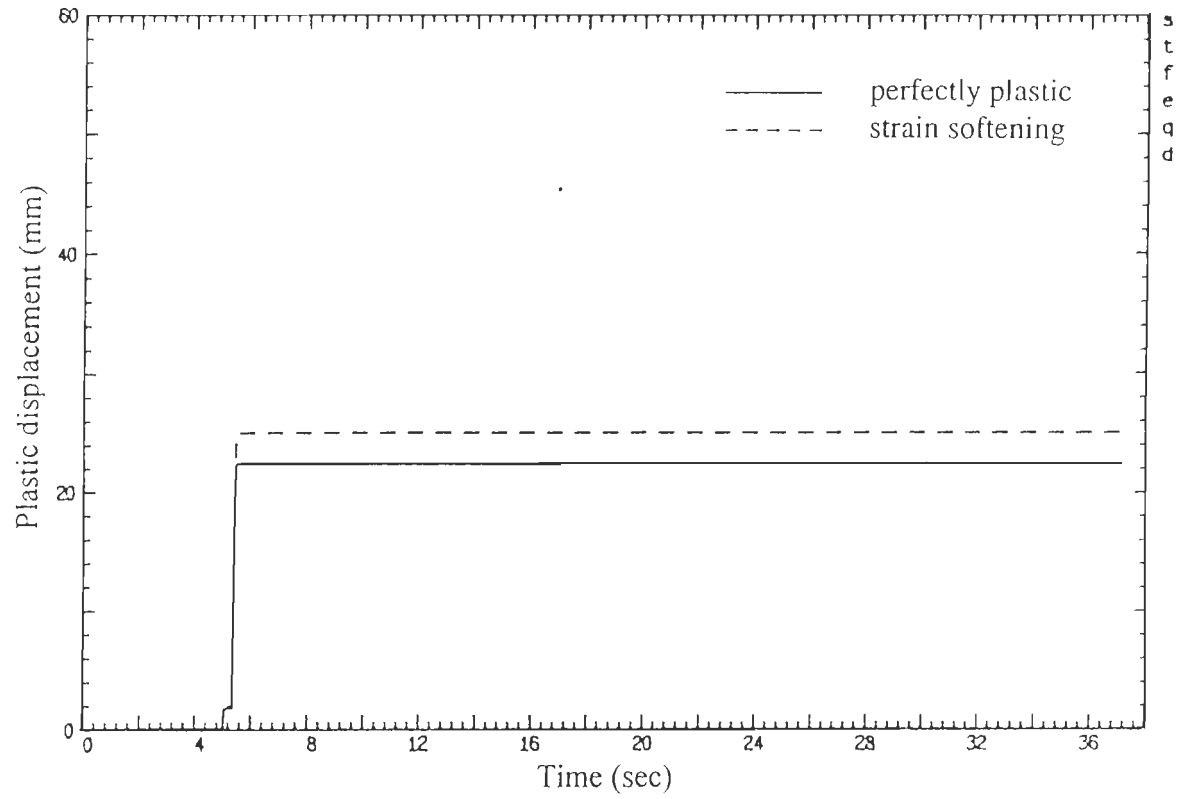

Fig. 5.23 Increase of plastic displacement with time ($P_{y_0} = 2.05 \times 10^5 N$)

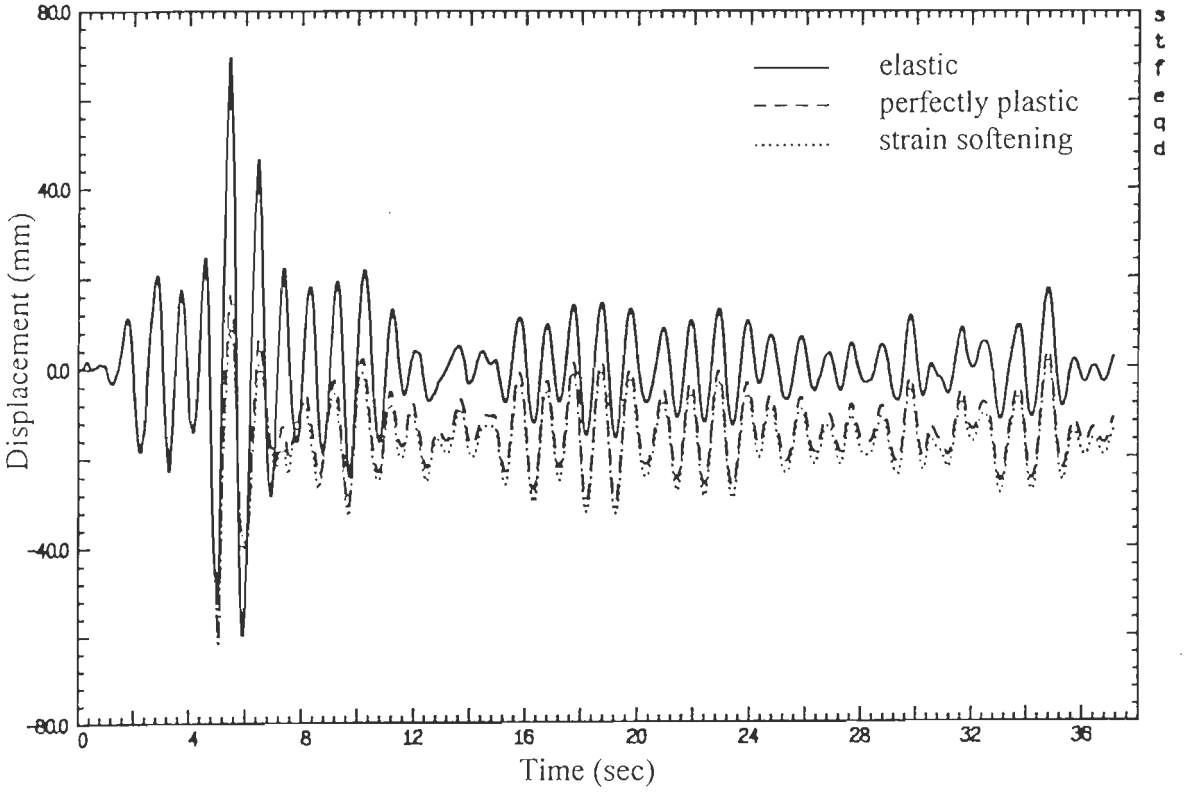

Fig. 5.24 Displacement time response of a SDF system with different characteristics to Uttarkashi earthquake excitation ($P_{y_0} = 1.23 \times 10^5 N$)

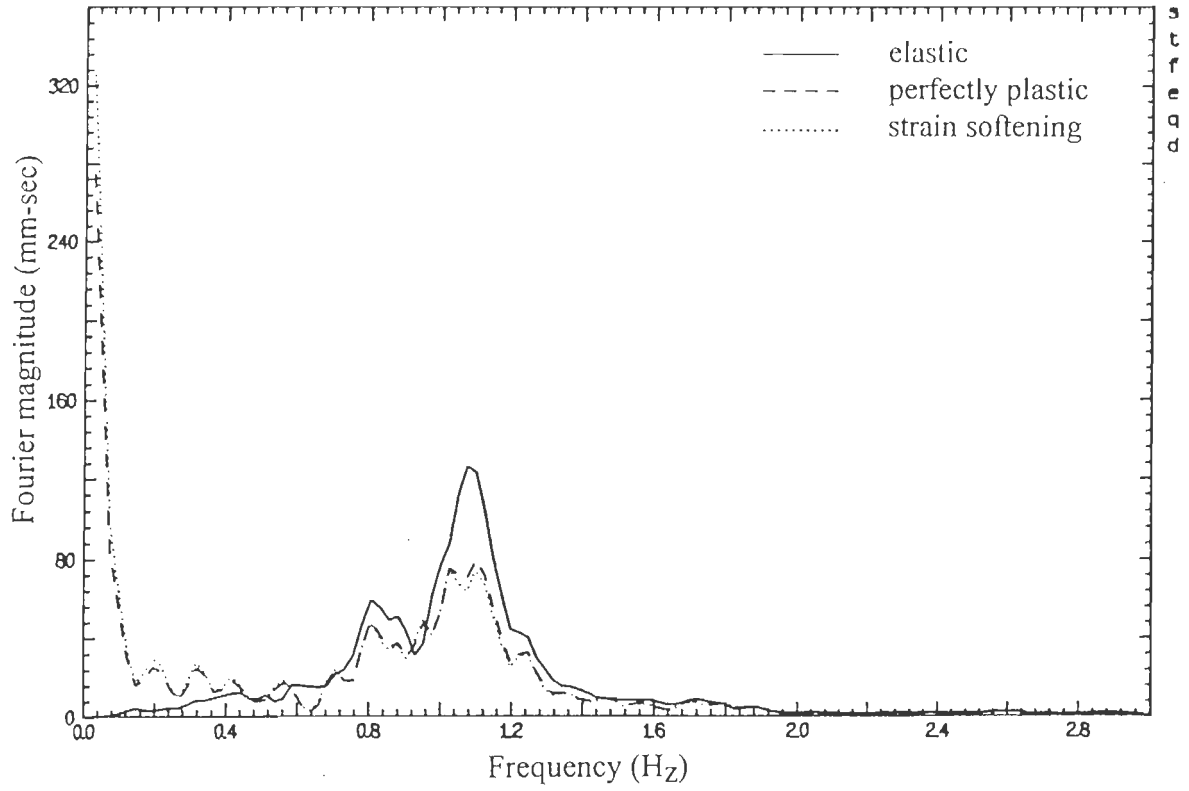

Fig. 5.25 Fourier magnitude plot of the displacement response ($P_{y_0} = 1.23 \times 10^5 N$)

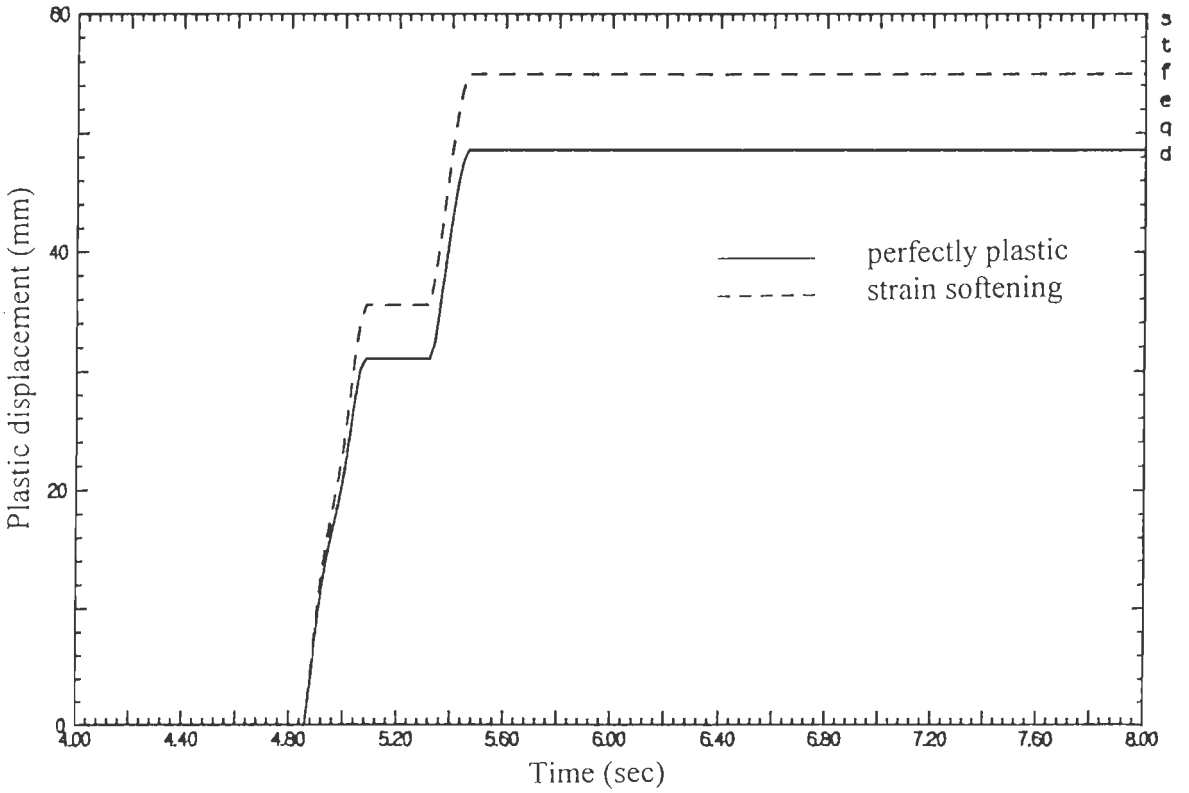

Fig. 5.26 Increase of plastic displacement with time ($P_{y_0} = 1.23 \times 10^5 N$)

References

Earthquake Engineering Studies, (1993) – Performance of strong motion instruments in Garhwal (U.P.), Earthquake of Oct. 20, 1991, Vol. 2, *Report of the Department of Earthquake Engineering*, No. EQ. 93-07, Roorkee.

Bathe, K.J. (1982) – Finite element procedures in Engineering analysis, Prentice Hall Inc. Englewood Cliffs.

Bathe, K.J. and Wilson, E.L. (1976) – Numerical methods in finite element analysis, Prentice Hall.

Bazant, Z.P. (1976) – Instability, ductility and size effect in strain softening concrete, *J. Eng. Mech., ASCE*, **102**(2), 331-344.

Bazant, Z.P. and Belytschko, T. (1985) – Wave propagation in a strain softening Bar: exact solution, *J. Eng. Mech., ASCE*, **111**(3), 381-389.

Bazant, Z.P. and Chang, T.P. (1987) – Nonlocal finite element analysis of strain softening solids, *J. Eng. Mech., ASCE*, **113**, 89-105.

Belytschko, T. (1978) – Explicit time integration of structural-mechanical systems, Advanced Structural Dynamics (Ed. Donea, J.), 97-122.

Belytschko, T., Xiao-Jun Wang, Bazant, Z.P. and Hyun, Y. (1987) – Transient solutions for one dimensional problems with strain softening, *J. App. Mech., ASCE*, **54**, 513-518.

Bicanic, N. and Pankaj (1990a) – On mesh design for concrete strain softening analysis, *Computer Aided Analysis and Design of Concrete Structures*, (Eds. Bicanic, N. and Mang, H.), Vol. 2, Pineridge Press, 959-974.

Bicanic, N. and Pankaj (1990b) – Some computational aspects of tensile strain localization modelling in concrete, Eng. Fract. Mech., 35(4/5), 697-707.

de Borst, R. (1986) – Nonlinear analysis of frictional materials, *Ph.D. Dissertation*, Delft University of Technology.

Crisfield, M.A. (1991) – Nonlinear finite element analysis of solids and structures; Vol. 1 Essentials, John Wiley and Sons.

Katona, M.G. and Zienkiewicz, O.C. (1985) – A unified set of single step algorithms, part 3: The beta -m method, a generalisation of Newmark scheme, *IJNME*, **21**, 1345-1359.

Marques, J.M.M.C. (1984) – Stress computations in elastoplasticity, *Engng. Comput.* **1**, 42-51.

Moin, K. and Pankaj (1994) – Strain softening in dynamic problems, *Tenth Symposium on Earthquake Engineering,* University of Roorkee, Roorkee, 893-905.

Mondker, D.P. and Powell, G.H. (1975) – Static and dynamic analysis of nonlinear structures, *EERC* 75-10.

Mondker, D.P. and Powell, G.H. (1978) – Evaluation of solution schemes for nonlinear structures, *Comp. Struct.*, **9**, 223-236.

Newmark, N.M. (1959) – A method of computation for structural dynamics, *J. Engng. Mech., ASCE*, **85**, 67-94.

Nyssen, C. (1981) – An efficient and accurate iterative method allowing large incremental steps to some elastoplastic problems, *Comp. Struct.*, **13**, 63-71.

Owen, D.R.J. and Hinton, E. (1980) – Finite elements in plasticity: Theory and Practice, Pineridge Press, U. K.

Pankaj, (1990) – Finite element analysis in strain softening and localization problems, *Ph.D. Thesis*, University College of Swansea, University of Wales, U.K.

Pankaj and Moin, K. (1996) – On the use of strain softening prediction of post-peak seismic response of structures, *Proceedings of Eleventh World Conference on Earthquake Engineering* to be held in Mexico, Jun. 23-28, 1996, to appear.

Pankaj, Moin, K. and Barthwal, G. (1994) – On single step algorithms in the solution of dynamic linear and nonlinear problems, *Bull. Ind. Soc. Earth. Tech.*, **31**, 117-139.

Ramm, E. and Matzenmiller, A. (1988) – Consistent linearisation in elastoplastic shell analysis, *Engng. Comput.*, **5**, 289-299.

Sandler, I.S. (1984) – Strain softening for static and dynamic problems, *Proceeding Symposium on Constitutive Equations, Micro, Macro and Computational Aspects*, (Edited by Willam, K. J.), 217-231.

Zienkiewicz, O.C. and Taylor, R.L. (1991) – The finite element method: solids and fluid mechanics dynamics and nonlinearity, Fourth edition, Vol. 2, McGraw Hill International Editions.

Zienkiewicz, O.C. and Wood, W.L. (1986) – Computational transient analysis, *Unpublished Notes*.

Zienkiewicz, O.C., Wood, W.L., Hines, N.W. and Taylor, R.L. (1984) – A unified set of single step algorithms, *IJNME*, **20**, 1524-1552.

Zienkiewicz, O.C., Wood, W.L. and Taylor, R.L. (1980) – An alternative single step algorithm for parabolic boundary value problems, *Int. J. Earth. Eng. Struct. Dyn.*, **8**, 31-40.

Chapter 6

Benchmark Problems

6.1 General

The analysis of industrial structures and substructures is often conducted using elastoplastic constitutive laws, in conjunction with the finite element method. The finite element codes may be used as "black box" by personnel who may be inadequately trained in the method. In order to train analysts and to check the validity of finite element codes, the benchmarks can be of paramount importance. Further, exact solutions in computational elastoplasticity cannot be used directly as these often pertain to solutions that are valid only for particular cases. However, these solutions can be used as benchmark tests to check the validity of finite element codes and accuracy of numerical solution procedures. A number of benchmarks have been devised for this purpose in computational elastoplasticity (Krieg and Krieg, 1977; A. Kamoulakos et al., 1985; Crisfield et al., 1987; Hinton and Ezzat, 1987; Jackman and White, 1987; Hinton et al., 1989; Hablot and Zarka, 1989; Pankaj and Moin, 1991; Sloan and Brooker, 1992; Pankaj and Moin, 1996).

In the present Chapter benchmark tests for three different yield criteria *viz.* von Mises, Mohr Coulomb and Hoffman are discussed. The perfectly plastic as well as strain hardening/softening hypotheses are considered. The tests are based on prescribed displacement field format.

6.2 Benchmark Testing

The benchmark tests discussed in this Chapter are based on single elements in a prescribed displacement field. Thus a displacement field is prescribed to the nodes of the element and then the corresponding strains and stresses are evaluated. While evaluation of strains from displacement involves only a strain-displacement transformation matrix, the computation of stresses from strains involves nonlinear material constitutive relationship. Here consideration is limited to isotropic elastoplastic benchmark tests for plane strain or three dimensional situations. The tests can be used to verify finite element packages with regard to their ability to (Hinton et al., 1989):

- Accurately predict first yield at various segments of the Mohr Coulomb, von Mises or Hoffman yield surfaces,
- Correctly predict flow on von Mises, Mohr Coulomb and Hoffman yield surface with or without hardening/softening.

6.3 Development of Benchmark Tests for von Mises Criterion

6.3.1 Perfect Plasticity

The exact integration of constitutive equations for an isotropic elasto-perfectly plastic von Mises material were developed by Krieg and Krieg (1977) by considering a constant strain rate vector of arbitrary direction for associated flow rule.

The basic steps for the evaluation of stress increment for a given strain increment can be outlined as follows

1. Find the radius R of the von Mises surface in deviatoric stress space as

$$R = \sqrt{\frac{2}{3}}\, Y_o$$

   where Y_o is the equivalent uniaxial yield stress.
2. Find contact deviatoric stress $\mathbf{S}_c$ at the contact starting stress (stress state on the yield surface) state $\boldsymbol{\sigma}$.
3. From the prescribed strain increment $\Delta\varepsilon$ find the deviatoric strain increment $\Delta\mathbf{e}$.
4. The elastic predictor deviatoric stress increment $\Delta\mathbf{S}_e$ is given by

$$\Delta\mathbf{S}_e = 2G\Delta\mathbf{e}$$

   where G is the shear modulus

5. The updated deviatoric stresses $\mathbf{S}_1$ can be found as

$$\mathbf{S}_1 = \alpha(\mathbf{S}_c + \beta\Delta\mathbf{S}_e)$$

where

$$\beta = \left[1 - C^2 + (1-C)^2 \cos\psi_c\right] R / \left(2C|\Delta\mathbf{S}_e|\right)$$

$$C = \mathrm{e}^{\left(-|\Delta\mathbf{S}_e|/R\right)}$$

$$\alpha = \frac{2C}{\left(1+C^2\right)+\left(1-C^2\right)\cos\psi_c}$$

$$\cos\psi_c = \frac{\mathbf{S}_c\,\Delta\mathbf{S}_e}{R|\Delta\mathbf{S}_e|}$$

$$|\Delta\mathbf{S}_e| = \left(\Delta S_{ex}^2 + \Delta S_{ey}^2 + \Delta S_{ez}^2 + 2\Delta\tau_{exy}^2 + 2\Delta\tau_{eyz}^2 + 2\Delta\tau_{ezx}^2\right)^{1/2}$$

and $\Delta S_{ex}, \Delta S_{ey}, \Delta S_{ez}$ are deviatoric elastic predictor stress increments in the x, y and z directions. Similarly $\Delta\tau_{exy}$ etc. are the elastic predictor shear stress increments.

This closed form solution is general enough to take into account any arbitrary strain increment. The solution has been extensively used as a benchmark test in von Mises plasticity (e.g. Hinton et al., 1989). This solution is however unable to tackle more general and practical cases like strain hardening/softening plasticity.

6.3.2 Hardening/Softening Plasticity

In general the stress increment during continued plastic loading needs to be computed by integrating the equations

$$d\boldsymbol{\sigma} = \mathbf{D}^{ep} d\boldsymbol{\varepsilon} \tag{6.1}$$

where the elastoplastic matrix

$$\mathbf{D}^{ep} = \mathbf{D} - \frac{(\mathbf{Da})(\mathbf{Da})^T}{\mathrm{A} + \mathbf{a}^T\mathbf{Da}} \tag{6.2}$$

Here $\mathbf{a}$ is the flow vector given by $\mathbf{a} = \partial F / \partial\boldsymbol{\sigma}$; $\mathbf{D}$ the elasticity matrix; and $d\boldsymbol{\sigma}$, $d\boldsymbol{\varepsilon}$ are infinitesimal stress and strain increments respectively. The parameter A is the hardening/softening parameter which for the yield function $F(\sigma, \kappa) = 0$ is given by

$$\mathrm{A} = -\frac{\partial F}{\partial\kappa}\left(\frac{\partial\kappa}{\partial\boldsymbol{\varepsilon}^p}\right)^T \frac{\partial F}{\partial\boldsymbol{\sigma}} \tag{6.3}$$

where κ is a parameter depending on plastic strain history and $\boldsymbol{\varepsilon}^p$ denotes plastic strain.

The stress increment is obtained by integrating Eqn. 6.1. This integration is straightforward if the elastoplastic matrix $\mathbf{D}^{ep}$ remains constant during the straining history. In general the $\mathbf{D}^{ep}$ matrix as given by Eqn. 6.2 keeps changing as the flow vector **a** and hardening parameter A are not constant during plastic loading. If a straining history is such that the flow vector **a** remains constant, then this will lead to a simple benchmark test. Clearly for linear hardening/softening the parameter A is constant and thus by merely ensuring a constant **a** the test will be able to include linear hardening/softening. It is easy to see that constancy of **a** for von Mises criterion can be ensured if the plastic strain direction is radial to yield surface in the $\pi-$plane. Such tests are considered in the following subsections.

6.4 Benchmark Tests for von Mises Criterion

6.4.1 Benchmark Test 1: Perfectly Plastic Element Under Uniaxial Tension

Consider a four noded square single element as shown in Fig. 6.1. Nodes 1 and 3 are restrained against all translations. Nodes 2 and 4 are permitted only prescribed translations in the x-direction. The prescribed displacement is induced in the x-direction at nodes 2 and 4. The principal stress directions will remain parallel to x, y and z axes throughout the straining history and therefore there will be no shear stress induced during straining. Moreover for a plane strain case the relationship $\sigma_y = \sigma_z$ will always be maintained. It is also easy to see that during such loading the elastoplastic matrix $\mathbf{D}^{ep}$ remains unchanged. As a first example, the case of perfect plasticity A = 0 was considered. The advantage of this test is that it is possible to verify the results using the methodology of Krieg and Krieg (1977) discussed in subsection 6.3.1.

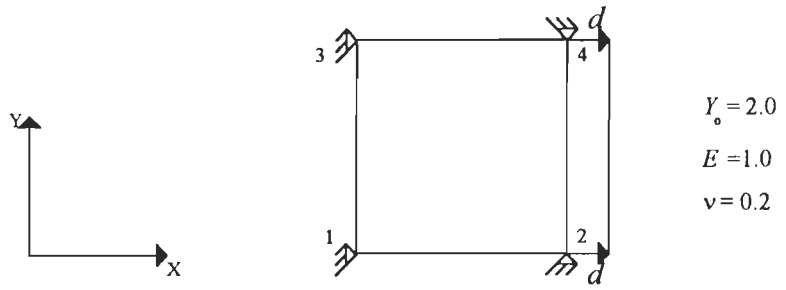

Fig. 6.1 Uniaxial tension test on a single element

The manner in which the stress states traverse the yield surface is shown in Fig. 6.2 and the numerical values obtained to be used as benchmark are presented in Table 6.1. Since the element is a square with unit sides, the prescribed displacements are the same as strain ε_x. The following observations can be made from Table 6.1 and Fig. 6.2.

- The first displacement increment ($\Delta x = 2.4$) is given in such a way that it takes the stress state elastically to the von Mises yield surface at which the stress state is given by

$$\sigma_x = \sigma_1 = \frac{(1-\nu)}{(1-2\nu)} Y_o$$

$$\sigma_y = \sigma_z = \sigma_2 = \sigma_3 = \frac{\nu}{(1-2\nu)} Y_o$$

with Y_o being the uniaxial yield strength of the virgin von Mises material. As perfect plasticity is considered in this test yield strength will continue to remain Y_o.

- On further stretching in x-direction the stress state traverses along the von Mises cylindrical yield surface. Stress state after each strain increment is marked by points 1-6 in Fig. 6.2.

Table 6.1: Uniaxial Tension with Perfect Plasticity

Increment	*Strain State Vector* $\begin{Bmatrix}\varepsilon_x\\ \varepsilon_y\\ \varepsilon_z\end{Bmatrix}$	*Flow Vector* $\begin{Bmatrix}\partial f/\partial\sigma_x\\ \partial f/\partial\sigma_y\\ \partial f/\partial\sigma_z\end{Bmatrix}$	*Stress Vector* $\begin{Bmatrix}\sigma_x\\ \sigma_y\\ \sigma_z\end{Bmatrix}$	*Effective Plastic Strain* $(=d\lambda)$	*Equivalent Stress Level*
1	$\begin{Bmatrix}2.40000\\ 0.00000\\ 0.00000\end{Bmatrix}$	$\begin{Bmatrix}0.00000\\ 0.00000\\ 0.00000\end{Bmatrix}$	$\begin{Bmatrix}2.66667\\ 0.66667\\ 0.66667\end{Bmatrix}$	0.00000	2.00000
2	$\begin{Bmatrix}3.01000\\ 0.00000\\ 0.00000\end{Bmatrix}$	$\begin{Bmatrix}1.00000\\ -0.50000\\ -0.50000\end{Bmatrix}$	$\begin{Bmatrix}3.00556\\ 1.00556\\ 1.00556\end{Bmatrix}$	0.40667	2.00000
3	$\begin{Bmatrix}3.51000\\ 0.00000\\ 0.00000\end{Bmatrix}$	$\begin{Bmatrix}1.00000\\ -0.50000\\ -0.50000\end{Bmatrix}$	$\begin{Bmatrix}3.28333\\ 1.28333\\ 1.28333\end{Bmatrix}$	0.74000	2.00000
4	$\begin{Bmatrix}4.01000\\ 0.00000\\ 0.00000\end{Bmatrix}$	$\begin{Bmatrix}1.00000\\ -0.50000\\ -0.50000\end{Bmatrix}$	$\begin{Bmatrix}3.56111\\ 1.56111\\ 1.56111\end{Bmatrix}$	1.07333	2.00000
5	$\begin{Bmatrix}5.01000\\ 0.00000\\ 0.00000\end{Bmatrix}$	$\begin{Bmatrix}1.00000\\ -0.50000\\ -0.50000\end{Bmatrix}$	$\begin{Bmatrix}4.11667\\ 2.11667\\ 2.11667\end{Bmatrix}$	1.74000	2.00000
6	$\begin{Bmatrix}6.01000\\ 0.00000\\ 0.00000\end{Bmatrix}$	$\begin{Bmatrix}1.00000\\ -0.50000\\ -0.50000\end{Bmatrix}$	$\begin{Bmatrix}4.67222\\ 2.67222\\ 2.67222\end{Bmatrix}$	2.40667	2.00000

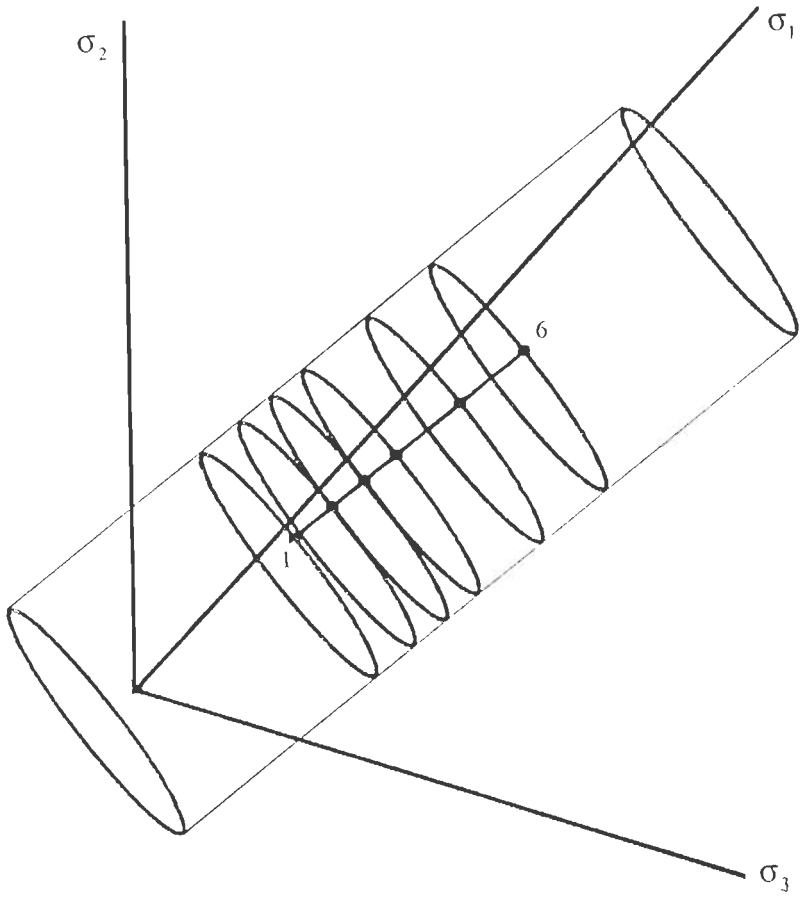

(a)

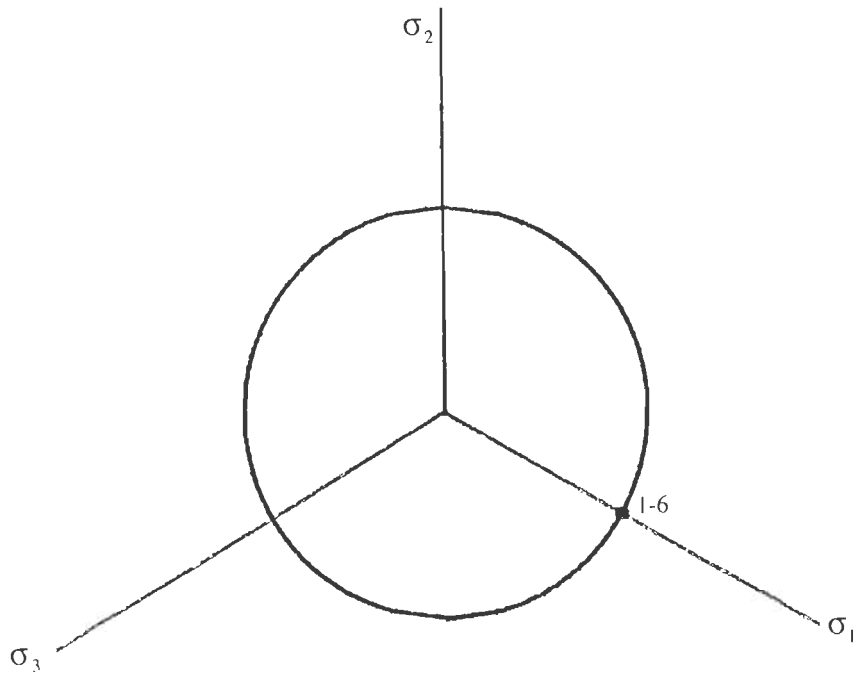

(b)

Fig. 6.2 Variation of the stress state on the Mises yield surface for uniaxial tension and perfect plasticity (a) in principal stress space (b) π−plane representation

From Fig. 6.2 it is clear that the tensile displacement of element (Fig. 6.1) keeps the stress points on tension side (all the traversed points on the von Mises yield surface lie on the positive sides of the $\sigma_1, \sigma_2, \sigma_3$ axes). It can be seen that the uniaxial stretching causes the mean stress to continuously increase (point 1 of Fig. 6.2(a) is nearest to the origin while point 6 is farthest to the origin).

The $\pi-$ plane representation of the stress changes is shown in Fig. 6.2(b). The figure illustrates that in the principal stress space all stress states lie on a single straight line. This line is the intersection of a plane projecting radially outwards from the axis of the von Mises cylinder (the hydrostatic axis). As a result, in the $\pi-$ plane all stress points coincide.

Although this test has been illustrated using a four noded element, it would be equally valid on any square element with larger number of nodes. Obviously in that case appropriate boundary conditions will need to be prescribed to all nodes on the edges. Since in this test perfect plasticity is assumed a verification with the solution proposed by Krieg and Krieg (1977) can be made as follows.

For verification the strain increment from step 1 to step 6 was considered. Using the steps outlined in subsection 6.3.1 various quantities can be evaluated as follows:

1. $R = 1.63299$

2. Starting contact stress state

$$\boldsymbol{\sigma} = \begin{Bmatrix} 2.66667 \\ 0.66667 \\ 0.00000 \\ 0.66667 \end{Bmatrix}$$

and starting deviatoric contact stress state

$$\mathbf{S}_c = \begin{Bmatrix} 1.33333 \\ -0.66667 \\ 0.00000 \\ -0.66667 \end{Bmatrix}$$

3. The strain increment from steps 1 to 6 is

$$\Delta\boldsymbol{\varepsilon} = \begin{Bmatrix} 3.61000 \\ 0.00000 \\ 0.00000 \\ 0.00000 \end{Bmatrix}$$

and the deviatoric strain increment is

$$\Delta\mathbf{e} = \begin{Bmatrix} 2.40667 \\ -1.20333 \\ 0.00000 \\ -1.20333 \end{Bmatrix}$$

4. The elastic predictor deviatoric stress increment using elastic properties of Fig. 6.1 is

$$\Delta\mathbf{S}_e = \begin{Bmatrix} 2.00555 \\ -1.00277 \\ 0.00000 \\ -1.00277 \end{Bmatrix}$$

5.

$$|\Delta\mathbf{S}_e| = 2.45629$$
$$\beta = 2.32714$$
$$C = 0.22220$$
$$\cos\psi_c = 1.00000$$
$$\mathbf{S}_1 = \begin{Bmatrix} 1.33333 \\ -0.66667 \\ 0.00000 \\ -0.66667 \end{Bmatrix}$$

The update stress is therefore

$$\boldsymbol{\sigma} = \begin{Bmatrix} 4.67222 \\ 2.67222 \\ 0.00000 \\ 2.67222 \end{Bmatrix}$$

It can be seen that this matches the stress state in step 6 of Table 6.1.

6.4.2 Benchmark Test 2: Strain Softening Element Under Uniaxial Tension

A test, similar to that discussed in the previous subsection, was conducted assuming the material of the element to be linearly strain softening. The procedure of Krieg and Krieg would not be applicable in this case. A work hardening hypothesis was assumed and the softening parameter $A = -0.25$ was used. The manner in which the stress state traverses the yield surface is shown in Fig. 6.3 and the numerical values are presented in Table 6.2. In this case the circles represented by the von Mises surface in the $\pi-$ plane

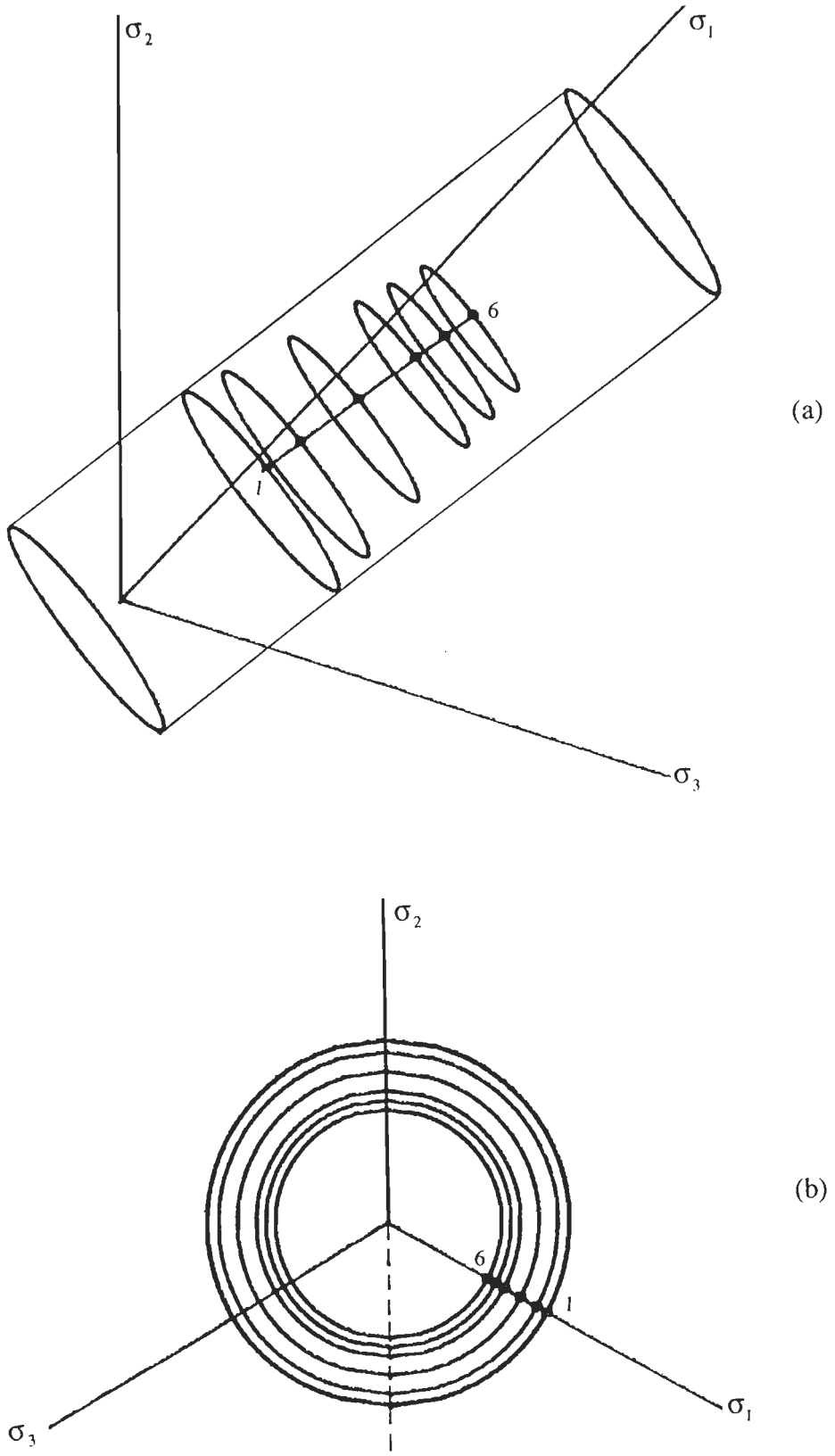

Fig. 6.3 Variation of the stress state on the Mises yield surface for uniaxial tension and strain softening (a) in principal stress space (b) $\pi-$plane representation

shrinks with increased loading. The Mises cylinder of Fig. 6.3 represents the first yield surface. The shrinking is illustrated by the decrease in the equivalent stress level of Table 6.2. As the flow vector remains constant along with the parameter A, no difficulty is encountered in integrating the rate equations of plasticity.

Table 6.2: Uniaxial Tension with Strain Softening

Increment	*Strain State Vector* $\begin{Bmatrix}\varepsilon_x\\ \varepsilon_y\\ \varepsilon_z\end{Bmatrix}$	*Flow Vector* $\begin{Bmatrix}\partial f/\partial\sigma_x\\ \partial f/\partial\sigma_y\\ \partial f/\partial\sigma_z\end{Bmatrix}$	*Stress Vector* $\begin{Bmatrix}\sigma_x\\ \sigma_y\\ \sigma_z\end{Bmatrix}$	*Effective Plastic Strain* $(=d\lambda)$	*Equivalent Stress Level*
1	$\begin{Bmatrix}2.40000\\ 0.00000\\ 0.00000\end{Bmatrix}$	$\begin{Bmatrix}0.00000\\ 0.00000\\ 0.00000\end{Bmatrix}$	$\begin{Bmatrix}2.66667\\ 0.66667\\ 0.66667\end{Bmatrix}$	0.00000	2.00000
2	$\begin{Bmatrix}3.01000\\ 0.00000\\ 0.00000\end{Bmatrix}$	$\begin{Bmatrix}1.00000\\ -0.50000\\ -0.50000\end{Bmatrix}$	$\begin{Bmatrix}2.92083\\ 1.04782\\ 1.04782\end{Bmatrix}$	0.50833	1.87292
3	$\begin{Bmatrix}4.01000\\ 0.00000\\ 0.00000\end{Bmatrix}$	$\begin{Bmatrix}1.00000\\ -0.50000\\ -0.50000\end{Bmatrix}$	$\begin{Bmatrix}3.33750\\ 1.67282\\ 1.67282\end{Bmatrix}$	1.34167	1.66458
4	$\begin{Bmatrix}5.01000\\ 0.00000\\ 0.00000\end{Bmatrix}$	$\begin{Bmatrix}1.00000\\ -0.50000\\ -0.50000\end{Bmatrix}$	$\begin{Bmatrix}3.75417\\ 2.29792\\ 2.29792\end{Bmatrix}$	2.17500	1.45625
5	$\begin{Bmatrix}5.51000\\ 0.00000\\ 0.00000\end{Bmatrix}$	$\begin{Bmatrix}1.00000\\ -0.50000\\ -0.50000\end{Bmatrix}$	$\begin{Bmatrix}3.96250\\ 2.61042\\ 2.61042\end{Bmatrix}$	2.59167	1.35208
6	$\begin{Bmatrix}6.01000\\ 0.00000\\ 0.00000\end{Bmatrix}$	$\begin{Bmatrix}1.00000\\ -0.50000\\ -0.50000\end{Bmatrix}$	$\begin{Bmatrix}4.17083\\ 2.92292\\ 2.92292\end{Bmatrix}$	3.00833	1.24792

6.4.3 Benchmark Test 3: Perfectly Plastic Element in Pure Shear

A four noded element was subjected to pure shear by prescribing displacements as shown in Fig. 6.4. This problem is again a plane strain type and the condition that the flow vector remains constant during loading process is maintained.

The traversed state of stress is shown in Fig. 6.5 and the numerical values obtained are presented in Table 6.3. It is observed from Fig. 6.5 and Table 6.3 that:

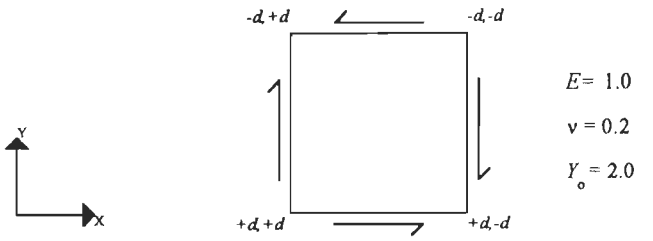

Fig 6.4 A plane strain element under pure shear

Table 6.3: Pure Shear with Perfect Plasticity

Increment	*Displacement Vector* $\begin{Bmatrix}\Delta x\\ \Delta y\end{Bmatrix}$	*Strain State Vector* $\begin{Bmatrix}\varepsilon_x\\ \varepsilon_y\\ \tau_{xy}\\ \varepsilon_z\end{Bmatrix}$	*Flow Vector* $\begin{Bmatrix}\partial f/\partial\sigma_x\\ \partial f/\partial\sigma_y\\ \partial f/\partial\tau_{xy}\\ \partial f/\partial\sigma_z\end{Bmatrix}$	*Stress Vector* $\begin{Bmatrix}\sigma_x\\ \sigma_y\\ \tau_{xy}\\ \sigma_z\end{Bmatrix}$	*Effective Plastic Strain* $(=d\lambda)$	*Equivalent Stress Level*
1	$\begin{Bmatrix}0.69282\\ 0.69282\end{Bmatrix}$	$\begin{Bmatrix}0.00000\\ 0.00000\\ -2.77128\\ 0.00000\end{Bmatrix}$	$\begin{Bmatrix}0.00000\\ 0.00000\\ 0.00000\\ 0.00000\end{Bmatrix}$	$\begin{Bmatrix}0.00000\\ 0.00000\\ -1.15470\\ 0.00000\end{Bmatrix}$	0.00000	2.00000
2	$\begin{Bmatrix}1.20000\\ 1.20000\end{Bmatrix}$	$\begin{Bmatrix}0.00000\\ 0.00000\\ -4.80000\\ 0.00000\end{Bmatrix}$	$\begin{Bmatrix}0.00000\\ 0.00000\\ -1.73205\\ 0.00000\end{Bmatrix}$	$\begin{Bmatrix}0.00000\\ 0.00000\\ -1.15470\\ 0.00000\end{Bmatrix}$	1.17128	2.00000
3	$\begin{Bmatrix}1.70000\\ 1.70000\end{Bmatrix}$	$\begin{Bmatrix}0.00000\\ 0.00000\\ -6.80000\\ 0.00000\end{Bmatrix}$	$\begin{Bmatrix}0.00000\\ 0.00000\\ -1.73205\\ 0.00000\end{Bmatrix}$	$\begin{Bmatrix}0.00000\\ 0.00000\\ -1.15470\\ 0.00000\end{Bmatrix}$	2.32598	2.00000
4	$\begin{Bmatrix}2.20000\\ 2.20000\end{Bmatrix}$	$\begin{Bmatrix}0.00000\\ 0.00000\\ -8.80000\\ 0.00000\end{Bmatrix}$	$\begin{Bmatrix}0.00000\\ 0.00000\\ -1.73205\\ 0.00000\end{Bmatrix}$	$\begin{Bmatrix}0.00000\\ 0.00000\\ -1.15470\\ 0.00000\end{Bmatrix}$	3.48068	2.00000
5	$\begin{Bmatrix}2.70000\\ 2.70000\end{Bmatrix}$	$\begin{Bmatrix}0.00000\\ 0.00000\\ -10.80000\\ 0.00000\end{Bmatrix}$	$\begin{Bmatrix}0.00000\\ 0.00000\\ -1.73205\\ 0.00000\end{Bmatrix}$	$\begin{Bmatrix}0.00000\\ 0.00000\\ -1.15470\\ 0.00000\end{Bmatrix}$	4.63538	2.00000
6	$\begin{Bmatrix}3.20000\\ 3.20000\end{Bmatrix}$	$\begin{Bmatrix}0.00000\\ 0.00000\\ -12.80000\\ 0.00000\end{Bmatrix}$	$\begin{Bmatrix}0.00000\\ 0.00000\\ -1.73205\\ 0.00000\end{Bmatrix}$	$\begin{Bmatrix}0.00000\\ 0.00000\\ -1.15470\\ 0.00000\end{Bmatrix}$	5.79008	2.00000

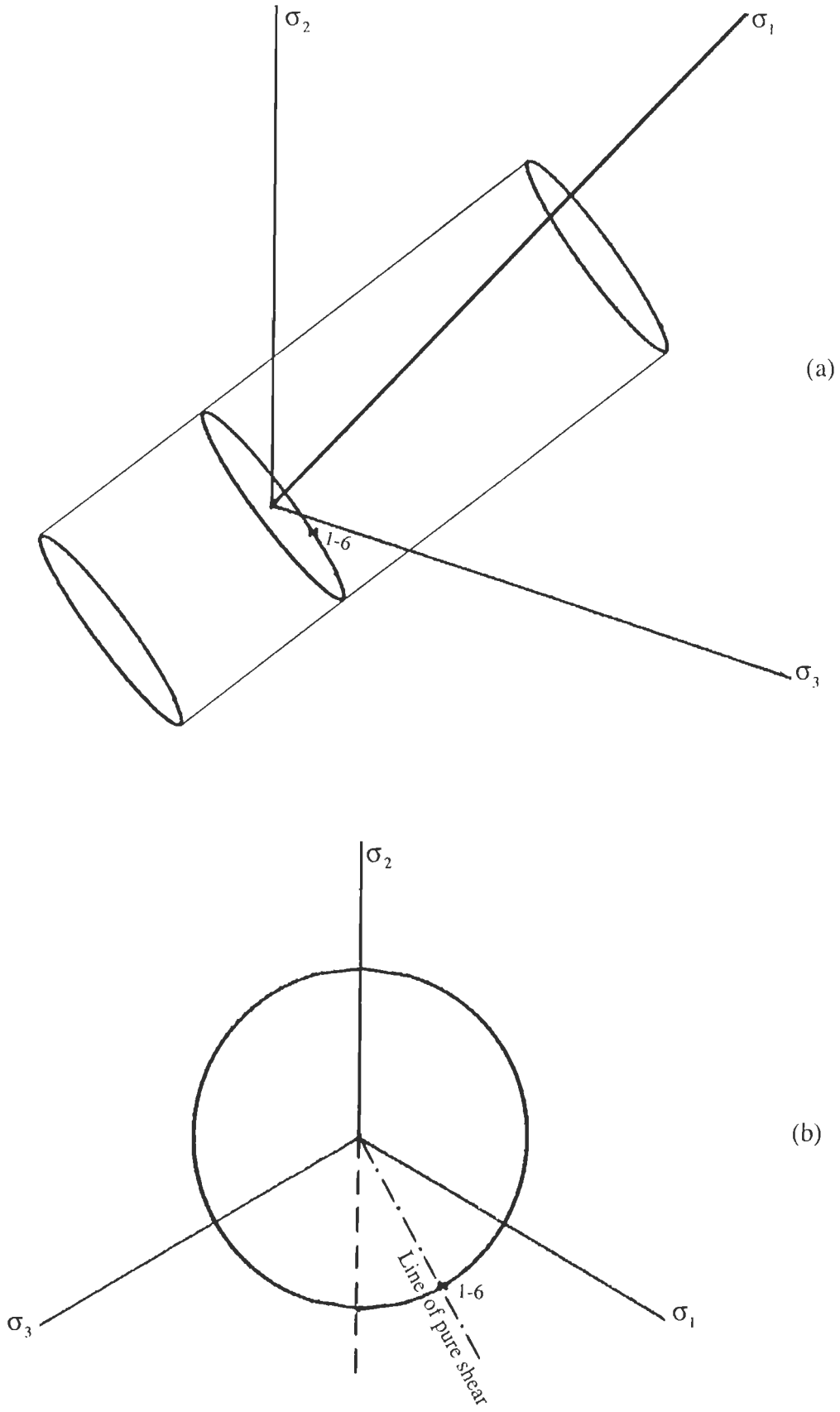

Fig. 6.5 Variation of the stress state on the Mises yield surface for pure shear and perfect plasticity (a) in principal stress space (b) $\pi-$plane representation

- The first step ($d = 0.69282$) takes the stress state elastically to the von Mises yield surface. The state of pure shear stress at the first yield is represented by

$$\tau_{xy} = Y_o / \sqrt{3}$$

The other components of the stress are obviously zero.

- Further increment in displacement causes the stress state to remain at the same position on the yield surface, since a constant state of stress ($\tau_{xy} = -1.15470$) is maintained throughout the post-yield straining process in which d is increased. This is because any additional shear strain after initial yield contributes only to the plastic strain increment. As elastic strain increment remains zero the stress state remains unchanged. For the purpose of plotting this state of pure shear was resolved into maximum and minimum principal stress components σ_1 and σ_2 as

$$\sigma_1 = \tau_{xy}$$

$$\sigma_2 = -\tau_{xy}$$

- In the $\pi-$plane representation it can be seen that the stress points lie on the line of pure shear.

6.4.4 Benchmark Test 4: Strain Softening Element in Pure Shear

The test of subsection 6.4.3 was repeated with a strain softening element. Linear strain softening with softening parameter $A = -0.25$ was assumed. The manner in which the stress state traverses the yield surface is shown in Fig. 6.6 respectively and the numerical values are presented in Table 6.4.

All stress points lie on a line projecting radially outwards from the origin as can be seen from Fig. 6.6. The figure also illustrates the changes in the radius of Mises cylinder.

6.5 Development Of Benchmark Tests For Mohr Coulomb Criterion

In this section exact solutions for Mohr Coulomb elastoplasticity that include linear strain hardening or softening plasticity, are developed (Pankaj and Moin, 1991,1996).

Table 6.4: Pure Shear with Strain Softening

Increment	*Displacement Vector* $\begin{Bmatrix}\Delta x\\ \Delta y\end{Bmatrix}$	*Strain State Vector* $\begin{Bmatrix}\varepsilon_x\\ \varepsilon_y\\ \tau_{xy}\\ \varepsilon_z\end{Bmatrix}$	*Flow Vector* $\begin{Bmatrix}\partial f/\partial\sigma_x\\ \partial f/\partial\sigma_y\\ \partial f/\partial\tau_{xy}\\ \partial f/\partial\sigma_z\end{Bmatrix}$	*Stress Vector* $\begin{Bmatrix}\sigma_x\\ \sigma_y\\ \tau_{xy}\\ \sigma_z\end{Bmatrix}$	*Effective Plastic Strain* $(=d\lambda)$	*Equivalent Stress Level*
1	$\begin{Bmatrix}0.69282\\ 0.69282\end{Bmatrix}$	$\begin{Bmatrix}0.00000\\ 0.00000\\ -2.77128\\ 0.00000\end{Bmatrix}$	$\begin{Bmatrix}0.00000\\ 0.00000\\ 0.00000\\ 0.00000\end{Bmatrix}$	$\begin{Bmatrix}0.00000\\ 0.00000\\ -1.15470\\ 0.00000\end{Bmatrix}$	0.00000	2.00000
2	$\begin{Bmatrix}1.20000\\ 1.20000\end{Bmatrix}$	$\begin{Bmatrix}0.00000\\ 0.00000\\ -4.80000\\ 0.00000\end{Bmatrix}$	$\begin{Bmatrix}0.00000\\ 0.00000\\ -1.73205\\ 0.00000\end{Bmatrix}$	$\begin{Bmatrix}0.00000\\ 0.00000\\ -0.94337\\ 0.00000\end{Bmatrix}$	1.46410	1.63397
3	$\begin{Bmatrix}1.70000\\ 1.70000\end{Bmatrix}$	$\begin{Bmatrix}0.00000\\ 0.00000\\ -6.80000\\ 0.00000\end{Bmatrix}$	$\begin{Bmatrix}0.00000\\ 0.00000\\ -1.73205\\ 0.00000\end{Bmatrix}$	$\begin{Bmatrix}0.00000\\ 0.00000\\ -0.73504\\ 0.00000\end{Bmatrix}$	2.90748	1.27313
4	$\begin{Bmatrix}2.20000\\ 2.20000\end{Bmatrix}$	$\begin{Bmatrix}0.00000\\ 0.00000\\ -8.80000\\ 0.00000\end{Bmatrix}$	$\begin{Bmatrix}0.00000\\ 0.00000\\ -1.73205\\ 0.00000\end{Bmatrix}$	$\begin{Bmatrix}0.00000\\ 0.00000\\ -0.52671\\ 0.00000\end{Bmatrix}$	4.35085	0.09123
5	$\begin{Bmatrix}2.70000\\ 2.70000\end{Bmatrix}$	$\begin{Bmatrix}0.00000\\ 0.00000\\ -10.80000\\ 0.00000\end{Bmatrix}$	$\begin{Bmatrix}0.00000\\ 0.00000\\ -1.73205\\ 0.00000\end{Bmatrix}$	$\begin{Bmatrix}0.00000\\ 0.00000\\ -0.31837\\ 0.00000\end{Bmatrix}$	5.79423	0.55144
6	$\begin{Bmatrix}3.60000\\ 3.60000\end{Bmatrix}$	$\begin{Bmatrix}0.00000\\ 0.00000\\ -13.80000\\ 0.00000\end{Bmatrix}$	$\begin{Bmatrix}0.00000\\ 0.00000\\ -1.73205\\ 0.00000\end{Bmatrix}$	$\begin{Bmatrix}0.00000\\ 0.00000\\ -0.00587\\ 0.00000\end{Bmatrix}$	7.95929	0.01077

The Mohr Coulomb yield surface in the principal stress space is a pyramid with six planes (Fig. 6.7). The difficulty with such an yield surface is the presence of singular regions due to the edges (where two planes meet) and apex (where all six planes meet). Here consideration is limited to the cases where either only one plane is involved or when any edge is involved, in the integration of the stress strain law. Solutions for each of these cases are derived in turn in the following subsections.

6.5.1 One Active Plane

The Mohr Coulomb yield criterion in terms of principal stresses can be written as (Owen and Hinton, 1980).

$$F = \frac{1}{2}(\sigma_1 - \sigma_3) + \frac{1}{2}(\sigma_1 + \sigma_3)\sin\phi - c\cos\phi = 0 \qquad (6.4)$$

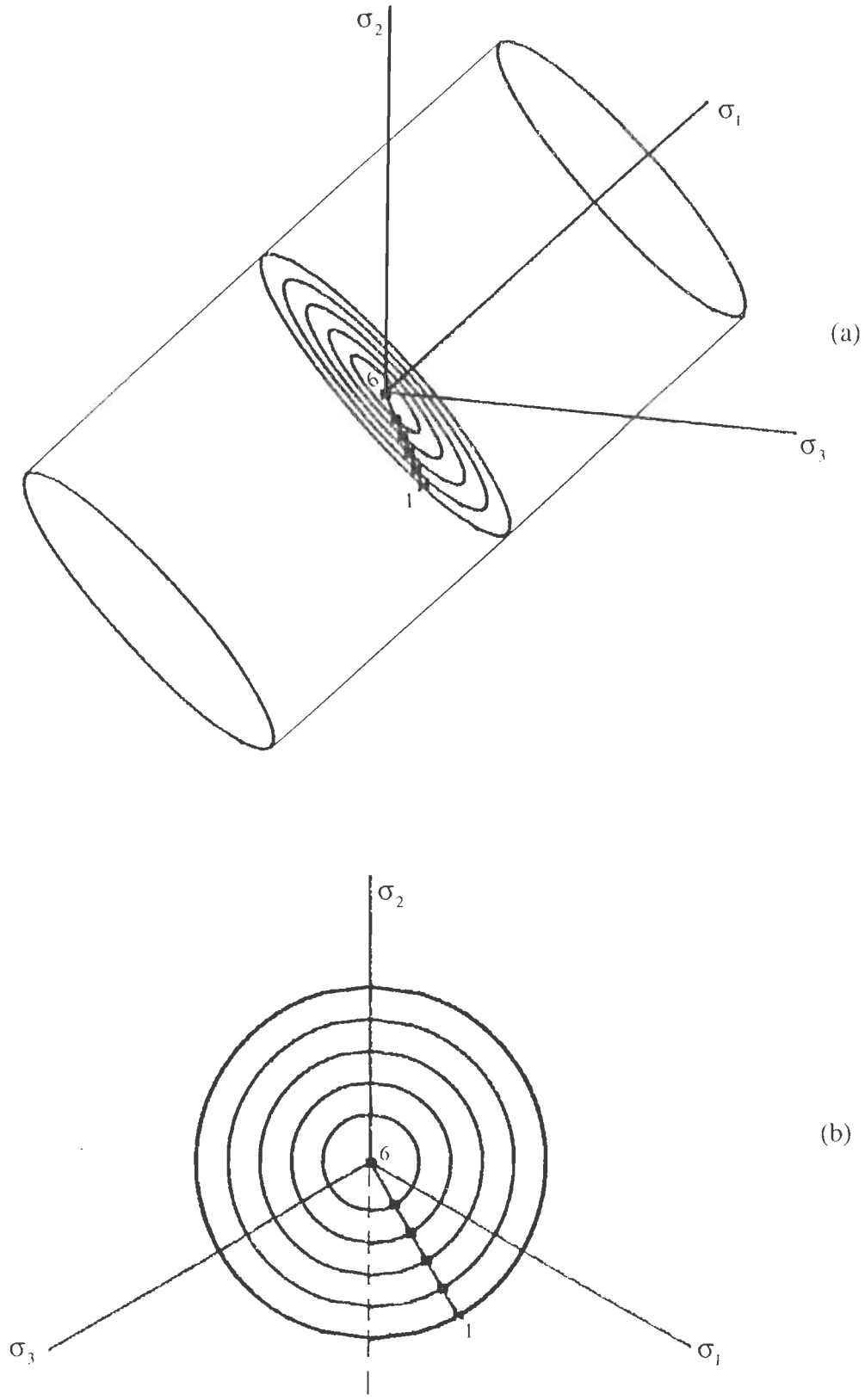

Fig. 6.6 Variation of the stress state on the Mises yield surface for pure shear and strain softening (a) in principal stress space (b) π−plane representation

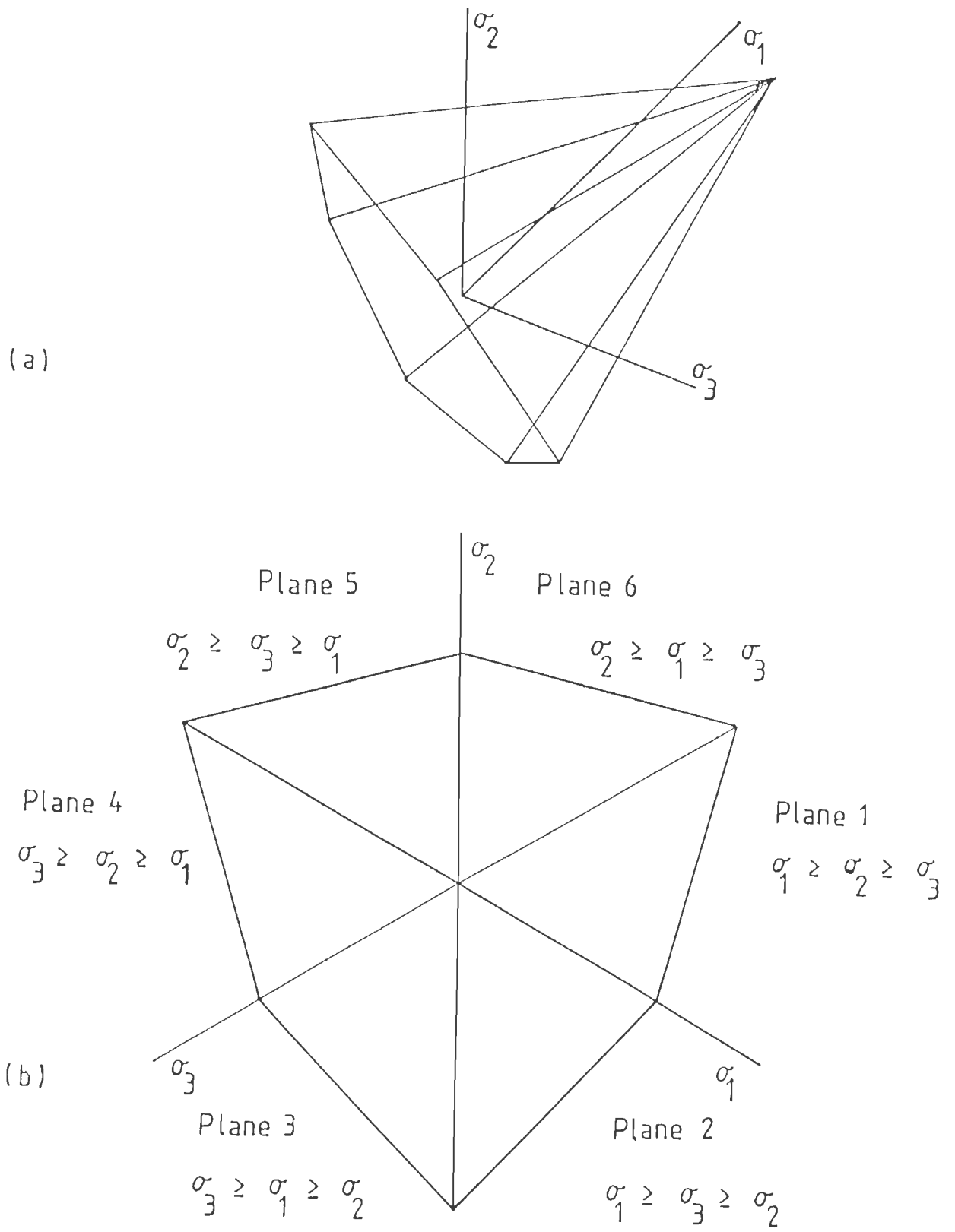

Fig. 6.7 Mohr Coulomb yield surface (a) in principal stress space (b) π−plane representation

where σ_1 and σ_3 are the principal stresses with $\sigma_1 \geq \sigma_2 \geq \sigma_3$; and c and ϕ are cohesion and friction angle respectively. The complete yield surface represents a set of six planes (Fig. 6.7) in the principal stress space and the use of Eqn. 6.4 implies using the sextant where $\sigma_1 \geq \sigma_2 \geq \sigma_3$ [Fig. 6.7(b)] (Pankaj and Bicanic, 1989).

Equation 6.4 is linear equation in terms of principal stresses σ_i; thereby if the Cartesian axes are aligned with the principal stress directions the flow vector **a** would comprise of six constants, of which those corresponding to intermediate principal stress and shear stress would be zero at any given stress state. If it can be ensured that this flow vector and parameter A do not change during plastic loading the elastoplastic matrix would become a constant making integration of Eqn. 6.1 straightforward. This can be ensured in the principal stress space if a test is devised in which (a) parameters A remain unchanged; (b) the finite principal strain increment is aligned in the direction of principal stress and; (c) the strain increment is such that the same plane remains active during the loading step.

For the above conditions one can work out $\mathbf{D}^{ep}$ with respect to the three principal directions using

$$\mathbf{a} = \begin{pmatrix} \frac{\partial f}{\partial \sigma_1} \\ \frac{\partial f}{\partial \sigma_1} \\ \frac{\partial f}{\partial \sigma_1} \end{pmatrix} = \frac{1}{2}\begin{pmatrix} s+1 \\ 0 \\ s-1 \end{pmatrix} \tag{6.5}$$

and

$$\mathbf{D} = \mathrm{B}\begin{pmatrix} 1-\nu & \nu & \nu \\ \nu & 1-\nu & \nu \\ \nu & \nu & 1-\nu \end{pmatrix} \tag{6.6}$$

where $s = \sin\phi$ and $\mathrm{B} = E/((1+\nu)(1-2\nu))$. The exact elastoplastic modulus matrix for this case can be evaluated and is given by

$$\mathbf{D}^{ep} = \begin{pmatrix} d_{11} & d_{12} & d_{13} \\ d_{21} & d_{22} & d_{23} \\ d_{31} & d_{32} & d_{33} \end{pmatrix} \tag{6.7}$$

where

$$d_{11} = \mathrm{B}(1-\nu) - k(1-4\nu+4\nu^2-4\nu s+2s+s^2)$$
$$d_{12} = \mathrm{B}\nu - k(2\nu s-4\nu^2 s+2\nu s^2)$$

$$
\begin{aligned}
d_{13} &= \mathrm{B}\nu - k(-1 + 4\nu - 4\nu^2 + s^2) \\
d_{21} &= d_{12} \\
d_{22} &= \mathrm{B}(1-\nu) - 4k\nu^2 s^2 \\
d_{23} &= \mathrm{B}\nu - k(-2\nu s + 4\nu^2 s + 2\nu s^2) \\
d_{31} &= d_{13} \\
d_{32} &= d_{23} \\
d_{33} &= \mathrm{B}(1-\nu) - k(1 - 4\nu + 4\nu^2 + 4\nu s - 2s + s^2)
\end{aligned} \tag{6.8}
$$

and

$$
k = \mathrm{B}^2 / [4\{\mathrm{A} + (\mathrm{B}/2)(1 - 2\nu + s^2)\}] \tag{6.9}
$$

Now the exact integration of Eqn. 6.1 is straightforward as the finite stress increment, for a single active plane, can be obtained simply by premultiplying the above evaluated $\mathbf{D}^{ep}$ matrix by the finite strain increment. It can be verified that the elastoplastic modulus matrix is singular, though unique, for perfect plasticity (A=0) and nonsingular for $\mathrm{A} > 0$.

6.5.2 Two active planes

When more than one "yield planes" become active simultaneously, in associated plasticity, Koiter (1953) showed that

$$
d\boldsymbol{\varepsilon}^{\mathrm{p}} = \sum_{j=1}^{m} d\lambda_j \frac{\partial F_j}{\partial \boldsymbol{\sigma}} \tag{6.10}
$$

where m is the number of active yield functions (m=2 in this case).Thus with the aid of Eqn. 6.10, the Eqn. 6.1 can be rewritten as

$$
d\boldsymbol{\sigma} = \mathbf{D}\left(d\boldsymbol{\varepsilon} - d\boldsymbol{\varepsilon}^{p}\right) = \mathbf{D}\left(d\boldsymbol{\varepsilon} - \sum_{j=1}^{m} d\lambda_j \mathbf{a}_j\right) \tag{6.11}
$$

where $\mathbf{a}_j = \partial F_j / \partial \boldsymbol{\sigma}$. It can be shown that the incremental plastic multiplier $d\lambda_i$ (i=1 *to* m) now need to be evaluated by solving the simultaneous equations (Pankaj and Bicanic, 1989)

$$
d\lambda_i + \sum_{j=1, j\neq i}^{m} \left(\frac{\mathrm{A}_{ij} + \mathbf{a}_i^T \mathbf{D} \mathbf{a}_j}{\mathrm{A}_{ii} + \mathbf{a}_i^T \mathbf{D} \mathbf{a}_i} \right) d\lambda_j = \frac{\mathbf{a}_i^T \mathbf{D} d\boldsymbol{\varepsilon}}{\mathrm{A}_{ii} + \mathbf{a}_i^T \mathbf{D} \mathbf{a}_i} \tag{6.12}
$$

where

$$A_{ij} = -\frac{\partial F_i}{\partial \kappa}\left(\frac{\partial \kappa}{\partial \varepsilon^p}\right)^T \frac{\partial F_j}{\partial \sigma} \tag{6.13}$$

Once again, for Mohr Coulomb plasticity, when two planes are active (m=2) then if (a) A_{ij} are kept constant; (b) the principal strain increments are aligned in the direction of principal stress; and (c) it is ensured that the same edge remain active during the finite strain increment; then it is easy to compute the elastoplastic modulus matrix which becomes a constant. Here it is important to point out that for strain hardening format the parameters A_{ij} become nonlinear functions of plastic multiplier $d\lambda_i$. In contrast, with work hardening format, A_{ij} (=A) for all i,j are the same (Pankaj and Moin, 1991) and it is easy to derive $\mathbf{D}^{ep}$ for multiple active yield planes.

In order to illustrate the above consider that in addition to the planes defined by Eqn. 6.47, the active plane is

$$F_2 = \frac{1}{2}(\sigma_1 - \sigma_2) + \frac{1}{2}(\sigma_1 + \sigma_2)\sin\phi - c\cos\phi = 0 \tag{6.14}$$

then the elements of matrix $\mathbf{D}^{ep}$ (Eqn. 6.7) with the aid of Eqns. 6.11-6.12 for the principal stress/strain directions are

$$\begin{aligned}
d_{11} &= \mathrm{B}(1-\nu) - \frac{\mathrm{B}^2}{2}(\mathrm{C}_1 - \mathrm{C}_2)\left(1 - 4\nu + 4\nu^2 - 4\nu s + 2s + s^2\right) \\
d_{12} &= \mathrm{B}\nu - \frac{\mathrm{B}^2}{4}(\mathrm{C}_1 - \mathrm{C}_2)\left[2\nu s(1 - 2\nu + s) + \left(-1 + 4\nu - 4\nu^2 + s^2\right)\right] \\
d_{13} &= d_{12} \\
d_{21} &= d_{12} \\
d_{22} &= \mathrm{B}(1-\nu) - \mathrm{C}_1\mathrm{B}^2\nu^2 s^2 + \mathrm{C}_2\mathrm{B}^2\nu s(-1 + 2\nu + s) - \frac{\mathrm{C}_1\mathrm{B}^2}{4}\left(1 - 4\nu - 2s + 4\nu^2 + 4\nu s + s^2\right) \\
d_{23} &= \mathrm{B}\nu + \mathrm{C}_2\mathrm{B}^2\nu^2 s^2 - \mathrm{C}_1\mathrm{B}^2\nu s(-1 + 2\nu + s) - \frac{\mathrm{C}_2\mathrm{B}^2}{4}\left(1 - 4\nu - 2s + 4\nu^2 + 4\nu s + s^2\right) \\
d_{31} &= d_{13} \\
d_{32} &= d_{23} \\
d_{33} &= d_{22}
\end{aligned} \tag{6.15}$$

where

$$\mathrm{C}_1 = \frac{\mathrm{A} + \frac{\mathrm{B}}{2}\left(1 - 2\nu + s^2\right)}{\left\{\mathrm{A} + \frac{\mathrm{B}}{2}(1 - 2\nu + s^2)\right\}^2 - \left\{\mathrm{A} + \frac{\mathrm{B}}{4}(1 - 2\nu + 2s - 4\nu s + s^2 + 2\nu s^2)\right\}^2}$$

$$C_2 = \frac{A + \frac{B}{4}\left(1 - 2\nu + 2s - 4\nu s + s^2 + 2\nu s^2\right)}{\{A + \frac{B}{2}(1 - 2\nu + s^2)\}^2 - \{A + \frac{B}{4}(1 - 2\nu + 2s - 4\nu s + s^2 + 2\nu s^2)\}^2} \tag{6.16}$$

Similarly, for any two active surfaces the constant elastoplastic modulus matrix can be computed.

It is seen that this matrix is rank deficient for perfect as well as for hardening/softening plasticity. However the matrix is unique and would yield a unique stress increment for a given strain increment.

6.6 Benchmark Tests for Mohr Coulomb Criterion

Five simple tests that follow a prescribed displacement field approach and are conducted on a single element are now described.

The loading considered here is in the form of prescribed displacements in x, y and z-directions. For each of the tests considered numerical values at the end of each increment are given in a tabular form. Stress changes are also illustrated using a three dimensional plot in the principal stress space. The same changes are also shown using a $\pi-$plane representation in many cases. As the mean stress changes, the $\pi-$plane on which the stress point lies also changes. The $\pi-$planes corresponding to stresses for each step have been plotted. Thus when the stress point moves towards the apex the corresponding $\pi-$plane polygon becomes smaller and as it moves away the polygon becomes larger. The basic data assumed is $E = 1.0$, $\nu = 0.2$, $\phi = 30°$ and $c\cos\phi = 2.25$.

6.6.1 Benchmark Tests 1: Biaxial Displacement with Perfect Plasticity

Prescribed displacements are applied to a single element as shown in Fig. 6.8. The manner in which the stress state traverses the yield surface is shown in Fig. 6.9 and the numerical values obtained on integrating the required equations are illustrated in Table 6.5. The following observations can be made from Fig. 6.9 and Table 6.5

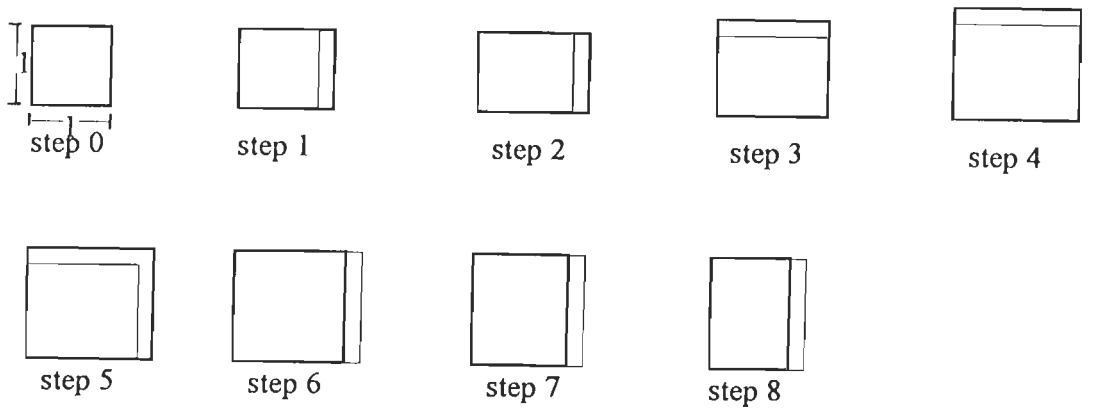

Fig. 6.8 Application of biaxial prescribed displacements to the element for perfect/hardening plasticity

1. The principal stress axes will remain in x, y and z-directions (Fig. 6.8) throughout the straining history and therefore, there will be no shear stress along these directions.

2. Step 1 takes the stress point elastically to the yield surface. At this point a corner in the Mohr Coulomb yield surface is encountered with

$$\sigma_x = \sigma_1 = \frac{2c\cos\phi(1-\nu)}{1-2\nu+\sin\phi}$$

$$\sigma_y = \sigma_z = \sigma_2 = \sigma_3 = \frac{\nu}{1-\nu}\sigma_1 \qquad (6.17)$$

3. Step 2 (further stretching in the x-direction) keeps the stress point on the same edge of the surface, the mean stress is increased and the stress point moves along the edge towards the apex of the Mohr Coulomb pyramid. In this step two yield planes become active and remain active during the stretching.

4. On stretching in the y-direction (Step 3) stress point moves away from the edge and only one plane of the yield surface is active with $\sigma_x > \sigma_y > \sigma_z$ *i.e.* $\sigma_1 > \sigma_2 > \sigma_3$.

5. On further stretching in the y-direction (Step 4) stress point moves to the edge where $\sigma_x = \sigma_y > \sigma_z$, *i.e.* $\sigma_1 = \sigma_2 > \sigma_3$. During this step care is taken to stretch it to an extent that during the stretching process only one plane remains active till the stress point moves to the edge.

6. In Step 5 the element is stretched simultaneously in x and y-directions. The stress point moves along the edge where $\sigma_x = \sigma_y$.

7. Compression in the x-direction (Step 6) brings the stress point back inside the yield surface.

8. Further compression in the x-direction first brings the stress point to the yield plane with $\sigma_y > \sigma_z > \sigma_x$ (Step 7) and still further compression (Step 8) keeps the stress point on that plane.

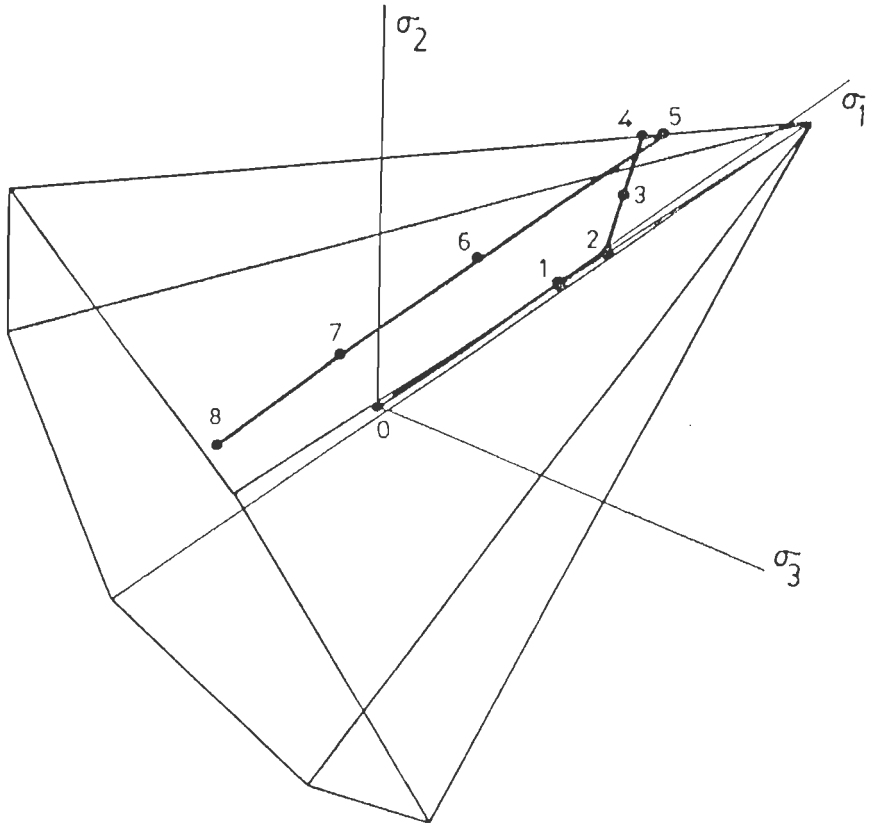

Fig. 6.9 Variation of the stress state on the Mohr Coulomb yield surface for biaxial displacement and perfect plasticity

Table 6.5: Biaxial Displacement with Perfect Plasticity

Step	$\Delta\varepsilon_x$	$\Delta\varepsilon_y$	σ_x	σ_y	σ_z	$c\cos\phi$
1	2.945	0.000	3.273	0.818	0.818	2.250
2	2.945	0.000	3.499	1.498	1.498	2.250
3	0.000	1.000	3.597	2.576	1.792	2.250
4	0.000	1.041	3.699	3.699	2.098	2.250
5	0.300	0.300	3.773	3.773	2.318	2.250
6	−3.000	0.000	0.439	2.939	1.485	2.250
7	−2.237	0.000	−2.046	2.318	0.863	2.250
8	−2.000	0.000	−4.252	1.582	0.275	2.250

In a similar manner several steps can be added to check the performance of any computer code in various regions of the surface.

6.6.2 Benchmark Tests 2: Biaxial Displacement with Hardening Plasticity

As has been discussed if a constant hardening modulus is assumed, it is straightforward to integrate the stress strain relations even for hardening plasticity. In this example (Pankaj and Moin, 1991) the manner in which prescribed displacements have been applied is the same as that done in the previous example. Work hardening format has been followed and $H = \partial c / \partial \varepsilon_y^p = 0.13333$ ($A_{ij} = 0.1$) has been assumed. The results are illustrated in Table 6.6. Clearly due to hardening the values of the prescribed displacements will be different if a stress path similar to the one in the previous example is to be traversed. Moreover, the yield surface will expand during Steps, 2,3,4,5 and 8.

6.6.3 Benchmark Tests 3: Biaxial Displacement with Softening Plasticity

To illustrate typical prescribed displacement format test with isotropic strain softening plasticity, a plane strain biaxial type test is considered. Displacements are prescribed as shown in Fig. 6.10. A work hardening hypothesis with $A_{ij} = -0.1$ was employed. The results are illustrated in Table 6.7 and the manner in which the stress state traverses the yield surface is shown in Fig. 6.11.

Table 6.6: Biaxial Displacement with Hardening Plasticity

Step	$\Delta\varepsilon_x$	$\Delta\varepsilon_y$	σ_x	σ_y	σ_z	$c\cos\phi$
1	2.945	0.000	3.273	0.818	0.818	2.250
2	2.945	0.000	3.958	1.519	1.519	2.589
3	0.000	1.473	4.141	3.114	1.948	2.618
4	0.000	1.070	4.273	4.273	2.261	2.640
5	0.300	0.300	4.422	4.422	2.469	2.699
6	−4.000	0.000	−2.255	3.311	1.357	2.699
7	−3.032	0.000	−3.391	2.469	0.515	2.699
8	−3.000	0.000	−6.704	1.405	−0.360	2.729

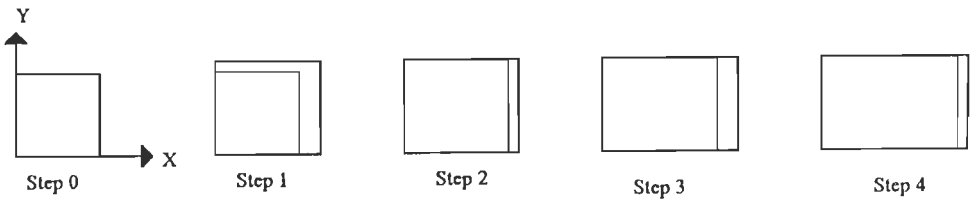

Fig. 6.10 Application of biaxial prescribed displacements to the element for strain softening

Table 6.7: Biaxial Displacement with Strain Softening

Step	$\Delta\varepsilon_x$	$\Delta\varepsilon_y$	σ_x	σ_y	σ_z	$c\cos\phi$
1	2.700000	1.350000	3.375000	2.250000	1.125000	2.250000
2	3.465825	0.000000	3.100908	2.462729	2.462729	1.710000
3	1.000000	0.000000	2.955060	2.683372	2.683372	1.545440
4	0.500000	0.000000	2.882135	2.793695	2.793695	1.463178

6.6.4 Benchmark Test 4: Triaxial Displacement with Perfect Plasticity

Prescribed displacements are applied to a single element as shown in Fig. 6.12. The manner in which the stress state traverses the yield surface is shown in Fig. 6.13. The numerical values obtained from the closed form solution discussed, are illustrated in Table 6.8. The following observations can be made from Fig. 6.13 and Table 6.8.

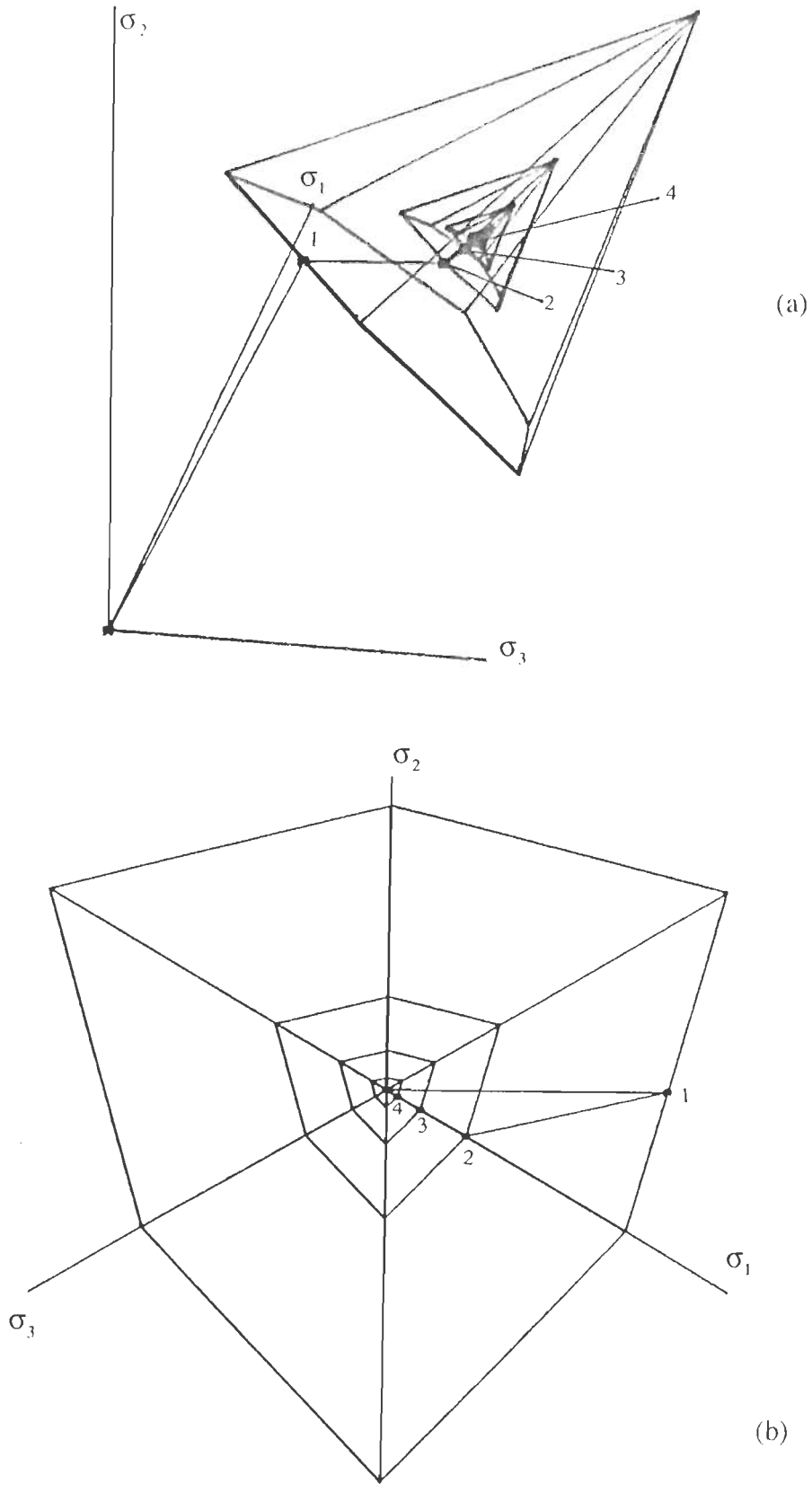

Fig. 6.11 Movement of stress point in and on the Mohr Coulomb yield surface for biaxial displacement and strain softening (a) in principal stress space (b) $\pi-$plane representation

1. The principal axes will remain in x, y and z-directions (Fig. 6.12) throughout the straining history and therefore, there will be no shear stresses along these directions. Thus one can employ $\sigma_1 \equiv \sigma_x$, $\sigma_2 \equiv \sigma_y$ and $\sigma_3 \equiv \sigma_z$.

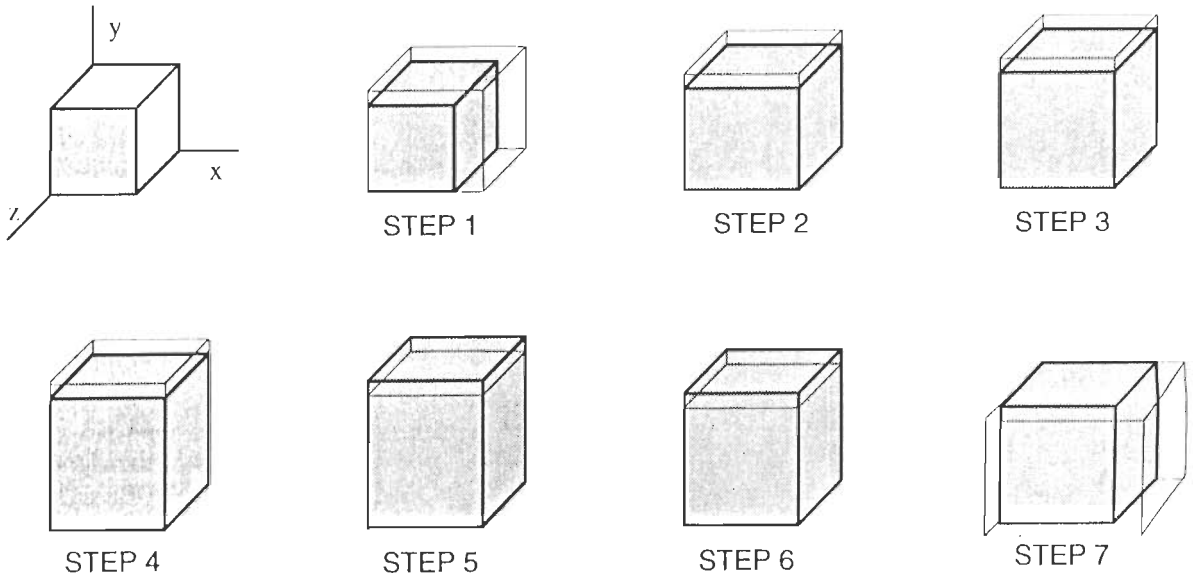

Fig. 6.12 Application of triaxial prescribed displacement to the element with perfect plasticity

2. Step 1 (stretching in x and y-directions) takes the stress point elastically to the yield surface. At the end of this step Plane 1 [Fig 6.7(b)] is reached elastically with

$$\sigma_x = \sigma_1 = \frac{2c\cos\phi(1-\nu/2)}{1-2\nu+\sin\phi(1+\nu)}$$

$$\sigma_y = \sigma_2 = \frac{c\cos\phi(1+\nu)}{1-2\nu+\sin\phi(1+\nu)}$$

$$\sigma_z = \sigma_3 = \frac{3c\nu\cos\phi}{1-2\nu+\sin\phi(1+\nu)} \qquad (6.18)$$

3. Step 2 (further stretching in y-direction only) keeps the stress point on Plane 1 and, therefore, only one plane remains active. Care is taken to limit this stretching to an extent that stress point just reaches the edge of Plane 1 and Plane 6 (refer Fig. 6.7). At this stage $\sigma_1 = \sigma_2 > \sigma_3$.

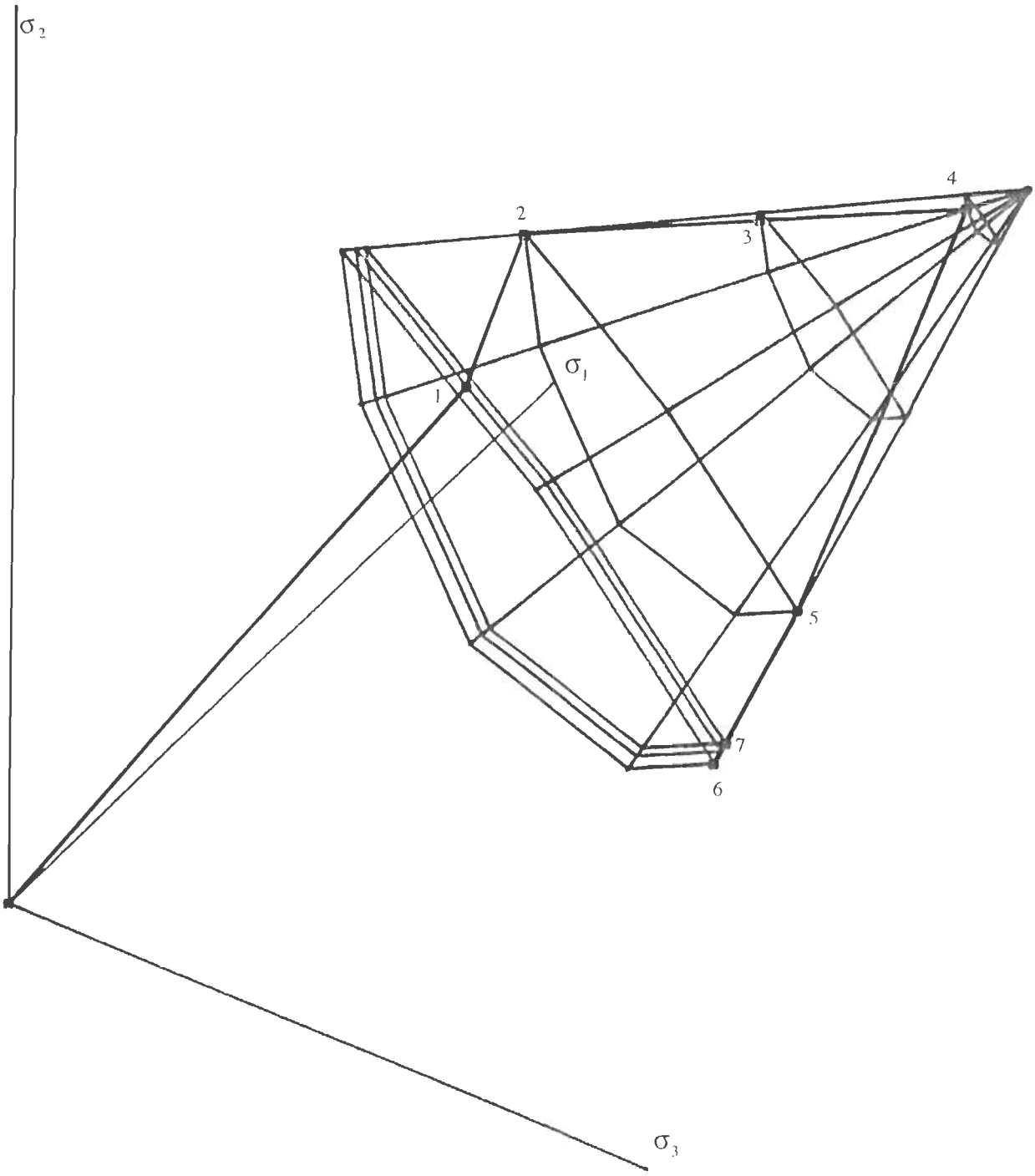

(a)

Continued

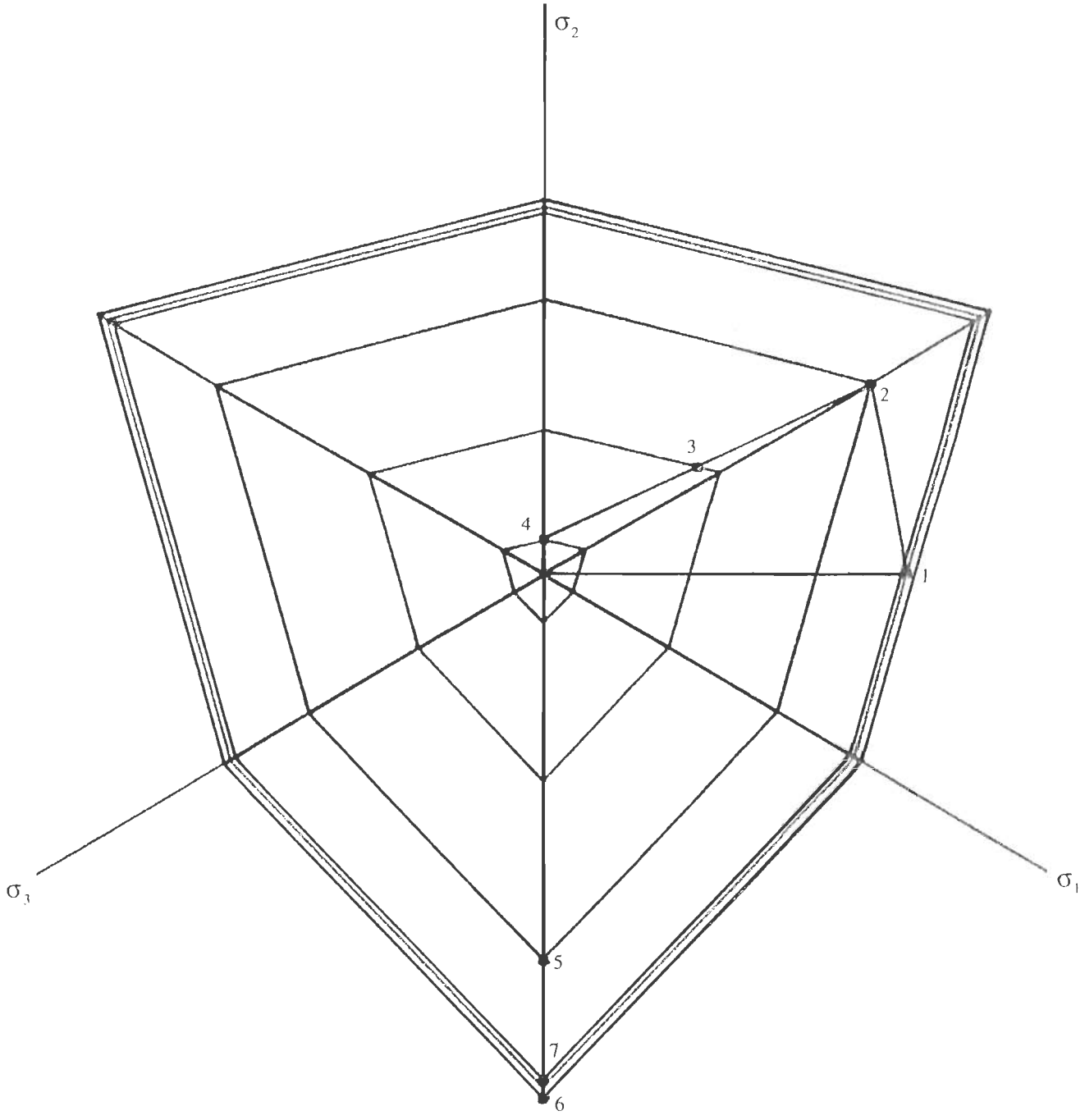

(b)

Fig. 6.13 Movement of stress point in and on the Mohr Coulomb yield surface for triaxial displacement and perfect plasticity (a) in principal stress space (b) π – plane representation

4. Further stretching in the y-direction (Step 3) the stress point immediately moves away from the edge and traverses on Plane 6 ($\sigma_2 > \sigma_1 > \sigma_3$). Thus once again during this stretching only one plane remains active.

5. In Step 4 stretching in the y-direction is continued till the edge of Plane 6 and Plane 5 is encountered where $\sigma_2 > \sigma_1 = \sigma_3$.

6. The element is now compressed in the y-direction (Step 5). This compression brings the stress points in the elastic regime. The compression is limited to an extent that the yield surface is just encountered at the edge of the intersection of planes 2 and 3 ($\sigma_1 = \sigma_3 > \sigma_2$). Clearly during this increment there will be no addition to the plastic strains.

7. In Step 6 the element is further compressed in the y-direction. The stress point remains on the edge of planes 2 and 3 as both planes become active in this step.

8. Tensile strains are applied simultaneously in x and z-directions in Step 7. During this prescribed straining, Planes 2 and 3 continue to remain active as before.

Table 6.8: Triaxial Displacement with Perfect Plasticity

Step	$\Delta\varepsilon_x$	$\Delta\varepsilon_y$	$\Delta\varepsilon_z$	σ_x	σ_y	σ_z	$c\cos\phi$
1	2.70000	1.35000	0.00000	3.37500	2.25000	1.12500	2.250
2	0.00000	1.14750	0.00000	3.48750	3.48750	1.46250	2.250
3	0.00000	4.00000	0.00000	3.87966	3.97770	2.93309	2.250
4	0.00000	3.51091	0.00000	4.22386	4.40795	4.22386	2.250
5	0.00000	−2.65090	0.00000	3.48750	1.46251	3.48750	2.250
6	0.00000	−1.00000	0.00000	3.12165	0.36494	3.12165	2.250
7	0.20000	0.00000	0.20000	3.17043	0.51129	3.17043	2.250

6.6.5 Benchmark Test 5: Triaxial Displacement with Hardening Plasticity

In the present example a constant $A_{ij} = 0.1$ was assumed *i.e.* $H = \partial c / \partial \varepsilon_y^p = 0.13333$. The prescribed displacement field was applied as shown in Fig. 6.14 and the results are illustrated in Fig. 6.15 and Table 6.9. It can be seen from Fig. 6.15 that the yield surface

expands with plastic loading, however, no difficulty is encountered in computing the exact stress increment. As in the last example π-planes corresponding to stresses in each step have been plotted and shown in Fig. 6.15(b). Observations similar to those made in the last example can be made in this example as well. In this example, however, the equivalent yield strength, represented by $c\cos\phi$, goes on increasing with plastic loading. This can be seen from the last column of Table 6.9.

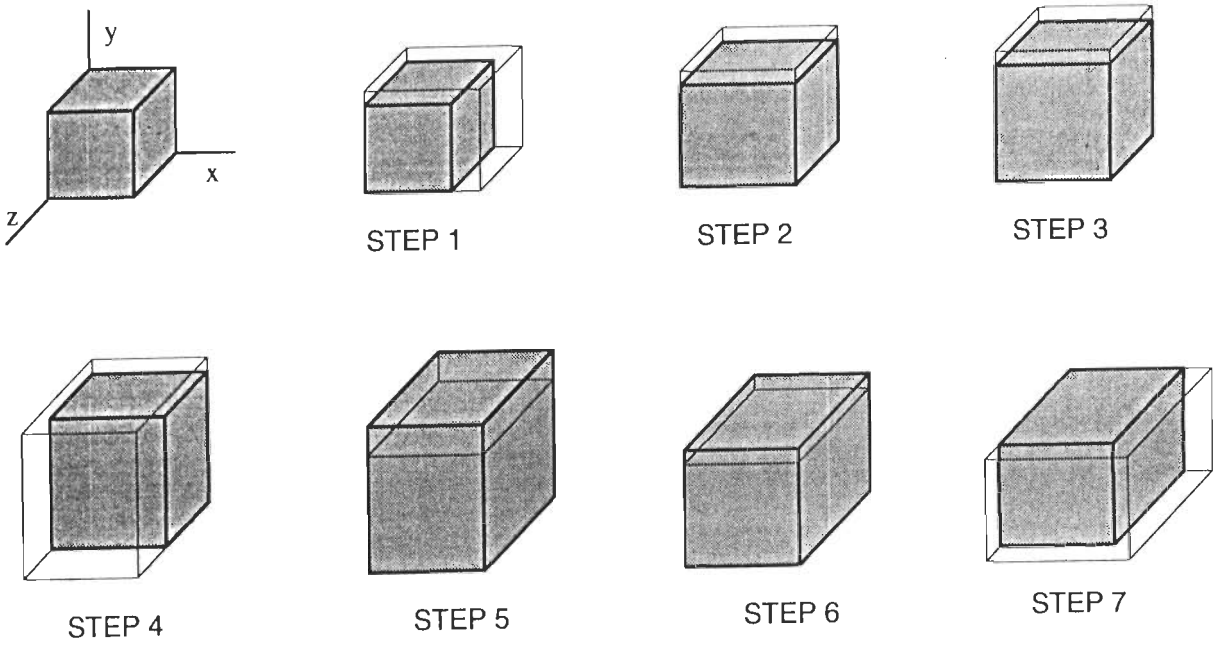

Fig. 6.14 Application of triaxial prescribed displacement to the element with hardening plasticity

Table 6.9: Triaxial Displacement with Hardening Plasticity

Step	$\Delta\varepsilon_x$	$\Delta\varepsilon_y$	$\Delta\varepsilon_z$	σ_x	σ_y	σ_z	$c\cos\phi$
1	2.70000	1.35000	0.00000	3.37500	2.25000	1.12500	2.250
2	0.00000	1.17299	0.00000	3.52054	3.52054	1.46722	2.274
3	0.00000	1.00000	0.00000	3.64462	3.78630	1.82185	2.384
4	0.00000	0.21818	2.18185	4.30825	4.61803	4.30826	2.386
5	0.00000	−4.46080	0.00000	3.06914	−0.33841	3.06914	2.386
6	0.00000	−1.00000	0.00000	2.72260	−1.43894	2.72261	2.402
7	0.20000	0.00000	0.20000	2.82161	−1.30033	2.82162	2.441

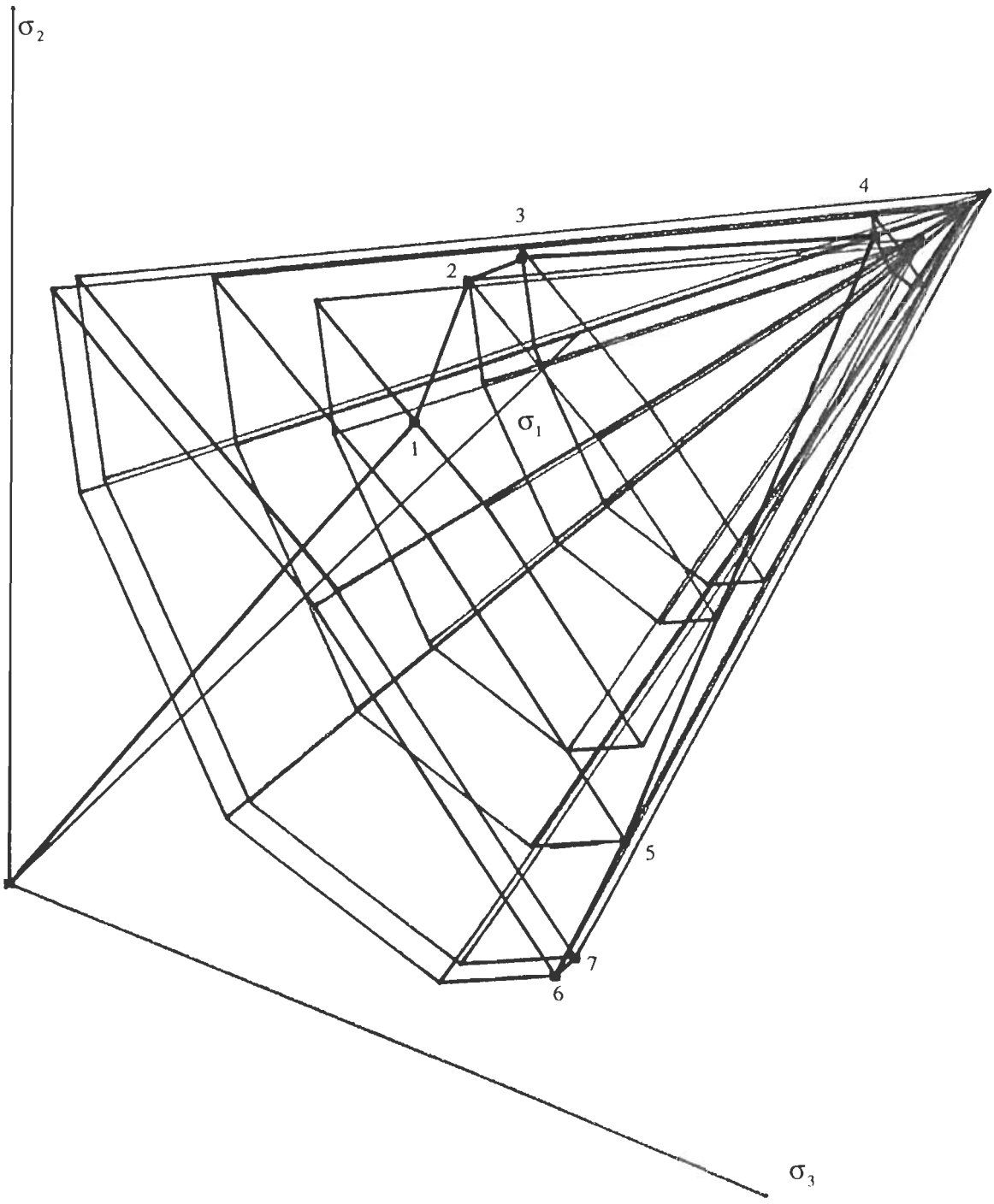

(a)

— *Continued*

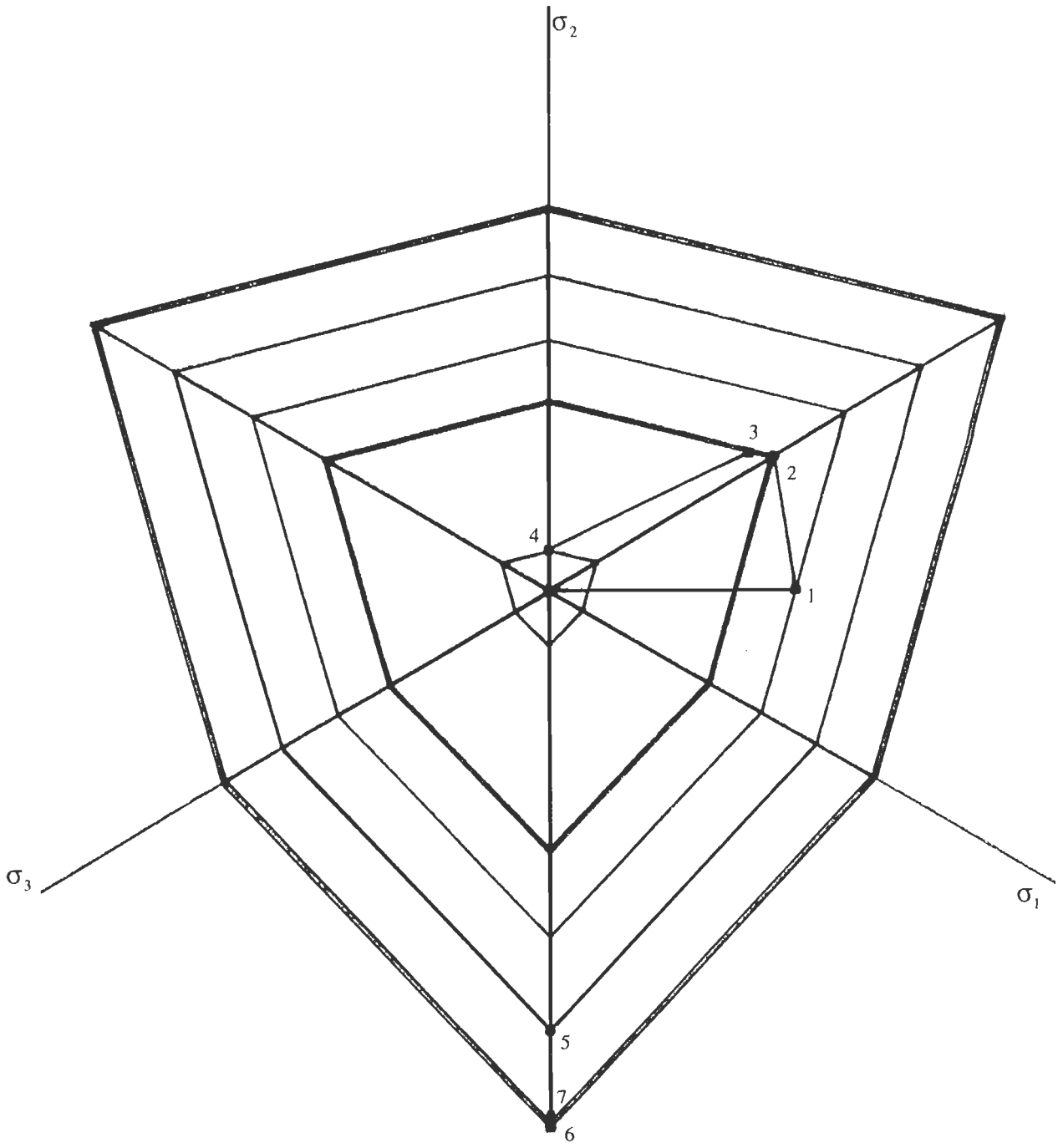

(b)

Fig. 6.15 Variation of the of the stress state in and on the Mohr Coulomb yield surface for triaxial displacement and hardening plasticity (a) in principal stress space (b) $\pi-$plane representation

6.7 Illustrative Tests for Hoffman Criterion

As discussed earlier the isotropic form of the Hoffman criterion is a cylindrical paraboloid in the principal stress space as shown in Fig. 6.16. As such it is not straightforward to

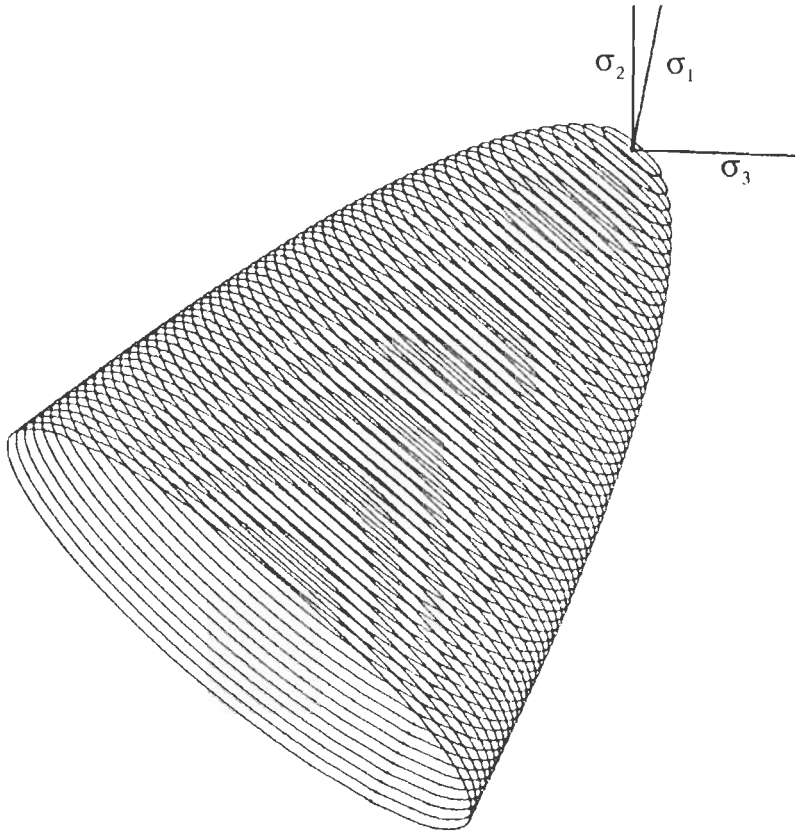

Fig. 6.16 Hoffman yield surface in principal stress space

evolve closed form solutions for this criterion. However, tests that can illustrate the stress changes in the principal stress space and can serve as tools for understanding are considered. The algorithm discussed earlier was used for stress computations. Once again tests are based on single elements on which prescribed displacements are applied.

6.7.1 Test 1: Uniaxial Tension with Perfect Plasticity

A four noded square plane strain single element with unit sides was subjected to a uniaxial strain as shown in Fig. 6.17. Once again for the plane strain case the relationship $\sigma_y = \sigma_z$ is always maintained.

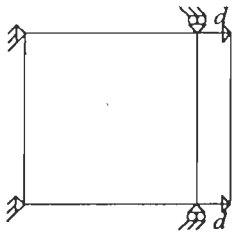

E = 200000.0
ν = 0.25
f_c = 10000.0
f_t = 1000.0 or 9000.0

Fig. 6.17 Uniaxial tension on a single element

The manner in which the stress state traverses the yield surface is shown in Fig. 6.18 and the numerical values are presented in Table 6.10. The first yield is encountered at

Table 6.10: Uniaxial Tension with Perfect Plasticity, (f_{co} = 10000 and f_{to} = 1000)

Increment	*Strain State Vector* $\begin{Bmatrix}\varepsilon_x\\ \varepsilon_y\\ \varepsilon_z\end{Bmatrix}$	*Flow Vector* $\begin{Bmatrix}\partial f/\partial\sigma_x\\ \partial f/\partial\sigma_y\\ \partial f/\partial\sigma_z\end{Bmatrix}$	*Stress Vector* $\begin{Bmatrix}\sigma_x\\ \sigma_y\\ \sigma_z\end{Bmatrix}$	*Effective Plastic Strain* $(=d\lambda)$	*Equivalent Stress Level*
1	$\begin{Bmatrix}0.00272\\ 0.00000\\ 0.00000\end{Bmatrix}$	$\begin{Bmatrix}0.00000\\ 0.00000\\ 0.00000\end{Bmatrix}$	$\begin{Bmatrix}653.99384\\ 217.99795\\ 217.99795\end{Bmatrix}$	0.00000	1.0×10^7
2	$\begin{Bmatrix}0.00880\\ 0.00000\\ 0.00000\end{Bmatrix}$	$\begin{Bmatrix}11549.00\\ 7725.00\\ 7725.00\end{Bmatrix}$	$\begin{Bmatrix}1.16016\times10^3\\ -1.14835\times10^2\\ -1.14835\times10^2\end{Bmatrix}$	0.00314	1.0×10^7
3	$\begin{Bmatrix}0.02380\\ 0.00000\\ 0.00000\end{Bmatrix}$	$\begin{Bmatrix}14806.00\\ 6096.80\\ 6096.80\end{Bmatrix}$	$\begin{Bmatrix}1.99365\times10^3\\ -9.09514\times10^2\\ -9.09514\times10^2\end{Bmatrix}$	0.01171	1.0×10^7
4	$\begin{Bmatrix}0.05380\\ 0.00000\\ 0.00000\end{Bmatrix}$	$\begin{Bmatrix}19006.00\\ 3997.00\\ 3997.00\end{Bmatrix}$	$\begin{Bmatrix}2.77866\times10^3\\ -2.22431\times10^3\\ -2.22431\times10^3\end{Bmatrix}$	0.03156	1.0×10^7
5	$\begin{Bmatrix}0.08380\\ 0.00000\\ 0.00000\end{Bmatrix}$	$\begin{Bmatrix}21514.00\\ 2743.10\\ 2743.10\end{Bmatrix}$	$\begin{Bmatrix}3.09670\times10^3\\ -3.16519\times10^3\\ -3.16519\times10^3\end{Bmatrix}$	0.05334	1.0×10^7
6	$\begin{Bmatrix}3.11380\\ 0.00000\\ 0.00000\end{Bmatrix}$	$\begin{Bmatrix}26999.00\\ 00000.01\\ 00000.01\end{Bmatrix}$	$\begin{Bmatrix}3.37037\times10^3\\ -5.62962\times10^3\\ -5.62962\times10^3\end{Bmatrix}$	2.52150	1.0×10^7

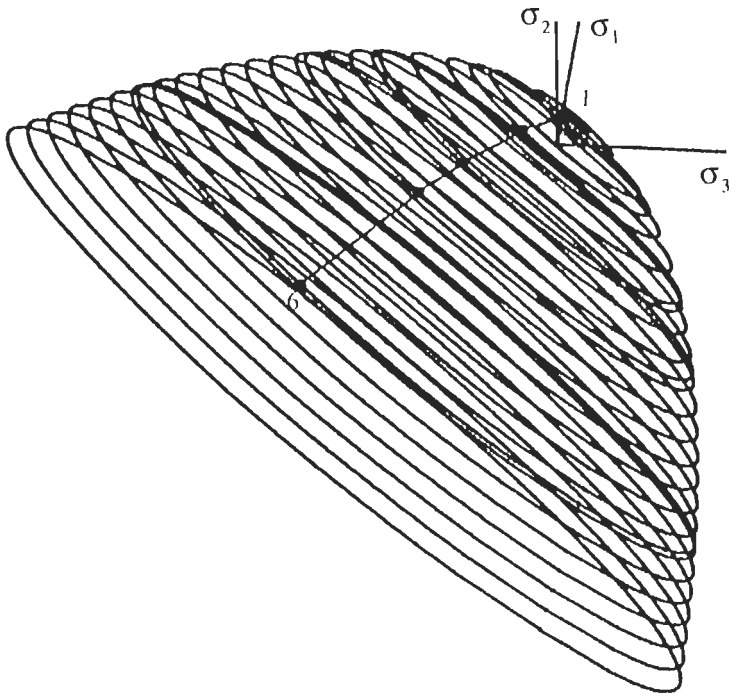

(a)

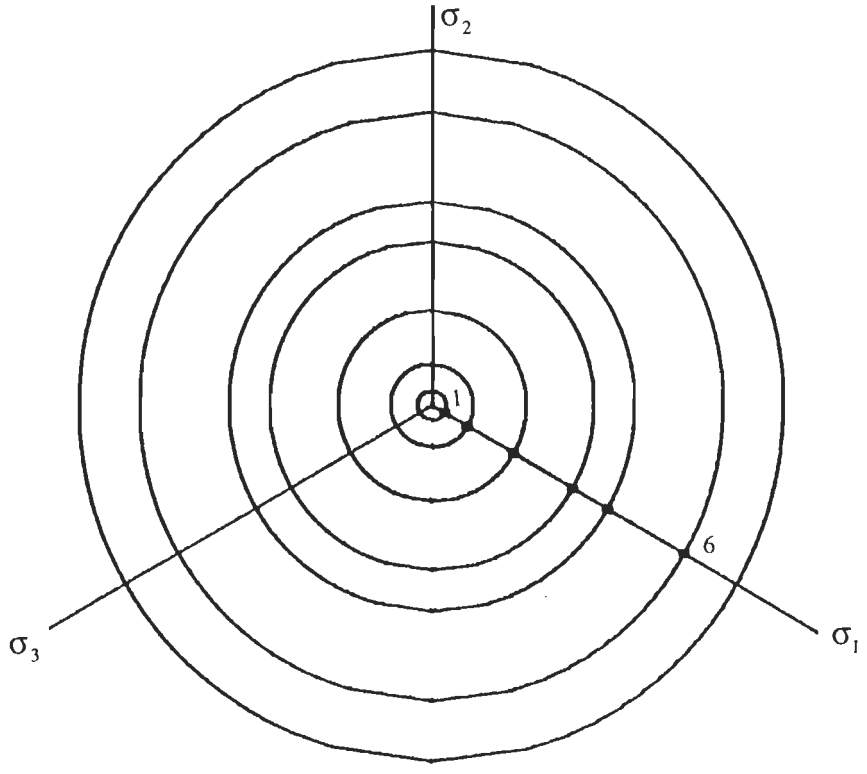

(b)

Fig. 6.18 Movement of stress point on the Hoffman yield surface for uniaxial tension and perfect plasticity with $f_{co} = 10000$ and $f_{to} = 1000$ (a) in principal stress space (b) $\pi-$plane representation

$$\sigma_x = \frac{(1-\nu)\left[-(1+\nu)(f_c - f_t) + \sqrt{(1+\nu)^2(f_c - f_t)^2 + 4f_c f_t (1-2\nu)^2}\right]}{2(1-2\nu)^2}$$

$$\sigma_y = \sigma_z = \left(\frac{\nu}{1-\nu}\right)\sigma_x \qquad (6.19)$$

After yielding the flow vector keeps changing for each step as shown in Table 6.10, while a constant stress level ($= f_c f_t$) is maintained. Once again the principal stress axes remain parallel to x, y and z direction throughout the straining history and no shear stresses are induced.

It is interesting to observe that the stress state tends to move towards the compressive side of the hydrostatic stress axis with increased tension as can be seen from Fig. 6.18. The reason is that while there is a monotonic increase in the tensile stress σ_x the σ_y and σ_z stresses become compressive in a manner causing a decrease in the mean stress (Table 6.10). This apparently is due to excessive dilatation caused by the criterion.

If f_c is kept at 10000 while f_t is increased to 9000 then the uniaxial straining test yields results as shown in Table 6.11 and Fig. 6.19. It can be seen that in this case the stress points move towards the apex of the Hoffman surface with increased uniaxial strain. This is a trend which is similar to that observed for the von Mises criterion.

Table 6.11: Uniaxial Tension with Perfect Plasticity, ($f_{co} = 10000$ and $f_{to} = 9000$)

Increment	*Strain State Vector* $\begin{Bmatrix}\varepsilon_x\\ \varepsilon_y\\ \varepsilon_z\end{Bmatrix}$	*Flow Vector* $\begin{Bmatrix}\partial f/\partial\sigma_x\\ \partial f/\partial\sigma_y\\ \partial f/\partial\sigma_z\end{Bmatrix}$	*Stress Vector* $\begin{Bmatrix}\sigma_x\\ \sigma_y\\ \sigma_z\end{Bmatrix}$	*Effective Plastic Strain* $(= d\lambda)$	*Equivalent Stress Level*
1	$\begin{Bmatrix}0.05199\\ 0.00000\\ 0.00000\end{Bmatrix}$	$\begin{Bmatrix}0.00000\\ 0.00000\\ 0.00000\end{Bmatrix}$	$\begin{Bmatrix}1.24782\times10^4\\ 4.15941\times10^3\\ 4.15941\times10^3\end{Bmatrix}$	0.00000	9.0×10^7
2	$\begin{Bmatrix}0.05809\\ 0.00000\\ 0.00000\end{Bmatrix}$	$\begin{Bmatrix}0.17383\times10^5\\ -0.71914\times10^4\\ -0.71914\times10^4\end{Bmatrix}$	$\begin{Bmatrix}1.30946\times10^4\\ 4.90322\times10^3\\ 4.90322\times10^3\end{Bmatrix}$	0.00461	9.0×10^7
3	$\begin{Bmatrix}0.07309\\ 0.00000\\ 0.00000\end{Bmatrix}$	$\begin{Bmatrix}0.16742\times10^5\\ -0.68712\times10^4\\ -0.68712\times10^4\end{Bmatrix}$	$\begin{Bmatrix}1.45957\times10^4\\ 6.72451\times10^3\\ 6.72451\times10^3\end{Bmatrix}$	0.01599	9.0×10^7
4	$\begin{Bmatrix}0.10309\\ 0.00000\\ 0.00000\end{Bmatrix}$	$\begin{Bmatrix}0.15394\times10^5\\ -0.61972\times10^4\\ -0.61972\times10^4\end{Bmatrix}$	$\begin{Bmatrix}1.75316\times10^4\\ 1.03344\times10^4\\ 1.03344\times10^4\end{Bmatrix}$	0.03891	9.0×10^7
5	$\begin{Bmatrix}0.13309\\ 0.00000\\ 0.00000\end{Bmatrix}$	$\begin{Bmatrix}0.13940\times10^5\\ -0.54698\times10^4\\ -0.54698\times10^4\end{Bmatrix}$	$\begin{Bmatrix}2.03603\times10^4\\ 1.38904\times10^4\\ 1.38904\times10^4\end{Bmatrix}$	0.06206	9.0×10^7
6	$\begin{Bmatrix}0.26309\\ 0.00000\\ 0.00000\end{Bmatrix}$	$\begin{Bmatrix}0.47984\times10^4\\ -0.18992\times10^4\\ -0.18992\times10^4\end{Bmatrix}$	$\begin{Bmatrix}2.91310\times10^4\\ 2.62318\times10^4\\ 2.62318\times10^4\end{Bmatrix}$	0.16607	9.0×10^7

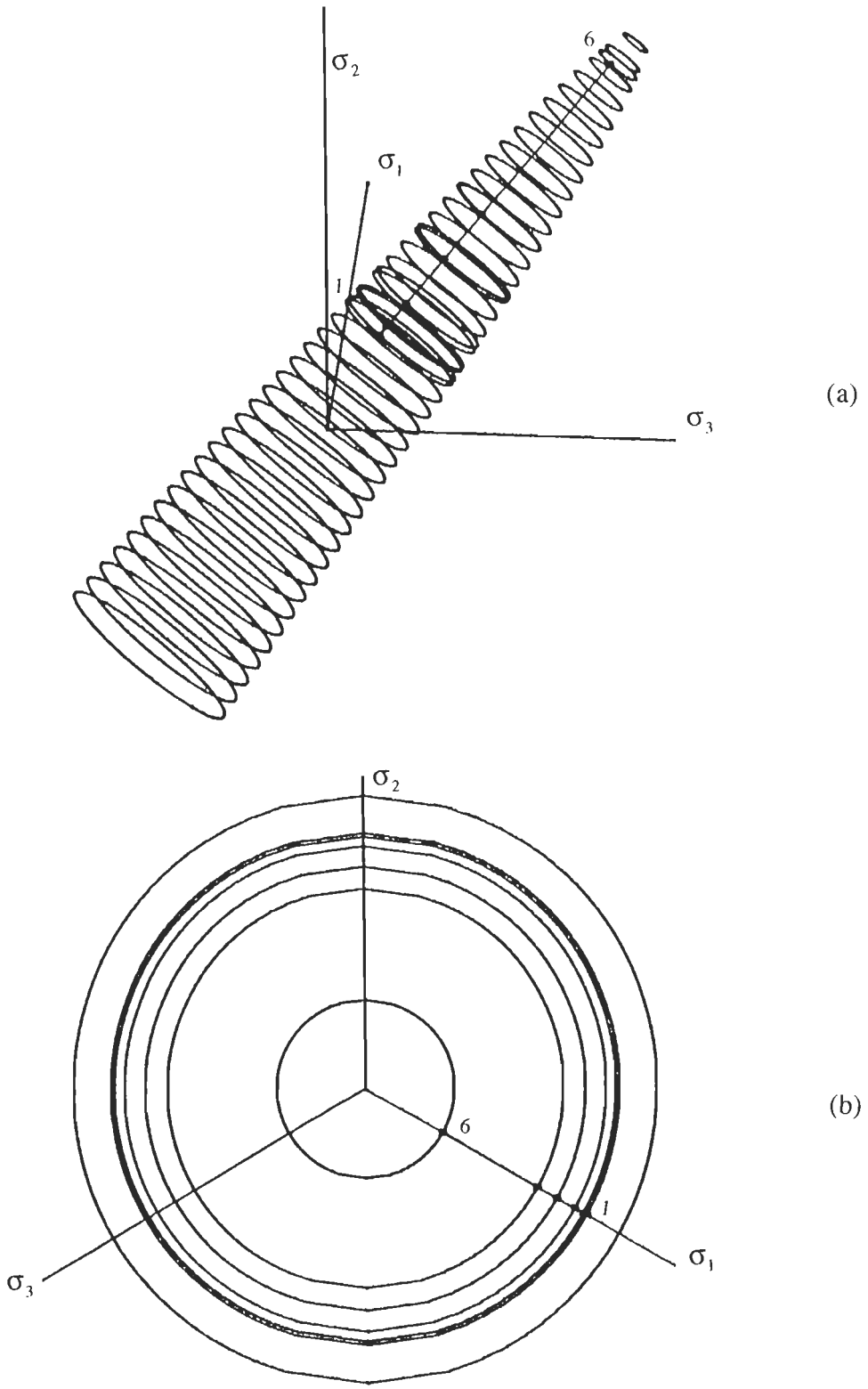

Fig. 6.19 Movement of stress point on the Hoffman yield surface for uniaxial tension and perfect plasticity with $f_{co} = 10000$ and $f_{to} = 9000$ (a) in principal stress space (b) $\pi-$plane representation

6.7.2 Test 2: Uniaxial Compression with Perfect Plasticity

A single element was subjected to a uniaxial compression as shown in Fig. 6.20.

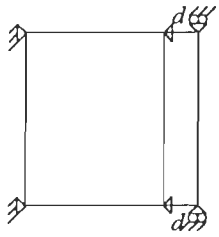

E = 200000.0 f_c = 10000.0
ν = 0.25 f_t = 1000.0

Fig. 6.20 Uniaxial compression on a single element

The manner in which the stresses traverse the yield surface is shown in Fig. 6.21 and numerical values are given in Table 6.12. The first yield is encountered at

$$\sigma_x = \frac{(1-\nu)\left[-(1+\nu)(f_c - f_t) - \sqrt{(1+\nu)^2(f_c - f_t)^2 + 4 f_c f_t (1-2\nu)^2}\right]}{2(1-2\nu)^2}$$

$$\sigma_y = \sigma_z = \left(\frac{\nu}{1-\nu}\right)\sigma_x \qquad (6.20)$$

Table 6.12: Uniaxial Compression with Perfect Plasticity, (f_{co} = 10000 and f_{to} = 1000)

Increment	*Strain State Vector* $\begin{Bmatrix}\varepsilon_x\\ \varepsilon_y\\ \varepsilon_z\end{Bmatrix}$	*Flow Vector* $\begin{Bmatrix}\partial f/\partial\sigma_x\\ \partial f/\partial\sigma_y\\ \partial f/\partial\sigma_z\end{Bmatrix}$	*Stress Vector* $\begin{Bmatrix}\sigma_x\\ \sigma_y\\ \sigma_z\end{Bmatrix}$	*Effective Plastic Strain* $(= d\lambda)$	*Equivalent Stress Level*
1	$\begin{Bmatrix}-0.14335\\ 0.00000\\ 0.00000\end{Bmatrix}$	$\begin{Bmatrix}0.00000\\ 0.00000\\ 0.00000\end{Bmatrix}$	$\begin{Bmatrix}-3.44039\times10^4\\ -1.14679\times10^4\\ -1.14679\times10^4\end{Bmatrix}$	0.00000	10^7
2	$\begin{Bmatrix}-0.16835\\ 0.00000\\ 0.00000\end{Bmatrix}$	$\begin{Bmatrix}-4.12293\times10^4\\ 3.41146\times10^4\\ 3.41146\times10^4\end{Bmatrix}$	$\begin{Bmatrix}-3.97337\times10^4\\ -1.46190\times10^4\\ -1.46190\times10^4\end{Bmatrix}$	0.00783	10^7
3	$\begin{Bmatrix}-0.19335\\ 0.00000\\ 0.00000\end{Bmatrix}$	$\begin{Bmatrix}-4.52447\times10^4\\ 3.61223\times10^4\\ 3.61223\times10^4\end{Bmatrix}$	$\begin{Bmatrix}-4.49564\times10^4\\ -1.78341\times10^4\\ -1.78341\times10^4\end{Bmatrix}$	0.01636	10^7
4	$\begin{Bmatrix}-0.24335\\ 0.00000\\ 0.00000\end{Bmatrix}$	$\begin{Bmatrix}-5.24667\times10^4\\ 3.97334\times10^4\\ 3.97334\times10^4\end{Bmatrix}$	$\begin{Bmatrix}-5.51015\times10^4\\ -2.43681\times10^4\\ -2.43681\times10^4\end{Bmatrix}$	0.03503	10^7
5	$\begin{Bmatrix}-0.29335\\ 0.00000\\ 0.00000\end{Bmatrix}$	$\begin{Bmatrix}-5.89125\times10^4\\ 4.29563\times10^4\\ 4.29563\times10^4\end{Bmatrix}$	$\begin{Bmatrix}-6.49719\times10^4\\ -3.10156\times10^4\\ -3.10156\times10^4\end{Bmatrix}$	0.05528	10^7
6	$\begin{Bmatrix}-0.39335\\ 0.00000\\ 0.00000\end{Bmatrix}$	$\begin{Bmatrix}-7.01936\times10^4\\ 4.85968\times10^4\\ 4.85968\times10^4\end{Bmatrix}$	$\begin{Bmatrix}-8.40982\times10^4\\ -4.45013\times10^4\\ -4.45013\times10^4\end{Bmatrix}$	0.09904	10^7

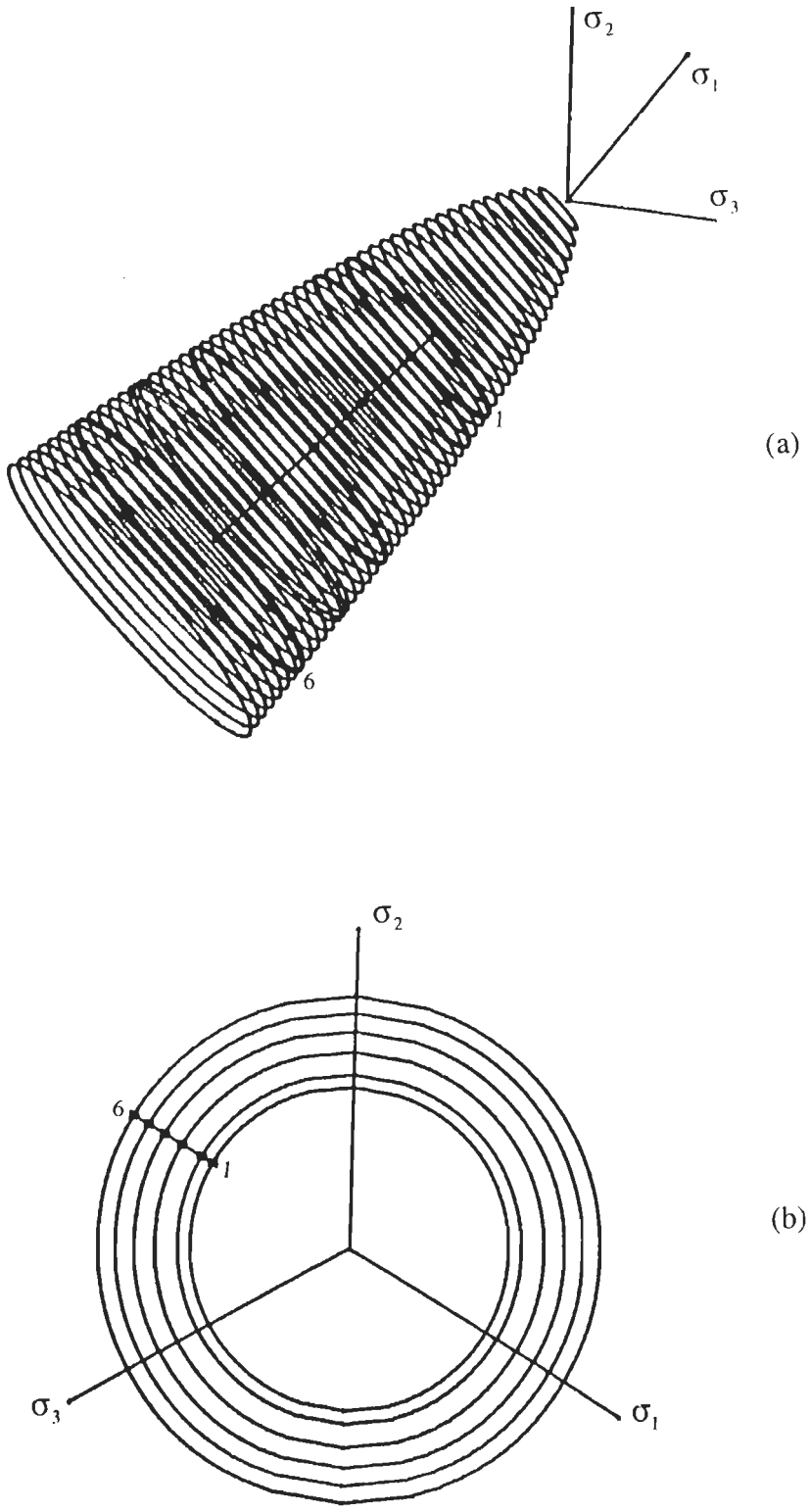

Fig. 6.21 Movement of stress point on the Hoffman yield surface for uniaxial compression and perfect plasticity with $f_{co} = 10000$ and $f_{to} = 1000$ (a) in principal stress space (b) $\pi-$plane representation

In this case it can be seen that all the stress components are compressive. The compressive stress continue to increase with increased uniaxial compressive strain.

6.7.3 Test 3: Pure Shear with Perfect Plasticity

A single element was subjected to pure shear strain by prescribing displacements as shown in Fig. 6.22. The variation of the stress state as shear strain is increased is shown in Fig. 6.23 and Table 6.13. The first yield is encountered at

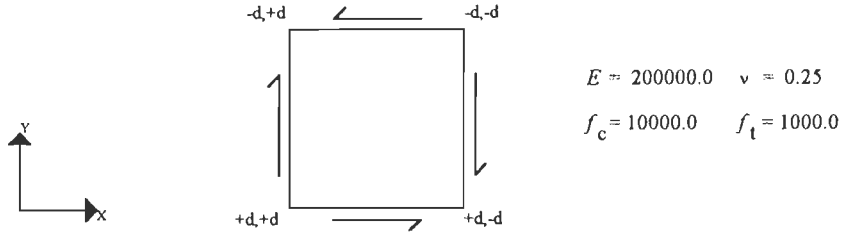

Fig 6.22 A plane strain element under pure shear

Table 6.13: Pure Shear with Perfect Plasticity, (f_{co} = 10000 and f_{to} = 1000)

Increment	*Displacement Vector* $\begin{Bmatrix}\Delta x\\ \Delta y\end{Bmatrix}$	*Strain State Vector* $\begin{Bmatrix}\varepsilon_x\\ \varepsilon_y\\ \tau_{xy}\\ \varepsilon_z\end{Bmatrix}$	*Flow Vector* $\begin{Bmatrix}\partial f/\partial\sigma_x\\ \partial f/\partial\sigma_y\\ \partial f/\partial\tau_{xy}\\ \partial f/\partial\sigma_z\end{Bmatrix}$	*Stress Vector* $\begin{Bmatrix}\sigma_x\\ \sigma_y\\ \tau_{xy}\\ \sigma_z\end{Bmatrix}$	*Effective Plastic Strain* $(=d\lambda)$	*Equivalent Stress Level*
1	$\begin{Bmatrix}0.00570\\ 0.00570\end{Bmatrix}$	$\begin{Bmatrix}0.00000\\ 0.00000\\ -0.02282\\ 0.00000\end{Bmatrix}$	$\begin{Bmatrix}0.00000\\ 0.00000\\ 0.00000\\ 0.00000\end{Bmatrix}$	$\begin{Bmatrix}0.00000\\ 0.00000\\ -1.82574\times10^{3}\\ 0.00000\end{Bmatrix}$	0.00000	1.00000×10^{7}
2	$\begin{Bmatrix}0.00307\\ 0.00307\end{Bmatrix}$	$\begin{Bmatrix}0.00000\\ 0.00000\\ -0.12300\\ 0.00000\end{Bmatrix}$	$\begin{Bmatrix}0.90000\times10^{4}\\ 0.90000\times10^{4}\\ -0.38129\times10^{4}\\ 0.90000\times10^{4}\end{Bmatrix}$	$\begin{Bmatrix}-4.11683\times10^{3}\\ -4.11683\times10^{3}\\ -6.35490\times10^{3}\\ -4.11683\times10^{3}\end{Bmatrix}$	0.02906	1.00000×10^{7}
3	$\begin{Bmatrix}0.13075\\ 0.13075\end{Bmatrix}$	$\begin{Bmatrix}0.00000\\ 0.00000\\ -0.52300\\ 0.00000\end{Bmatrix}$	$\begin{Bmatrix}0.90000\times10^{4}\\ 0.90000\times10^{4}\\ -0.78441\times10^{5}\\ 0.90000\times10^{4}\end{Bmatrix}$	$\begin{Bmatrix}-1.86203\times10^{4}\\ -1.86203\times10^{4}\\ -1.30735\times10^{4}\\ -1.86203\times10^{4}\end{Bmatrix}$	0.21858	1.00000×10^{7}
4	$\begin{Bmatrix}0.23075\\ 0.23075\end{Bmatrix}$	$\begin{Bmatrix}0.00000\\ 0.00000\\ -0.92300\\ 0.00000\end{Bmatrix}$	$\begin{Bmatrix}0.90000\times10^{4}\\ 0.90000\times10^{4}\\ -0.10111\times10^{6}\\ 0.90000\times10^{4}\end{Bmatrix}$	$\begin{Bmatrix}-3.11812\times10^{4}\\ -3.11812\times10^{4}\\ -1.68512\times10^{4}\\ -3.11812\times10^{4}\end{Bmatrix}$	0.42705	1.00000×10^{7}
5	$\begin{Bmatrix}0.33075\\ 0.33075\end{Bmatrix}$	$\begin{Bmatrix}0.00000\\ 0.00000\\ -1.32300\\ 0.00000\end{Bmatrix}$	$\begin{Bmatrix}0.90000\times10^{4}\\ 0.90000\times10^{4}\\ -0.11766\times10^{6}\\ 0.90000\times10^{4}\end{Bmatrix}$	$\begin{Bmatrix}-4.23635\times10^{4}\\ -4.23635\times10^{4}\\ -1.96113\times10^{4}\\ -4.23635\times10^{4}\end{Bmatrix}$	0.64173	1.00000×10^{7}
6	$\begin{Bmatrix}0.53075\\ 0.53075\end{Bmatrix}$	$\begin{Bmatrix}0.00000\\ 0.00000\\ -2.12300\\ 0.00000\end{Bmatrix}$	$\begin{Bmatrix}0.90000\times10^{4}\\ 0.90000\times10^{4}\\ -0.14229\times10^{6}\\ 0.90000\times10^{4}\end{Bmatrix}$	$\begin{Bmatrix}-6.21180\times10^{4}\\ -6.21180\times10^{4}\\ -2.37148\times10^{4}\\ -6.21180\times10^{4}\end{Bmatrix}$	1.07960	1.00000×10^{7}

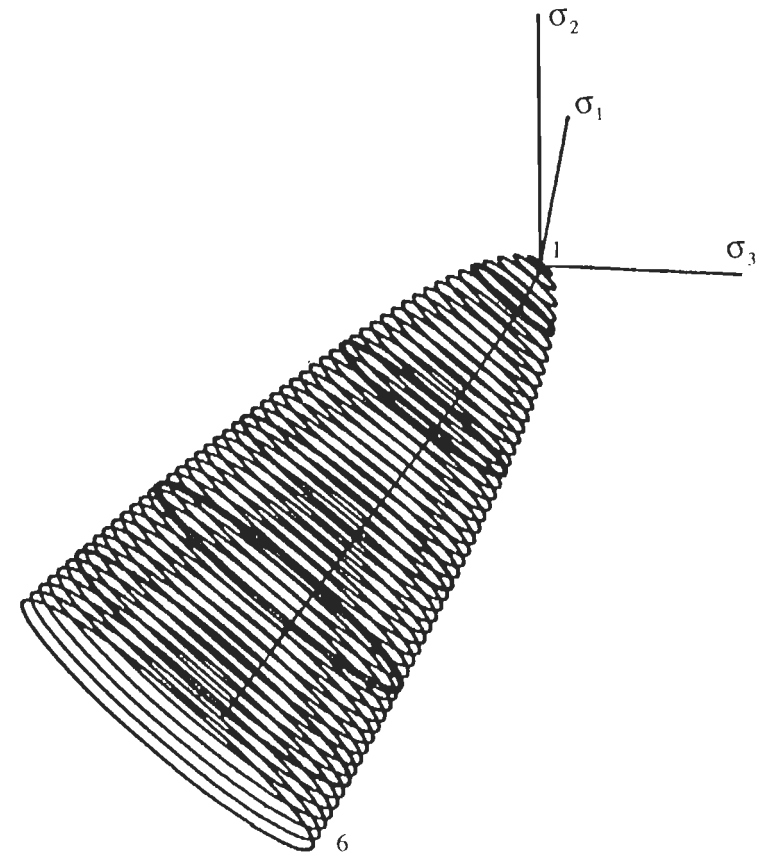

(a)

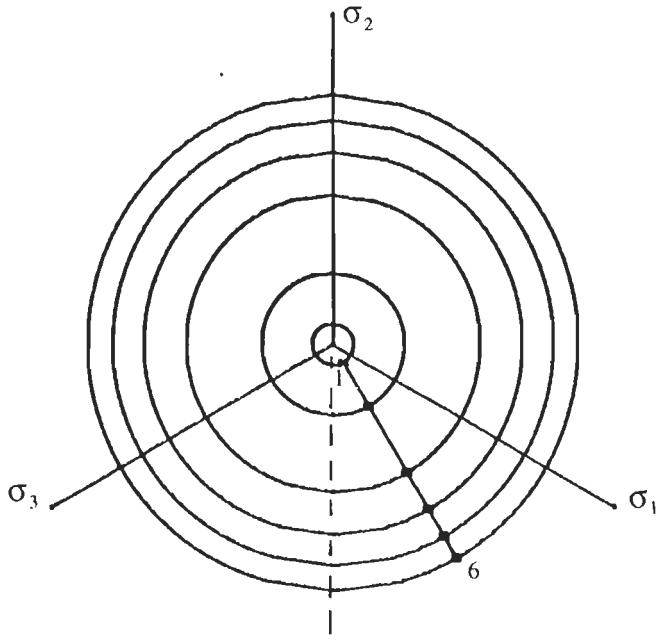

(b)

Fig. 6.23 Movement of stress point on the Hoffman yield surface for pure shear and perfect plasticity with $f_{co} = 10000$ and $f_{to} = 1000$ (a) in principal stress space (b) $\pi-$plane representation

$$\tau_{xy} = \sqrt{\frac{f_c f_t}{3}}$$

which happens at displacement (refer Fig. 6.22) $d = 0.022822$. Fig 6.23b shows that the stress state varies along the line of pure shear. The compressive normal stress increase monotonically as can be observed from Fig. 6.23 and Table 6.13.

6.8 Hoffman Criterion with Strain Softening

The evolution of the isotropic Hoffman yield surface under strain softening has generally been considered assuming a gradual decrease of the uniaxial tensile strength f_t while the uniaxial compressive stress f_c is assumed to remain constant (Bicanic et al., 1994). As discussed in Chapter 4, this study also examines the case when both f_c and f_t reduce by the same factor. The evolution of the surfaces for these cases was illustrated in Figs. 4.2 and 4.3. An exponential form of strain softening is assumed for both cases wherein f_t or both f_c and f_t reduce as per the following equation

$$f_t = f_{t_o} \, e^{-\left(\varepsilon_y^p / \varepsilon_c\right)^2}$$

where f_t and f_{t_o} are the uniaxial yield stress in tension at the current and virgin state of the material respectively. The parameters f_c and f_{c_o} can also be substituted in place of f_t and f_{t_o} when both f_c and f_t are assumed to reduce. ε_y^p indicates the equivalent plastic strain while ε_c is a constant that is responsible for the slope of the softening branch.

6.8.1 Test 4: Uniaxial Tension with Strain Softening

As discussed above two cases emerge for softening *viz.* (a) when a decline of both f_c and f_t is considered and (b) when only f_t is assumed to reduce. Illustrative tests for these cases are discussed.

(a) Both f_c and f_t Decline

A uniaxial tensile strain as shown in Fig. 6.17 is applied. Tensile strength $f_{t_o} = 1000$ and $f_{c_o} = 10000$ and $\varepsilon_c = 0.05$ are assumed. The results are illustrated in Fig. 6.24 and Table 6.14. In Fig. 6.24 the yield surface is plotted only for the virgin state of the material. It can be seen that while initially the stresses move towards the compressive direction of the hydrostatic axis, they change direction with increased strain. However when

$f_{to} = 9000$ is assumed the mean stress continues to move towards the tensile direction of the hydrostatic axis. The results for this case are illustrated in Fig. 6.25 and Table 6.15.

In each case the yield surface plotted corresponds to the virgin material. In the former case the stress point moves towards the compressive direction of the hydrostatic axes before curving back towards the tensile direction (Fig. 6.24). Thus, as the yield surface becomes narrower as it shrinks, a reversal in the stress path takes place. In the latter case, the stress point continues to move towards the tensile end (Fig. 6.25).

Table 6.14: Uniaxial Tension with Strain Softening, f_c and f_t Both Reduce ($f_{co} = 10000$ and $f_{to} = 1000$)

Increment	*Strain State Vector* $\begin{Bmatrix}\varepsilon_x\\ \varepsilon_y\\ \varepsilon_z\end{Bmatrix}$	*Flow Vector* $\begin{Bmatrix}\partial f/\partial\sigma_x\\ \partial f/\partial\sigma_y\\ \partial f/\partial\sigma_z\end{Bmatrix}$	*Stress Vector* $\begin{Bmatrix}\sigma_x\\ \sigma_y\\ \sigma_z\end{Bmatrix}$	*Effective Plastic Strain* $(= d\lambda)$	*Equivalent Stress Level*
1	$\begin{Bmatrix}0.00272\\ 0.00000\\ 0.00000\end{Bmatrix}$	$\begin{Bmatrix}0.00000\\ 0.00000\\ 0.00000\end{Bmatrix}$	$\begin{Bmatrix}653.99384\\ 217.99795\\ 217.99795\end{Bmatrix}$	0.00000	1.0×10^{7}
2	$\begin{Bmatrix}0.00880\\ 0.00000\\ 0.00000\end{Bmatrix}$	$\begin{Bmatrix}.11510\times10^{5}\\ .76871\times10^{4}\\ .76871\times10^{4}\end{Bmatrix}$	$\begin{Bmatrix}1.15811\times10^{3}\\ -1.16214\times10^{2}\\ -1.16214\times10^{2}\end{Bmatrix}$	0.00311	9.92280×10^{6}
3	$\begin{Bmatrix}0.01380\\ 0.00000\\ 0.00000\end{Bmatrix}$	$\begin{Bmatrix}.12634\times10^{5}\\ .69789\times10^{4}\\ .69789\times10^{4}\end{Bmatrix}$	$\begin{Bmatrix}1.48855\times10^{3}\\ -3.96403\times10^{2}\\ -3.96403\times10^{2}\end{Bmatrix}$	0.00585	9.72942×10^{6}
4	$\begin{Bmatrix}0.02380\\ 0.00000\\ 0.00000\end{Bmatrix}$	$\begin{Bmatrix}.14180\times10^{5}\\ .55863\times10^{4}\\ .55863\times10^{4}\end{Bmatrix}$	$\begin{Bmatrix}1.93720\times10^{3}\\ -9.27472\times10^{2}\\ -9.27472\times10^{2}\end{Bmatrix}$	0.01188	8.90600×10^{6}
5	$\begin{Bmatrix}0.03380\\ 0.00000\\ 0.00000\end{Bmatrix}$	$\begin{Bmatrix}0.14900\times10^{5}\\ 0.41143\times10^{4}\\ 0.41143\times10^{4}\end{Bmatrix}$	$\begin{Bmatrix}2.16969\times10^{3}\\ -1.42557\times10^{3}\\ -1.42557\times10^{3}\end{Bmatrix}$	0.01859	7.58441×10^{6}
6	$\begin{Bmatrix}0.04380\\ 0.00000\\ 0.00000\end{Bmatrix}$	$\begin{Bmatrix}0.14717\times10^{5}\\ 0.25737\times10^{4}\\ 0.25737\times10^{4}\end{Bmatrix}$	$\begin{Bmatrix}2.18221\times10^{3}\\ -1.86557\times10^{3}\\ -1.86557\times10^{3}\end{Bmatrix}$	0.02606	5.75985×10^{6}
7	$\begin{Bmatrix}0.05380\\ 0.00000\\ 0.00000\end{Bmatrix}$	$\begin{Bmatrix}0.13587\times10^{5}\\ 0.10328\times10^{4}\\ 0.10328\times10^{4}\end{Bmatrix}$	$\begin{Bmatrix}1.97297\times10^{3}\\ -2.21177\times10^{3}\\ -2.21177\times10^{3}\end{Bmatrix}$	0.03447	3.79921×10^{6}
8	$\begin{Bmatrix}0.06380\\ 0.00000\\ 0.00000\end{Bmatrix}$	$\begin{Bmatrix}0.11511\times10^{5}\\ -0.34248\times10^{3}\\ -0.34248\times10^{3}\end{Bmatrix}$	$\begin{Bmatrix}1.54365\times10^{3}\\ -2.40747\times10^{3}\\ -2.40747\times10^{3}\end{Bmatrix}$	0.04401	2.04278×10^{6}
9	$\begin{Bmatrix}0.07380\\ 0.00000\\ 0.00000\end{Bmatrix}$	$\begin{Bmatrix}0.86803\times10^{4}\\ -0.13107\times10^{4}\\ -0.13107\times10^{4}\end{Bmatrix}$	$\begin{Bmatrix}9.57420\times10^{2}\\ -2.37290\times10^{3}\\ -2.37290\times10^{3}\end{Bmatrix}$	0.05471	7.95385×10^{5}
10	$\begin{Bmatrix}0.08380\\ 0.00000\\ 0.00000\end{Bmatrix}$	$\begin{Bmatrix}0.56428\times10^{4}\\ -0.17178\times10^{4}\\ -0.17178\times10^{4}\end{Bmatrix}$	$\begin{Bmatrix}4.04637\times10^{2}\\ -2.04889\times10^{3}\\ -2.04889\times10^{3}\end{Bmatrix}$	0.06617	2.50471×10^{5}
11	$\begin{Bmatrix}0.09380\\ 0.00000\\ 0.00000\end{Bmatrix}$	$\begin{Bmatrix}0.30664\times10^{4}\\ -0.16512\times10^{4}\\ -0.16512\times10^{4}\end{Bmatrix}$	$\begin{Bmatrix}7.03256\times10^{1}\\ -1.50220\times10^{3}\\ -1.50220\times10^{3}\end{Bmatrix}$	0.07721	4.00190×10^{4}

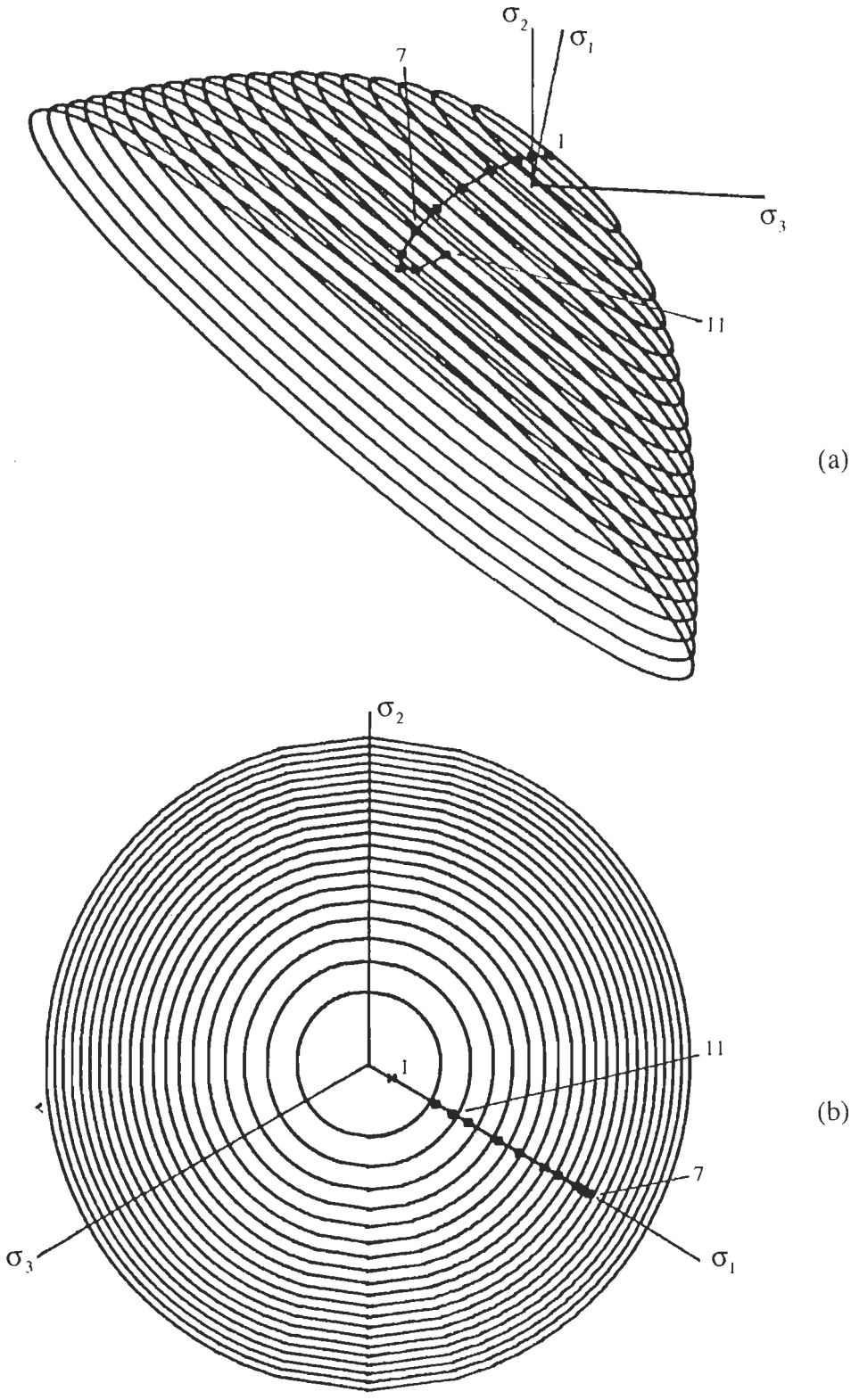

Fig. 6.24 Variation of the stress state on the Hoffman yield surface for uniaxial tension and strain softening (f_c and f_t both reduce) with $f_{co} = 10000$ and $f_{to} = 1000$ (a) in principal stress space (b) $\pi-$plane representation

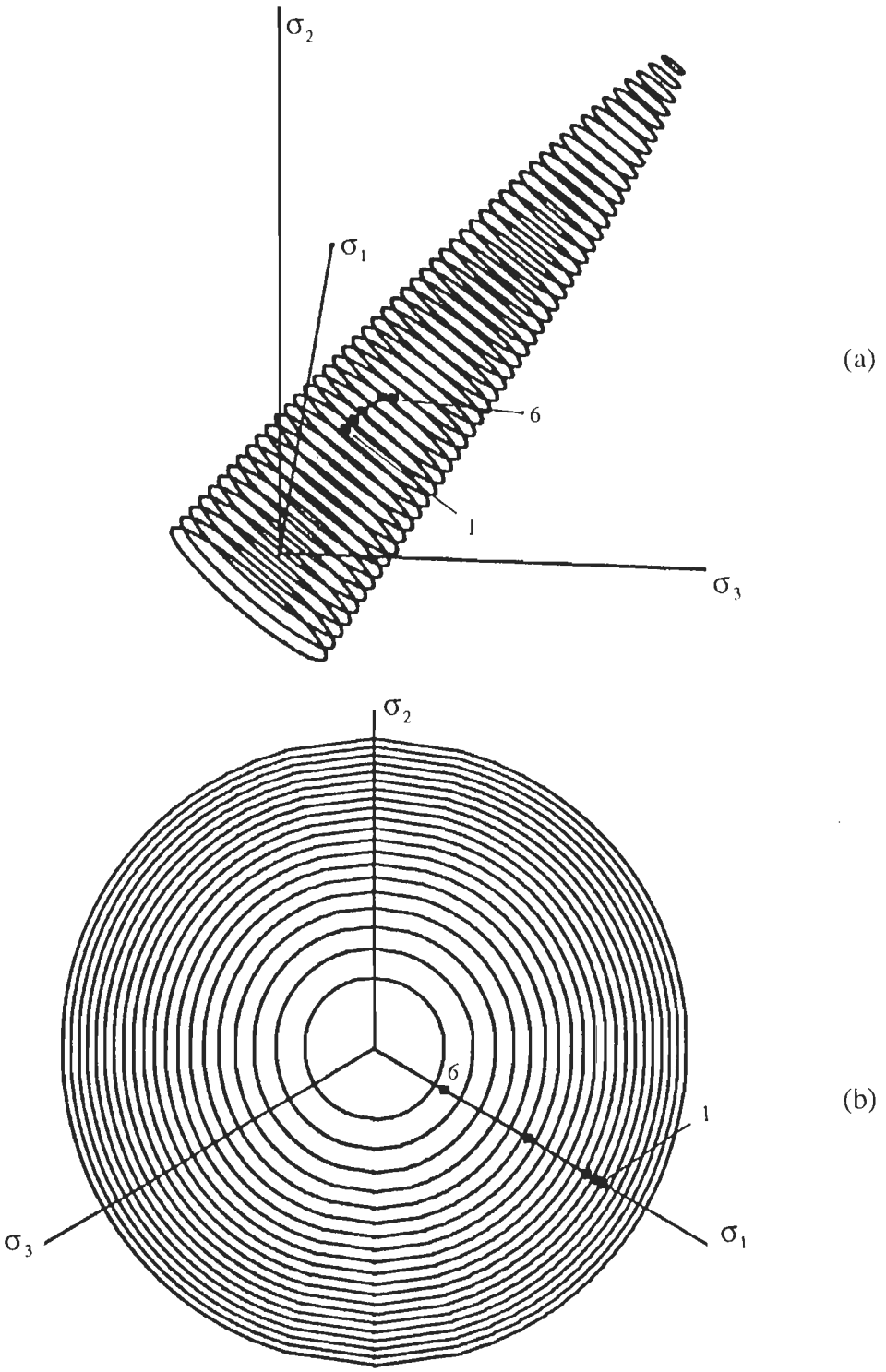

Fig. 6.25 Variation of the stress state on the Hoffman yield surface for uniaxial tension and strain softening (f_c and f_t both reduce) with $f_{co} = 10000$ and $f_{to} = 9000$ (a) in principal stress space (b) π−plane representation

Table 6.15: Uniaxial Tension with Strain Softening, f_c and f_t Both Reduce ($f_{co} = 10000$ and $f_{to} = 9000$)

Increment	*Strain State Vector* $\begin{Bmatrix}\varepsilon_x\\ \varepsilon_y\\ \varepsilon_z\end{Bmatrix}$	*Flow Vector* $\begin{Bmatrix}\partial f/\partial\sigma_x\\ \partial f/\partial\sigma_y\\ \partial f/\partial\sigma_z\end{Bmatrix}$	*Stress Vector* $\begin{Bmatrix}\sigma_x\\ \sigma_y\\ \sigma_z\end{Bmatrix}$	*Effective Plastic Strain* $(=d\lambda)$	*Equivalent Stress Level*
1	$\begin{Bmatrix}0.05199\\ 0.00000\\ 0.00000\end{Bmatrix}$	$\begin{Bmatrix}0.00000\\ 0.00000\\ 0.00000\end{Bmatrix}$	$\begin{Bmatrix}1.24782\times10^4\\ 4.15941\times10^3\\ 4.15941\times10^3\end{Bmatrix}$	0.00000	9.0×10^7
2	$\begin{Bmatrix}0.05309\\ 0.00000\\ 0.00000\end{Bmatrix}$	$\begin{Bmatrix}0.17583\times10^5\\ -0.72961\times10^4\\ -0.72961\times10^4\end{Bmatrix}$	$\begin{Bmatrix}1.25876\times10^4\\ 4.29435\times10^3\\ 4.29435\times10^3\end{Bmatrix}$	0.00084	8.99488×10^7
3	$\begin{Bmatrix}0.05809\\ 0.00000\\ 0.00000\end{Bmatrix}$	$\begin{Bmatrix}0.17090\times10^5\\ -0.71957\times10^4\\ -0.71957\times10^4\end{Bmatrix}$	$\begin{Bmatrix}1.30206\times10^4\\ 4.92532\times10^3\\ 4.92532\times10^3\end{Bmatrix}$	0.00502	8.81750×10^7
4	$\begin{Bmatrix}0.06309\\ 0.00000\\ 0.00000\end{Bmatrix}$	$\begin{Bmatrix}0.160215\times10^5\\ -0.70999\times10^4\\ -0.70999\times10^4\end{Bmatrix}$	$\begin{Bmatrix}1.33051\times10^4\\ 5.59799\times10^3\\ 5.59799\times10^3\end{Bmatrix}$	0.01000	8.29387×10^7
5	$\begin{Bmatrix}0.07309\\ 0.00000\\ 0.00000\end{Bmatrix}$	$\begin{Bmatrix}0.97774\times10^4\\ -0.69748\times10^4\\ -0.69748\times10^4\end{Bmatrix}$	$\begin{Bmatrix}1.28062\times10^4\\ 7.22214\times10^3\\ 7.22214\times10^3\end{Bmatrix}$	0.02614	5.19177×10^7
6	$\begin{Bmatrix}0.07809\\ 0.00000\\ 0.00000\end{Bmatrix}$	$\begin{Bmatrix}0.73730\times10^4\\ -0.68841\times10^4\\ -0.68841\times10^4\end{Bmatrix}$	$\begin{Bmatrix}1.08571\times10^4\\ 8.31667\times10^3\\ 8.31667\times10^3\end{Bmatrix}$	0.043714	1.92545×10^7

(b) Only f_t Declines

Uniaxial tension test with $f_{to} = 1000$ and only f_t declining does not cause a stress reversal (Fig. 6.26 and Table 6.16) as was the case when both f_c and f_t were assumed to decline . This is apparently because of the expansion of the yield surface towards the compressive direction of the hydrostatic axis. However, when $f_{to} = 9000$ is assumed the direction of stress traversal is reversed (Fig. 6.27 and Table 6.17).

Table 6.16: Uniaxial Tension with Strain Softening, f_t Reduces, ($f_{co} = 10000$ and $f_{to} = 1000$)

Increment	*Strain State Vector* $\begin{Bmatrix}\varepsilon_x\\ \varepsilon_y\\ \varepsilon_z\end{Bmatrix}$	*Flow Vector* $\begin{Bmatrix}\partial f/\partial\sigma_x\\ \partial f/\partial\sigma_y\\ \partial f/\partial\sigma_z\end{Bmatrix}$	*Stress Vector* $\begin{Bmatrix}\sigma_x\\ \sigma_y\\ \sigma_z\end{Bmatrix}$	*Effective Plastic Strain* $(= d\lambda)$	*Equivalent Stress Level*
1	$\begin{Bmatrix}0.00272\\ 0.00000\\ 0.00000\end{Bmatrix}$	$\begin{Bmatrix}0.00000\\ 0.00000\\ 0.00000\end{Bmatrix}$	$\begin{Bmatrix}6.53994\times10^2\\ 2.17997\times10^2\\ 2.17997\times10^2\end{Bmatrix}$	0.00000	1.0×10^7
2	$\begin{Bmatrix}0.00880\\ 0.00000\\ 0.00000\end{Bmatrix}$	$\begin{Bmatrix}0.11549\times10^5\\ 0.77252\times10^4\\ 0.77252\times10^4\end{Bmatrix}$	$\begin{Bmatrix}1.15017\times10^3\\ -1.16590\times10^2\\ -1.16590\times10^2\end{Bmatrix}$	0.00311	9.95349×10^6
3	$\begin{Bmatrix}0.01380\\ 0.00000\\ 0.00000\end{Bmatrix}$	$\begin{Bmatrix}0.12776\times10^5\\ 0.71119\times10^4\\ 0.71119\times10^4\end{Bmatrix}$	$\begin{Bmatrix}1.49088\times10^3\\ -3.97165\times10^2\\ -3.97165\times10^2\end{Bmatrix}$	0.00585	9.84314×10^6
4	$\begin{Bmatrix}0.04380\\ 0.00000\\ 0.00000\end{Bmatrix}$	$\begin{Bmatrix}0.17849\times10^5\\ 0.45752\times10^4\\ 0.45752\times10^4\end{Bmatrix}$	$\begin{Bmatrix}2.51027\times10^3\\ -1.91454\times10^3\\ -1.91454\times10^3\end{Bmatrix}$	0.02495	7.41895×10^6
5	$\begin{Bmatrix}0.07380\\ 0.00000\\ 0.00000\end{Bmatrix}$	$\begin{Bmatrix}0.20940\times10^5\\ 0.30300\times10^4\\ 0.30300\times10^4\end{Bmatrix}$	$\begin{Bmatrix}2.87315\times10^3\\ -3.09684\times10^3\\ -3.09684\times10^3\end{Bmatrix}$	0.04641	3.83857×10^5
6	$\begin{Bmatrix}0.21380\\ 0.00000\\ 0.00000\end{Bmatrix}$	$\begin{Bmatrix}0.26357\times10^5\\ 0.32122\times10^3\\ 0.32122\times10^3\end{Bmatrix}$	$\begin{Bmatrix}3.27515\times10^3\\ -5.40363\times10^3\\ -5.40363\times10^3\end{Bmatrix}$	0.15514	6.59145×10^2

Table 6.17: Uniaxial Tension with Strain Softening, f_t Reduces, ($f_{co} = 10000$ and $f_{to} = 9000$)

Increment	*Strain State Vector* $\begin{Bmatrix}\varepsilon_x\\ \varepsilon_y\\ \varepsilon_z\end{Bmatrix}$	*Flow Vector* $\begin{Bmatrix}\partial f/\partial\sigma_x\\ \partial f/\partial\sigma_y\\ \partial f/\partial\sigma_z\end{Bmatrix}$	*Stress Vector* $\begin{Bmatrix}\sigma_x\\ \sigma_y\\ \sigma_z\end{Bmatrix}$	*Effective Plastic Strain* $(= d\lambda)$	*Equivalent Stress Level*
1	$\begin{Bmatrix}0.05199\\ 0.00000\\ 0.00000\end{Bmatrix}$	$\begin{Bmatrix}0.00000\\ 0.00000\\ 0.00000\end{Bmatrix}$	$\begin{Bmatrix}1.24782\times10^4\\ 4.15941\times10^3\\ 4.15941\times10^3\end{Bmatrix}$	0.00000	9.00000×10^7
2	$\begin{Bmatrix}0.05509\\ 0.00000\\ 0.00000\end{Bmatrix}$	$\begin{Bmatrix}0.17421\times10^5\\ -0.72105\times10^4\\ -0.72105\times10^4\end{Bmatrix}$	$\begin{Bmatrix}1.27572\times10^4\\ 4.54673\times10^3\\ 4.54673\times10^3\end{Bmatrix}$	0.00253	8.97650×10^7
3	$\begin{Bmatrix}0.05709\\ 0.00000\\ 0.00000\end{Bmatrix}$	$\begin{Bmatrix}0.17145\times10^5\\ -0.70727\times10^4\\ -0.70727\times10^4\end{Bmatrix}$	$\begin{Bmatrix}1.28817\times10^4\\ 4.80898\times10^3\\ 4.80898\times10^3\end{Bmatrix}$	0.00446	8.927213×10^7
4	$\begin{Bmatrix}0.05909\\ 0.00000\\ 0.00000\end{Bmatrix}$	$\begin{Bmatrix}0.16669\times10^5\\ -0.68343\times10^4\\ -0.68343\times10^4\end{Bmatrix}$	$\begin{Bmatrix}1.29211\times10^4\\ 5.08686\times10^3\\ 5.08686\times10^3\end{Bmatrix}$	0.00683	8.83111×10^7
5	$\begin{Bmatrix}0.06009\\ 0.00000\\ 0.00000\end{Bmatrix}$	$\begin{Bmatrix}0.16287\times10^5\\ -0.66436\times10^4\\ -0.66436\times10^4\end{Bmatrix}$	$\begin{Bmatrix}1.28802\times10^4\\ 5.23658\times10^3\\ 5.23658\times10^3\end{Bmatrix}$	0.00831	8.75028×10^7
6	$\begin{Bmatrix}0.06109\\ 0.00000\\ 0.00000\end{Bmatrix}$	$\begin{Bmatrix}0.15697\times10^5\\ -0.63483\times10^4\\ -0.63483\times10^4\end{Bmatrix}$	$\begin{Bmatrix}1.27473\times10^4\\ 5.39899\times10^3\\ 5.39899\times10^3\end{Bmatrix}$	0.01025	8.62607×10^7

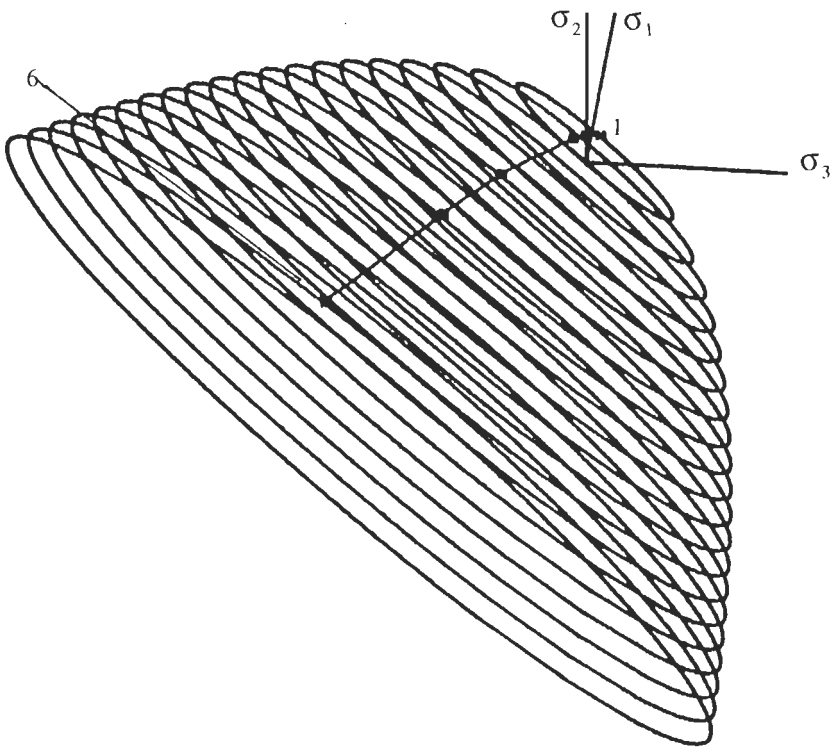

(a)

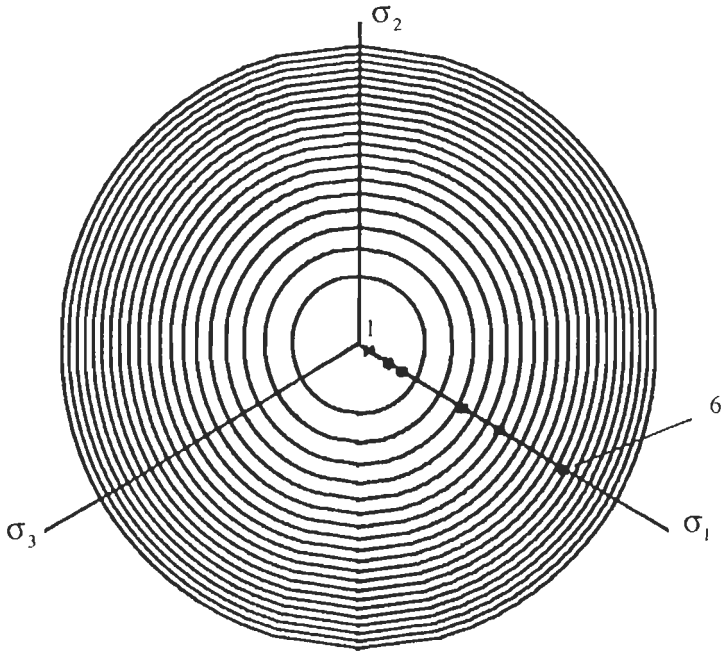

(b)

Fig. 6.26 Variation of the stress state on the Hoffman yield surface for uniaxial tension and strain softening (only f_t reduces) with $f_{co} = 10000$ and $f_{to} = 1000$ (a) in principal stress space (b) $\pi-$plane representation

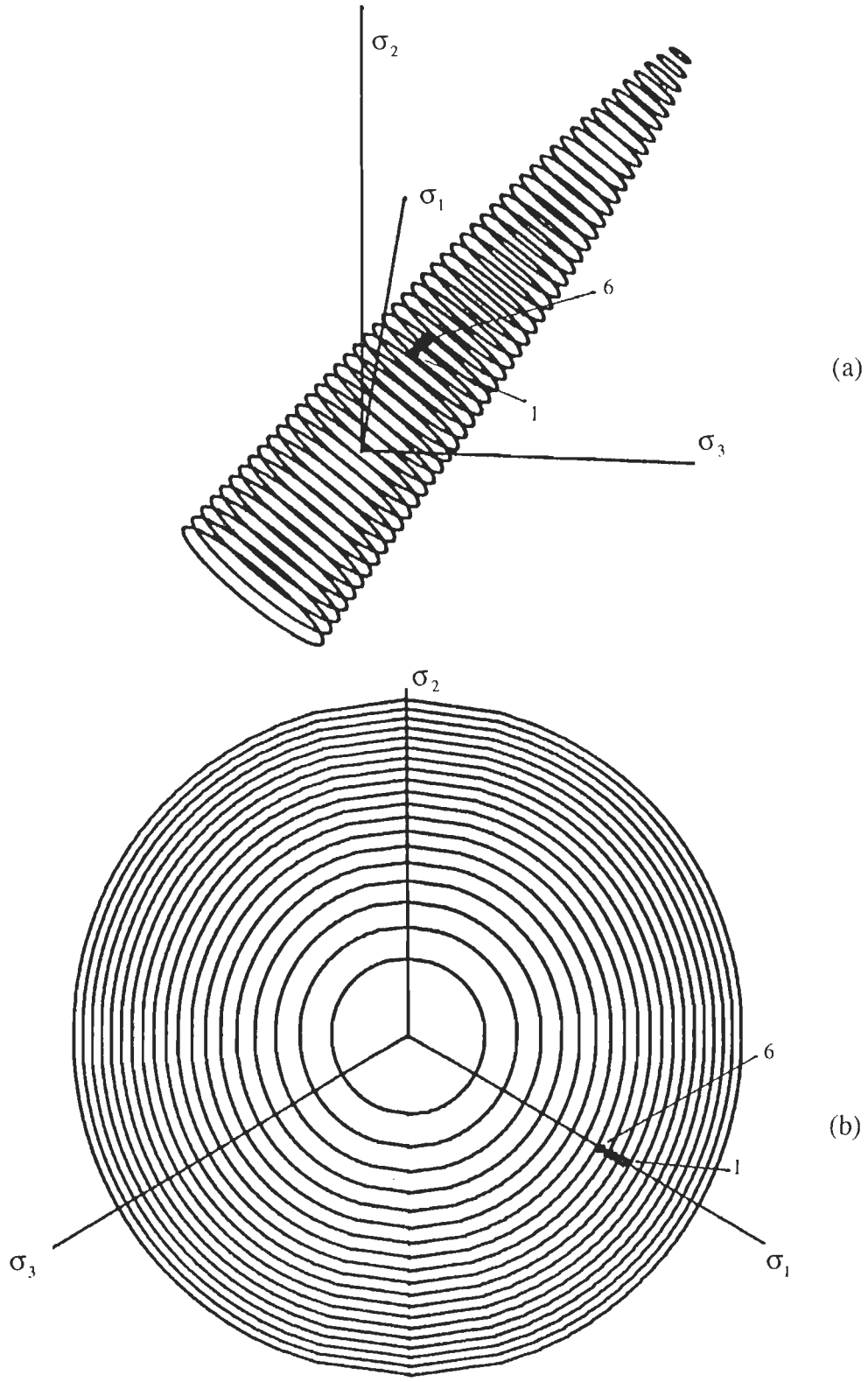

Fig. 6.27 Variation of the stress state on the Hoffman yield surface for uniaxial tension and strain softening (only f_t reduces) with $f_{co} = 10000$ and $f_{to} = 9000$ (a) in principal stress space (b) $\pi-$plane representation

References

Bicanic, N., Pearce, C.J. and Owen, D.R.J. (1994) – Failure predictions of concrete like materials using softening Hoffman plasticity model, *Computational Modelling of Concrete Structures,* (Eds. Mang, H., Bicanic, N. and Borst, R.D.), Pineridge Press, 185-198.

Crisfield, M.A. (1987) – Consistent schemes for plasticity computations with Newton Raphson method, *Computational Plasticity: Models, Software and Applications, Part I,* (Eds. Owen, D.R.J., Hinton, E. and Onate, E.), Pineridge Press, 133-159.

Hablot, J.M. and Zarka, J. (1989) – On the use of an inverse method to build exact solutions in elastoplasticity, *Computational Plasticity: Models, Software and Applications, Part I,* (Eds. Owen, D.R.J., Hinton, E. and Onate, E.), Pineridge Press, 409-419.

Hinton, E. and Ezzat, M.H. (1987) – Fundamental tests for two- and three-dimensional, small strains, elastoplastic finite element analysis, *NAFEMS Publications, RBPWMB.*

Hinton, E., Hellen, T.K. and Lyons, L.P.R. (1989) – On elasto-plastic benchmark philosophies, *Computational Plasticity: Models, Software and Applications, Pat I,* (Eds. Owen, D.R.J., Hinton, E. and Onate, E.), Pineridge Press, 389-407.

Jackman, R.H. and White, P.H. (1987) – Review of benchmark problems for nonlinear material behaviour, *NAFEMS Publication, RBPWMB.*

Kamoulakas, S.A., Davies, G.A.O. and Hitchings, D. (1985) – Benchmark tests for various finite element assemblies, *NAFEMS Publication,* C1.

Koiter, W.T. (1953) – Stress-strain relations, uniqueness and variational theorems for elasto-plastic materials with a singular yield surface, *Q. Appl. Math.*, **11**, 350-354.

Krieg, R.D. and Krieg, D.B. (1977) – Accuracies of numerical solution methods for the elasto-perfectly plastic models, *J. Pressure Vassal Technology, ASME*, **99**, 510-515.

Owen, D.R.J. and Hinton, E. (1980) – Finite elements in plasticity: Theory and Practice, Pineridge Press, U.K.

Pankaj and Bicanic, N. (1989) – On multivector stress returns in Mohr Coulomb elastoplasticity, *Computational Plasticity: Models, Software and Applications, Part I* (Eds. Owen, D.R.J., Hinton, E. and Onate, E.), Pineridge Press, 420-436.

Pankaj and Moin, K. (1991) – Benchmark tests in Mohr Coulomb elastoplasticity, *Proc. Asian Pacific Conf. on Computational mechanics*, A.A. Balkema, 753-759.

Pankaj and Moin, K. (1996) – Exact prescribed displacement field solutions in Mohr Coulomb elastoplasticity, *Engng. Comput.*, **13**(1), 4-14.

Sloan, S.W. and Brooker, J.R. (1992) – Integration of Tresca and Mohr-Coulomb Constitutive relations in plane strain elastoplasticity, *IJNME*, **33**, 163-196.

Chapter 7

Post-Peak Behaviour

7.1 Introduction

In the last Chapter a number of illustrative tests were developed by prescribing a displacement field on single element. In the present Chapter, a number of tests, once again involving single elements, are considered wherein mixed field conditions are prescribed. In general a mixture of displacement and boundary tractions are prescribed. The aim is to study the behaviour of elastoplastic von Mises, Mohr Coulomb and Hoffman materials in the post elastic regime. Predominant objective is to analyse response when perfectly plastic and strain softening characteristics are assumed. In addition to the movement of the stress point in the principal stress space emphasis is laid on the load displacement behaviour. Clearly only post-peak behaviour at the local or element level can lead to an overall post-peak structural response of general structures. In addition to the above study the Chapter also considers the analysis of the so called "acoustic tensor" which has been used as a localization indicator (Rudnicki and Rice, 1975; Ortiz, 1987; Ortiz et al., 1987; Willam and Sobh, 1987; Leroy and Ortiz, 1989).

7.2 Post-peak Response

Post-peak response can be described as the response of a structure that is incapable of sustaining any additional loads. The post-peak behaviour is associated with progressive failure of the structure, which in turn can be modelled using softening plasticity. Failure is often (not always) associated with localization which indicates discontinuous strain and

stress fields. The condition for localization can be expressed using the acoustic tensor as discussed in the earlier Chapter. In the absence of normality localization can take place even under hardening condition and is thus not necessarily associated with a post-peak material response (Leroy and Ortiz, 1989). Traditionally failure was also associated with the loss of positive tangent stiffness properties. This in elastoplasticity is associated with the hardening modulus A becoming zero in case of perfectly plastic behaviour or negative in case of strain softening behaviour. Perfect plasticity and strain softening lead to a constant and declining equivalent yield strength parameter respectively. This does not however imply post-peak (declining) load-deflection response at the structural level in which case the load might actually increase. This apparent increase of load is often due to the triaxial load path adopted by the material. In this Chapter attention is confined to the study of the load path, load deflection behaviour and localization indicators. In each case, either a perfectly plastic or strain softening properties are assumed.

7.3 von Mises Criterion

7.3.1 Perfect Plasticity

Consider a plane strain element shown in Fig. 7.1. A single element being treated like a structure is subjected to uniaxial compression through prescription of displacements in the x-direction. The element is assumed to be free in the transverse direction. Thus while displacements are prescribed in one direction, zero stresses are prescribed in the other. Perfect plasticity is assumed. A load deflection curve relating the applied displacement in the x-direction to the corresponding response loads in the same direction is shown in Fig. 7.2. It can be seen from Fig. 7.2 that the first yield is encountered at point A after which the element continues to carry increased loads till point B. After point B the load deflection curve becomes horizontal. Thus perfect plasticity in this case does not imply a flat load deflection curve immediately after first yield as in case of idealized one dimensional problems. A peak is attained at point B after which the stress state remains unchanged. The variation of stress state in the principal stress space is shown in Fig. 7.3.

An acoustic tensor analysis was conducted for the above problem and the normalized determinant of the acoustic tensor are shown in Fig. 7.4. In this figure θ indicates the angle of the normal of the localization band from the horizontal axis. The minimum determinant at point A is obtained at $\pm 42^{\circ}$. The localization condition is however satisfied

only at point B (Fig. 7.2) and at this state the normal to the localization band is inclined at $\pm 45^{\circ}$ from the horizontal axis.

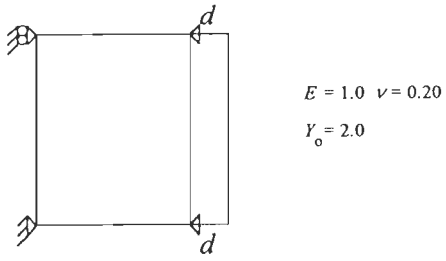

Fig. 7.1 Plane strain element under uniaxial compression

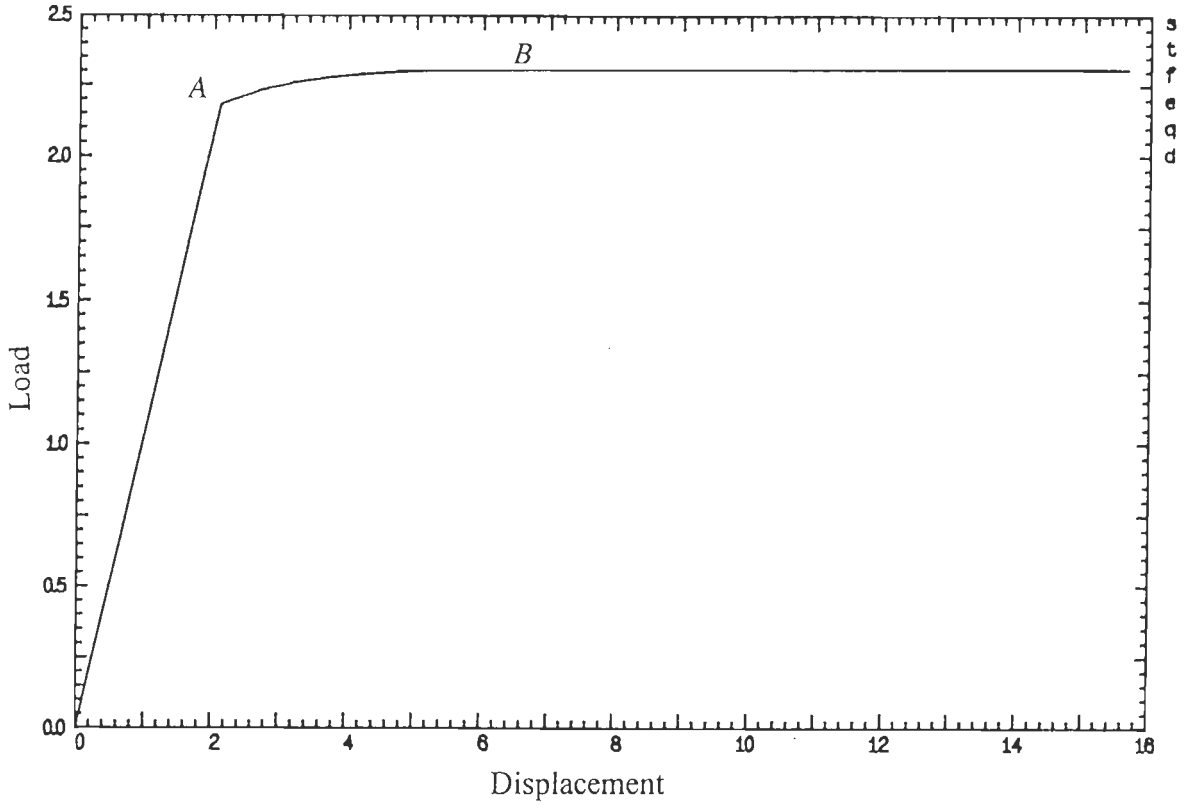

Fig. 7.2 Load deflection curve using von Mises yield criterion for uniaxial compression and perfect plasticity

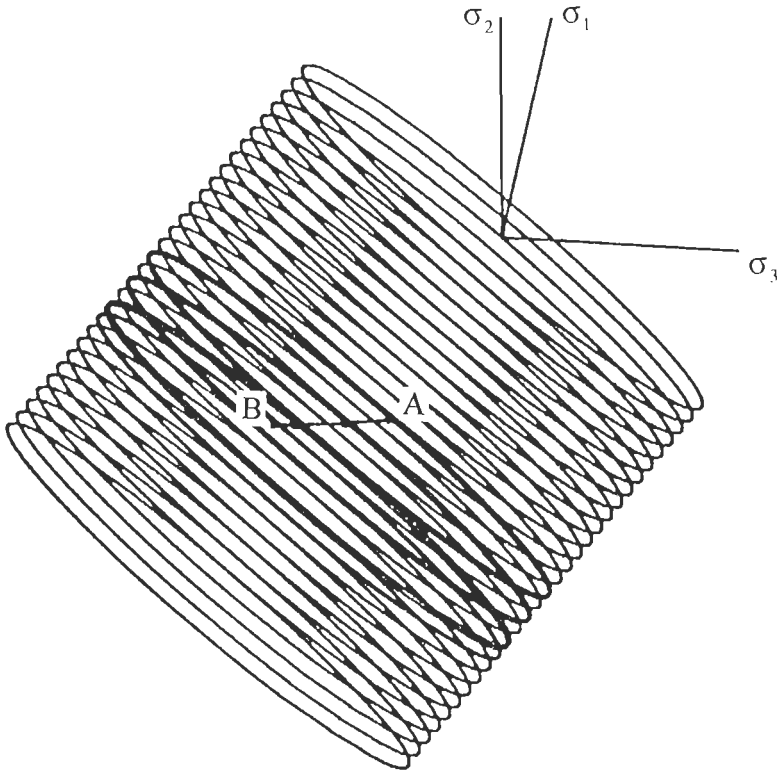

(a)

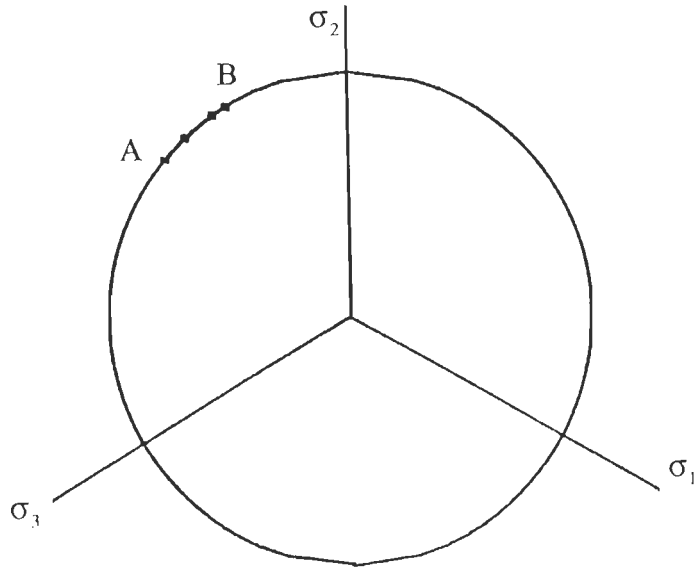

(b)

Fig. 7.3 Movement of the stress point on the von Mises yield surface for uniaxial compression and perfect plasticity (a) in principal stress space (b) $\pi-$ plane representation

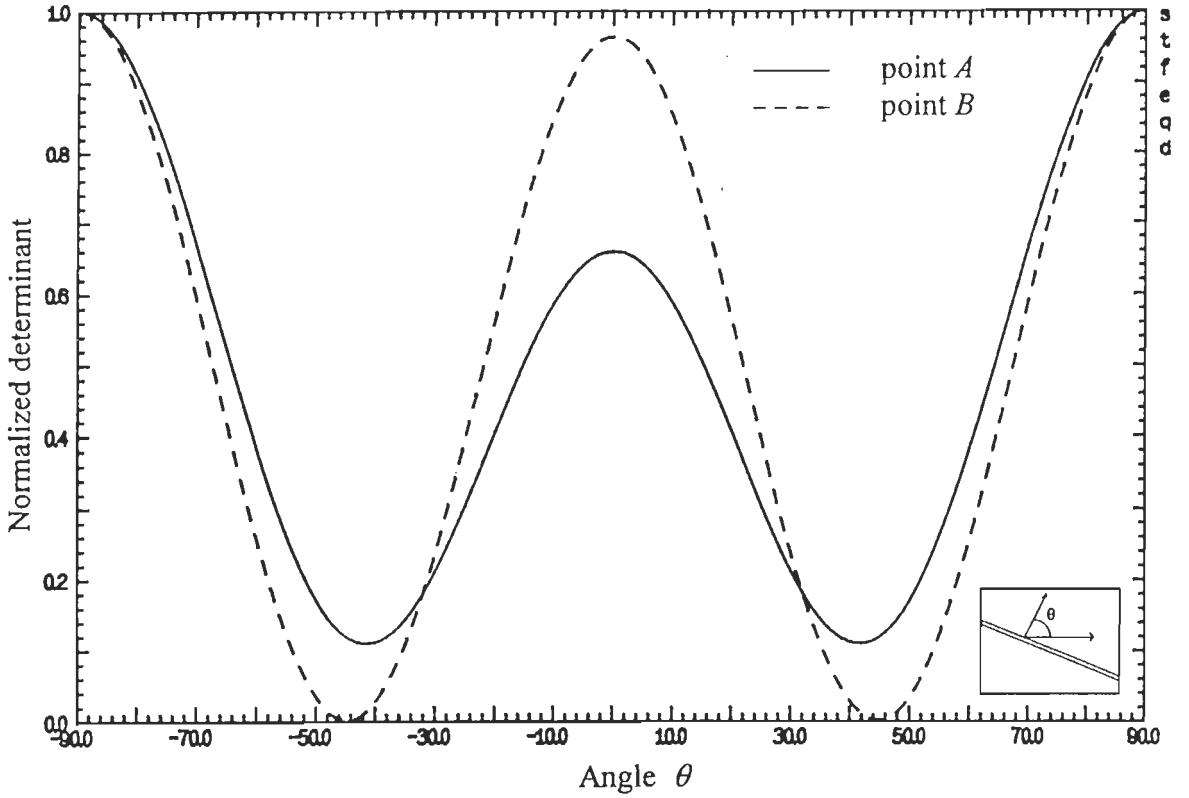

Fig. 7.4 Localization indicator using von Mises yield criterion for uniaxial compression and perfect plasticity

7.3.2 Softening Plasticity

For the example considered in the last subsection an increasing load carrying capacity was observed after first yield under perfect plasticity. Perfect plasticity implies that in the expression for $\mathbf{D}^{ep}$ which is

$$\mathbf{D}^{ep} = \frac{(\mathbf{Da})(\mathbf{Da})^T}{\mathrm{A} + \mathbf{a}^T\mathbf{Da}}$$

the value of the hardening parameter $\mathrm{A} = 0$. Clearly if softening plasticity or a negative value for A is assigned in the problem of the last subsection and the magnitude of A is increased, then at a critical value A_{cr} it should be possible to satisfy the localization condition immediately on first yield. Method for doing this has been discussed by Willam et at. 1994. For the uniaxial compression problem (Fig. 7.1) the critical value of the hardening parameter A at which the localization condition is satisfied immediately on the first yield is found to be $\mathrm{A}_{cr} = -0.107$. The load deflection curve under this condition is shown in Fig. 7.5 where the localization condition is satisfied immediately at point A. The normalized determinant of the acoustic tensor are illustrated in Fig 7.6. In this figure

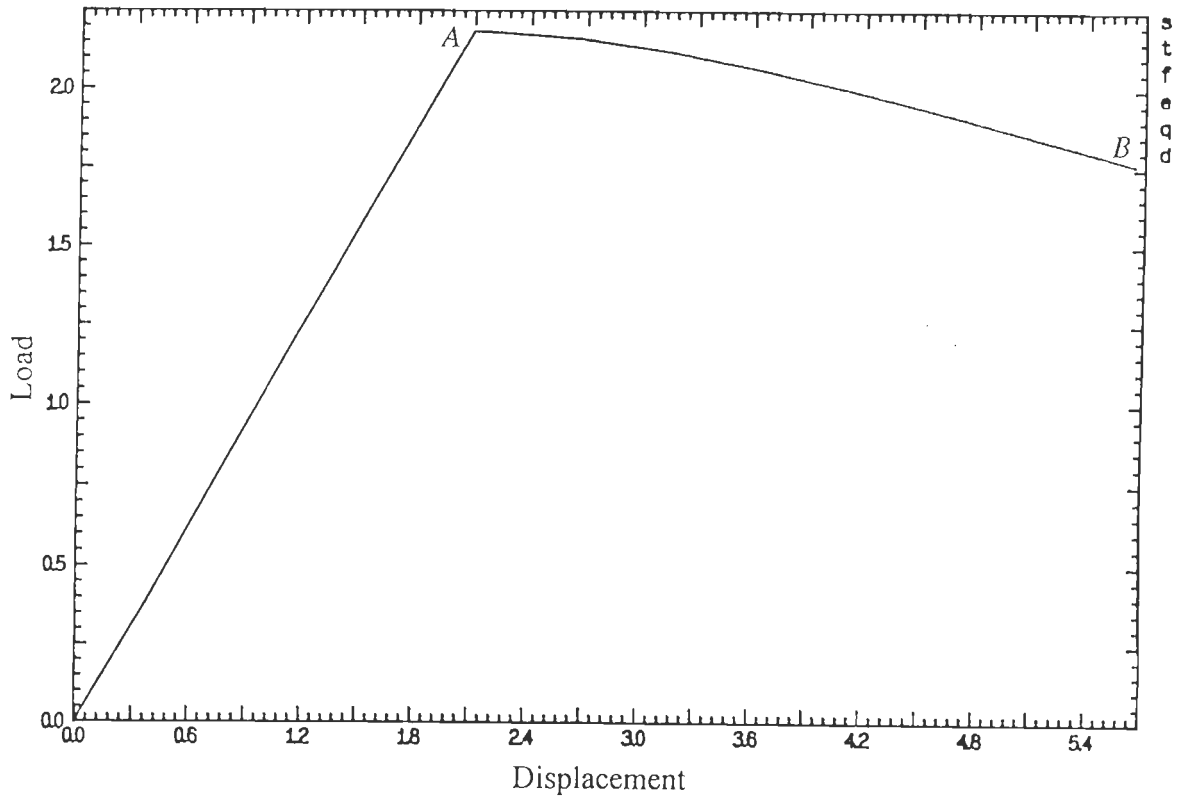

Fig. 7.5 Load deflection curve using von Mises yield criterion for uniaxial compression and strain softening ($A = A_{cr} = -0.107$)

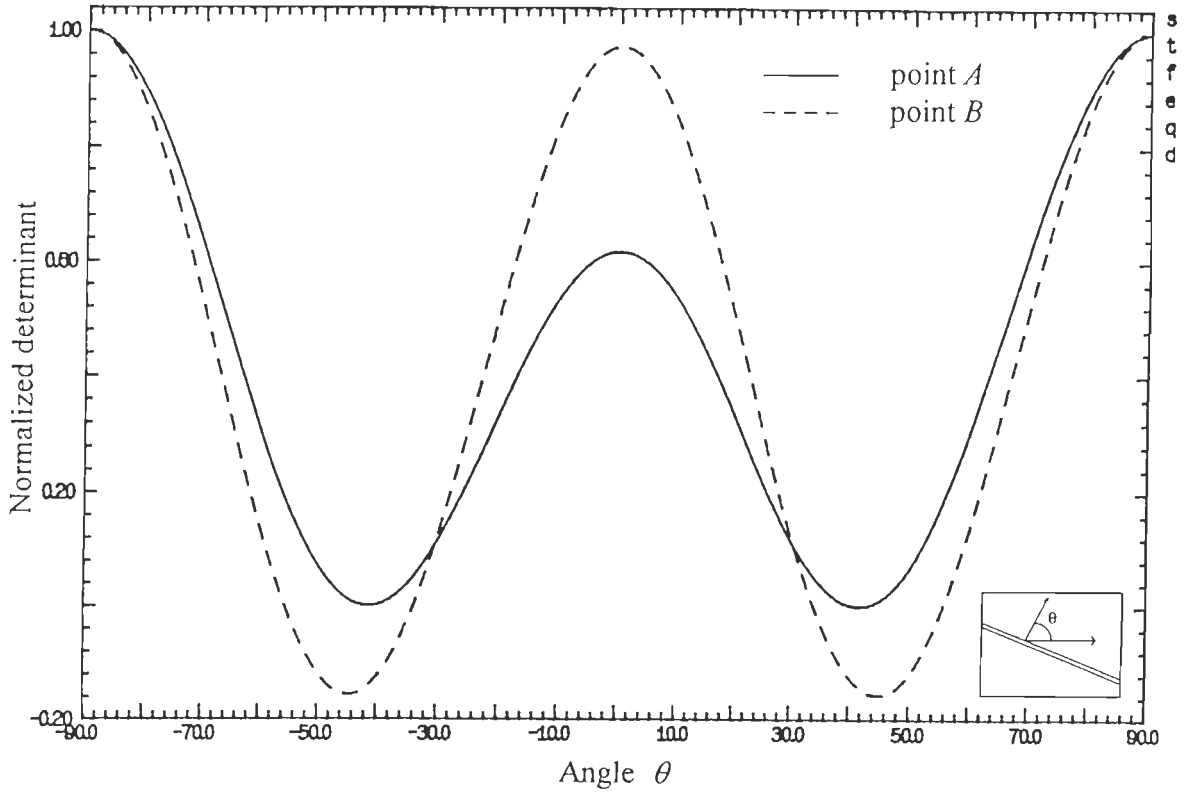

Fig. 7.6 Localization indicator using von Mises yield criterion for uniaxial compression and strain softening ($A = A_{cr} = -0.107$)

zero determinant is observed at an angle of ±42° when calculated at point A of the load deflection curve. With continued compression the determinant of the acoustic tensor becomes negative for a range of angles. At point B of load deflection curve (Fig. 7.5) the minimum determinant is at ±45° (Fig. 7.6).

If the hardening parameter A is selected such that $0 > A > A_{cr}$ then the load deflection curve of the problem under consideration should show a rising load deflection curve after first yield which may subsequently have a peak followed by a decline of load response. This is indeed observed to happen when, for example, A = – 0.05 (Fig. 7.7). The results of the acoustic tensor analysis are shown in Fig. 7.8. As expected the minimum normalized determinant is positive at first yield and reduces with continued compression.

Similarly when $A < A_{cr}$ then a decline of the load deflection curve is observed immediately after first yield (Fig. 7.9). This is accompanied by a negative determinant of the acoustic tensor at point A itself (Fig. 7.10).

7.3.3 Softening and Instability

In all cases with $A < 0$ continued compression leads to a stage when the determinant of the acoustic tensor is zero or negative within intervals of angles (Fig. 7.8 and 7.10). The size of these intervals can be increased by reducing the value of A. In fact localization can be made to occur at ±90° by appropriately working out $A = A_{cr90}$. For the problem under consideration $A_{cr90} = -0.98214$. The acoustic tensor analysis in this case yields a zero determinant for $\theta = \pm 90°$ (Fig. 7.11). In this case the determinant is negative for all angles remaining from −90° to +90°. A slight increase in A = – 0.60 reduces the range of possible localization angles (Fig. 7.11).

A finite element analysis of the problem with $A = A_{cr90}$ does not lead to convergence. The apparent reason is localization at $\theta = \pm 90°$ from the horizontal. These are the directions in which the single element structure is unrestrained and therefore undergoes increasing displacements in this (vertical) direction. Thus it can be safely stated that for this problem $A \leq A_{cr90}$ leads to instability, a requirement which may often be more stringent than the local uniqueness requirement (Willam et al., 1987) *viz.* $A + \mathbf{a}^T\mathbf{D}\mathbf{a} > 0$. It may be noted that for $A = A_{cr90}$, $A + \mathbf{a}^T\mathbf{D}\mathbf{a} = 0.26786$.

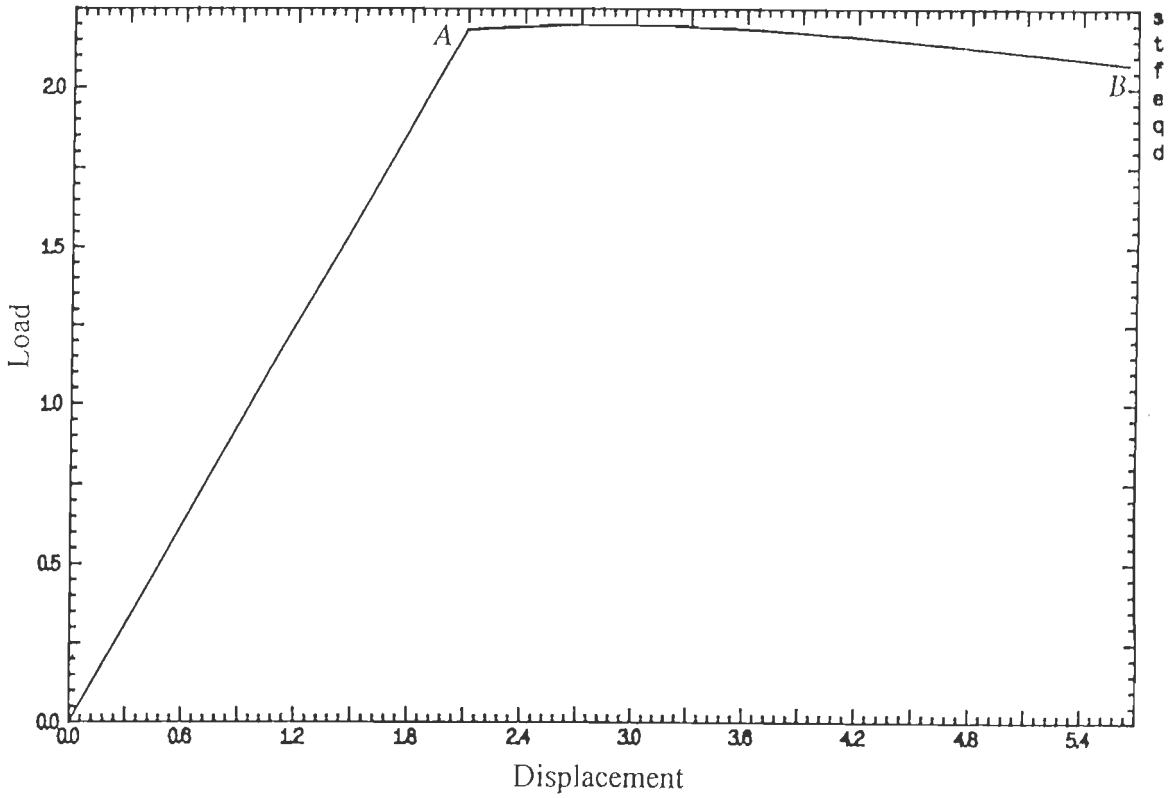

Fig. 7.7 Load deflection curve using von Mises yield criterion for uniaxial compression and strain softening ($0 > A > A_{cr}$)

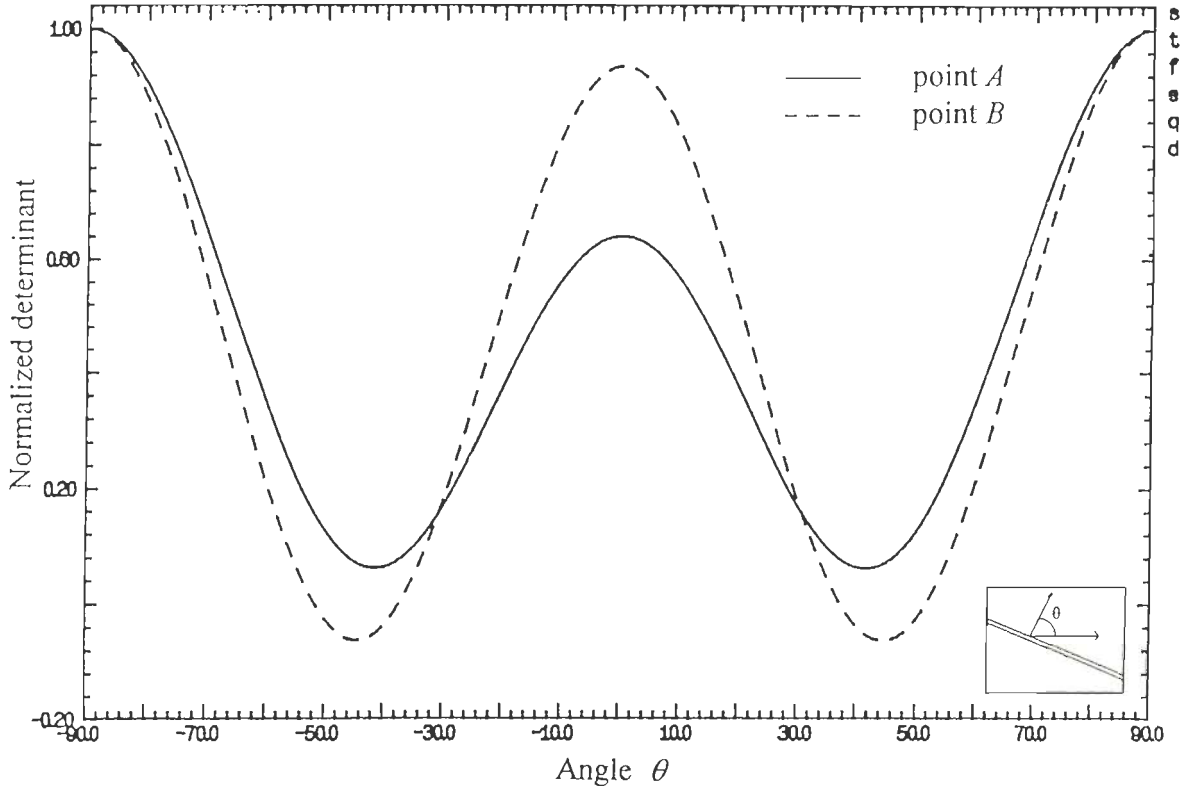

Fig. 7.8 Localization indicator using von Mises yield criterion for uniaxial compression and strain softening ($0 > A > A_{cr}$)

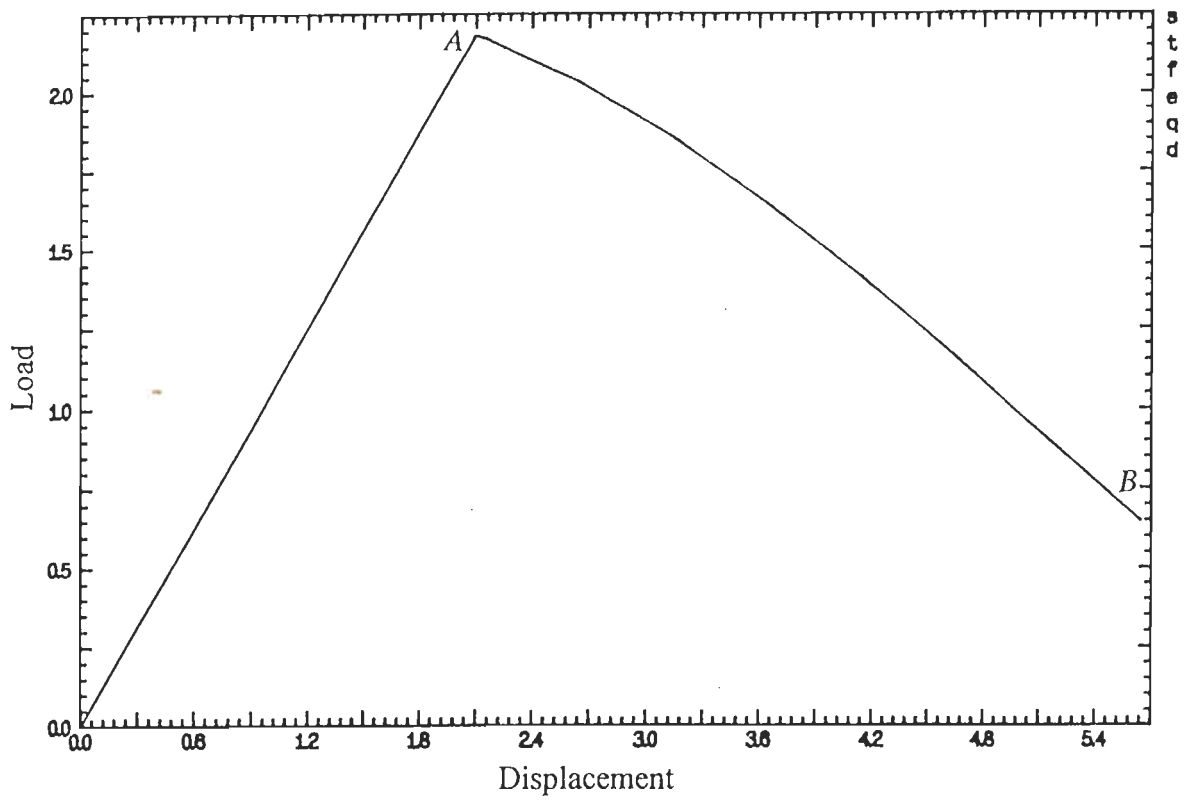

Fig. 7.9 Localization indicator using von Mises yield criterion for uniaxial compression and strain softening ($A < A_{cr}$)

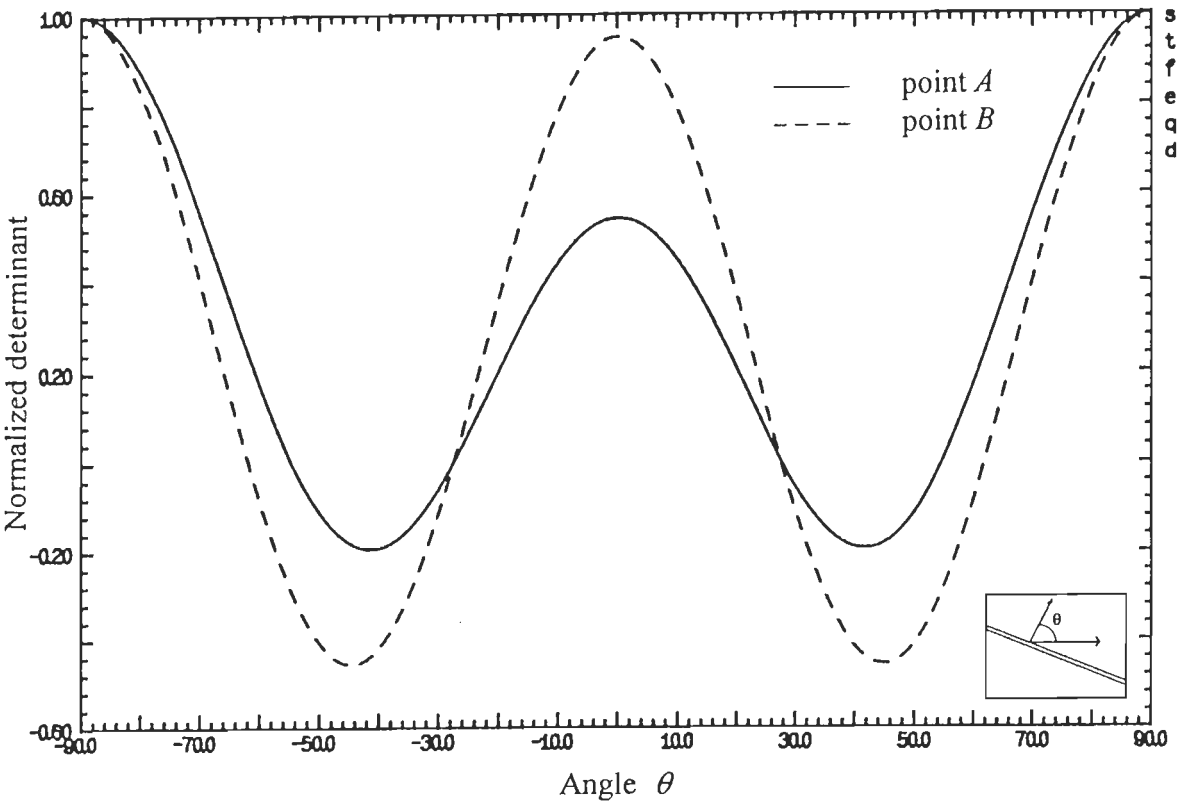

Fig. 7.10 Load deflection curve using von Mises yield criterion for uniaxial compression and strain softening ($A < A_{cr}$)

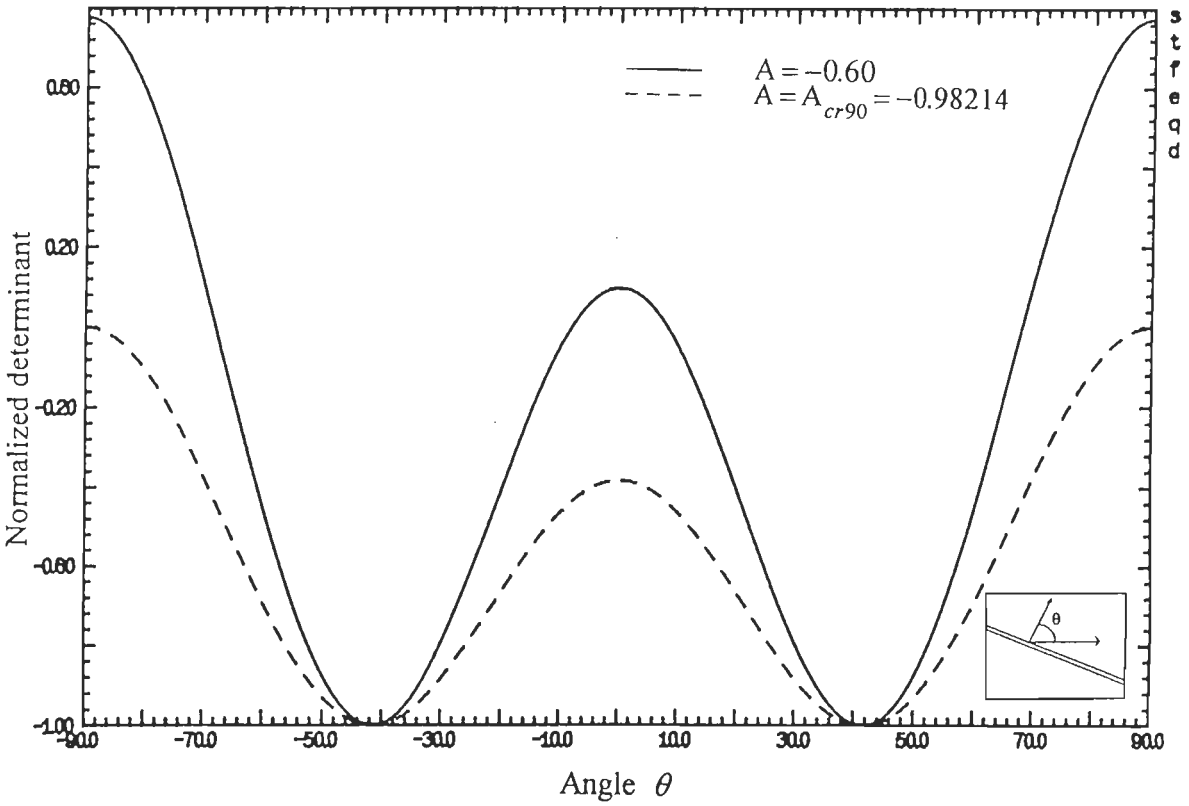

Fig. 7.11 Localization indicator using von Mises yield criterion for uniaxial compression and strain softening ($A_{cr90} = -0.98214$)

7.4 Mohr Coulomb Criterion

The problem of Fig. 7.1 with the element assumed to be of Mohr Coulomb material with $c\cos\phi = 2.25$ and $\phi = 30^\circ$ was considered. The elastic constants $E = 1.0$ and $\nu = 0.20$ were assumed. Once again associated plasticity is assumed.

7.4.1 Perfect Plasticity

Uniaxial compression for this problem with A = 0 or perfect plasticity leads to a flat load deflection response immediately after first yield (Fig. 7.12). In this case the stress state remains unchanged with continued compression after first yield (Fig. 7.13). The acoustic tensor analysis at all post yield stages indicates that the normal to the localization plane from the horizontal is inclined at an angle of ±60° (Fig. 7.14). This is in fact the result that is obtained using elementary soil mechanics expression *viz.*

$$\alpha = -\beta + \left(\frac{\pi}{4} + \frac{\phi}{2}\right)$$

where α and β are directions of localization band and maximum principal stress from the horizontal.

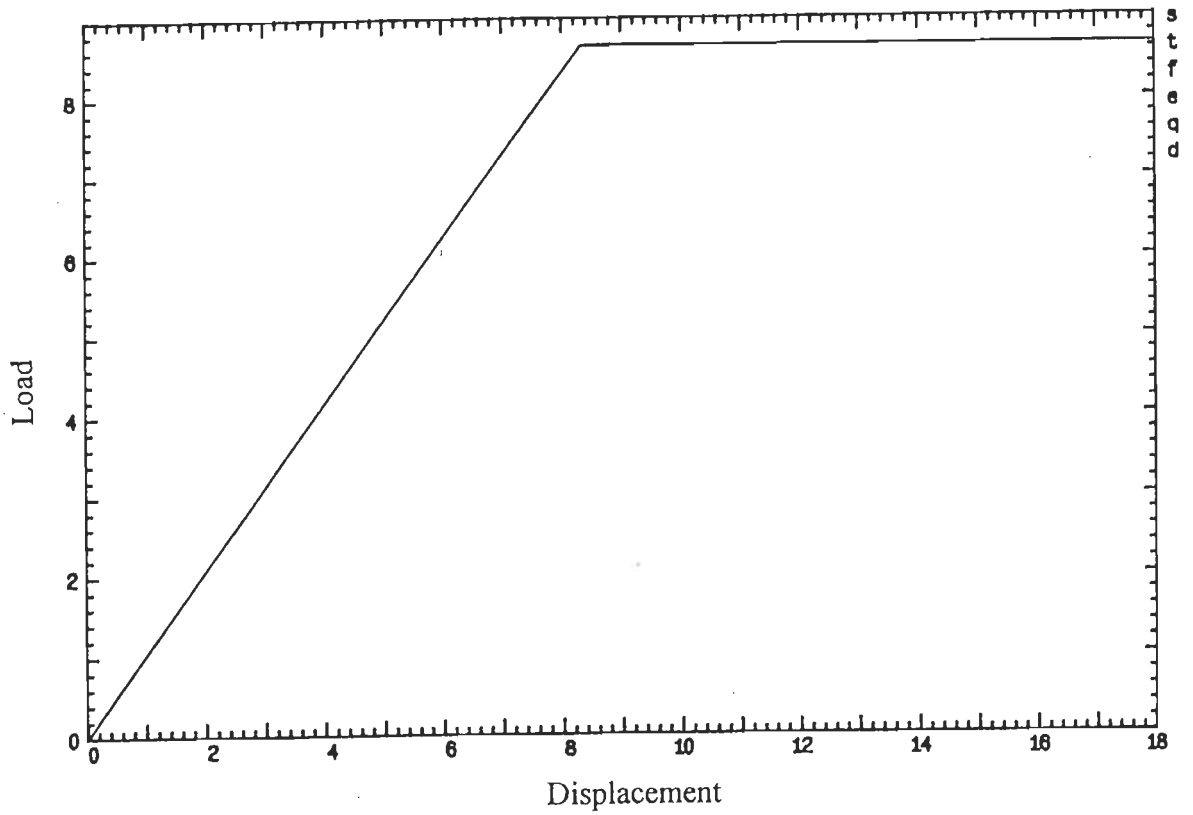

Fig. 7.12 Load deflection curve using Mohr Coulomb yield criterion for uniaxial compression and perfect plasticity

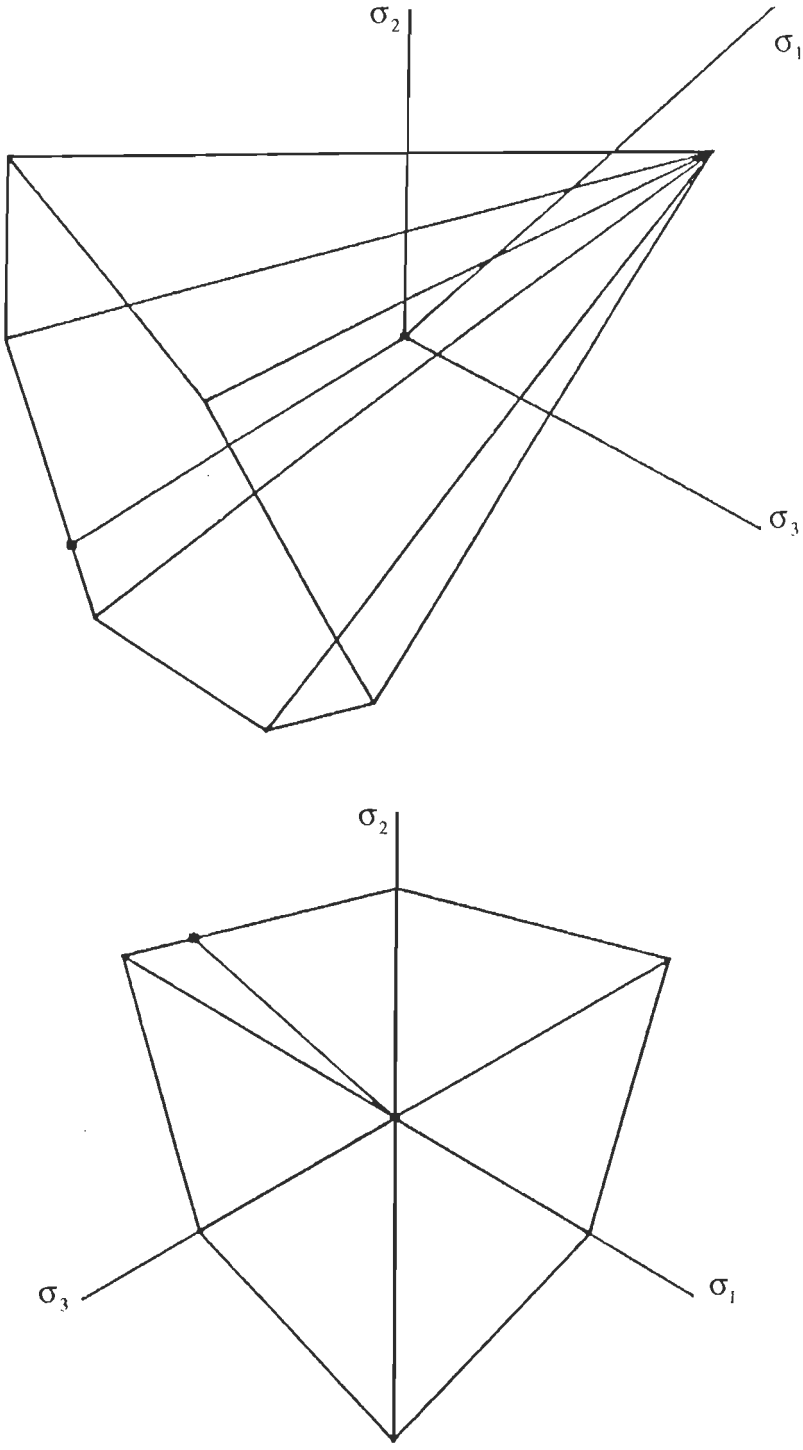

Fig. 7.13 Movement of the stress point on the Mohr Coulomb yield surface for uniaxial compression and perfect plasticity (a) in principal stress space (b) $\pi-$ plane representation

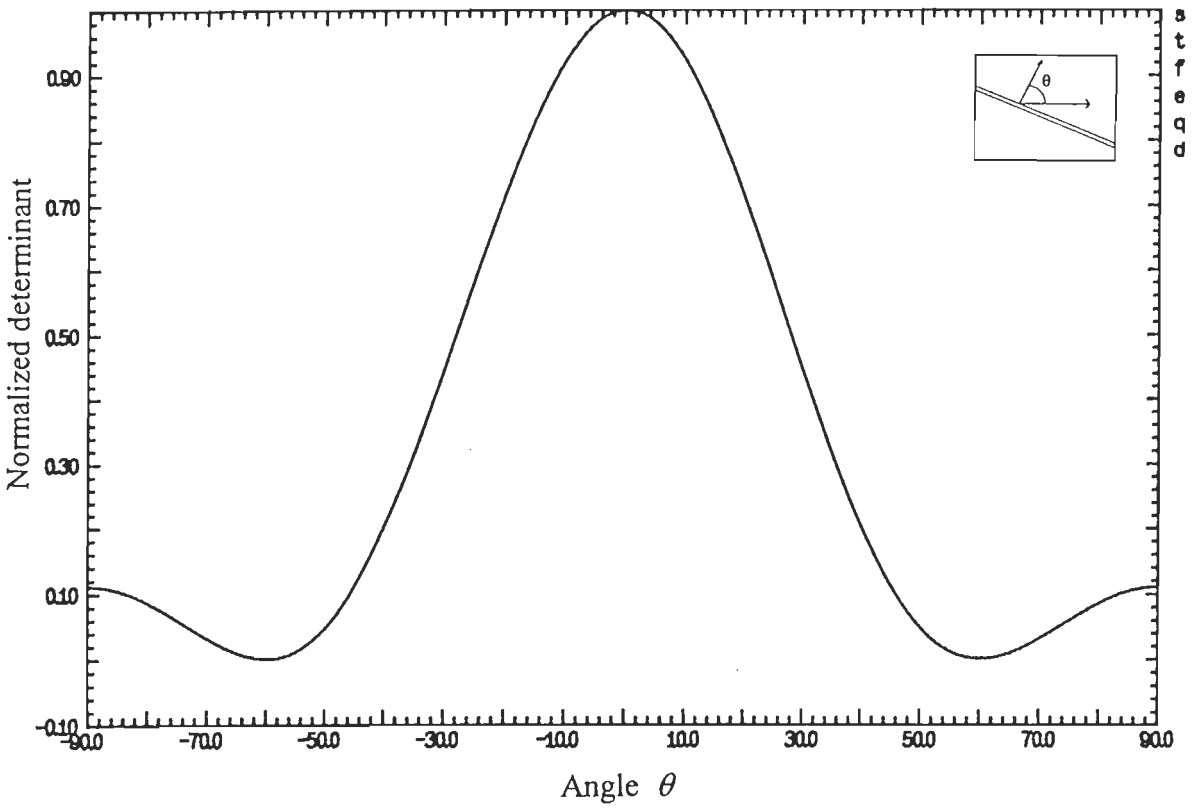

Fig. 7.14 Localization indicator using Mohr Coulomb yield criterion for uniaxial compression and perfect plasticity

7.4.2 Softening Plasticity

A reduction in the hardening parameter A leads to an immediate decline in the load deflection curve (Fig. 7.15). Typically for softening plasticity the yield surface will contract and the variation of the stress state will be as shown in Fig. 7.16.

For Mohr coulomb plasticity too a critical value of $A = A_{cr90}$ can be found such that the normal to localization band is inclined at an angle of $\pm 90^{\circ}$ from the horizontal. For this problem $A_{cr90} = -0.066$ was worked out. The corresponding results of the acoustic tensor analysis are shown in Fig. 7.17. A uniaxial compression with $A = A_{cr90}$ once again leads to instability which in finite element analysis results in a non convergent solution state.

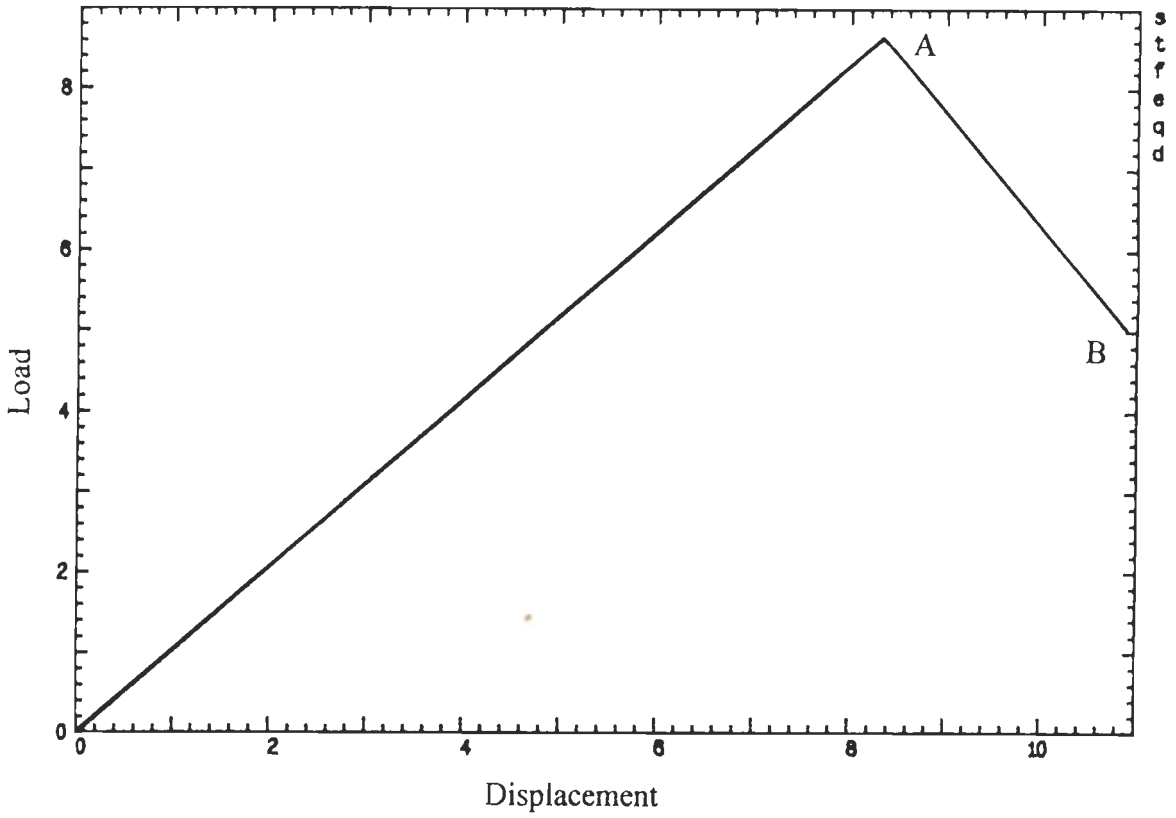

Fig. 7.15 Load deflection curve using Mohr Coulomb yield criterion for uniaxial compression and strain softening

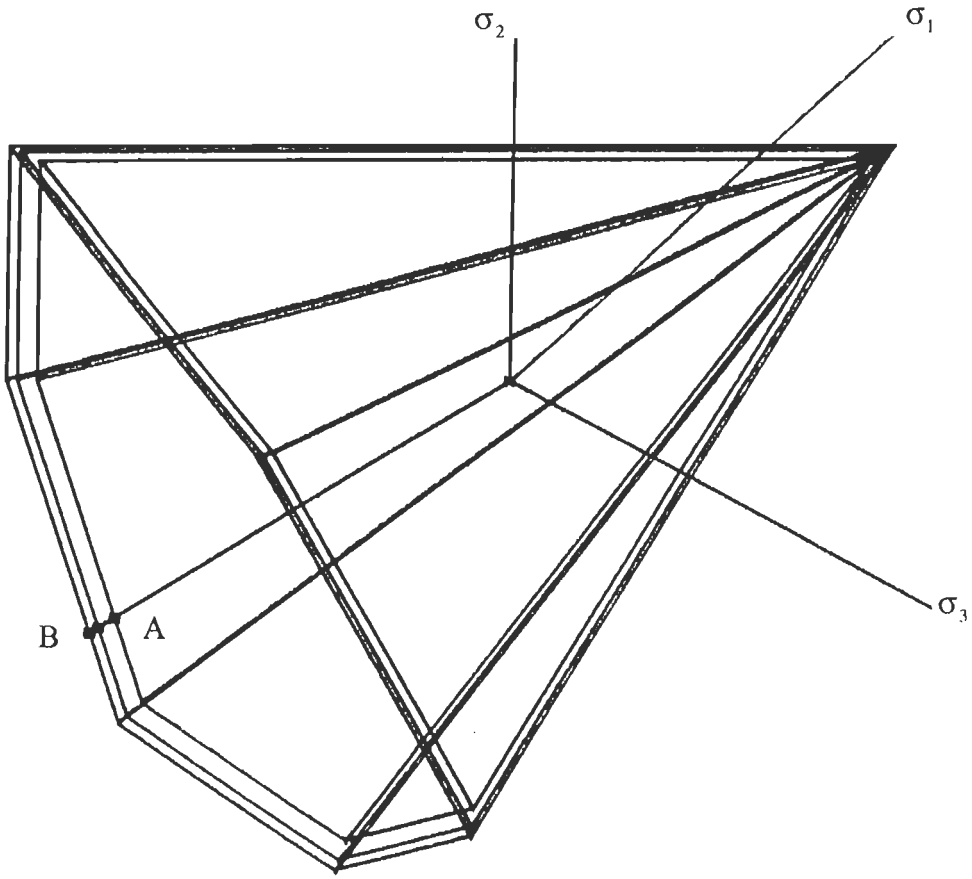

(a)

— *Continued*

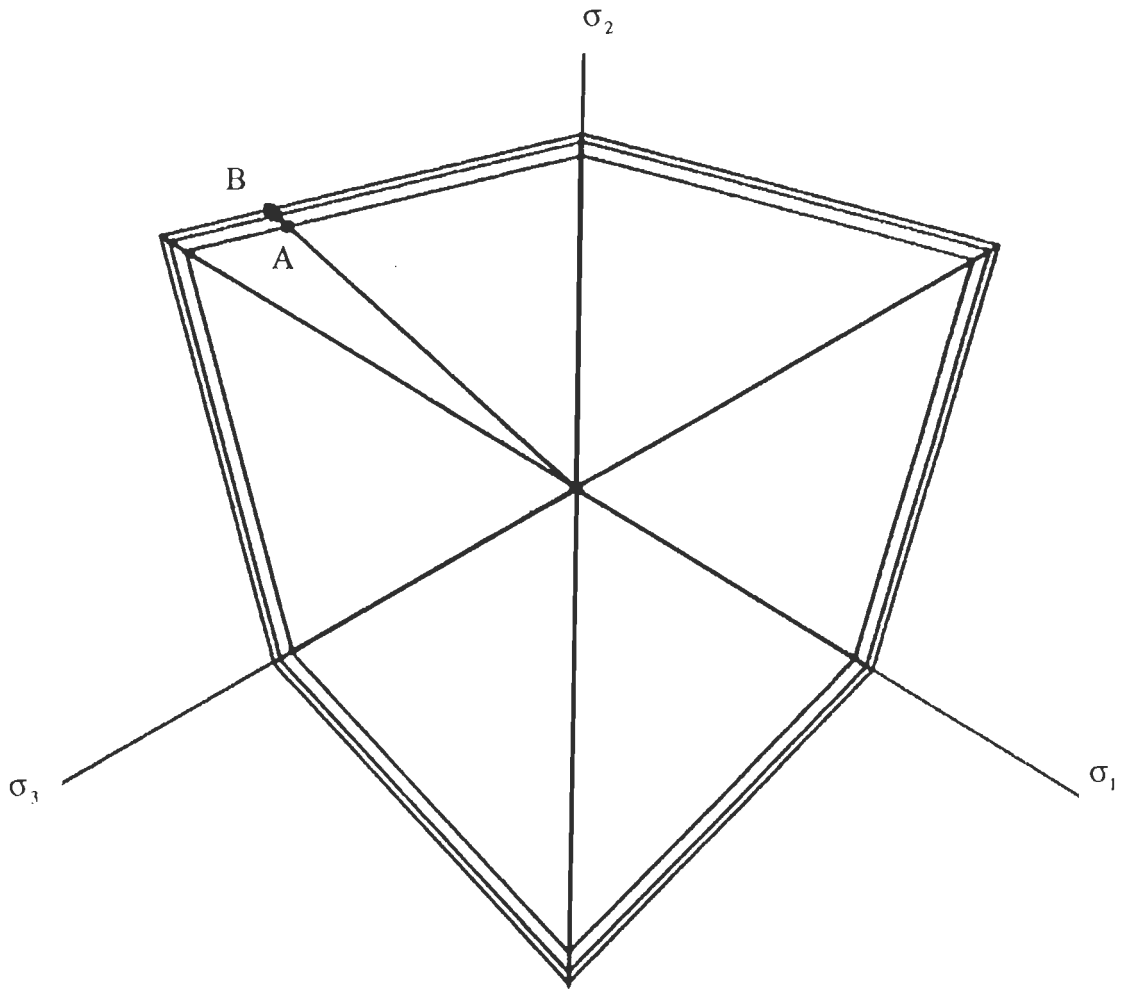

(b)

Fig. 7.16 Movement of the stress point on the Mohr Coulomb yield surface for uniaxial compression and strain softening (a) in principal stress space (b) $\pi-$ plane representation

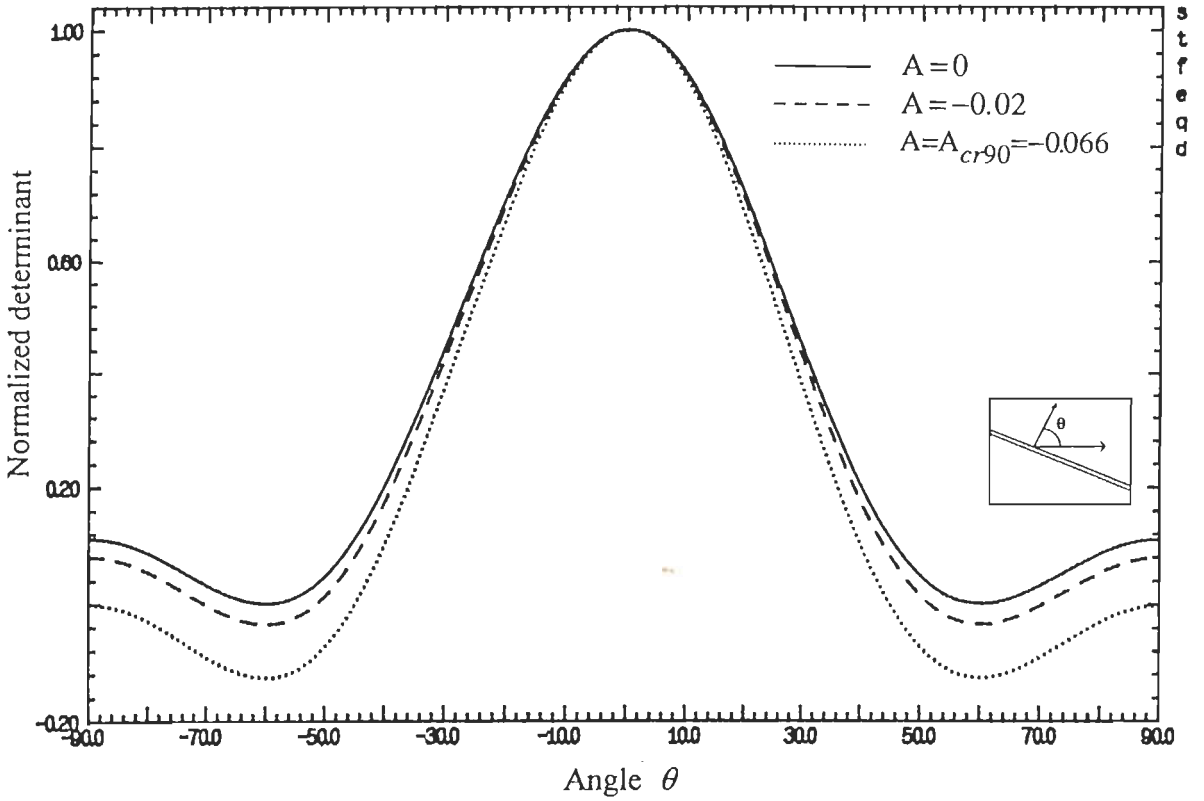

Fig. 7.17 Localization indicator using Mohr coulomb yield criterion for uniaxial compression and strain softening for different hardening parameters

7.5 Hoffman Criterion

The uniaxial compression problem of Fig. 7.1 is reconsidered in conjunction with the Hoffman criterion. The elastic constants $E = 2 \times 10^5$ and $\nu = 0.25$ were assumed.

7.5.1 Perfect Plasticity

In the first instance the element is assumed to be perfectly plastic with $f_{co} = 10000$, $f_{to} = 1000$. The resulting load deflection curve is shown in Fig. 7.18 and the variation of stress on the yield surface is shown in Fig. 7.19. Similar to what was observed with the von Mises criterion the load deflection curve ascends before becoming flat. During this rise from point A to B (Fig. 7.18) the stress state curves from point A to point B as shown in Fig. 7.19. At point B the stresses become constant and remain unchanged thereafter. The results of the acoustic tensor analysis conducted at points A and B are illustrated in Fig. 7.20. The localization condition is satisfied only when the load deflection curve becomes flat. The minimum determinant is observed at $\theta \approx \pm 58^\circ$. Clearly

this value depends on the f_c/f_t ratio. When $f_c = f_t$ this criterion changes to von Mises criterion in which case θ has already been found to be ±45°.

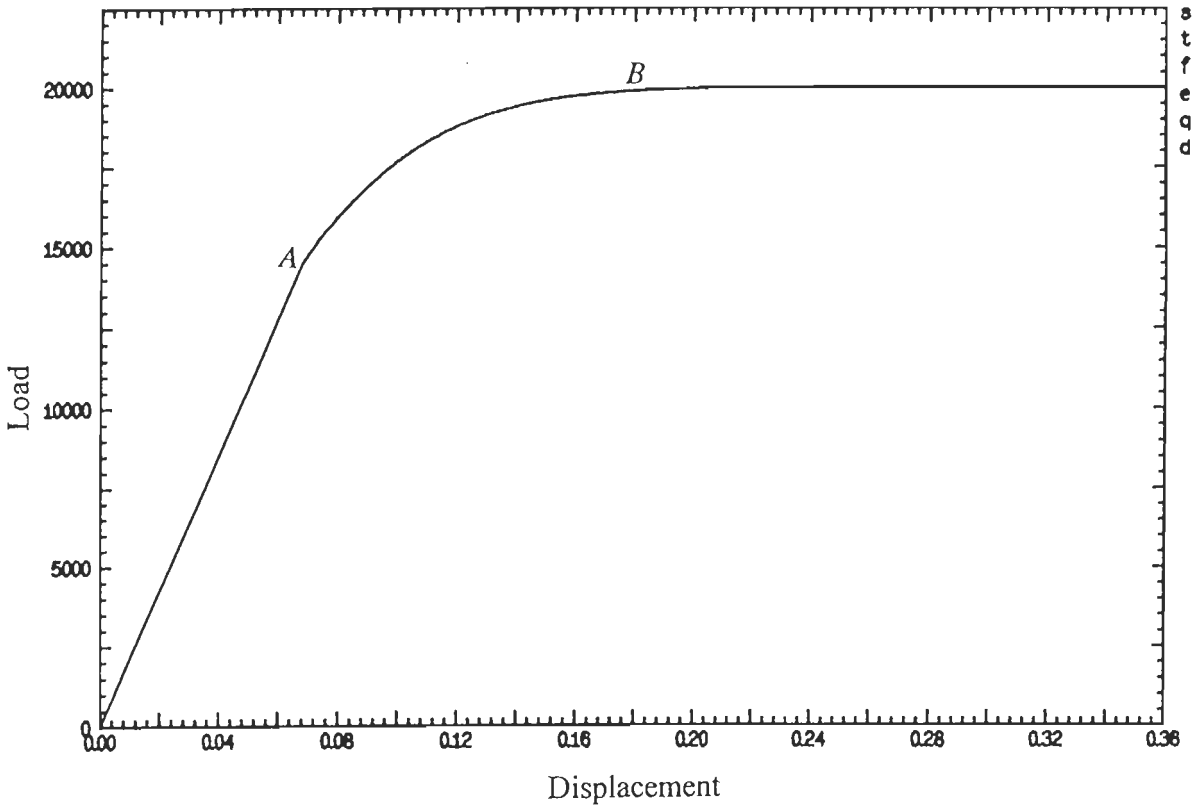

Fig. 7.18 Load deflection curve using Hoffman yield criterion for uniaxial compression and perfect plasticity

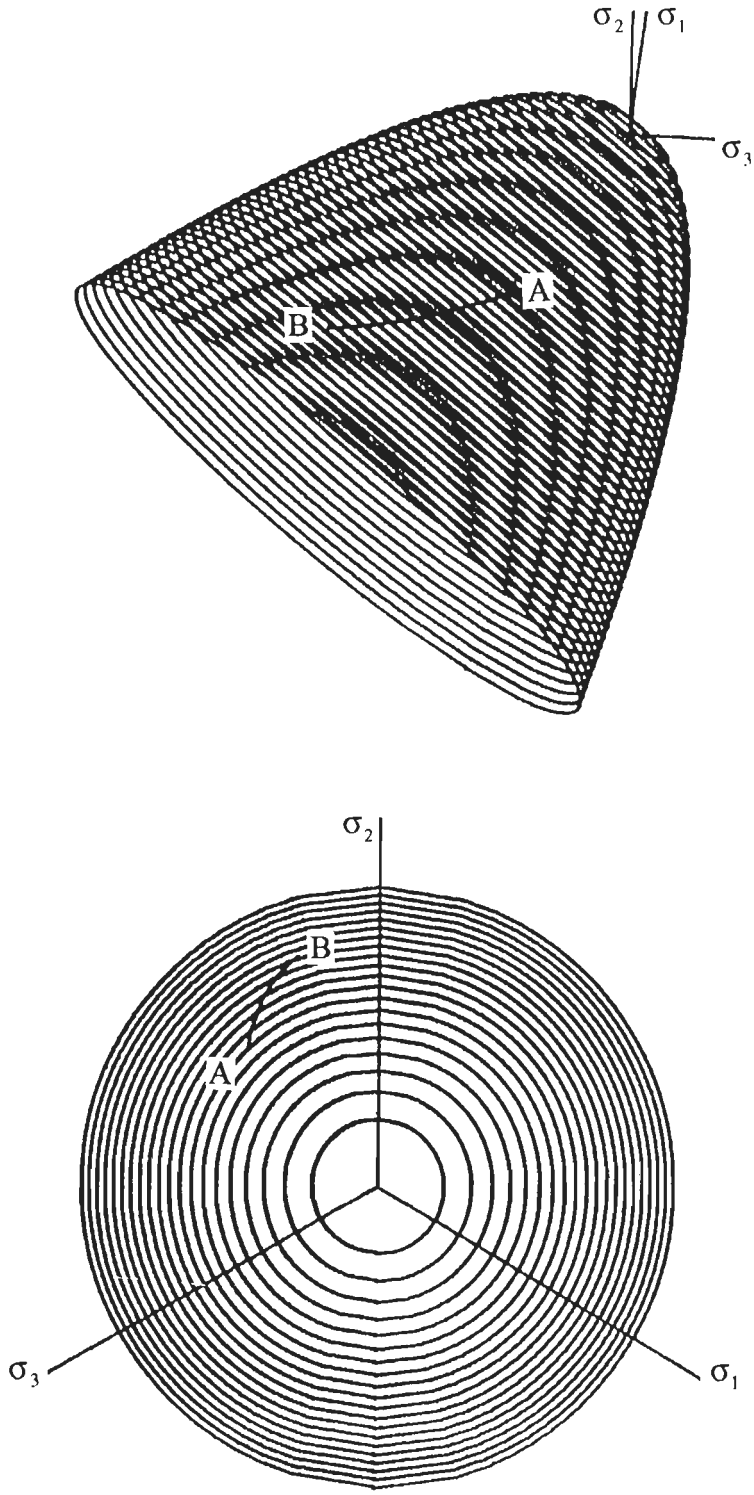

Fig. 7.19 Movement of the stress point on the Hoffman yield surface for uniaxial compression and perfect plasticity (a) in principal stress space (b) $\pi-$ plane representation

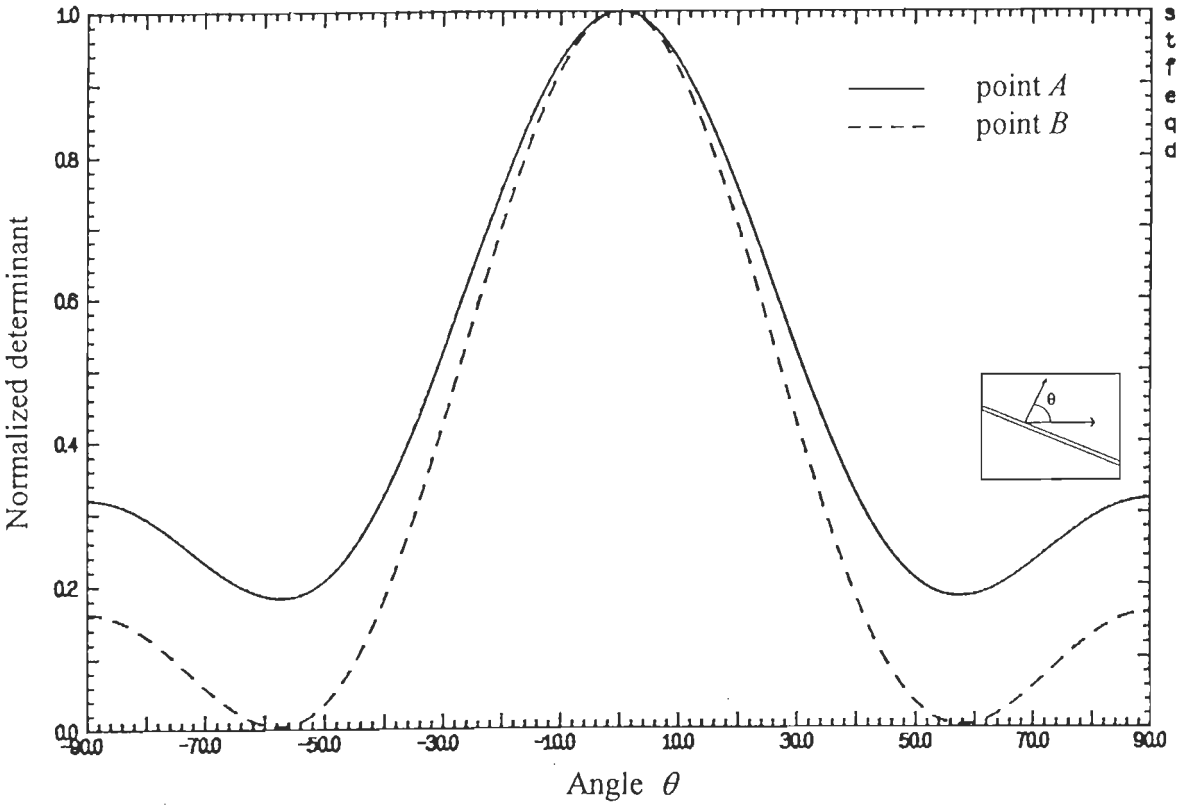

Fig. 7.20 Localization indicator using Hoffman yield criterion for uniaxial compression and perfect plasticity

7.5.2 Softening Plasticity

In this case the problem under consideration was tackled considering a decline in (a) f_t only and (b) both f_c and f_t. In both cases an exponential softening as discussed in the last Chapter with $\varepsilon_c = 0.15$ was used.

For the former case in which softening is confined to f_t only uniaxial compression led to a load deflection curve as shown in Fig. 7.21. The figure illustrates the absence of a peak and therefore a post-peak load deflection response. The normalized determinant of the acoustic tensor analysis are illustrated in Fig. 7.22 corresponding to points A and B of the load deflection curve. The localization condition is not satisfied as the minimum determinant remains positive. Thus with only a decline in f_t, uniaxial compression of the kind considered does not produce localization and post-peak response. The reason for this is apparently hardening of the yield surface in the compression regime as discussed in the last Chapter.

The latter case wherein softening was assumed to be both with regard to f_c and f_t, a peak and a post-peak (declining) response is observed as shown in Fig. 7.23. The acoustic tensor analysis at points A (first yield), B (near the peak) and C (on the descending branch

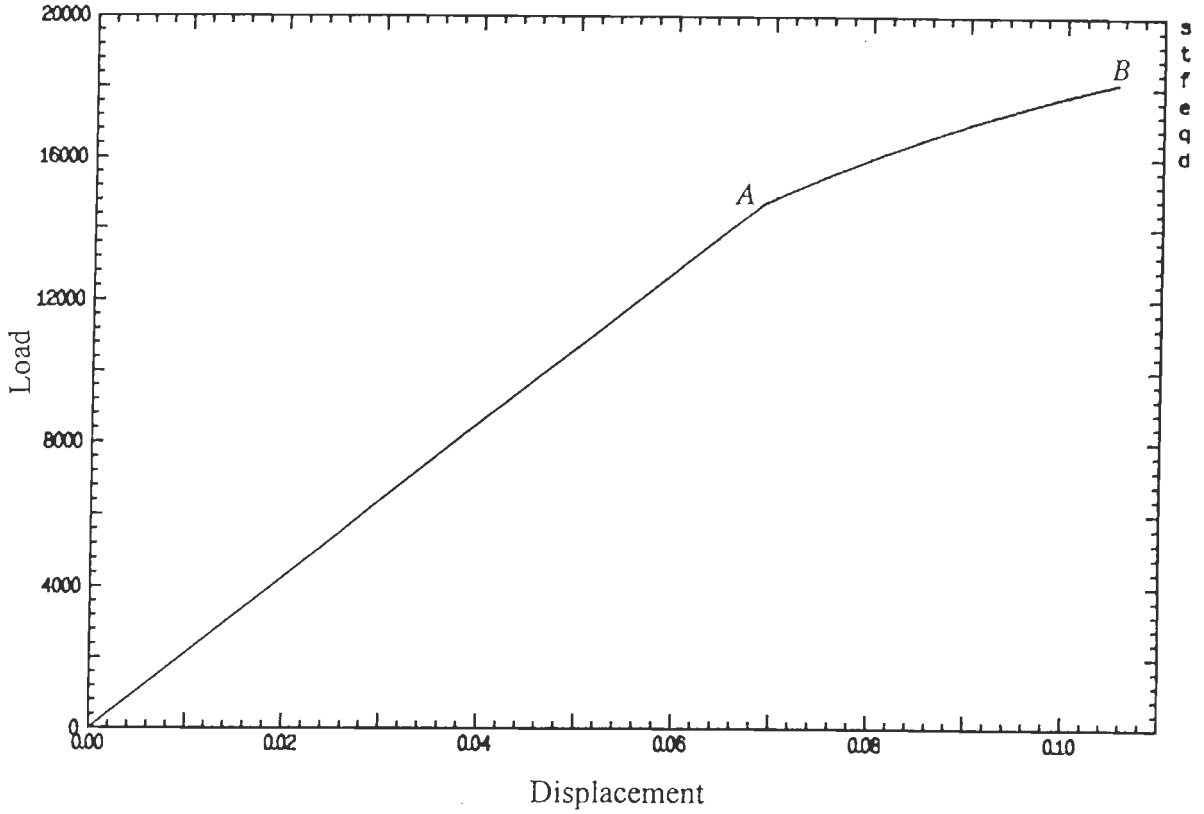

Fig. 7.21 Load deflection curve using Hoffman yield criterion for uniaxial compression and perfect plasticity, $f_{co} = 10000$ and $f_{to} = 1000$ (only f_t reduces)

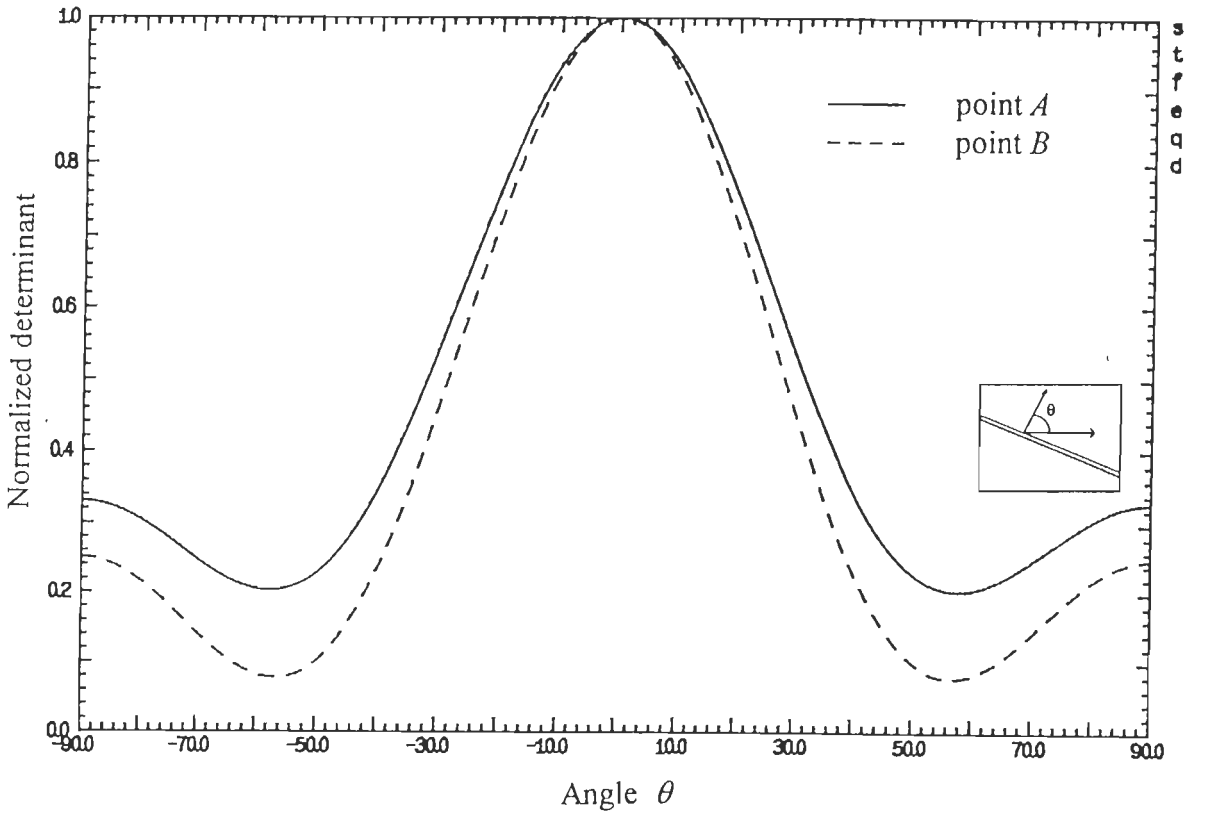

Fig. 7.22 Localization indicator using Hoffman yield criterion for uniaxial compression and perfect plasticity, $f_{co} = 10000$ and $f_{to} = 1000$ (only f_t reduces)

of the load deflection curve) is shown in Fig. 7.24. It can be seen that point B corresponds to a near satisfaction of the localization condition. The minimum determinant at this stage is found to be at $\theta \approx \pm 58^{\circ}$. At point C the localization condition is satisfied for a finite range of localization angles.

If f_{co}/f_{to} ratio is decreased by assuming $f_{co} = 10000$ and $f_{to} = 9000$ a more gradual post-peak behaviour is observed (Fig. 7.25). The acoustic tensor analysis corresponding to this case is shown in Fig. 7.26. In this case the localization angle reduces to $\theta \approx \pm 45^{\circ}$.

7.6 Mesh Sensitivity Issues

The mesh sensitivity issues can be broadly classified into two streams (Bicanic and Pankaj, 1990; Pankaj, 1990; Pankaj and Bicanic, 1991).

(a) Element size sensitivity or mesh objectivity.
(b) Discretisation sensitivity *i.e.* mesh ability/inability to capture localization.

The former aspect related to strain softening whereas the latter is relevant for non-softening localization problems as well.

With regard to the former issue, it is known that the choice of element size affects the finite element solution of strain softening problems, if no provision for non-local material model is made (Pankaj, 1990). Thus two meshes that "appear similar" in terms of element shapes and layout, but are different in terms of element sizes would yield different responses if softening modulus is treated as a material property. So in order to obtain mesh objective responses, some provisions for incorporating nonlocal moduli, (e.g. by using the concept of constant fracture energy) has to be made.

Localization has been defined as a strain discontinuity (Willam et al., 1994), which in the limit will represent a displacement discontinuity as well. In the finite element context, it has been argued (Bicanic and Pankaj, 1990; Willam et al. 1994) that meshes need to be fine in order to obtain a near displacement discontinuous solution and that the element boundaries need to be aligned with the localization band directions. In this study, consideration is limited to element size sensitivity issue. A simple compression panel problem is considered (Pietruszczak and Mroz, 1980,1981; Pankaj, 1990) for the study, where, apparently, the localization directions can be determined a priori with the aid of acoustic tensor studies discussed earlier.

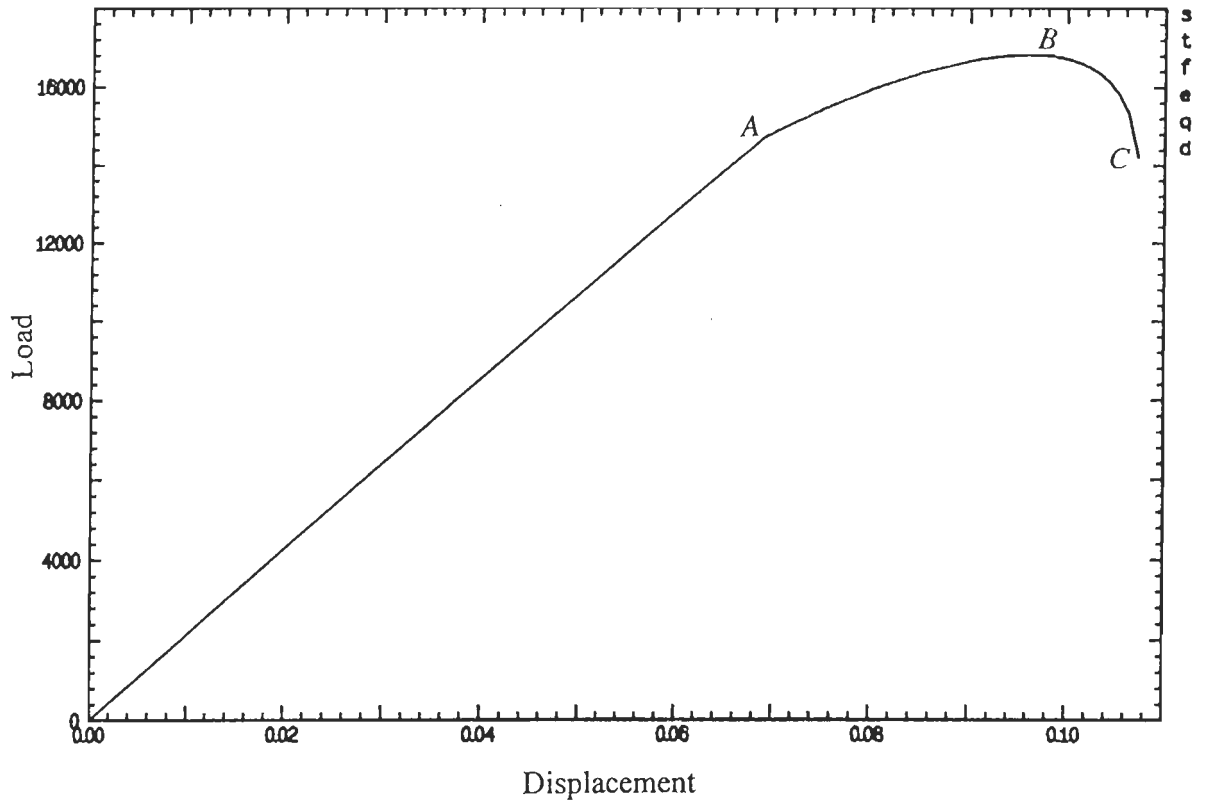

Fig. 7.23 Load deflection curve using Hoffman yield criterion for uniaxial compression and perfect plasticity, $f_{co} = 10000$ and $f_{to} = 1000$ (f_c and f_t both reduce)

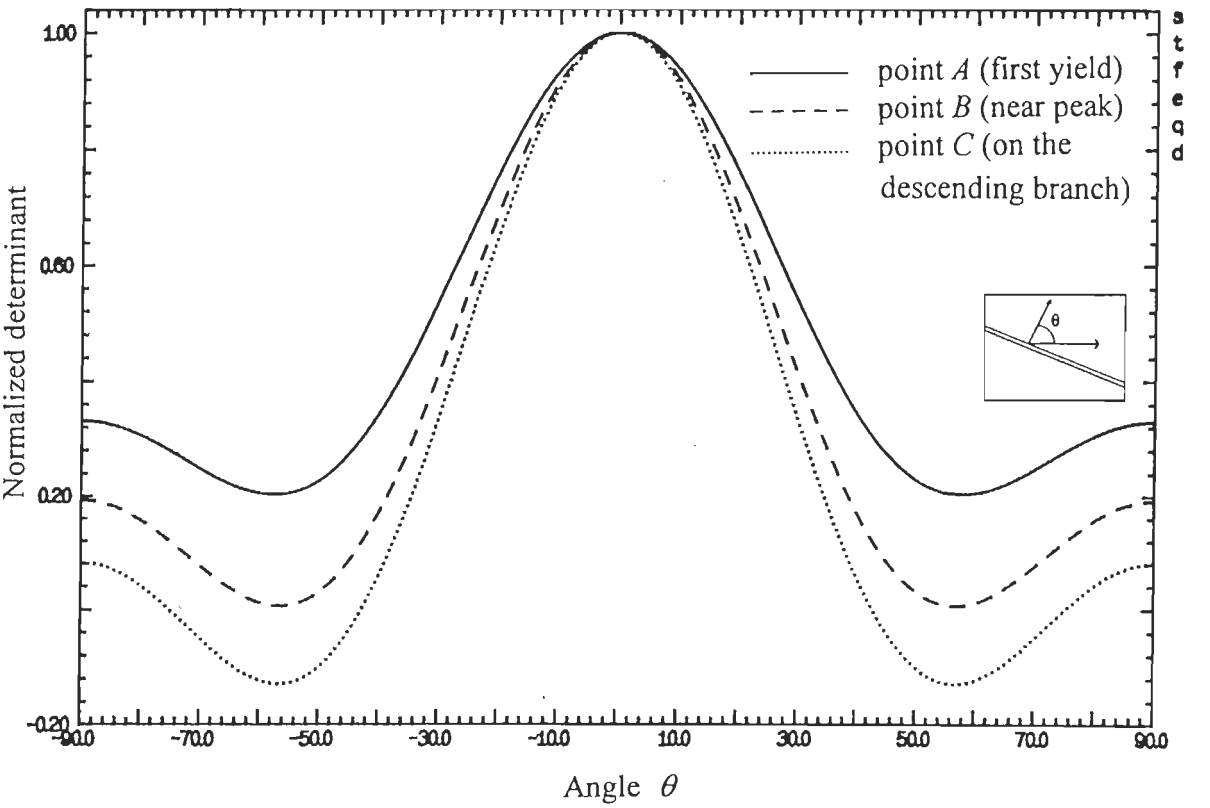

Fig. 7.24 Localization indicator using Hoffman yield criterion for uniaxial compression and perfect plasticity, $f_{co} = 10000$ and $f_{to} = 1000$ (f_c and f_t both reduce)

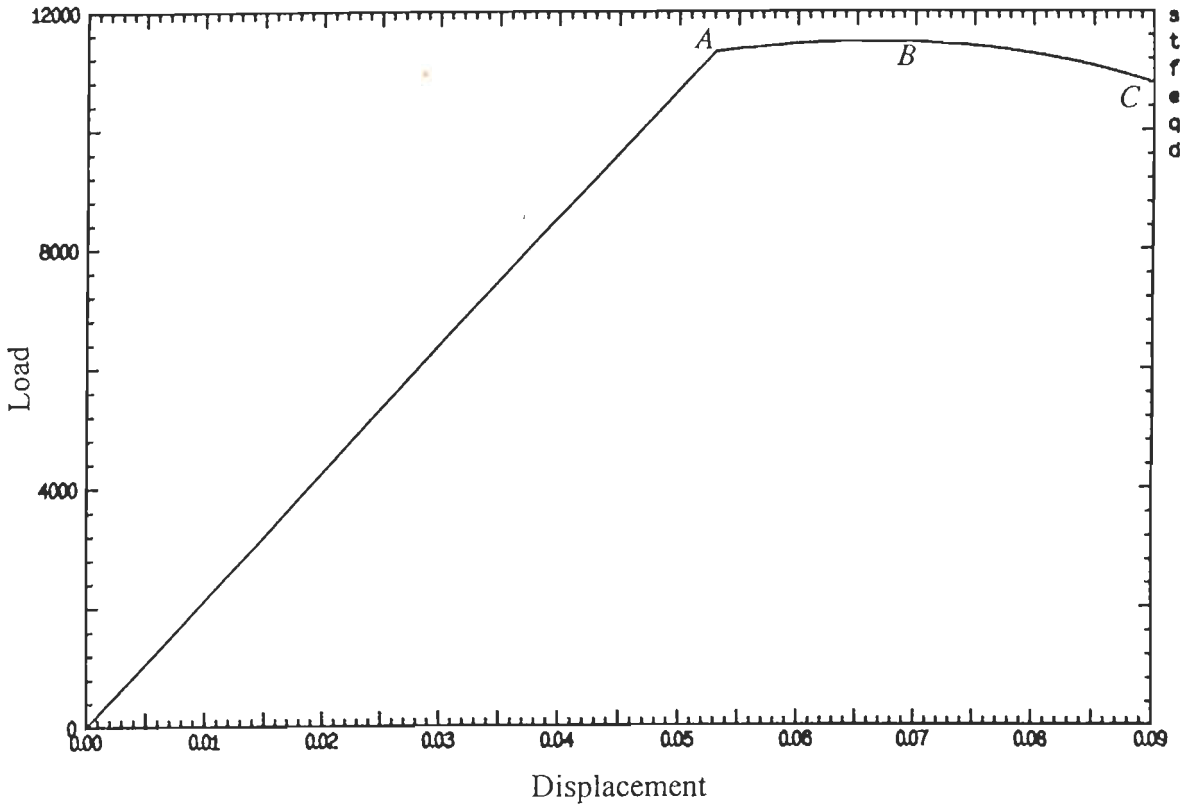

Fig. 7.25 Load deflection curve using Hoffman yield criterion for uniaxial compression and perfect plasticity, $f_{co} = 10000$ and $f_{to} = 1000$ (f_c and f_t both reduce)

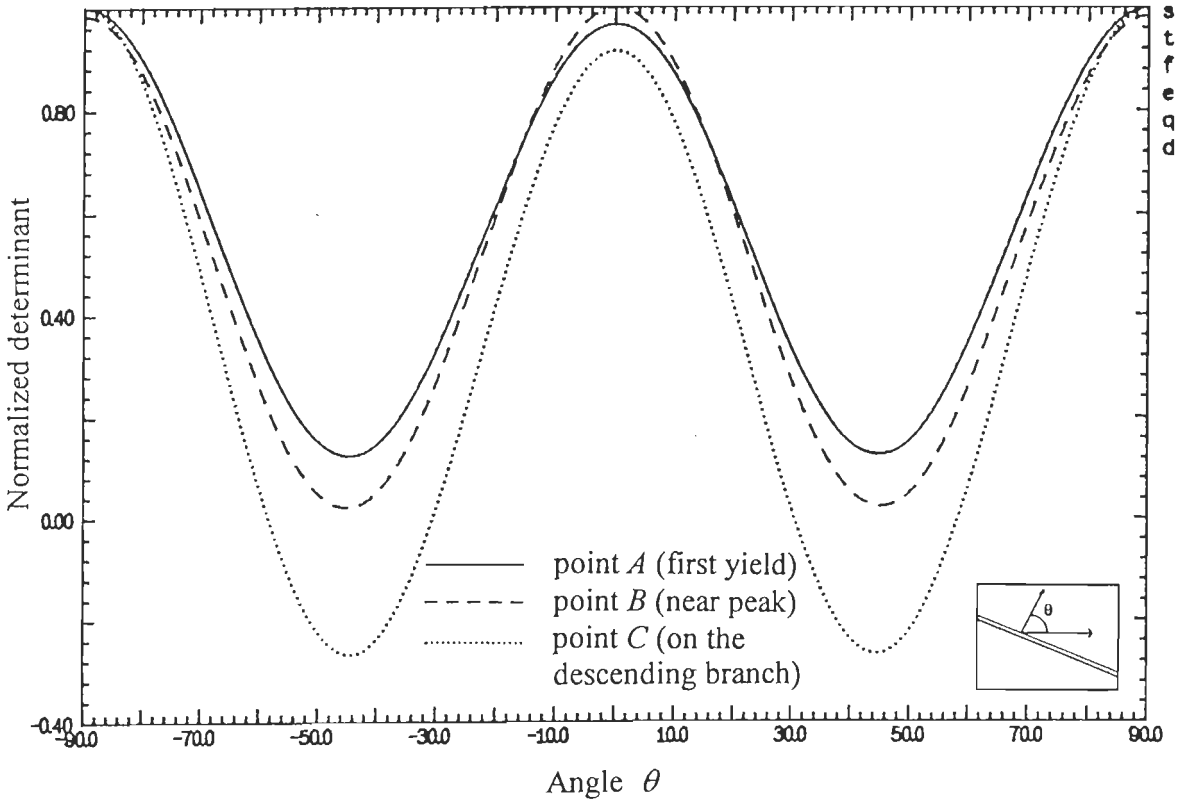

Fig. 7.26 Localization indicator using Hoffman yield criterion for uniaxial compression and perfect plasticity, $f_{co} = 10000$ and $f_{to} = 9000$ (f_c and f_t both reduce)

Assuming that the loss of strength in the damaged material decreases exponentially to zero as shown in Fig. 7.27 (Eqn. 4.15), the energy released from the band of Fig. 7.28a on full rupture will be

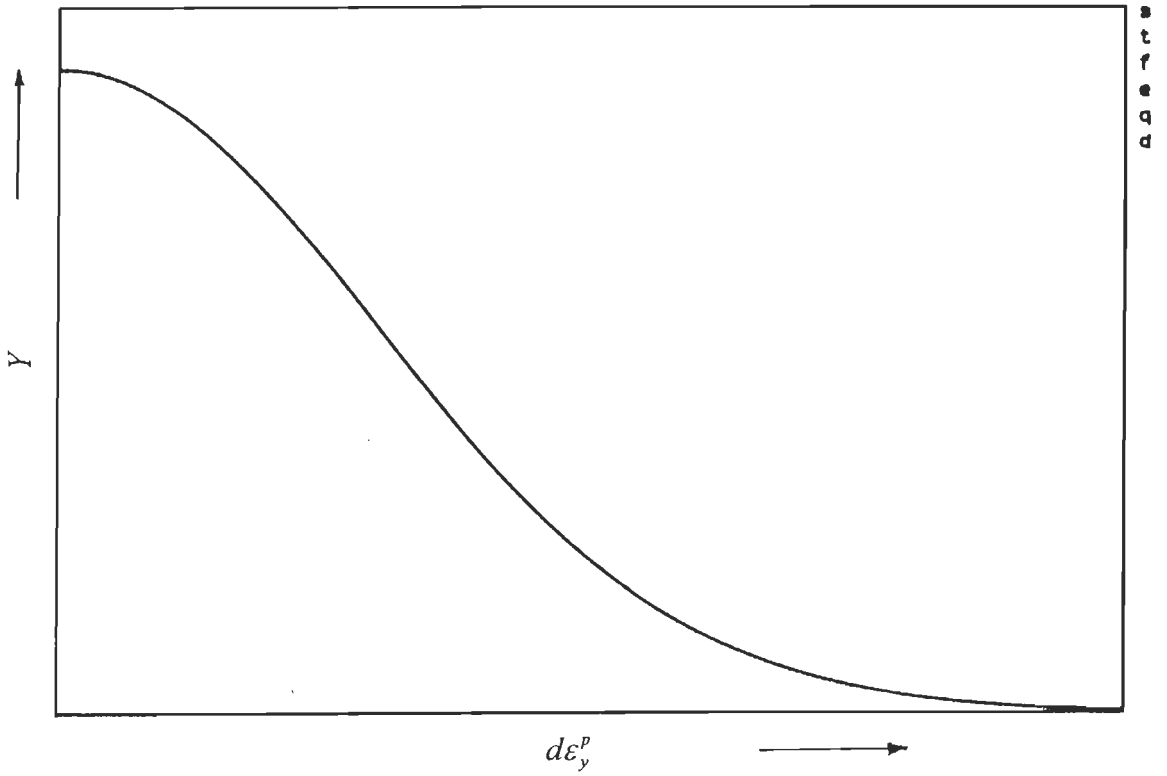

Fig. 7.27 Exponential decay of strength in the damaged material

$$\begin{aligned}\Delta E &= V_{t1}\int_0^\infty Y d\,\varepsilon_y^p = V_{t1}Y_\circ\int_0^\infty e^{-\left(\varepsilon_y^p/\varepsilon_{c1}\right)^2} d\varepsilon_y^p \\ &= \frac{\sqrt{\pi}}{2}Y_\circ\varepsilon_{c1}V_{t1} = \frac{\sqrt{\pi}}{2}Y_\circ\varepsilon_{c1}d_1l_1t \\ &= \frac{\sqrt{\pi}}{2}Y_\circ\varepsilon_{c1}A_1t\end{aligned} \tag{7.1}$$

If this is same as the band of Fig. 7.28b, then

$$\begin{aligned}\Delta E &= \frac{\sqrt{\pi}}{2}Y_\circ\varepsilon_{c2}d_2l_2t \\ &= \frac{\sqrt{\pi}}{2}Y_\circ\varepsilon_{c2}A_2t\end{aligned} \tag{7.2}$$

Equating Eqns. 7.1 and 7.2, one obtains

$$\frac{A_1}{A_2} = \frac{\varepsilon_{c2}}{\varepsilon_{c1}} \tag{7.3}$$

Thus, the parameter ε_c is inversely proportional to the area of the localization band. An appropriate choice of ε_c can be made if it is noted that the fracture energy per unit area G_c can be written as

$$G_c = \frac{\Delta E}{lt} \tag{7.4}$$

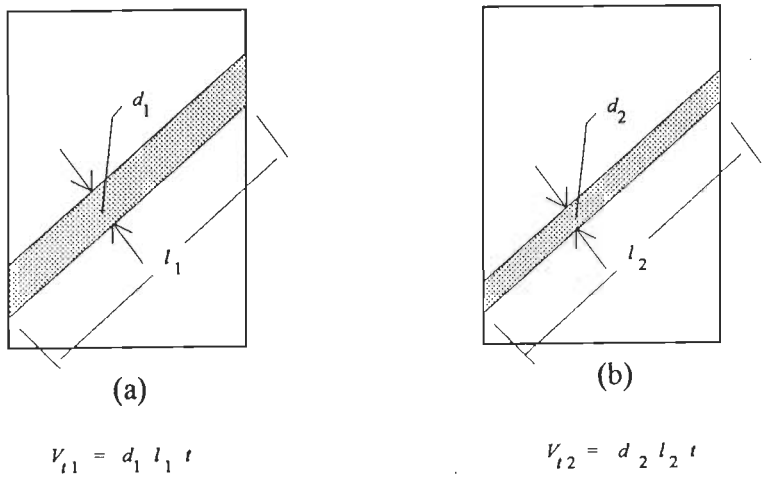

Fig. 7.28 Panel with two different localization band widths

7.7 Compression Panel under Softening von Mises Plasticity

A plane strain compression panel analysed by Pietruszczak and Mroz (1980,1981) and Pankaj (1990), shown in Fig. 7.29, was considered. The loading platens were assumed to be lubricated and frictionless. Thus, if the material of the panel is without defects, then the entire panel would deform uniformly. Clearly in such a case, a family of possible failure mechanism exists and the problem is of a bifurcation type. However, the bifurcation problem can be reduced to a limit load problem with, perhaps, a unique localization response if a defect is introduced (de Borst, 1986).

Uniaxial compression tests on a single element with freedom to expand in the transverse direction, with von Mises plasticity, discussed earlier in this Chapter showed that localization occurs at an angle of 45° from the direction of loading. Strictly, the results of the acoustic tensor analysis are not valid once homogeneity is lost. However, in

this case the possibility of the initial localization direction being maintained was considered.

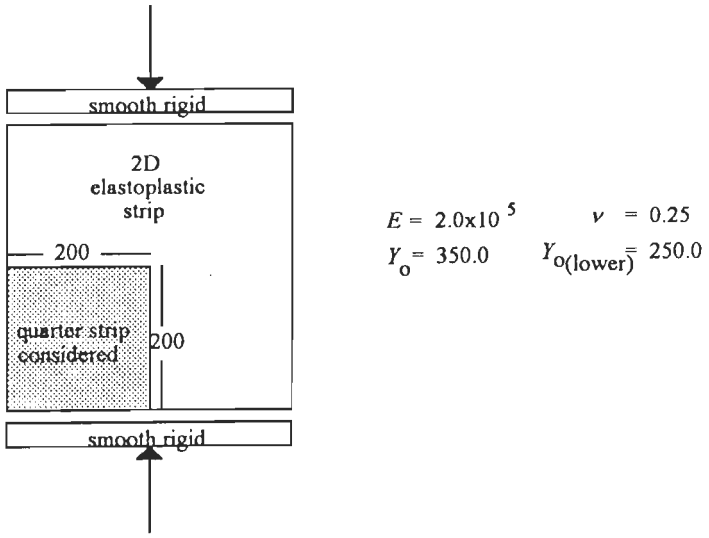

Fig. 7.29 Plane strain elastoplastic compression panel with von Mises plasticity

With this knowledge in the background, and also keeping in mind that the localization bands tend to follow element boundaries, finite element meshes as shown in Fig. 7.30 were designed. Three noded triangular elements with one point integration rule were used. Each of these meshes represents a quarter of the panel shown in Fig. 7.29. It can be seen that in each case, a band of elements spans along the diagonal from the lower left corner to the upper right corner.

7.7.1 Panel with a Weaker Band and no ε_c Modification

In the first series of numerical experiments, the von Mises material inside the band was assumed to have a lower yield level (by 28 %) as compared to the material outside the band. In this case, the parameter ε_c was not modified *i.e.* it was kept identical for all the four meshes of Fig. 7.30. In each case it was observed that the diagonal band becomes the localization band. The principal strain plots at the end of loading in each case are shown in Fig. 7.31. The material outside the band elastically unloads. Clearly the strain magnitudes in the localization band increase as the band becomes thinner.

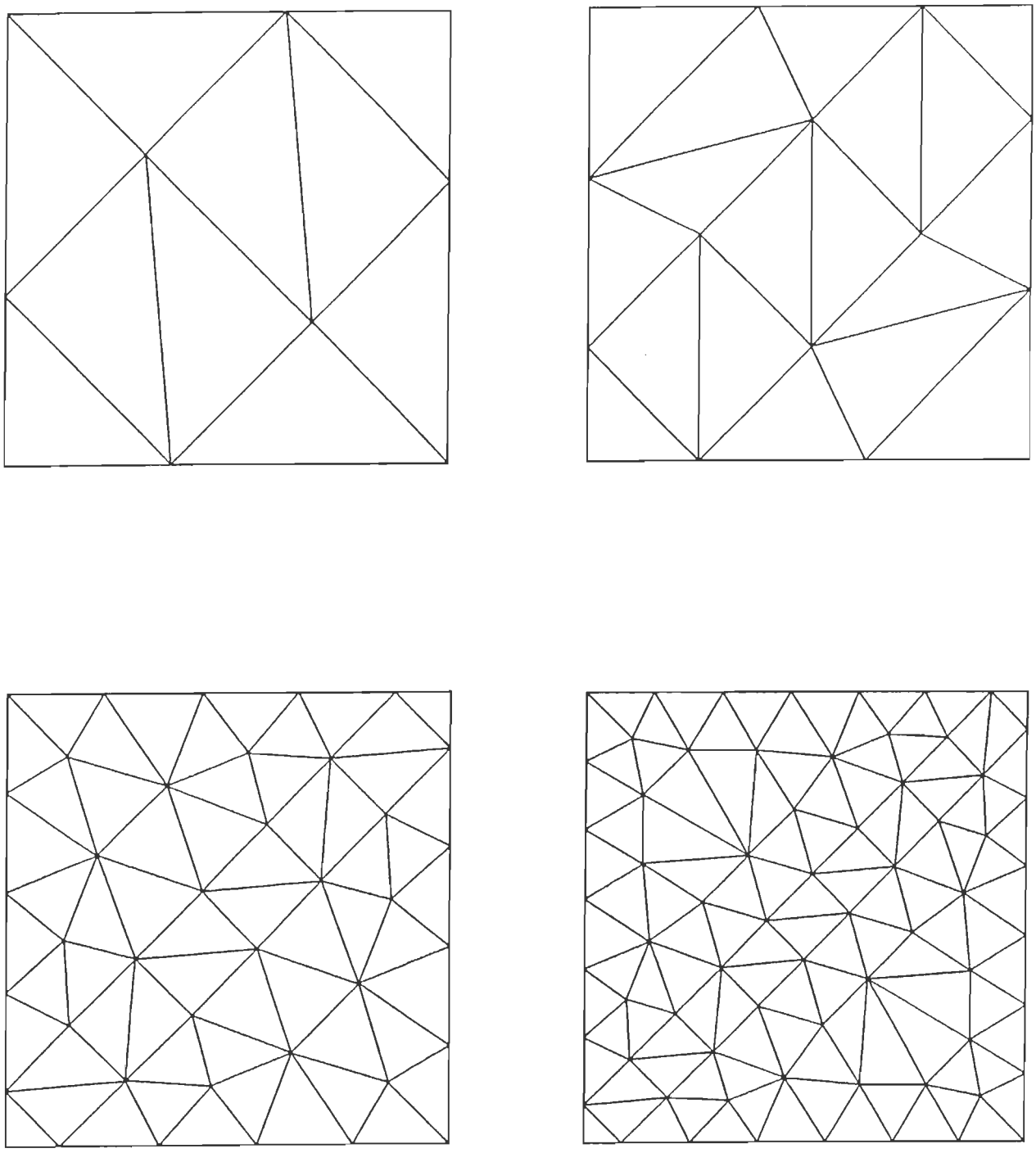

Fig. 7.30 Different mesh discretisations for compression panel with von Mises plasticity

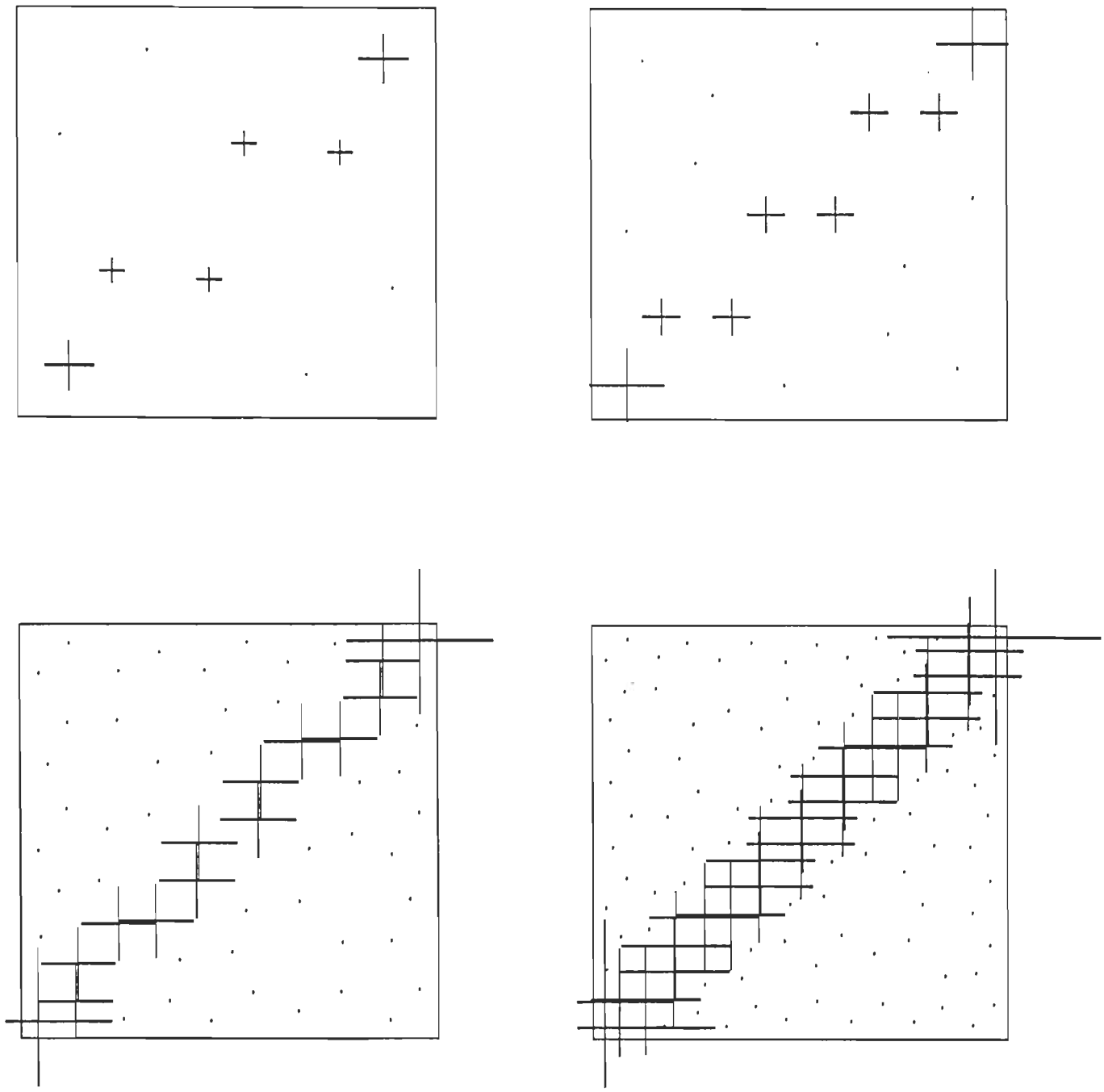

Fig. 7.31 Principal strains plots at the end of loading (compression panel with von Mises plasticity, Problem 7.7.1)

A comparison of the load deflection behaviour is shown in Fig. 7.32. It can be seen that the response is highly mesh sensitive. Thus, while the localization remains confined, mesh sensitivity due to *treating softening as a material property* is established again.

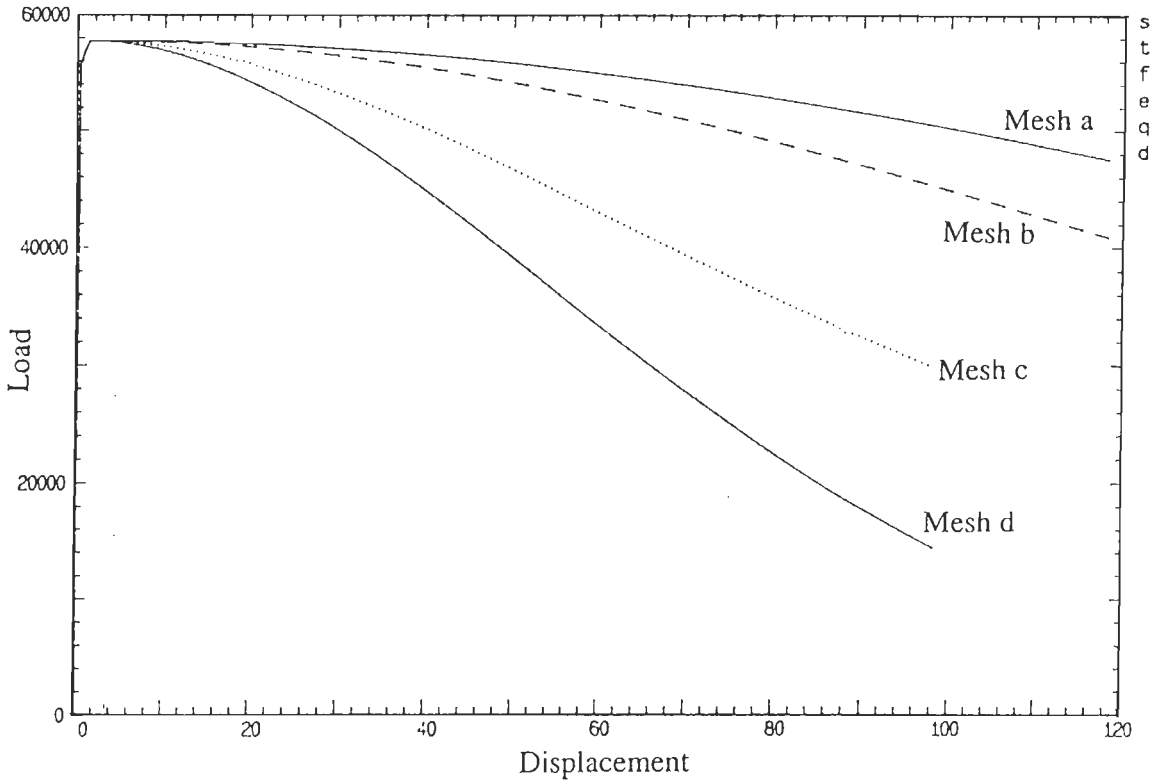

Fig. 7.32 Comparison of the load deflection behaviour (compression panel with von Mises plasticity, Problem 7.7.1)

7.7.2 Panel with Weaker Band and ε_c Modification

Once again, the compression panel problem discussed in the last subsection along with the meshes of Fig. 7.29 was analysed. In this case, softening was not treated as a material property and was modified as per the law discussed in Section 7.6. Once again the localization remains limited to the diagonal band and the corresponding principal strain plots are shown in Fig. 7.33. It can be seen that the strains inside the band become higher as the band becomes finer.

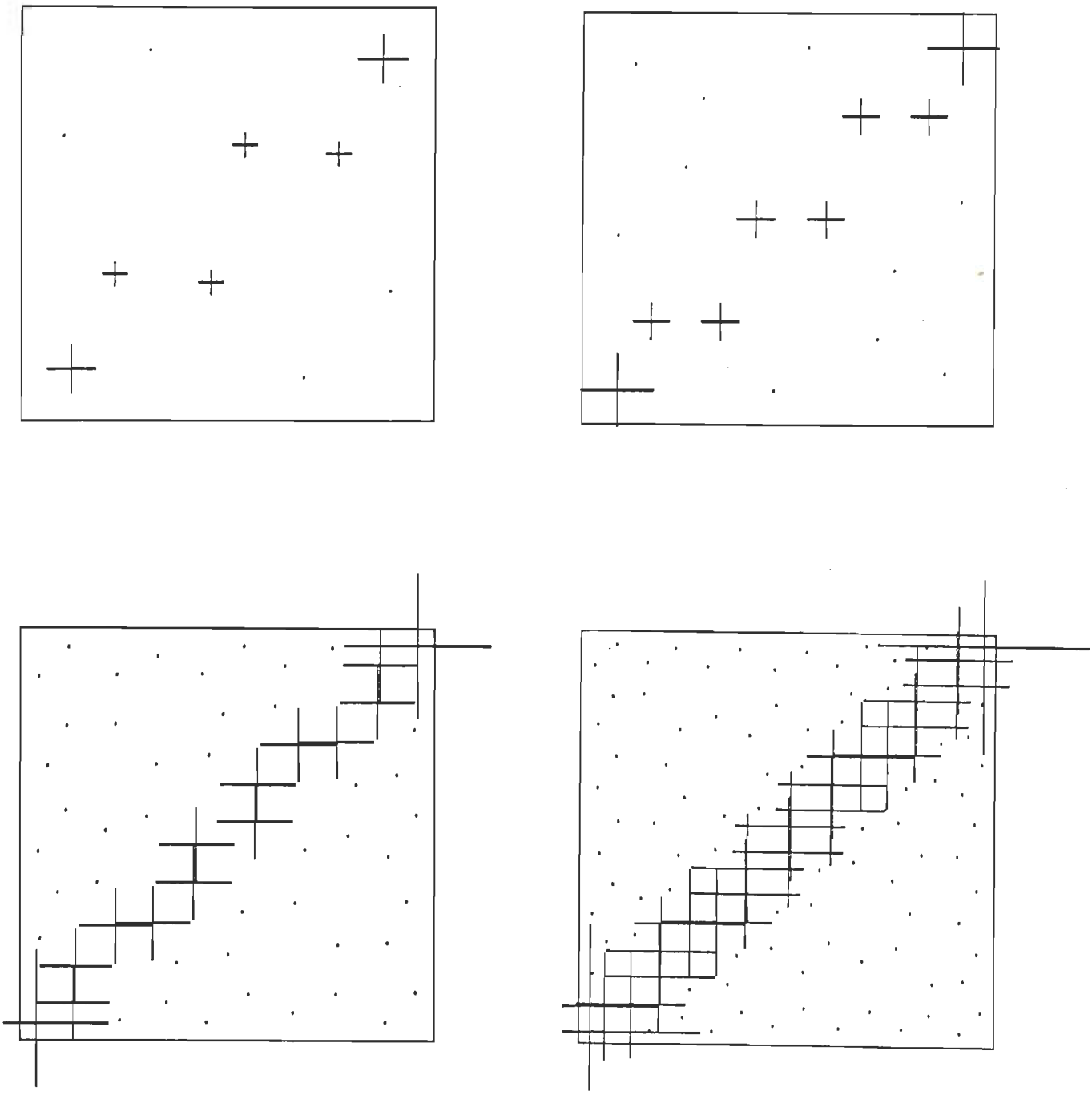

Fig. 7.33 Principal strains plots at the end of loading (compression panel with von Mises plasticity, Problem 7.7.2)

The load deflection graph for this case is shown in Fig. 7.34. It can be seen that the match for various meshes is reasonably good. Thus, it appears that mesh sensitivity that arises due to element size changes, can be taken care of by appropriately modifying the softening rules as the meshes change.

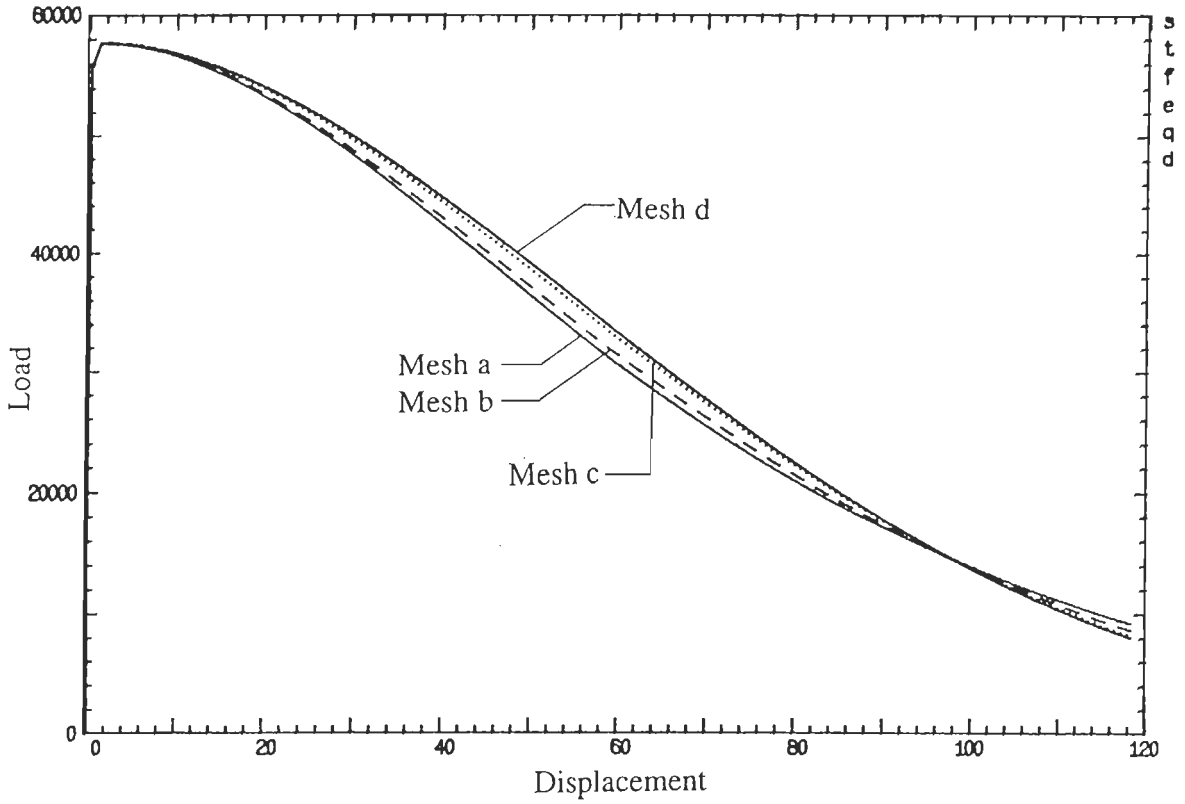

Fig. 7.34 Comparison of the load deflection behaviour (compression panel with von Mises plasticity, Problem 7.7.2)

7.7.3 Panel with Defective Element and ε_c Modification

Once again, the panel of Fig. 7.29 along with the meshes of Fig. 7.30 was analysed. In this case, only the lower left corner element was assumed to be weaker (or defective). This was done by making its yield level 28 % lower. On compression, this lower left corner element yielded first in each case. This was followed by a localization band initiation which started from this lower left corner and stretched diagonally along the band to the upper right corner. The principal strain plots are shown in Fig. 7.35 and the load displacement curves are shown in Fig. 7.36. Once again the match is reasonable. Clearly, the peak level

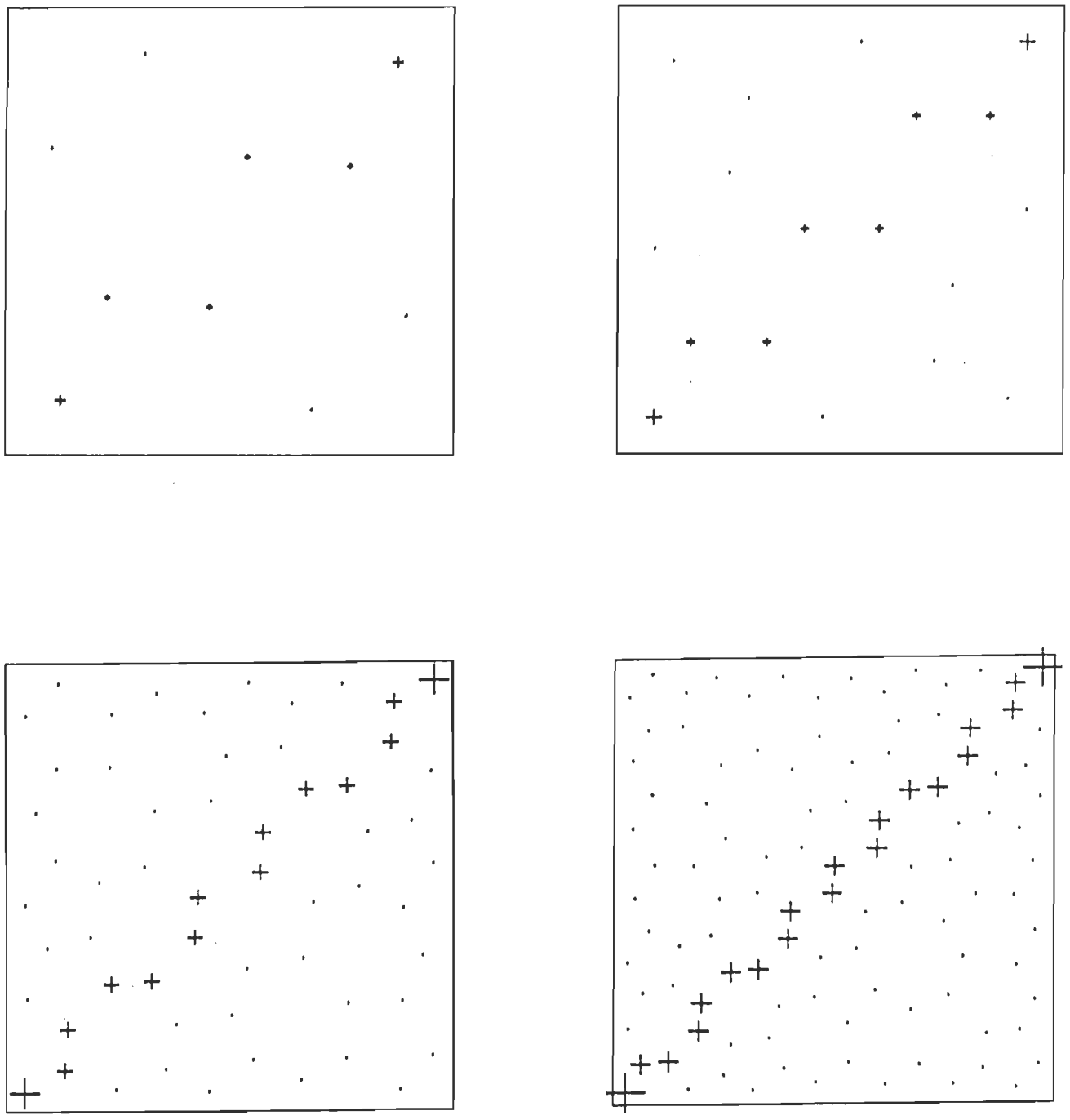

Fig. 7.35 Principal strains plots at the end of loading (compression panel with von Mises plasticity, Problem 7.7.3)

increases as the band becomes finer due to the defective element becoming smaller and smaller.

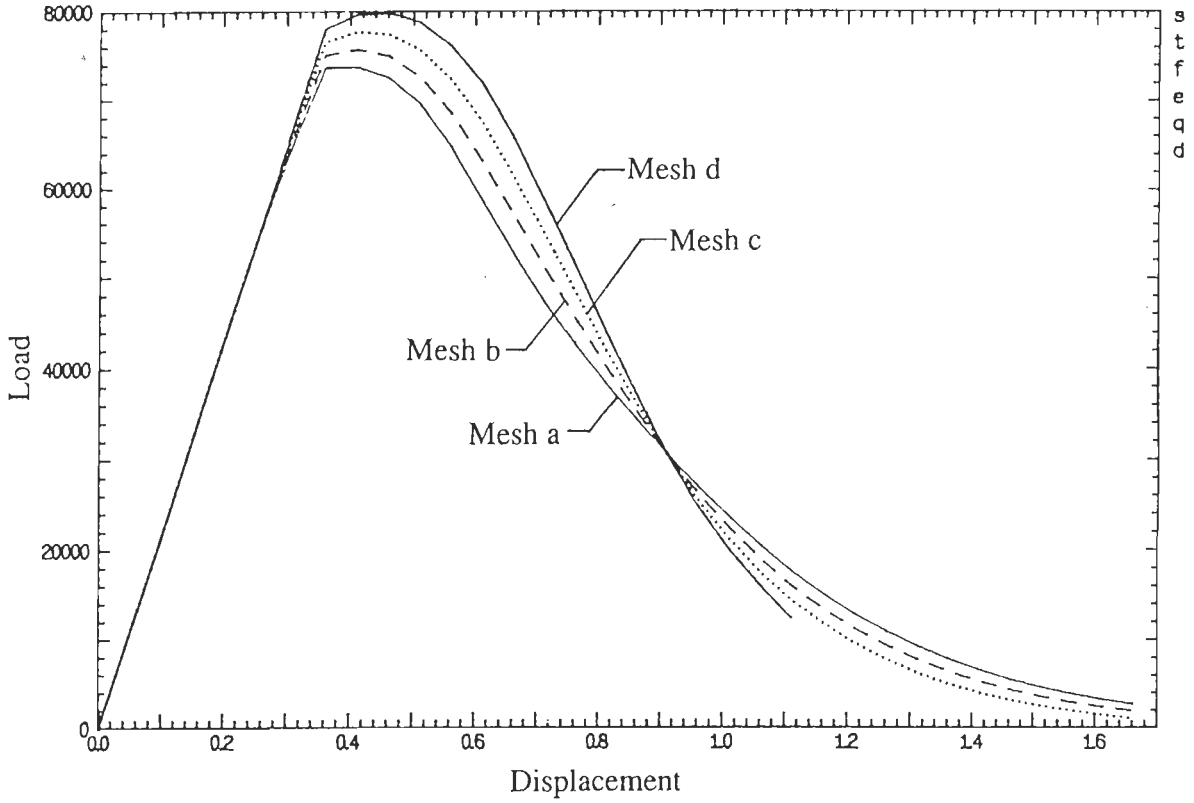

Fig. 7.36 Comparison of the load deflection behaviour (compression panel with von Mises plasticity, Problem 7.7.3)

7.8 Shear Panel with von Mises plasticity

A square panel as shown in Fig. 7.37 was subjected to a pure shear. Clearly, in this case, the principal stress direction will be aligned along the diagonals of the panel *i.e.* at 45° to the x / y axis. The expected direction of localization, if it remains unchanged, would therefore be either in the x or in the y-direction. Four meshes as shown in Fig. 7.38 consisting of eight noded quadrilateral elements with two point Gauss quadrature were used. In order to help the shear panel in finding the localization band, the central horizontal band was made weaker (28 % lower yield strength) in each case. Shearing of the panel as discussed led to a localization that remained confined to this weak band. The deformed shapes in each case are shown in Fig. 7.39 and the principal strain plots are

shown in Fig. 7.40. The load deflection curve for the four meshes (Fig. 7.41) is seen to coincide exactly if ε_c modification depending on element size as discussed are made. In fact, this problem is a kind of a one dimensional problem, as only a single stress component *viz.* shear is involved. So modification in softening parameter depending on element size leads to a complete removal of mesh sensitivity in this case.

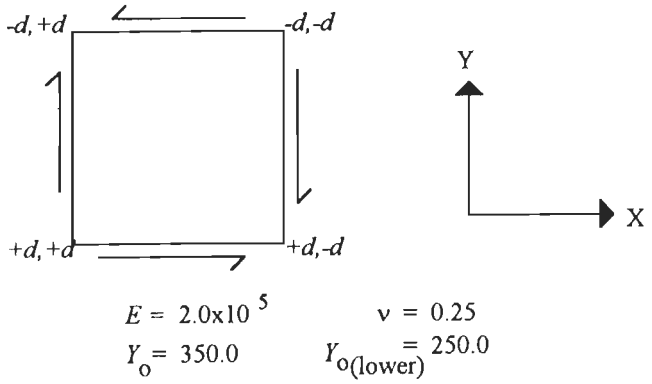

Fig. 7.37 Prescribed displacements to produce a state of pure shear

7.9 Compression Panel with Hoffman Plasticity

It was seen earlier in this Chapter that an element under compression with freedom to expand in a transverse direction does not satisfy the condition of localization if only f_t is assumed to decline. Therefore, for this study, the model wherein both f_c and f_t decline was adopted. From the study of the localization direction, it was seen earlier that the normal to the localization band would be inclined at $\theta \approx 58^\circ$ from the direction of compression loading (when $f_{co} = 10000$ and $f_{to} = 1000$). With this in view, a panel as shown in Fig. 7.42 was analysed. Once again it was assumed that the initial localization direction would be maintained, though this is not really true once homogeneity is lost. The size of the panel was selected such that the diagonal is at an angle of 58° from the horizontal. Once again, a quarter panel as shown in Fig. 7.42 was analysed. Two meshes as shown in Fig. 7.43 with visible diagonal band spanning from the lower left corner to the upper right corner were designed. In each case, defect was introduced by lowering both f_c and f_t parameters by 30 % in the lower left corner.

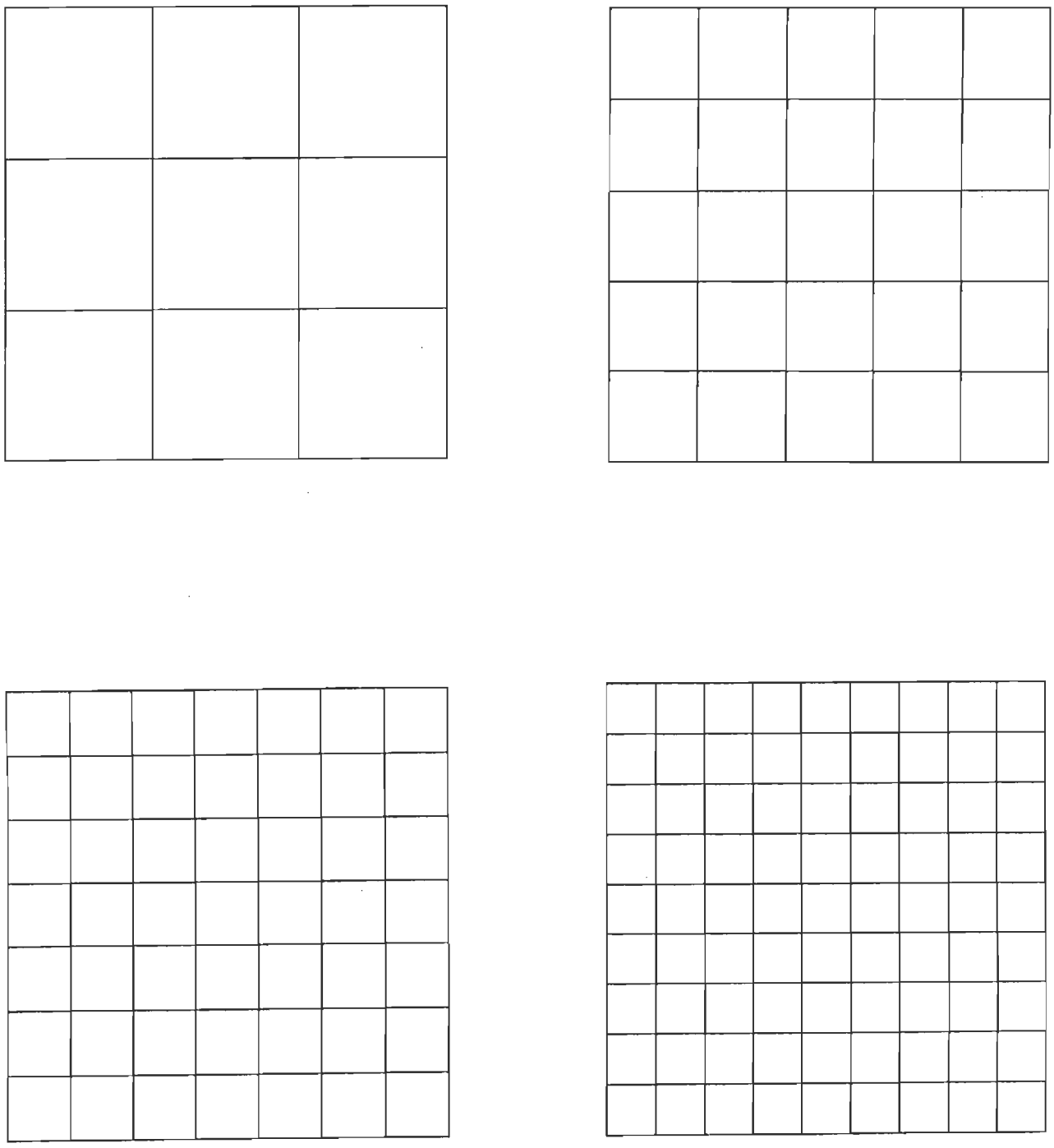

Fig. 7.38 Different mesh discretisations for shear panel with von Mises plasticity, Problem 7.8

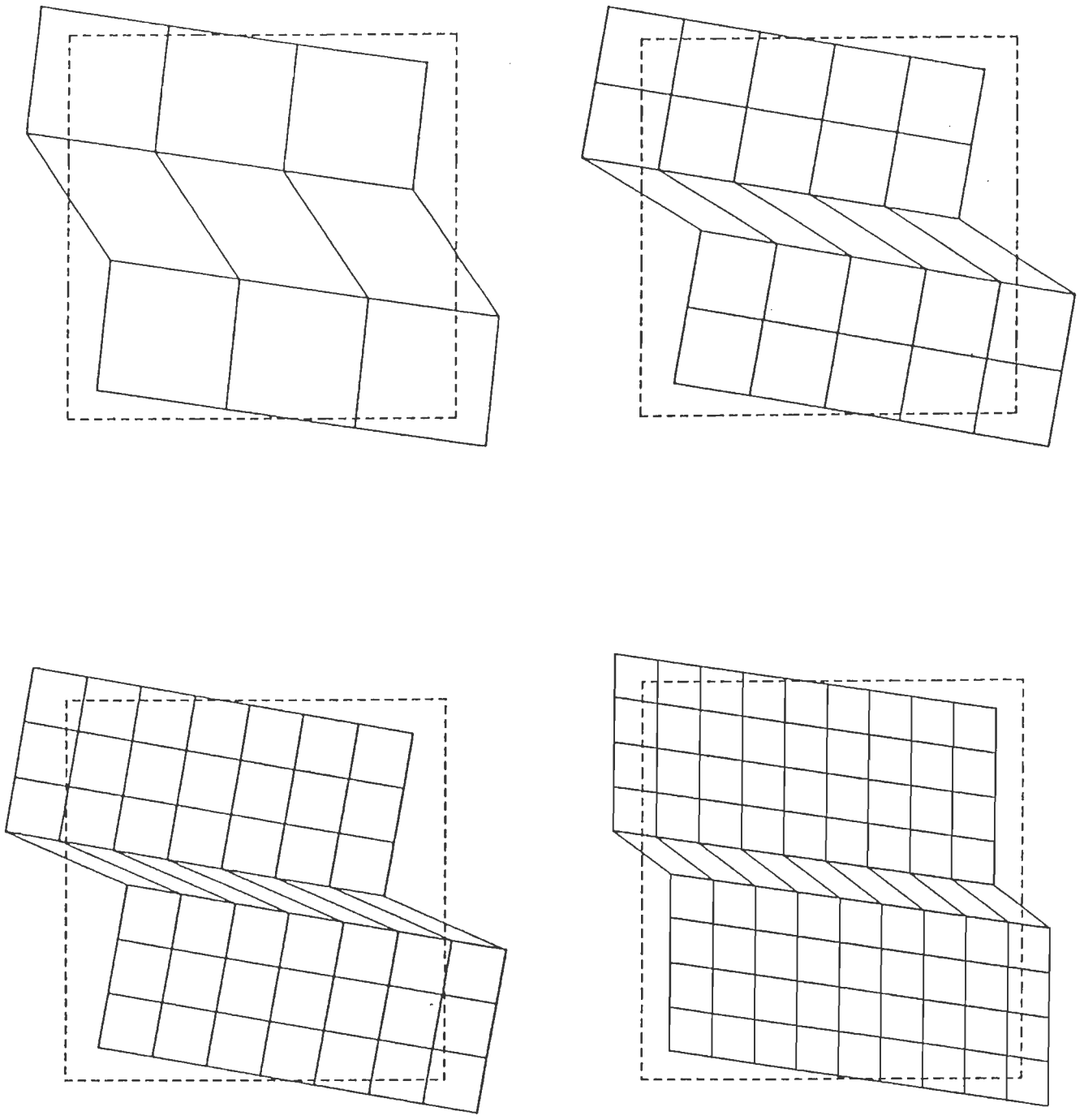

Fig. 7.39 Deformed shapes at the end of loading for shear panel with von Mises plasticity, Problem 7.8

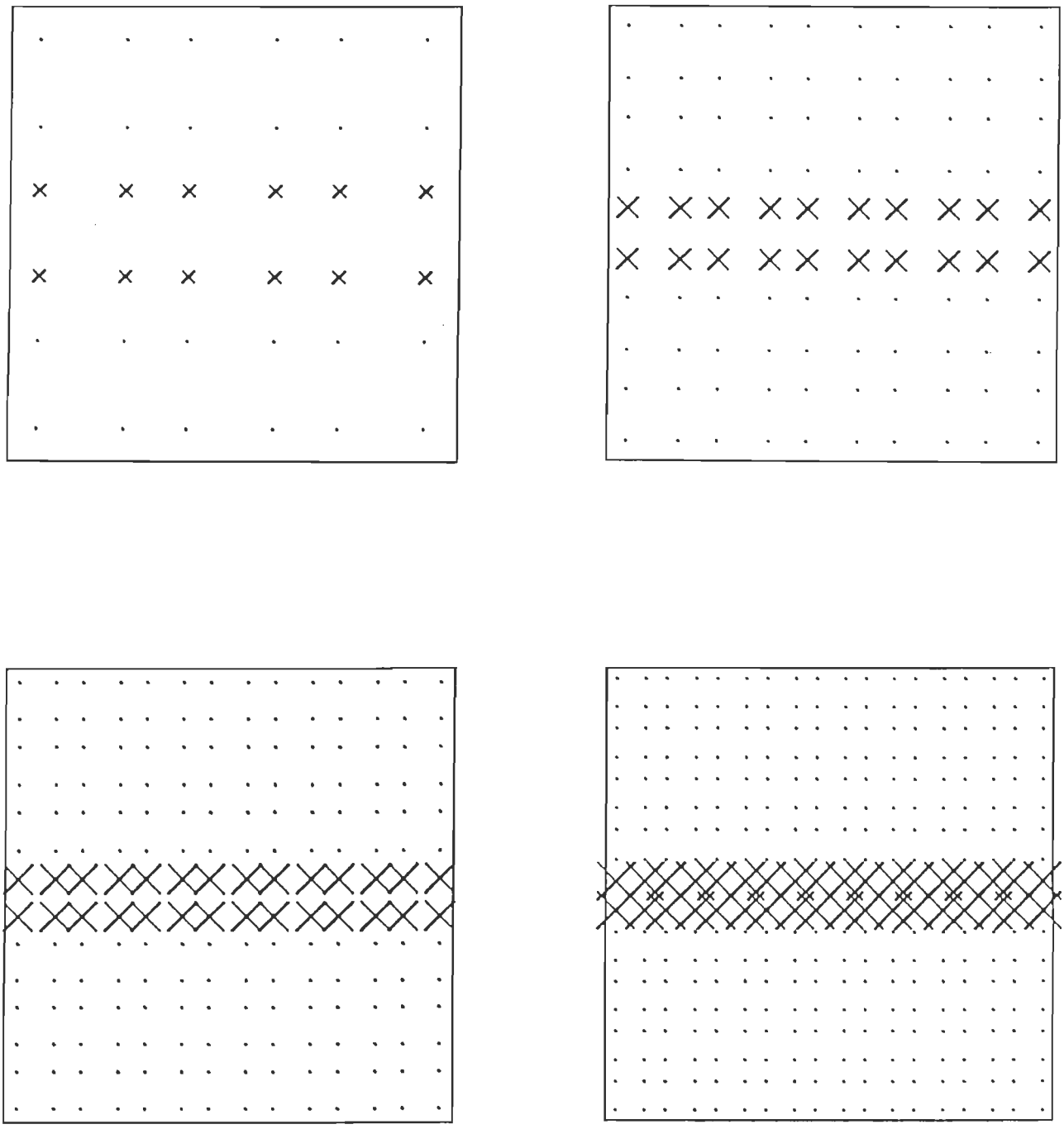

Fig. 7.40 Principal strains plots at the end of loading for shear panel with von Mises Plasticity, Problem 7.8

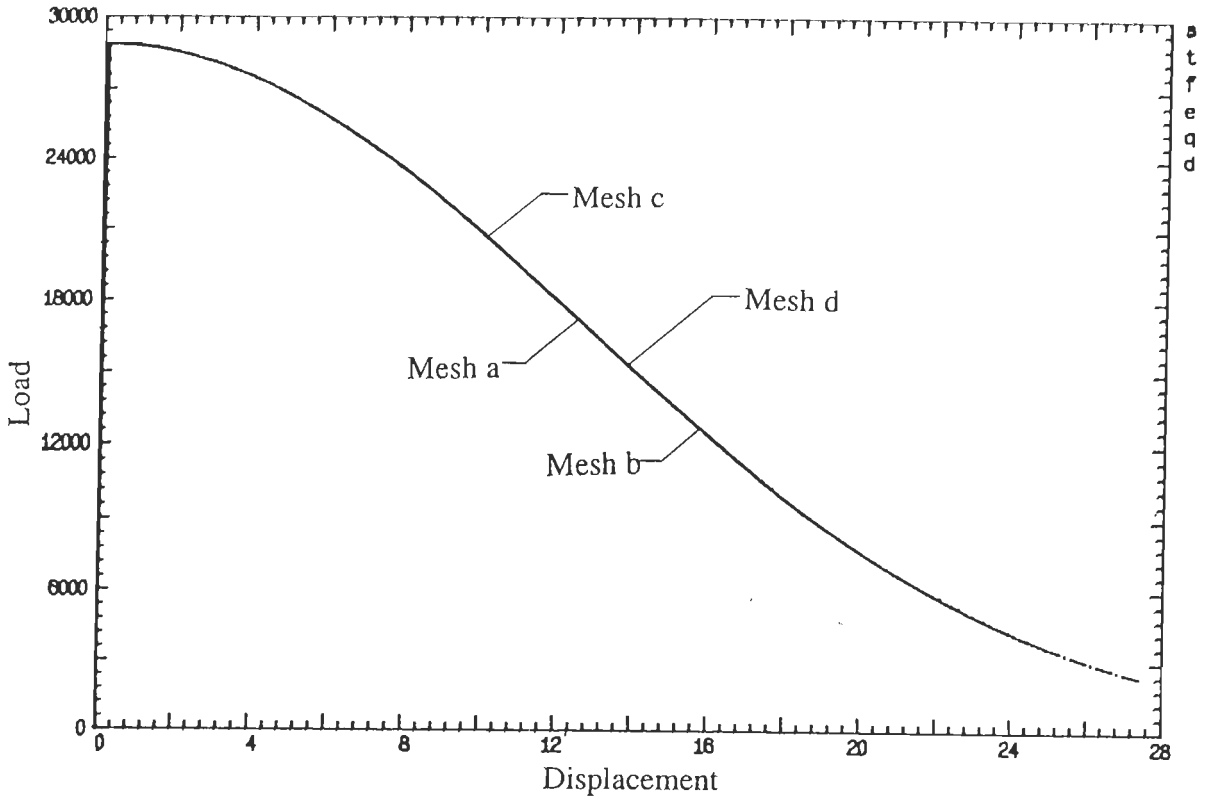

Fig. 7.41 Comparison of the load deflection behaviour for shear panel with von Mises plasticity, Problem 7.8

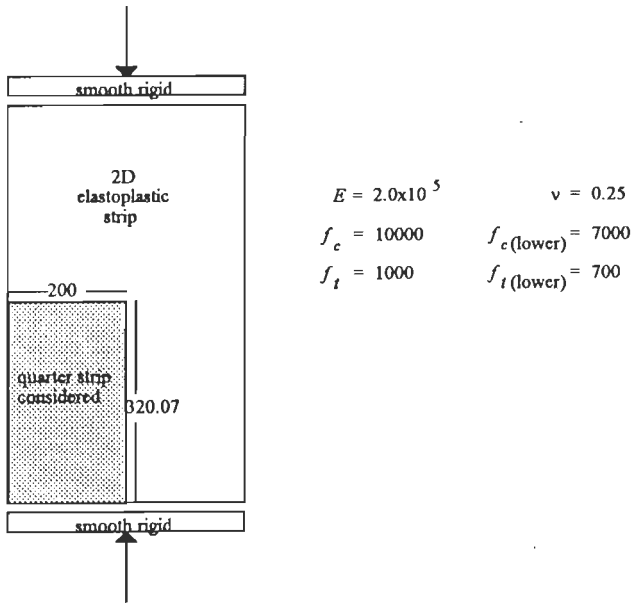

Fig. 7.42 Plane strain elastoplastic compression panel with Hoffman plasticity

Upon compression, the localization in the mesh of Fig. 7.43a remained confined to the diagonal band. The corresponding principal strain plot is shown in Fig. 7.44a. With regard to the mesh of Fig. 7.43b, the author observed that while the localization tends to move in the diagonal direction, the yielding spreads to the entire panel before a post-peak response can be attained. The post-peak principal strain is shown in Fig. 7.44b. As the yielding spreads in the entire panel, more or less uniform principal strains are observed at all integration points. Moreover, considerable numerical difficulties in convergence of the solution were encountered in the post-peak regime for these problems. The load deflection graph for the two meshes with and without the modification of ε_c are shown in Fig. 7.45. Numerical experiments were also conducted wherein $f_{co} = 10000$ and $f_{to} = 9000$ were employed. This makes the Hoffman criterion fairly close to the von Mises yield condition. No difficulty was encountered in this case and localization at 45° in a square panel was obtained. Other numerical experiments involved using $f_{co} = 10000$ and $f_{to} = 5000$. Appropriate compression panel to permit the localization was designed for this case. Once again, a tendency of spreading rather than localizing was observed.

It appears, that localization in plasticity using the finite element method strongly depends upon the yield criterion being employed.

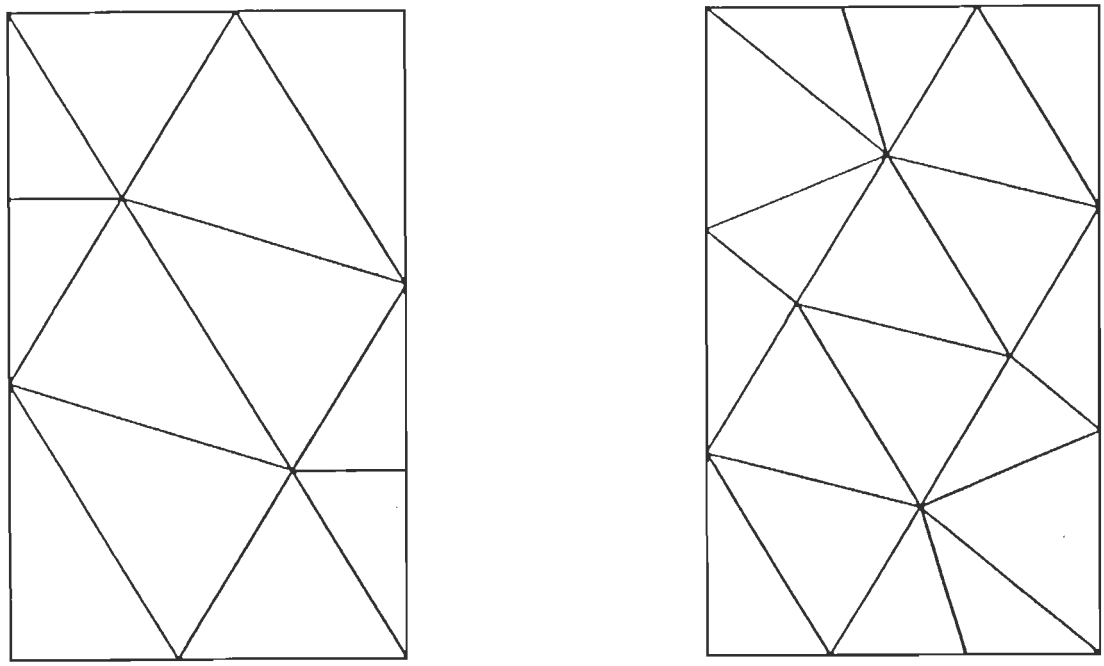

(a) (b)

Fig. 7.43 Meshes discretisations for compression panel with Hoffman plasticity, Problem 7.9 (a) thicker band (b) finer band

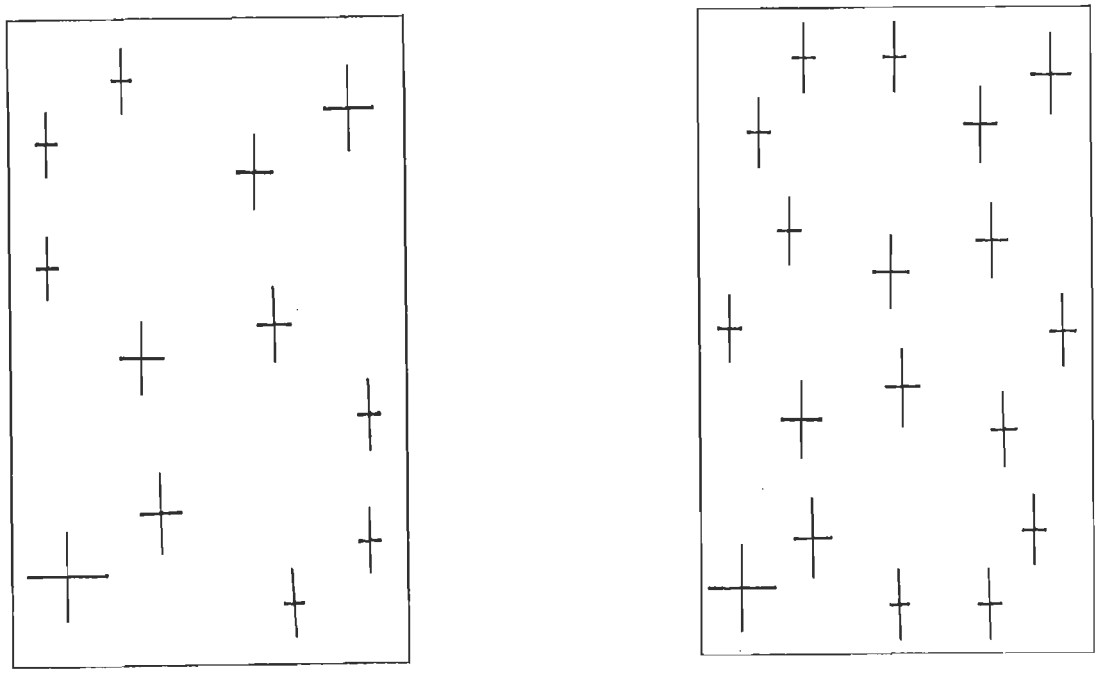

(a) (b)

Fig. 7.44 Principal strains plots at the end of loading for compression panel with Hoffman plasticity, Problem 7.9 (a) thicker band (b) finer band

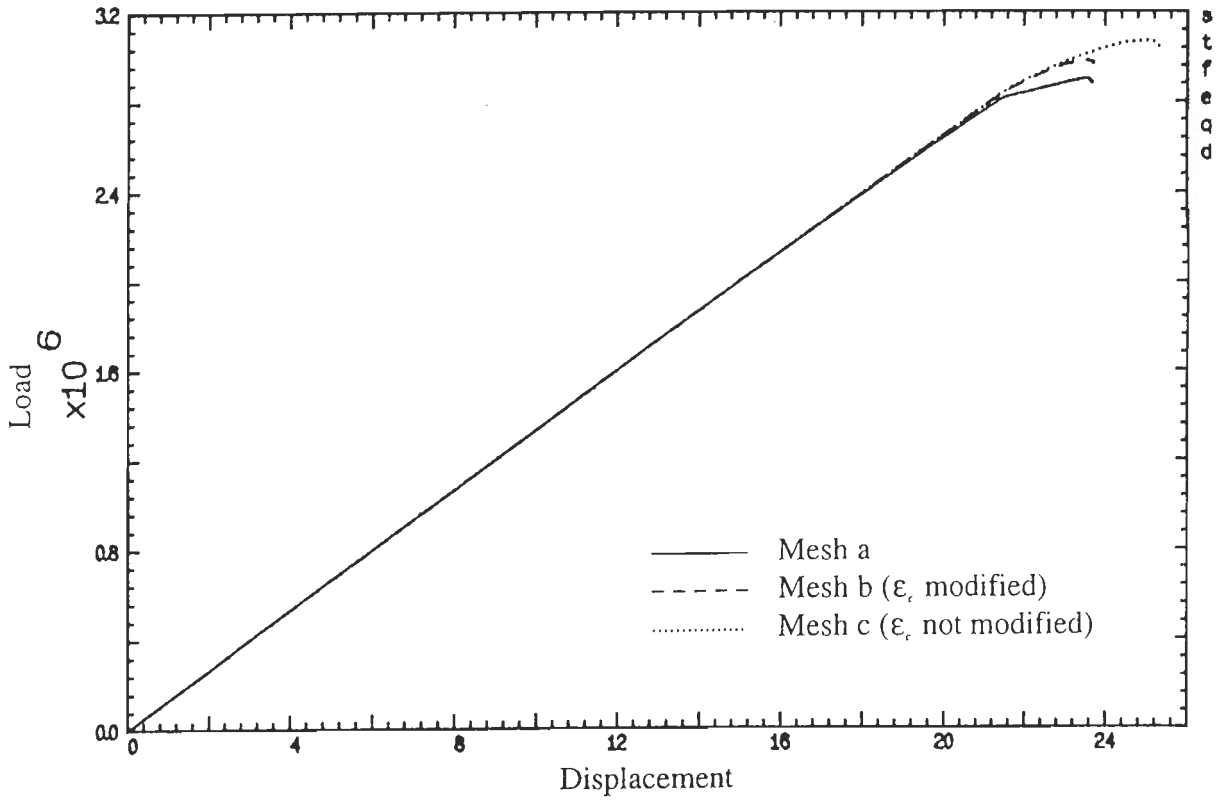

Fig. 7.45 Comparison of the load deflection behaviour with and without ε_c modification for compression panel with Hoffman Plasticity, Problem 7.9

References

Bicanic, N. and Pankaj (1990) – On mesh design for concrete strain softening analysis, *Computer Aided Analysis and Design of Concrete Structures*, (Eds. Bicanic, N. and Mang, H.), Vol. 2, Pineridge Press, 959-974.

de Borst, R. (1986) – Nonlinear analysis of frictional materials, *Ph.D. Dissertation*, Delft University of Technology.

Leroy, Y. and Ortiz, M. (1989) – Finite element analysis of strain localization in frictional materials, *Int. J. Num. Ana. Meth. Geomech.*, **13**, 53-74.

Ortiz, M. (1987) – An analytical study of the localized failure modes of concrete in mechanics of materials, *North Holland*, **6**, 159-174.

Ortiz, M., Leroy, Y. and Needleman, A. (1987) – A finite element method for localized failure analysis, *Computer Methods in Applied Mechanics & Engineering*, **61**, 189-214.

Pankaj (1990) – Finite element analysis in strain softening and localization problems, *Ph.D. Thesis*, University College of Swansea, University of Wales.

Pankaj and Bicanic, N. (1991) – Mesh sensitivity issues in strain softening and localization analysis, *Computational Mechanics*, (Eds. Cheung, Y.K., Lee, J.W.H. and Leung, A.Y.T.), Balkema, Roterdam, 1303-1308.

Pietruszczak, S.T. and Mroz, Z. (1980) – Numerical analysis of elastic-plastic compression of pillars accounting for material hardening and softening, *Int. J. Rock Mech. Min. Sci. and Geomech. Abstr.*, **17**, 199-207.

Pietruszczak, S.T. and Mroz, Z. (1981) – Finite element analysis of strain softening materials, *IJNME*, **10**, 327-334.

Rudnicki, J.W. and Rice, J.R. (1975) – Conditions for the localization of deformation of pressure-sensitive dilatent materials, *J. Mech. Phys. Solids*, **23**, 371-394.

Willam, K., Munz, T., Etse, G. and Menetrey, P. (1994) – Failure condition and localization in concrete, *Computational Modelling of Concrete Structures, EURO-C*, (Eds. Mang, H., Bicanic, N. and de Borst, R.), Vol. I, Pineridge Press, 263-281.

Willam, K., Pramono, E. and Sture, S. (1987) – Uniqueness and stability issues of strain softening computations, *Constitutive Laws for Engineering Materials: Theory and Applications*, (Eds. Desai, C.S. et al.), 249-260.

Willam, K. and Sobh, N. (1987) – Bifurcation analysis of tangential material operators, *Numerical Methods in Engineering: Theory and Application*, (Eds. Middleton, J. and Pande, G.N.).

Applications

8.1 General

The ideas and algorithms developed earlier are applied to some engineering problems. The post-peak load deflection behaviour and the localization patterns of different structures are considered.

8.2 Cantilever Beam Problem

A plane strain cantilever beam was subjected to prescribed end displacements (applied in increments) as shown in Fig. 8.1. The structure is discretised using eight noded quadrilateral elements (Fig. 8.2) with 2×2 Gauss quadrature. The numerical solution was simulated using the initial stiffness approach. An elastic strain softening idealisation for the material behaviour with exponential softening (as discussed earlier) is considered.

Strain softening von Mises and Hoffman yield criteria were employed. With von Mises plasticity, a uniaxial equivalent yield strength $Y_o = 3170$ is considered while with Hoffman plasticity a uniaxial compressive yield strength $f_{co} = 10000$ and uniaxial tensile yield strength $f_{to} = 1000$ is considered. The reason for this choice is that it yields $Y_o(\text{von Mises}) \approx \sqrt{f_{co} f_{to}}$ and the results may be some what comparable.

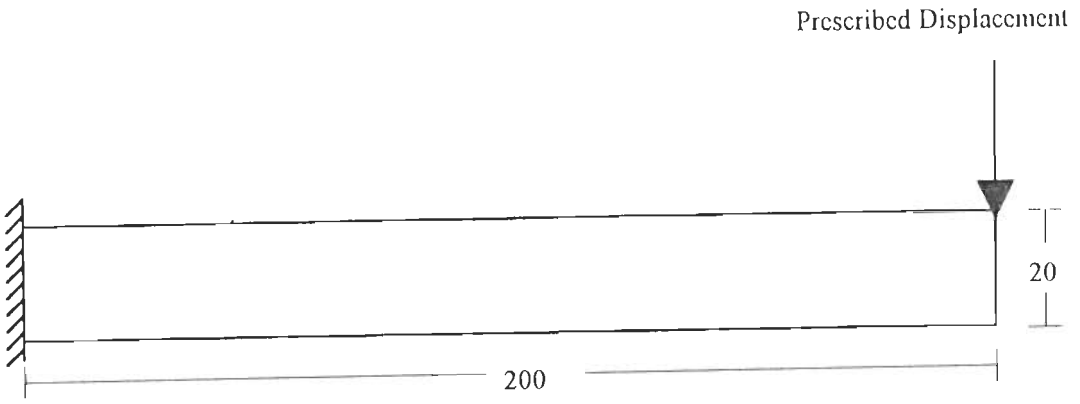

$E = 200000$ $\nu = 0.25$

Fig. 8.1 Geometry of the cantilever beam

Fig. 8.2 Finite element discretisation of the cantilever beam

For Hoffman, only the case in which both f_c and f_t decline is considered. Parameter $\varepsilon_c = 0.1$ has been assumed. The load deflection curves for the two cases are shown in Fig. 8.3. The Hoffman criterion leads to a lower peak load. The deflected shapes for a displacement of 54.6 are shown in Fig. 8.4. While the two shapes look similar, the principal strain plots (Fig. 8.5) and the Gauss point state plots (Fig 8.6) are quite different. In the principal strain plot the double line indicates tension while single line indicates compression at the Gauss points. Circles in the Gauss point state plot indicate that the point has experienced at least some yielding while crosses indicate that the point is still elastic. Figures 8.5 and 8.6 illustrate the state at maximum displacement of Fig. 8.3. For

(a)

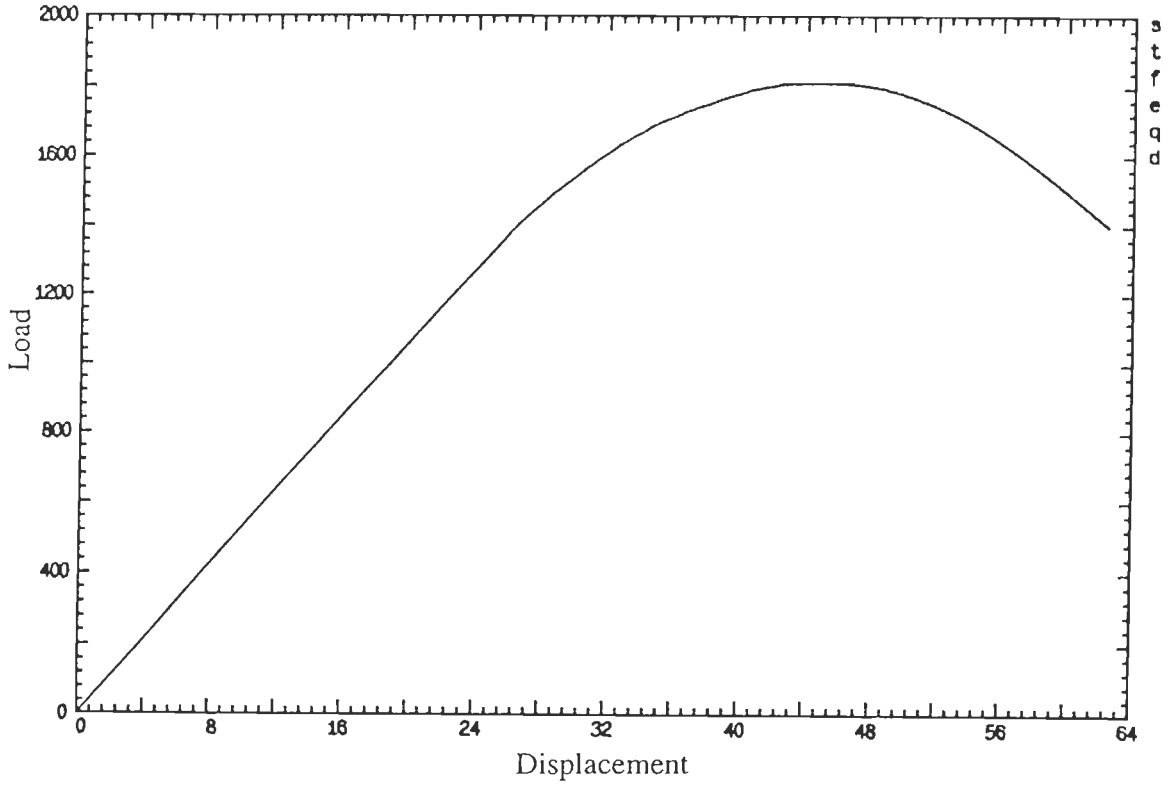

(b)

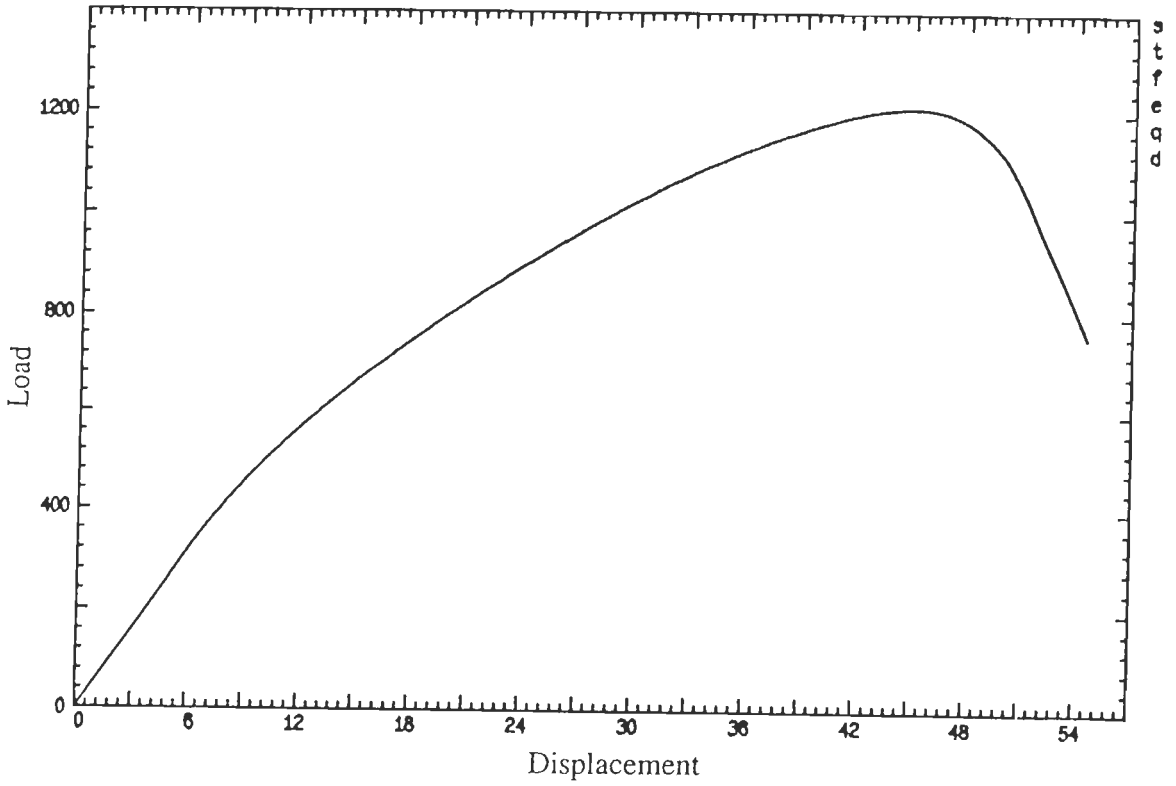

Fig. 8.3 Load deflection behaviour of the cantilever beam using (a) von Mises criterion and (b) Hoffman criterion

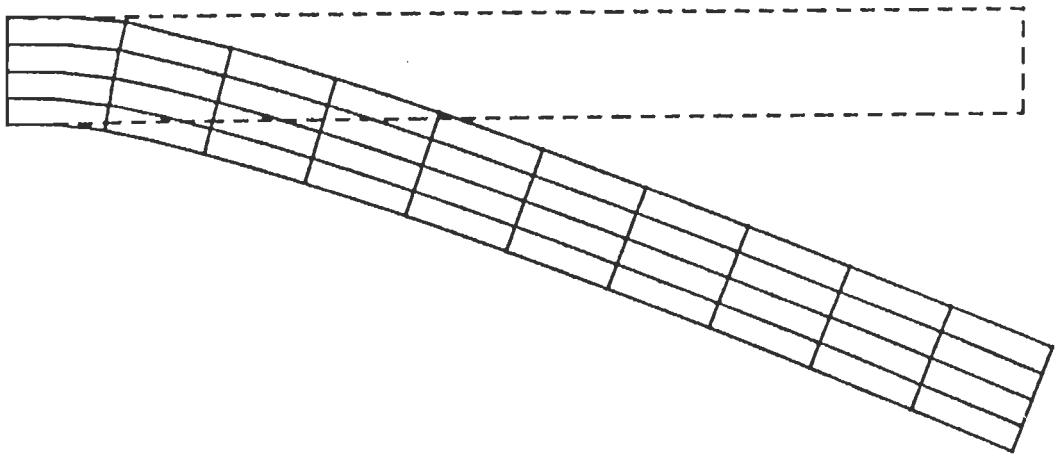

(a)

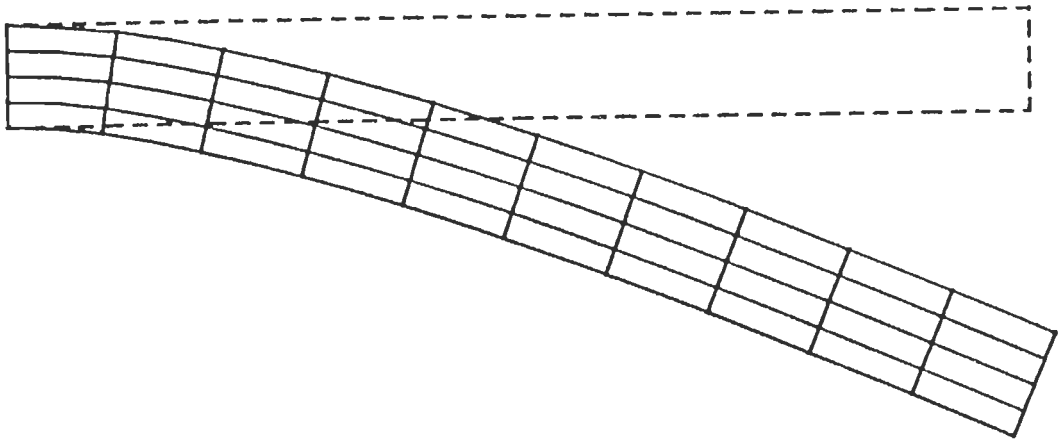

(b)

Fig. 8.4 Deformed shape (a) Hoffman criterion and (b) von Mises criterion

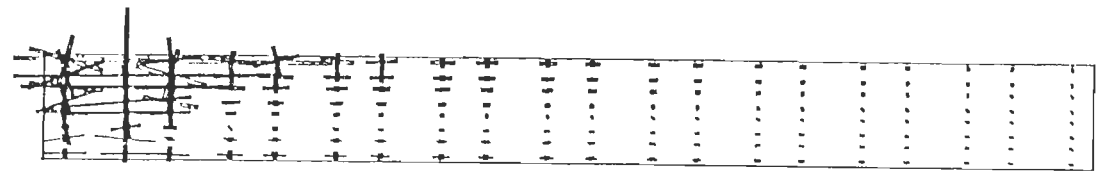

(a)

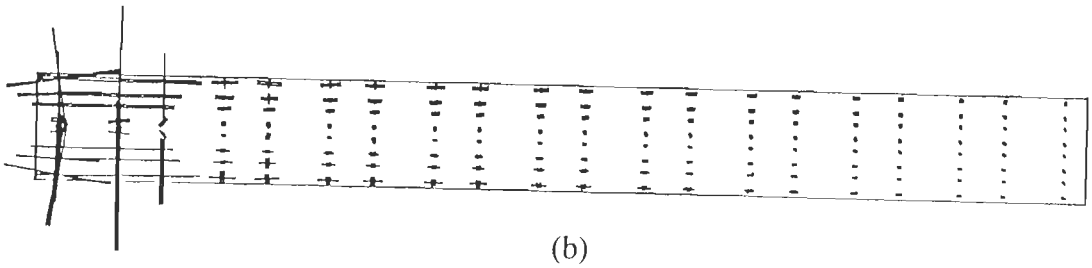

(b)

Fig. 8.5 Principal strain plot (a) Hoffman criterion and (b) von Mises criterion

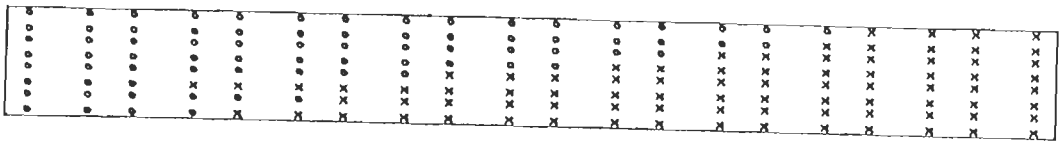

(a)

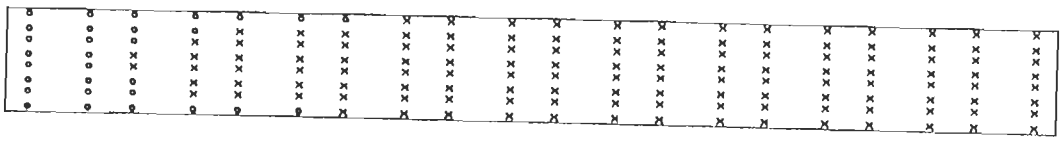

(b)

Fig. 8.6 Gauss point state plot (a) Hoffman criterion and (b) von Mises criterion

the Hoffman criterion there is considerable yielding on upper surface before a post-peak response is observed. On the other hand the localization zone is much narrower for the von Mises criterion. Moreover, the post-peak states for the Hoffman criterion are predominantly due to tensile stresses whereas for the von Mises criterion the post-peak state is expectedly due to both tension on the top and compression on the bottom. Thus for the von Mises criterion, yielding starts and propagates from the top and bottom regions simultaneously. It is felt that the Hoffman criterion has a tendency to produce a diffuse localization as compared to von Mises criterion.

8.3 Plane Strain Tension Specimen

The tension specimen used is shown in Fig. 8.7a and is similar to the one analysed by Moran et al. (1987) and Ortiz (1987). The material properties considered are the same as that of the previous example. A displacement is prescribed at the top end of the specimen which is also free to move in the transverse direction. The bottom end is kept fixed. The finite element discretisation is shown in Fig. 8.7b. The analysis is performed using triangular elements with one point integration rule. A defect in the form of lower yield strength, is introduced in the center of the specimen (shaded elements of Fig. 8.7b) in order to trigger localization. As the analysis proceeds, the material starts yielding which is initiated from the weak elements.

The progress of yielding for the two criteria is shown in Figs. 8.8 and 8.9. A defect in the centre of the specimen should cause two cross bands of localization, however, Fig. 8.8 illustrates that one direction is preferred as compared to the other. This is apparently due to the slight mesh bias in the mesh discretisation of Fig. 8.7b. Once again, the yielding is highly localized when the von Mises criterion is used and quite diffused with the Hoffman criterion.

The principal strain plots and deformed shapes for the two criteria are shown in Figs. 8.10 and 8.11. In both cases, necking at the centre is observed. In this problem, the Hoffman criterion exhibits much high peak load level as compared to the von Mises criterion (Fig. 8.12). This is apparently because of the diffused localization exhibited by the criterion. Considerable difficulties were encountered in numerical integration after the peak load level was achieved. As a result the analysis had to be terminated soon after the post-peak level was obtained.

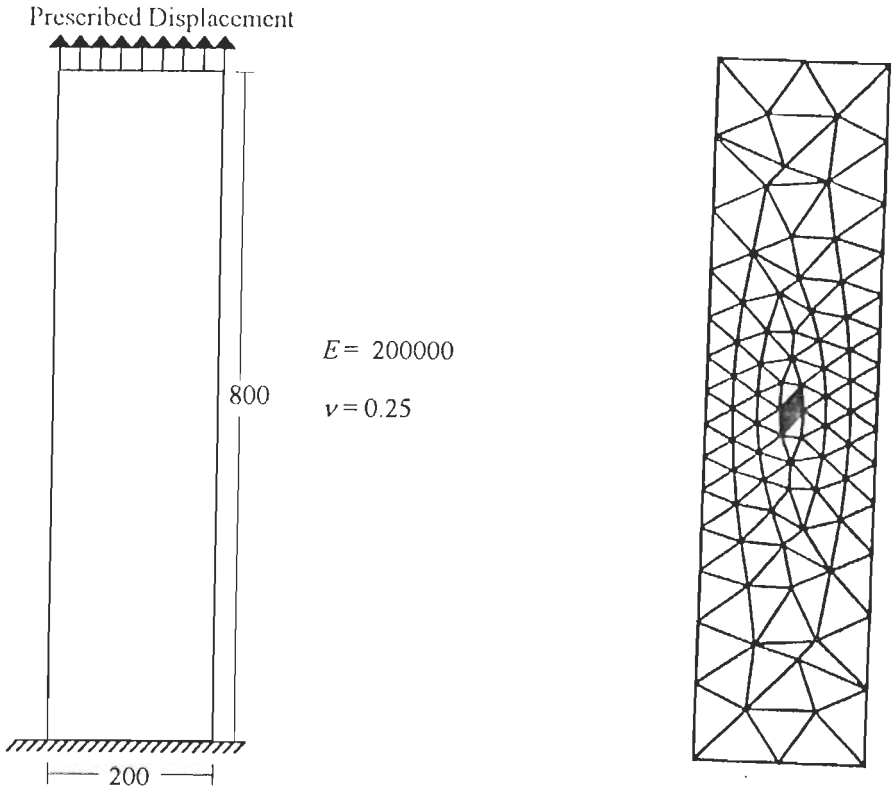

Fig. 8.7 (a) Geometry of the plane strain tension specimen (b) Finite element discretisation

8.4 Notched Shear Beam

A notched shear beam was tested by Arrea and Ingraffea (1982) and was analysed using the Mohr Coulomb criterion (Pankaj, 1990). The support and the loading conditions are non-symmetric with respect to the notch as shown in Fig. 8.13. Three noded triangular elements with one point Gauss integration rule were used in the study and the finite element discretization is shown in Fig. 8.14. Displacements are prescribed at points A and B, which is different from the original test in which loads were prescribed.

The load displacement response using the two criteria is shown in Fig. 8.15. The post-peak state could be traced more easily for the von Mises criterion as compared to Hoffman criterion. Once again, the Hoffman criterion yields a higher peak load.

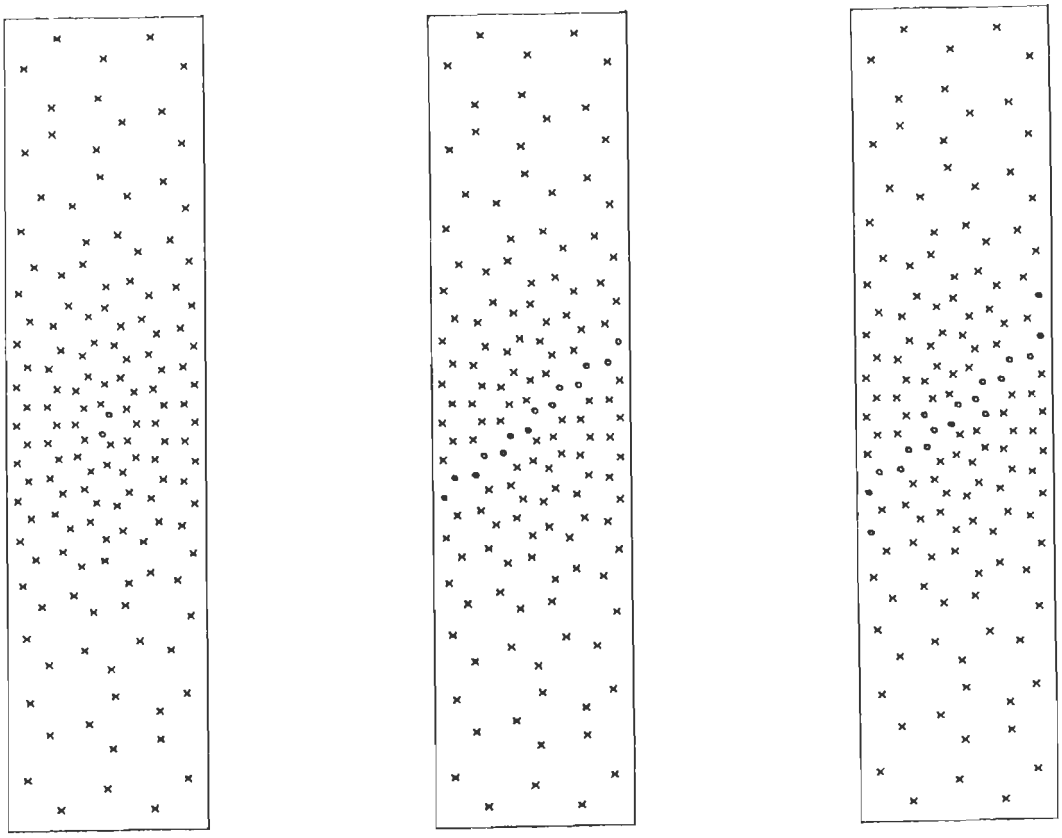

Fig. 8.8 Gauss point state plot at different stages of loading using von Mises criterion

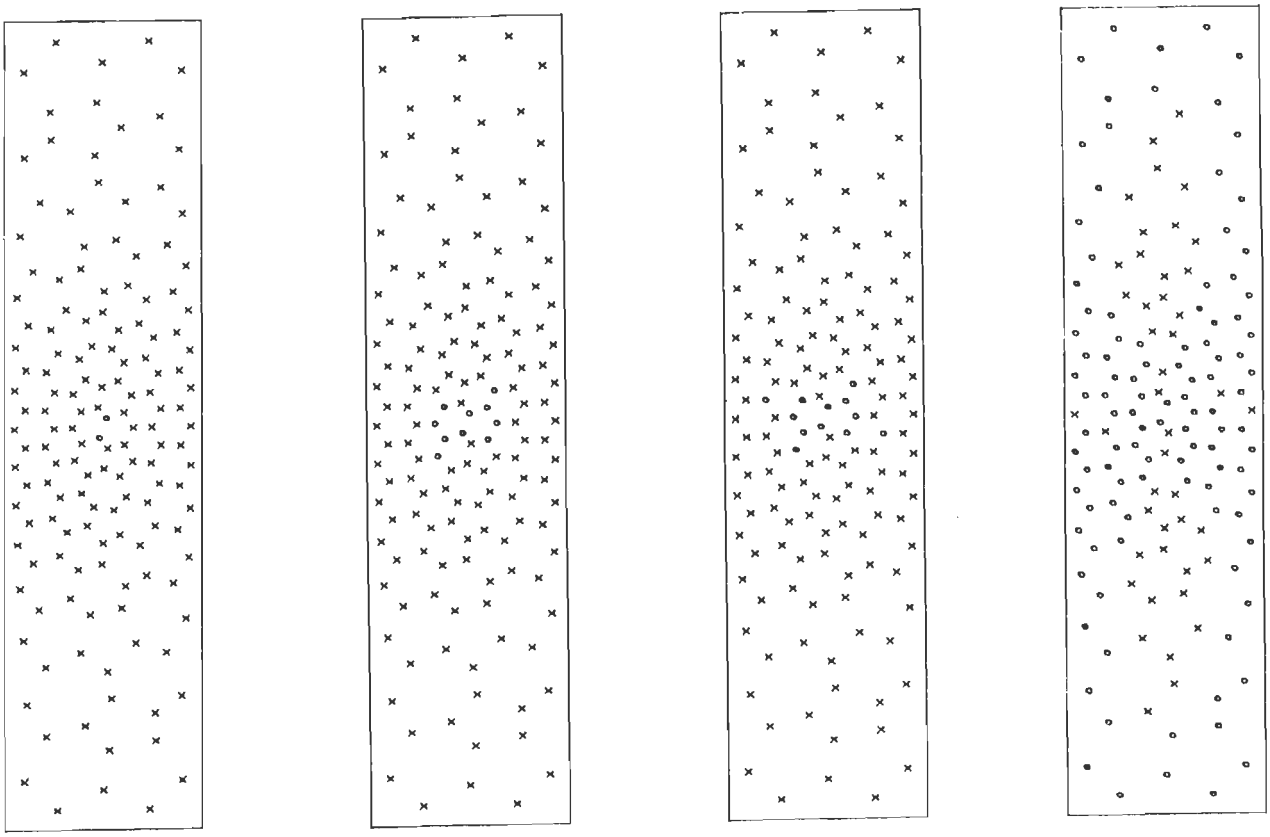

Fig. 8.9 Gauss point state plot at different stages of loading using Hoffman criterion

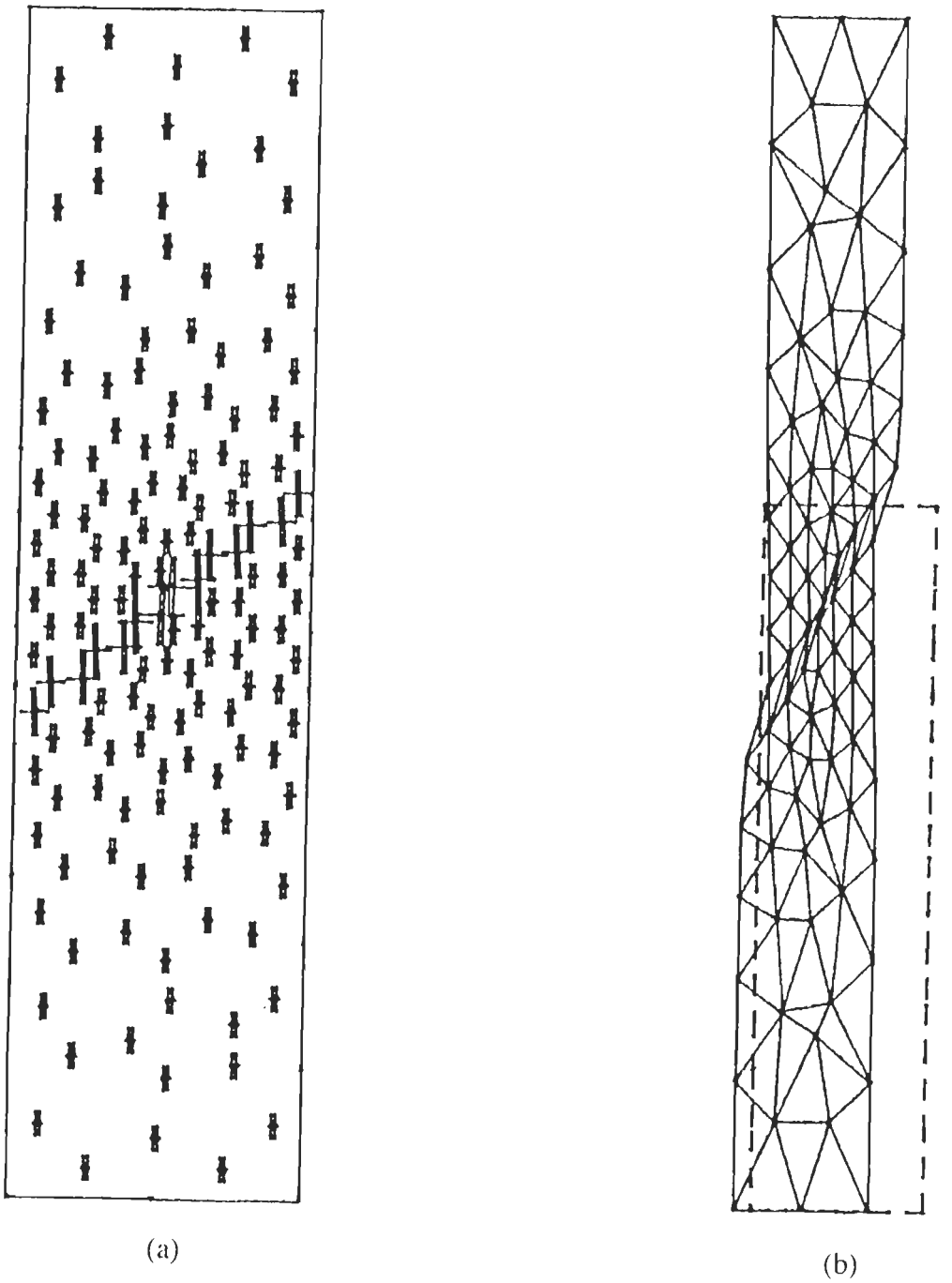

Fig. 8.10 Response using von Mises criterion at the end of the analysis (a) principal strain plot (b) deformed shape

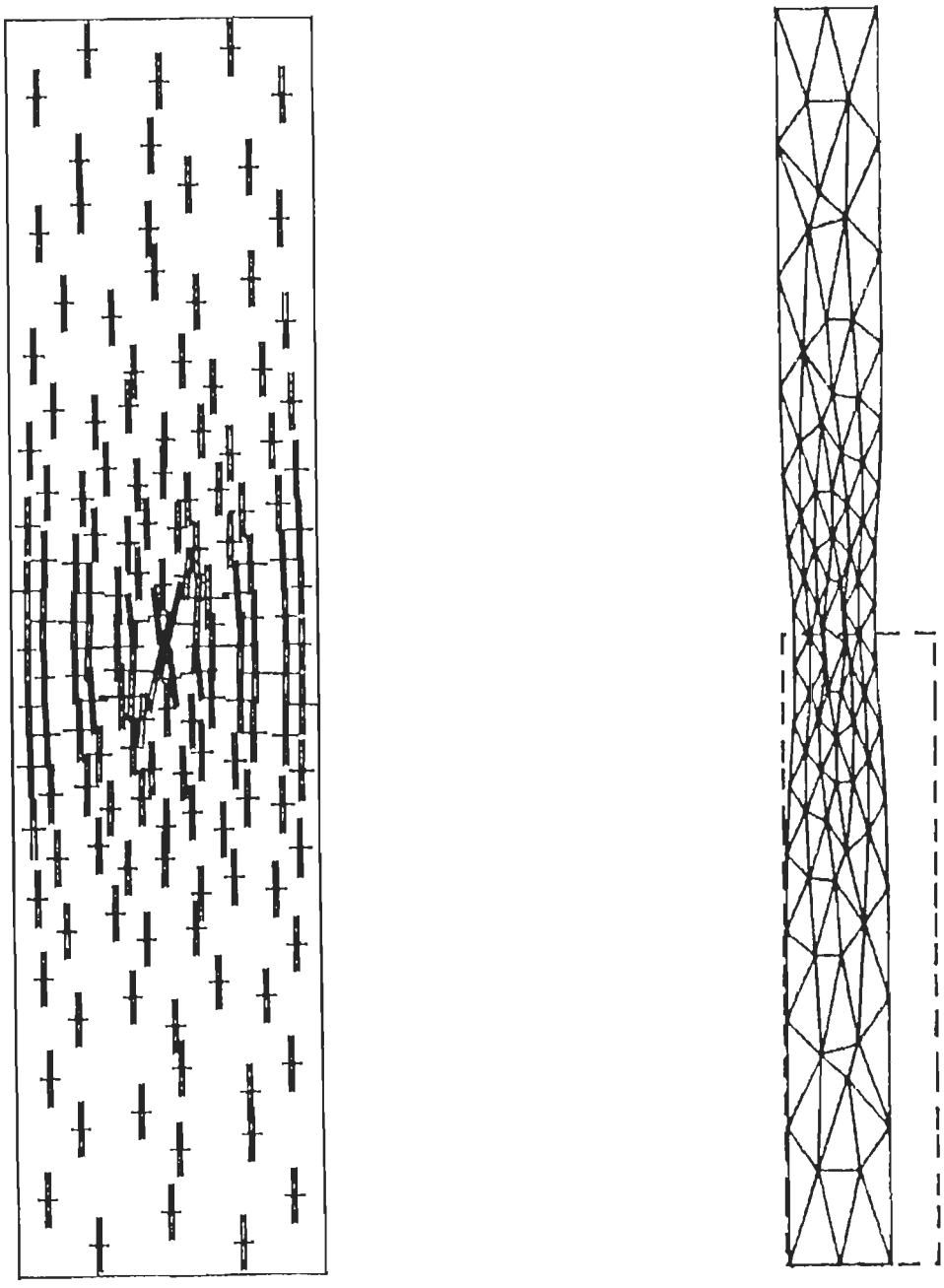

Fig. 8.11 Response using Hoffman criterion at the end of the analysis (a) principal strain plot (b) deformed shape

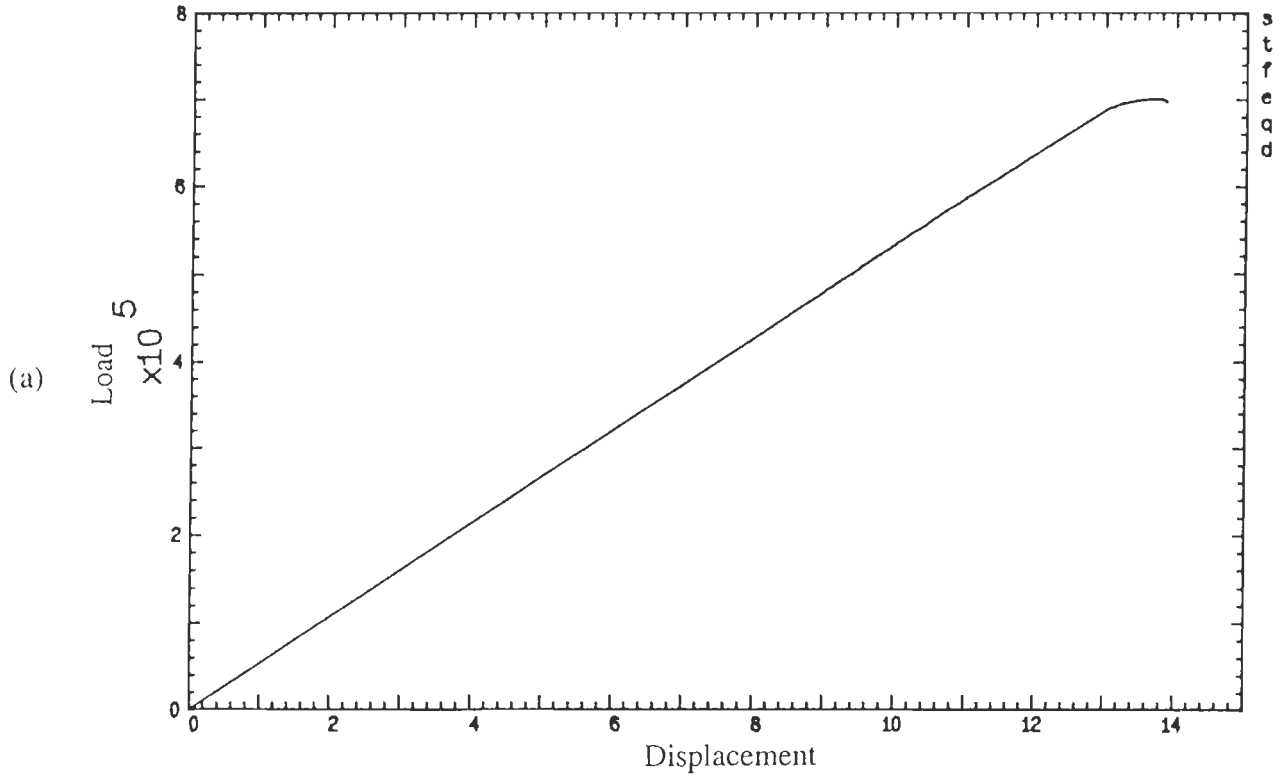

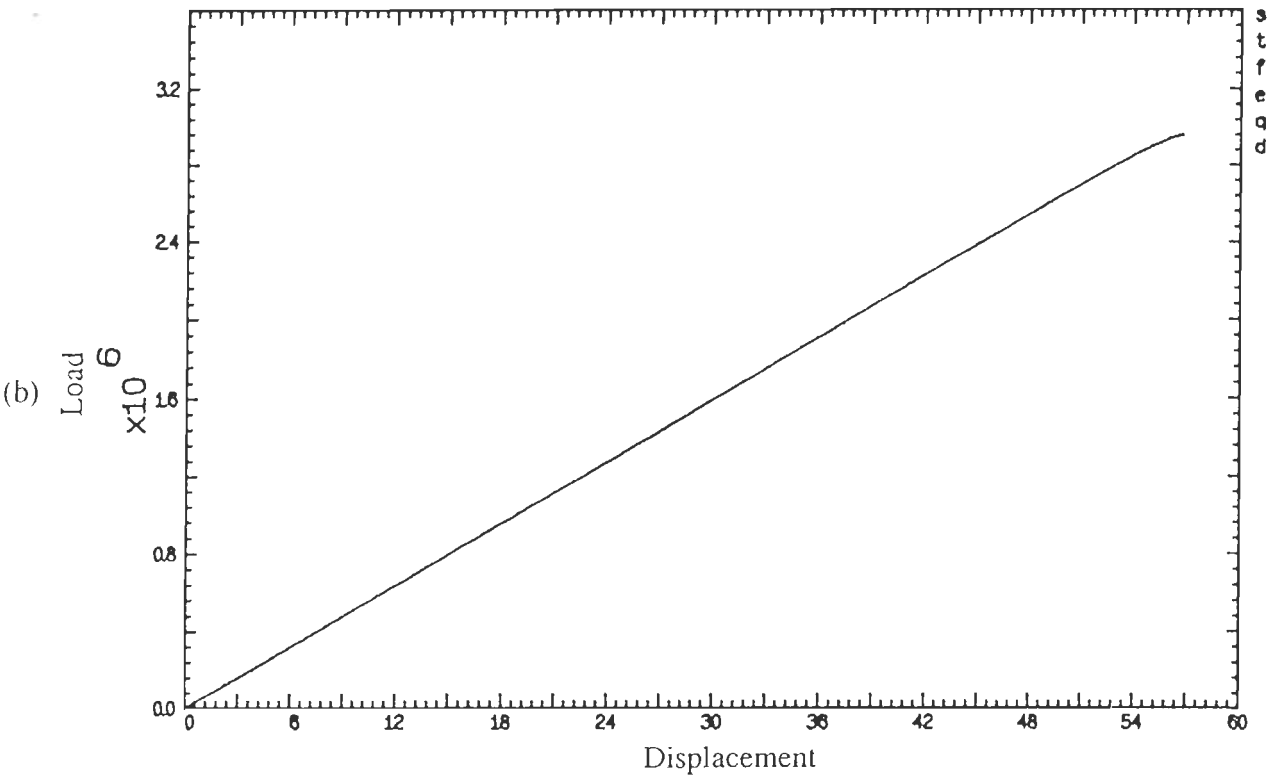

Fig. 8.12 Load deflection behaviour for necking problem using (a) von Mises criterion and (b) Hoffman criterion

Figures 8.16 and 8.17 show the principal strain plot, gauss point state plot and the deformed shape at the end of loading shown in the load displacement diagram (Fig. 8.15). The Hoffman criterion leads to a large area of the beam going into the post-yield range. The region of yielding for the von Mises criterion is more localized. However, both the criteria indicate a vertical localization surface starting from the notch. This is perhaps because of the imposed boundary conditions which do not permit any other localization pattern. In fact, similar results were obtained using the Mohr Coulomb criterion by Pankaj (1990). An interesting feature observed from the deformation plot is that the von Mises criterion tends to close the notch whereas the notch opens up when the Hoffman criterion is employed.

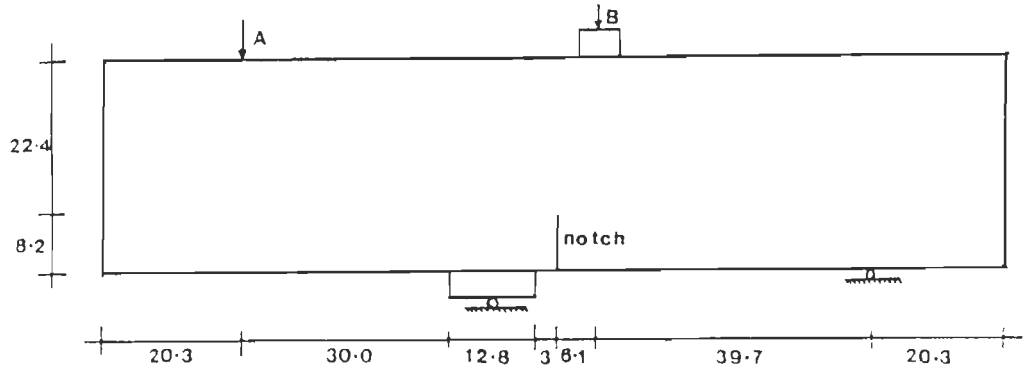

Fig. 8.13 Geometry of the notched shear beam

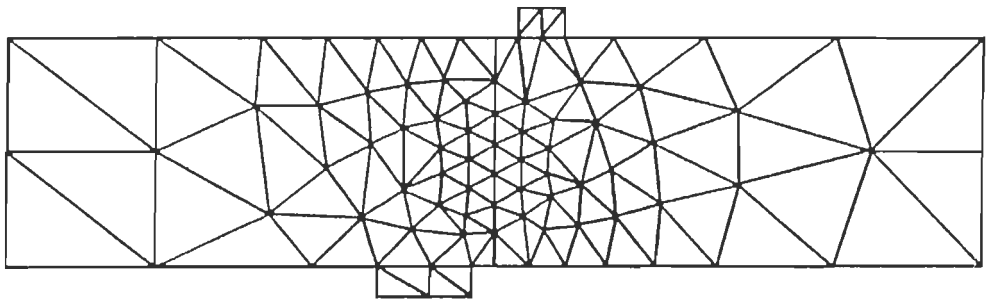

Fig. 8.14 Finite element discretisation of the notched shear beam

(a)

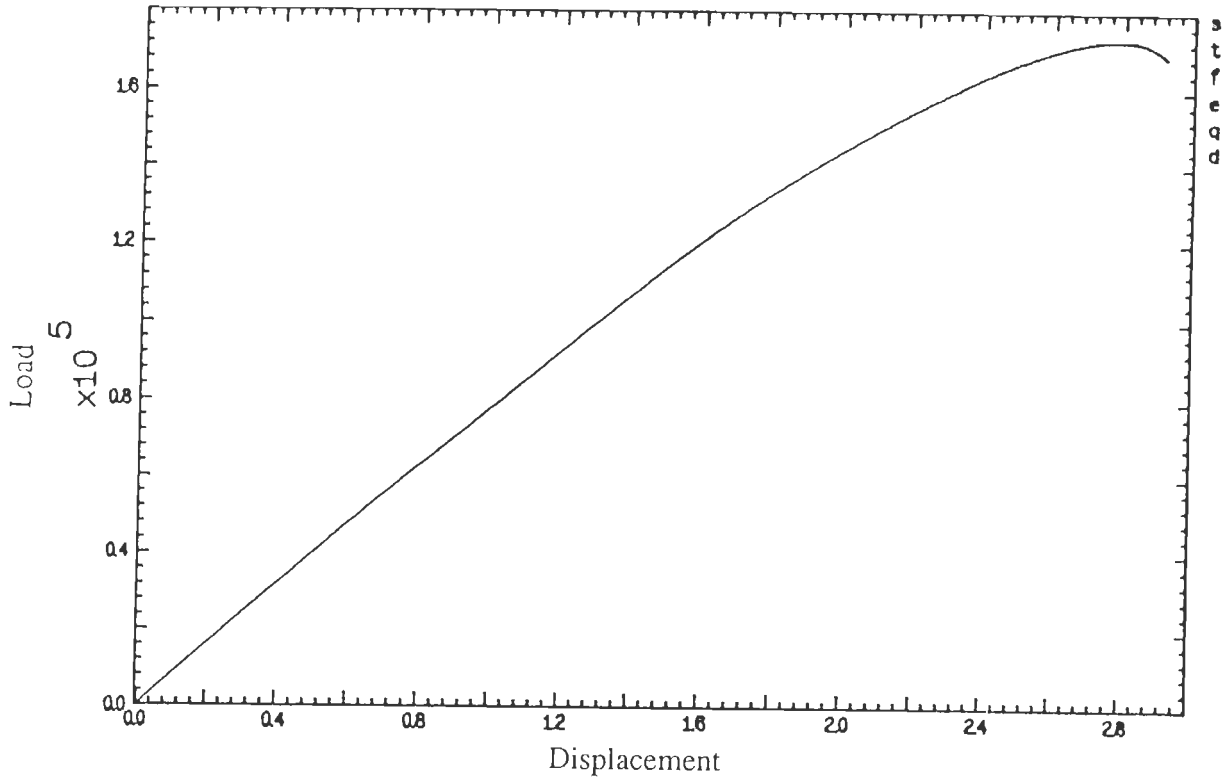

(b)

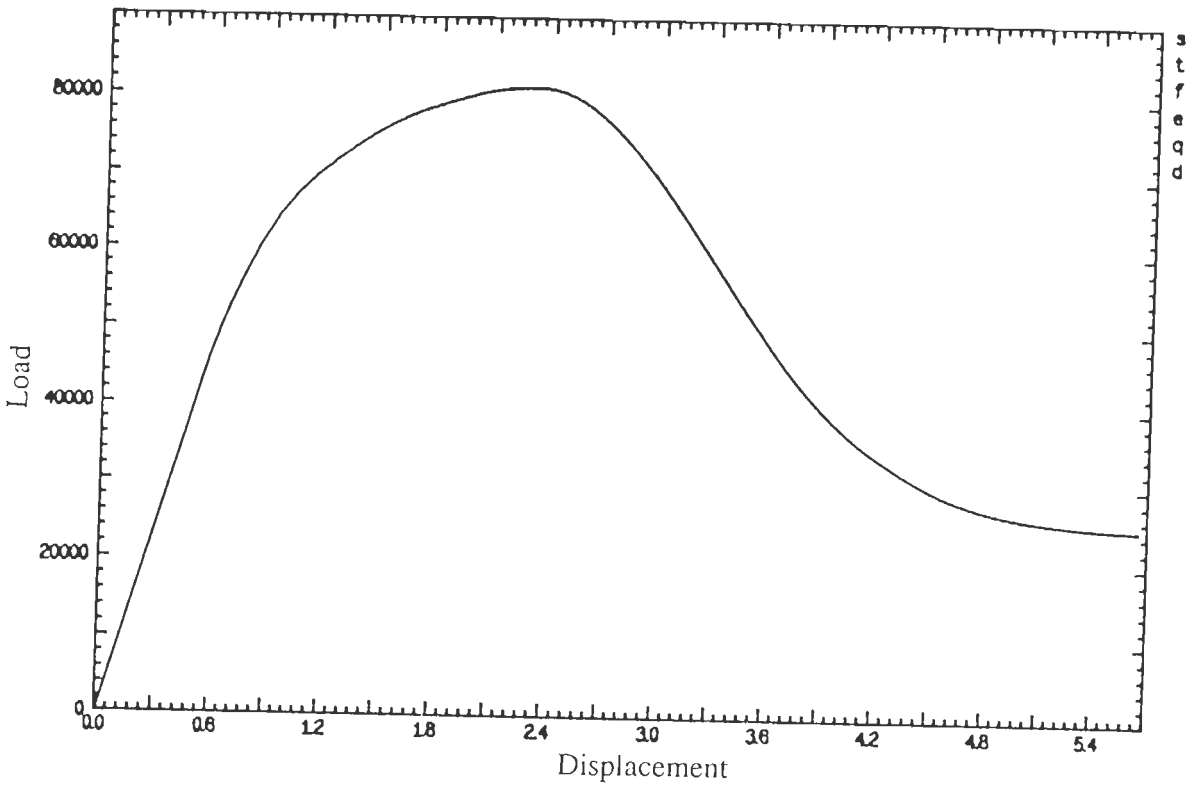

Fig. 8.15 Load deflection behaviour for notched beam problem using (a) Hoffman criterion and (b) von Mises criterion

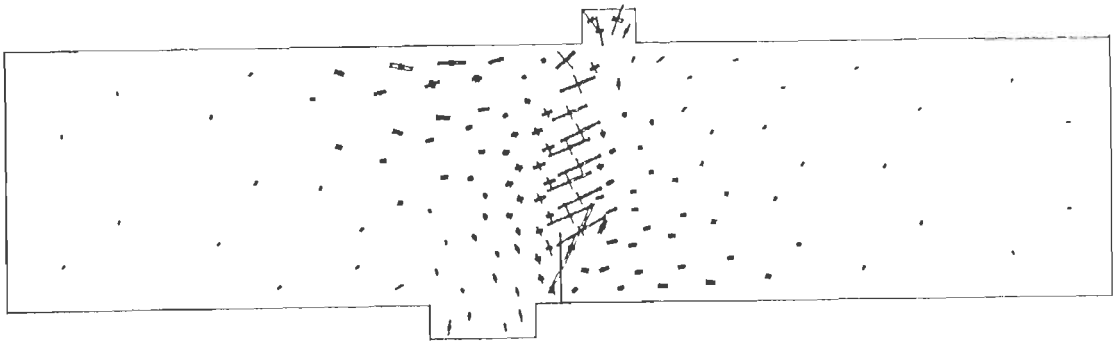

(a)

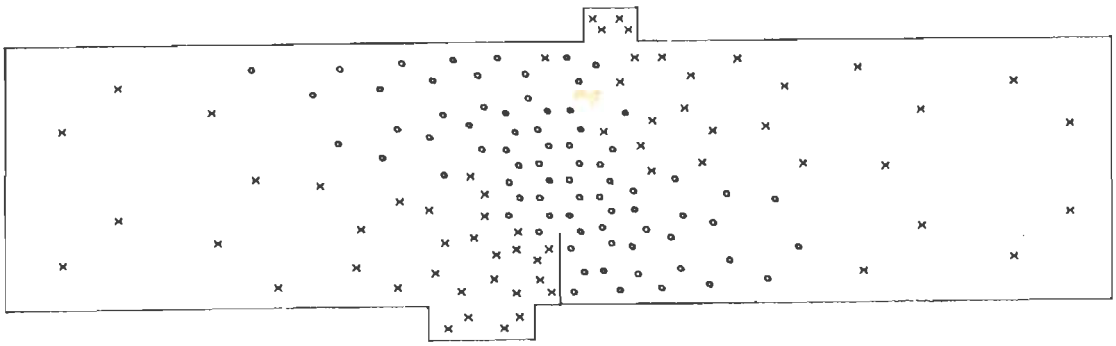

(b)

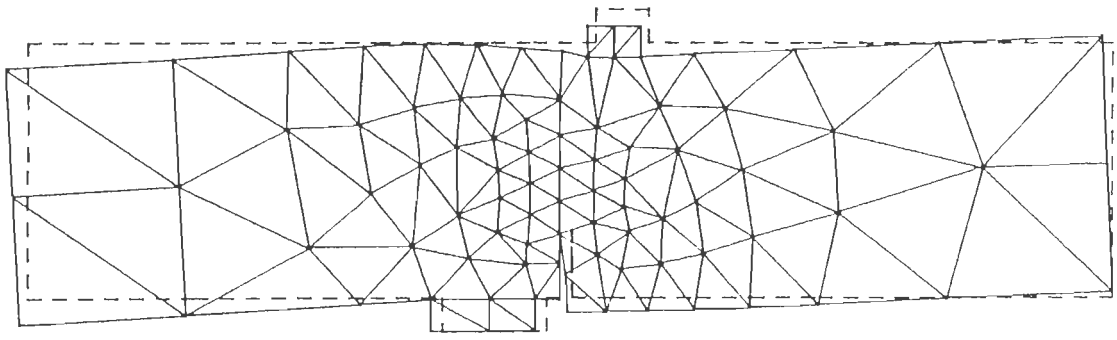

(c)

Fig. 8.16 Response using Hoffman criterion at the end of the analysis (a) principal strain plot (b) Gauss point state plot and (c) deformed shape

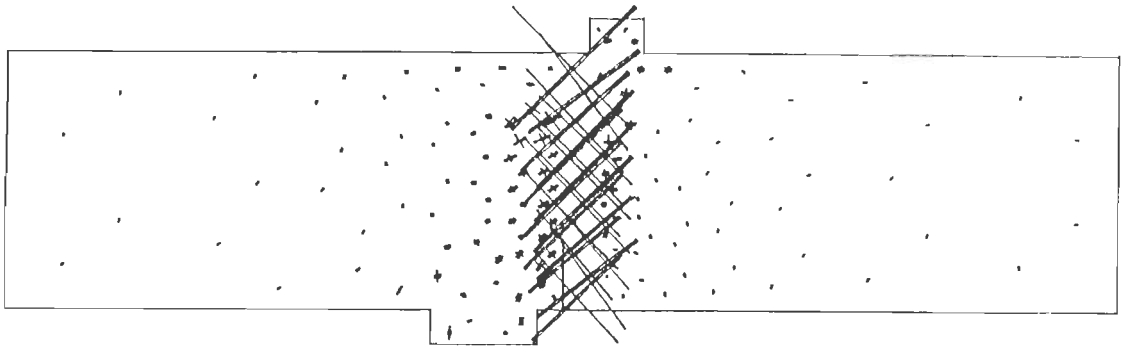

(a)

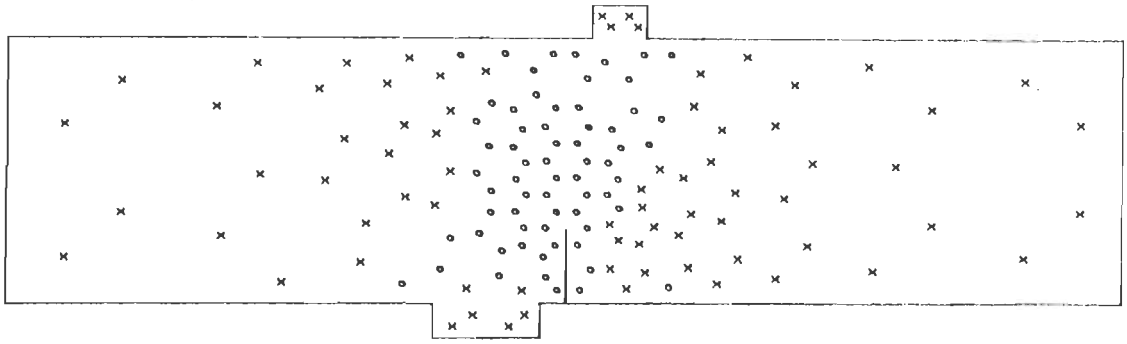

(b)

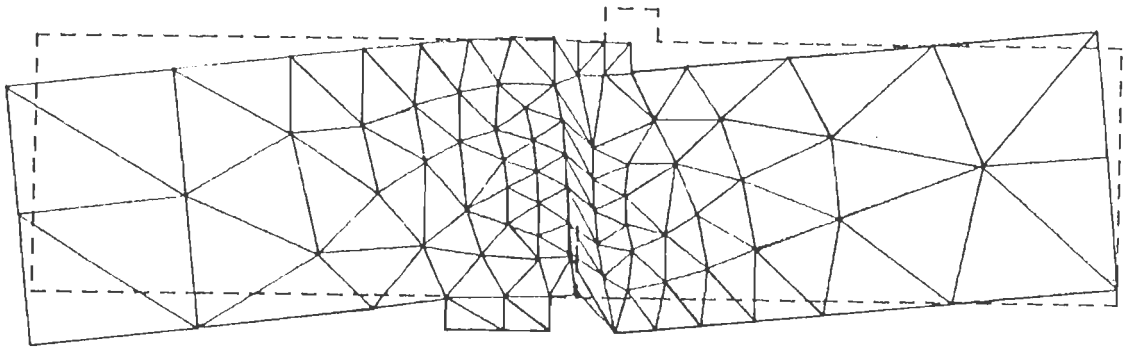

(c)

Fig. 8.17 Response using von Mises criterion at the end of the analysis (a) principal strain plot (b) Gauss point state plot and (c) deformed shape

8.5 Slope Failure Problem

Larsson et al. (1993) analysed a slope with a footing resting on its crest using the von Mises criterion. Similar problem has also been analysed by Bicanic et al. (1991). The footing was assumed to be rigid as compared to the slope. The geometry of the problem is shown in Fig. 8.18. Displacements are prescribed in the downward direction at the centre of the footing. The material properties used by Larsson et al. (1993) were adopted viz. $E = 2 \times 10^6$, $\nu = 0.45$ and the initial equivalent yield stress for von Mises $Y_o = 0.2$. Exponential softening with $\varepsilon_c = 0.01$ was employed. For the Hoffman criterion with both f_c and f_t permitted to decline, a series of analyses with a constant $f_{co} = 0.2$ and varying $f_{to} = 0.195, 0.15$ and 0.05 were conducted (Moin and Pankaj, 1996).

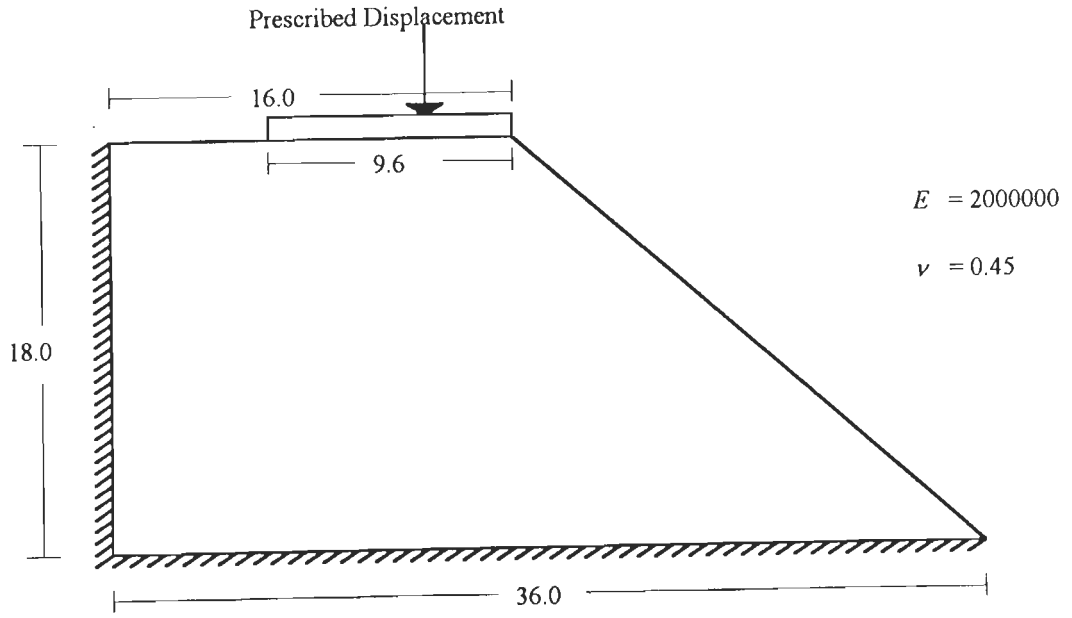

Fig. 8.18 Slope with a rigid footing

In the analysis, a pronounced mesh bias was introduced in the finite element mesh as shown in Fig. 8.19. The slip circle bias was determined using elementary soil mechanics principles.

The post-peak response in the form of principal strain plots, using $f_{co} = f_{to} = 0.20$ (von Mises); $f_{co} = 0.2$ and $f_{to} = 0.195$; $f_{co} = 0.2$ and $f_{to} = 0.15$; $f_{co} = 0.2$ and $f_{to} = 0.05$

is shown in Figs. 8.20-8.23. It can be seen that failure patterns predicted by the von Mises criterion follows the slip circle and the principal strains are localized. As the difference between f_{co} and f_{to} increases, a more diffused localization region is observed. In fact, from Fig. 8.23, it appears that a localization mode starting from the right end of the footing also develops. Thus a strong influence of yield criterion is observed from the failure mode. The Gauss point state plots and the deformation plots for the four cases are shown in Figs. 8.24-8.27. Conclusions similar to those discussed earlier can be derived from the Gauss point state plots. The deformation plot shows that the rigid footing gets more inclined as the f_{co} and f_{to} values come closer. Thus for the von Mises criterion, the downward displacement of the footing on the left edge is much more than the right edge. This difference is less when the Hoffman criterion is used especially when f_{co} and f_{to} are farthest from each other (Fig. 8.27b). This is Obviously because of the strain softening behaviour of the elements below the right edge of the footing for the case illustrated in Fig. 8.27. The load displacement plots for the four cases are shown in Fig. 8.28-8.31. It is interesting to see that as f_{co} and f_{to} move apart, the peak load predictions also rise.

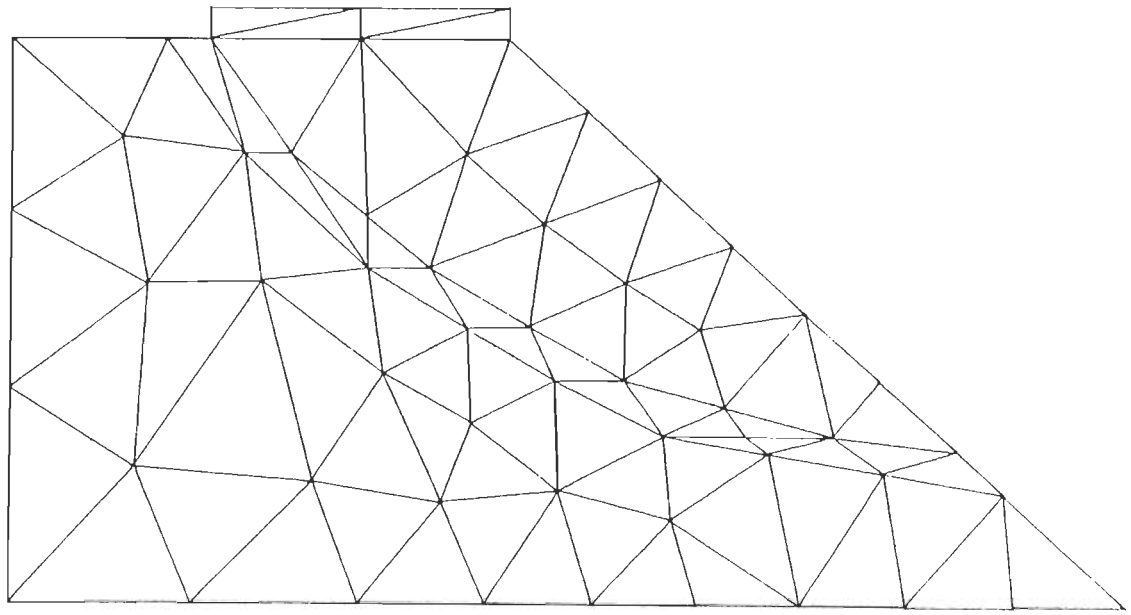

Fig. 8.19 Finite element discretisation of slope with rigid footing

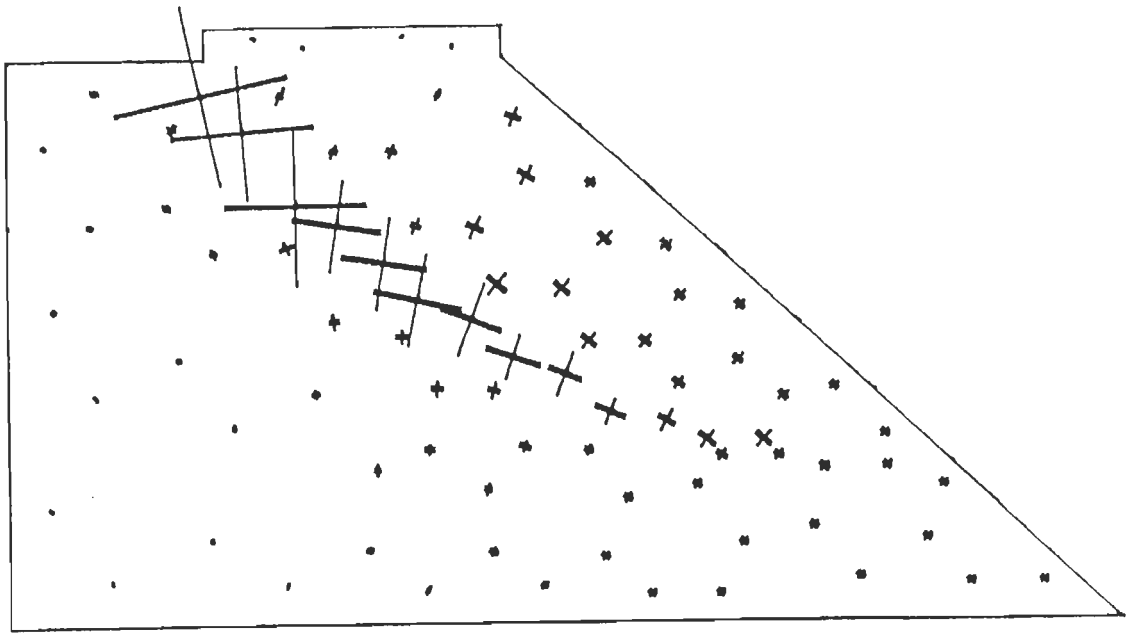

Fig. 8.20 Principal strain plot (von Mises)

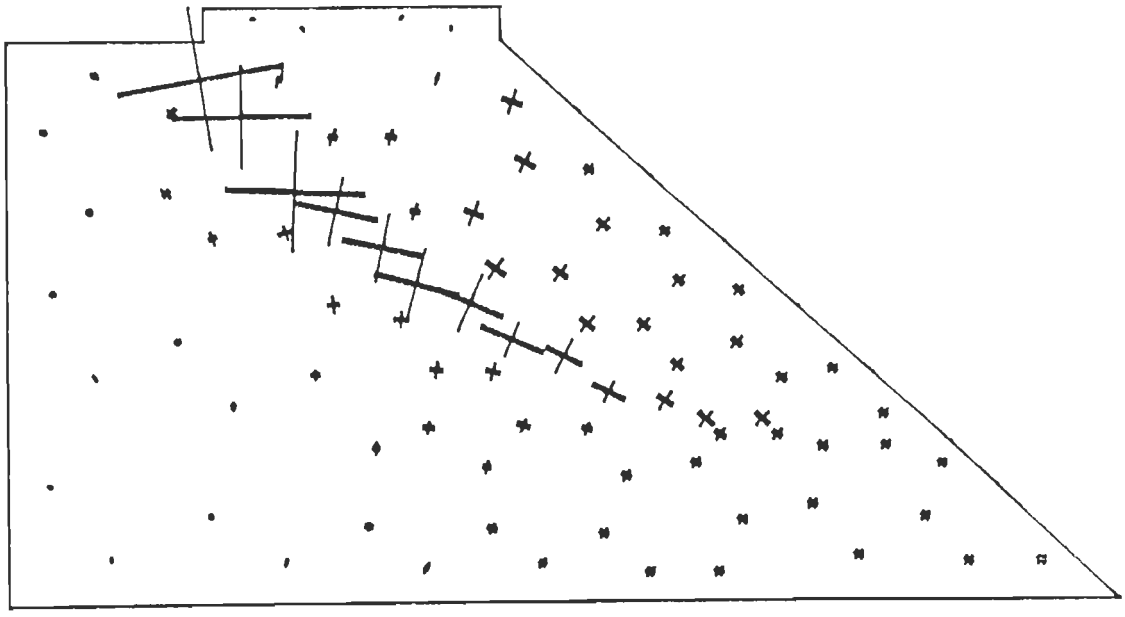

Fig. 8.21 Principal strain plot (Hoffman) $f_{co} = 0.20, f_{to} = 0.195$

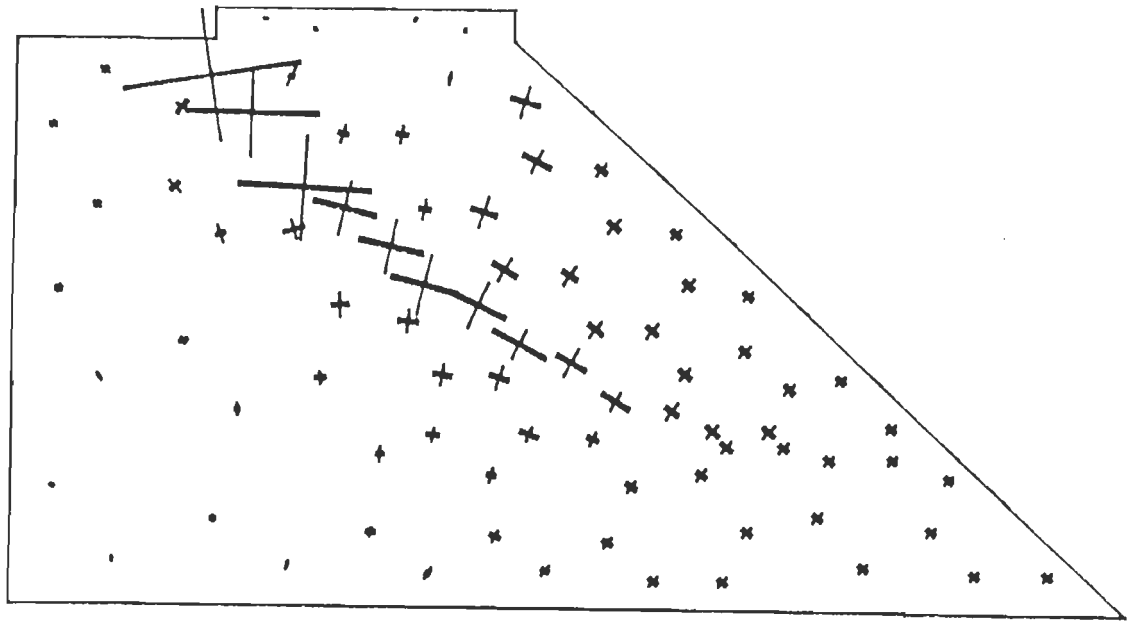

Fig. 8.22 Principal strain plot (Hoffman) $f_{co} = 0.20, f_{to} = 0.15$

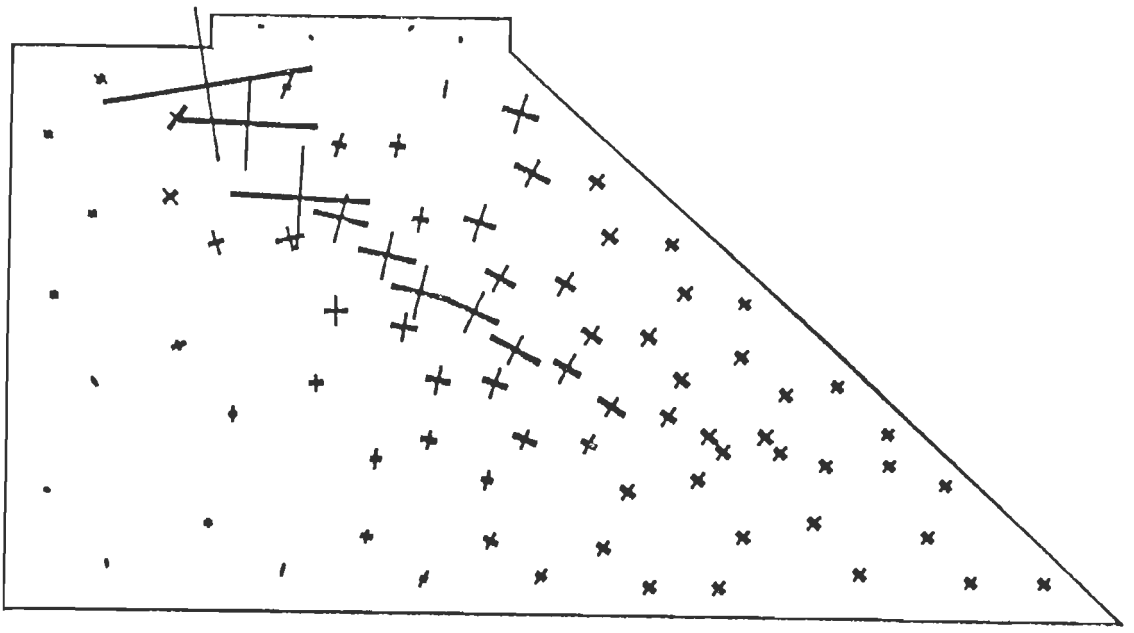

Fig. 8.23 Principal strain plot (Hoffman) $f_{co} = 0.20, f_{to} = 0.05$

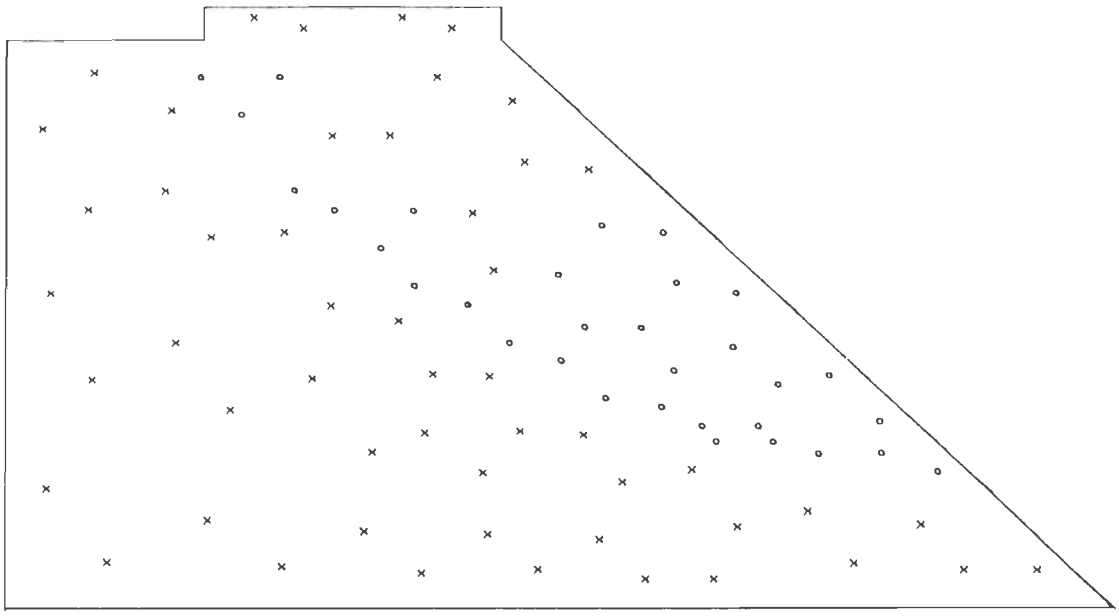

(a)

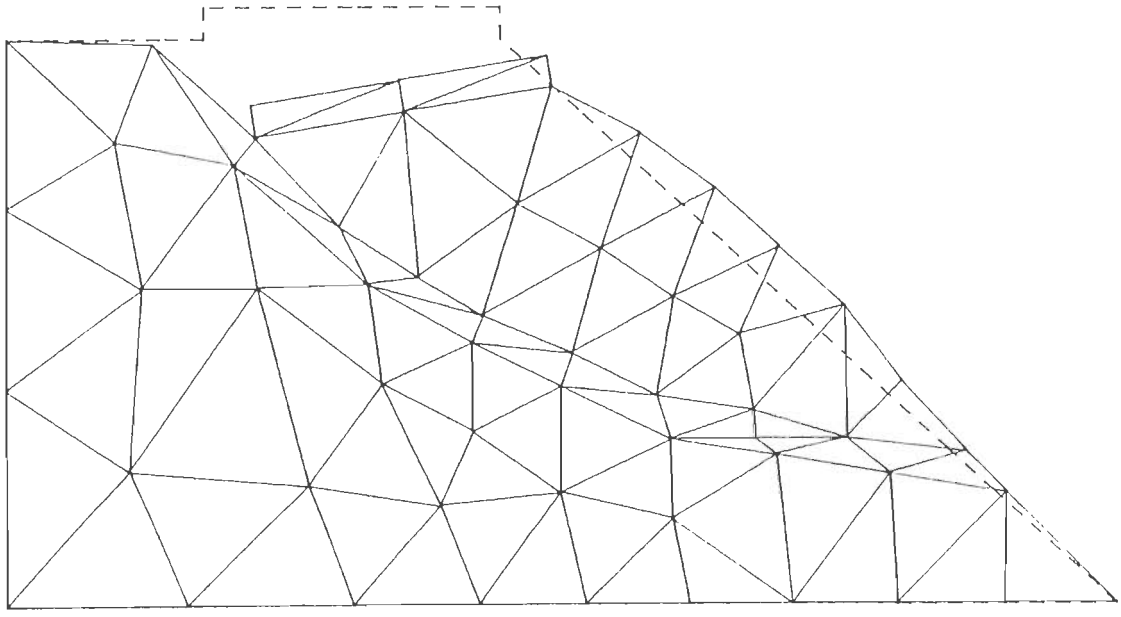

(b)

Fig. 8.24 Stability analysis using von Mises plasticity (a) Gauss point state plot and (b) deformed shape

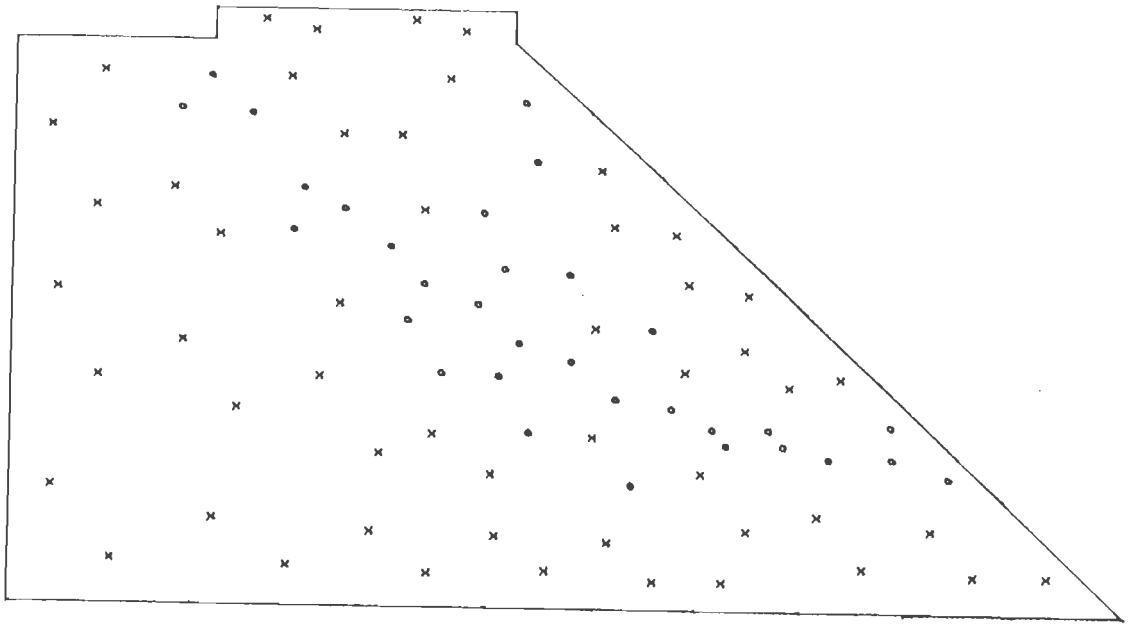

(a)

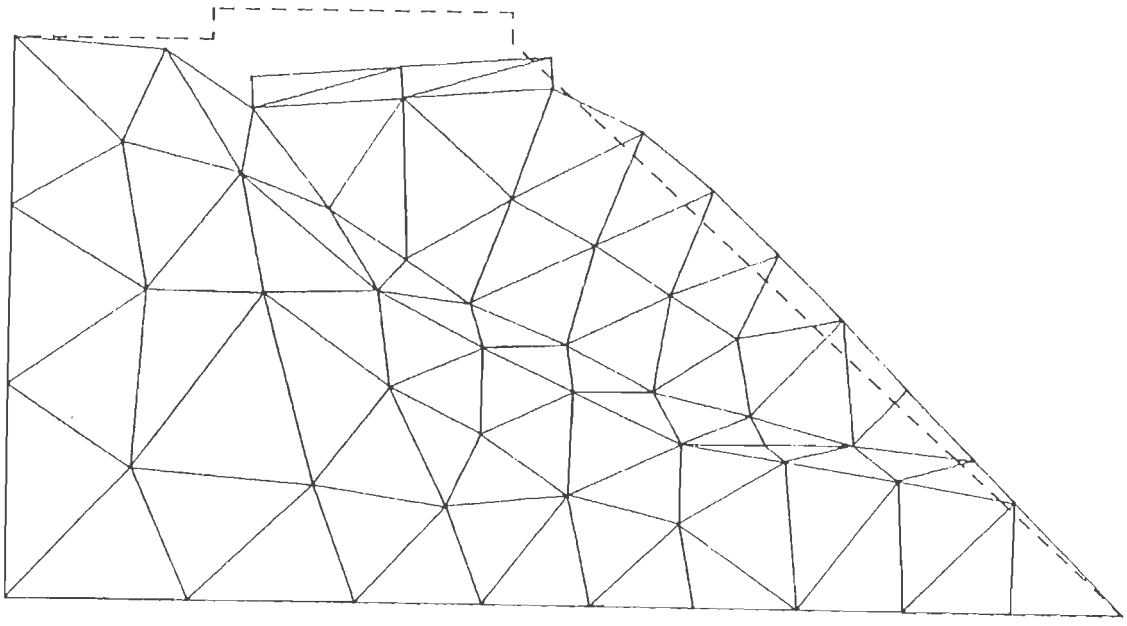

(b)

Fig. 8.25 Stability analysis using Hoffman plasticity ($f_{co} = 0.20, f_{to} = 0.195$) (a) Gauss point state plot and (b) deformed shape

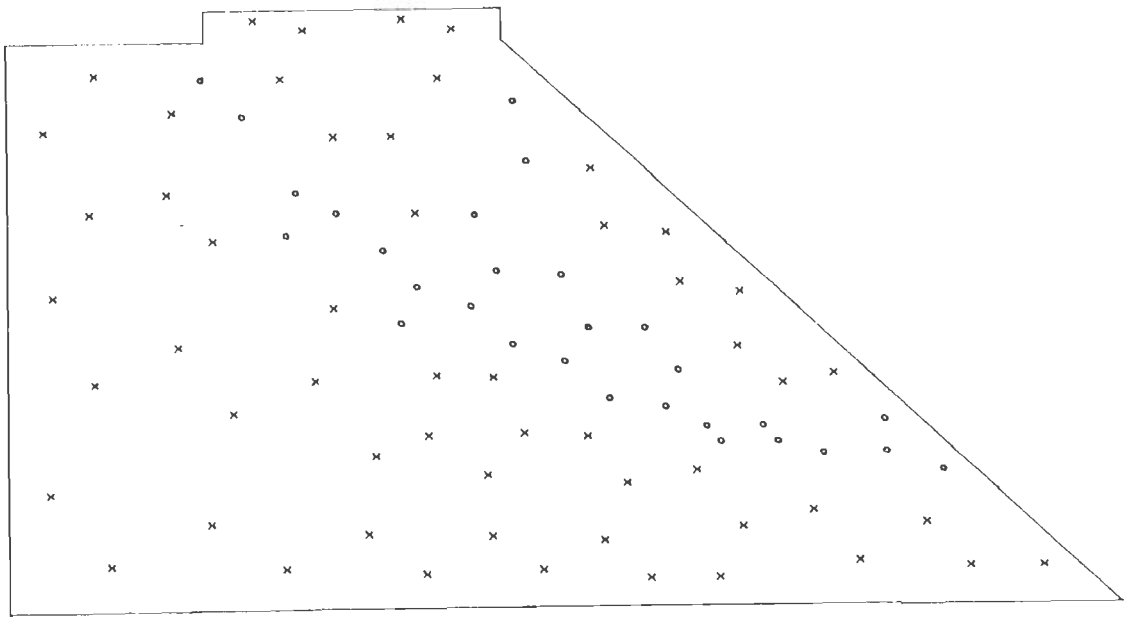

(a)

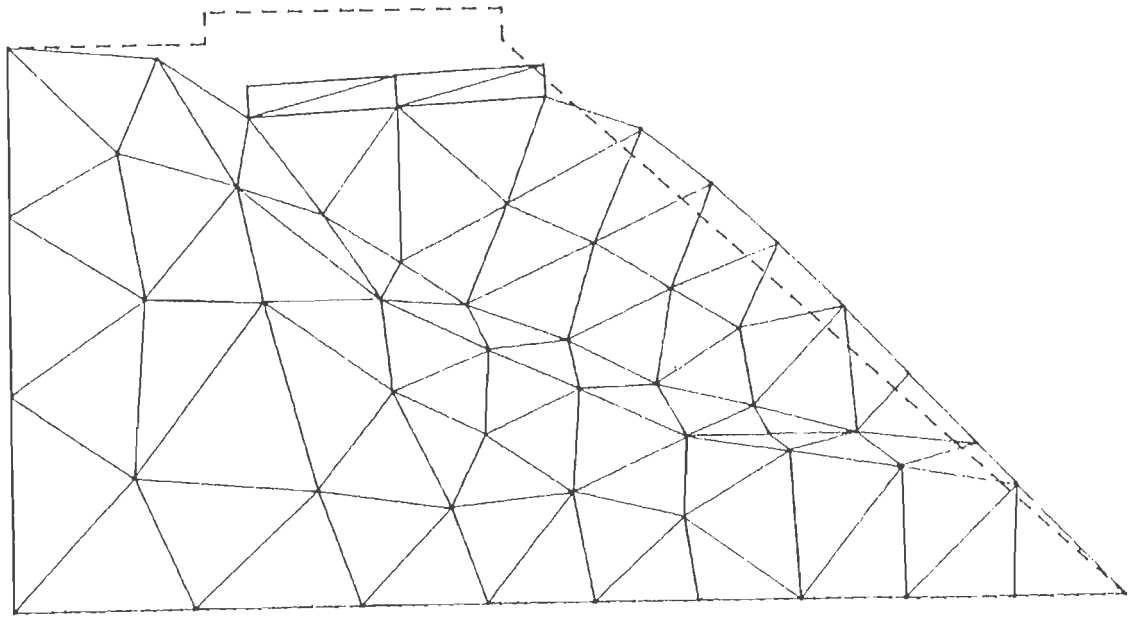

(b)

Fig. 8.26 Stability analysis using Hoffman plasticity ($f_{co} = 0.20, f_{to} = 0.15$) (a) Gauss point state plot and (b) deformed shape

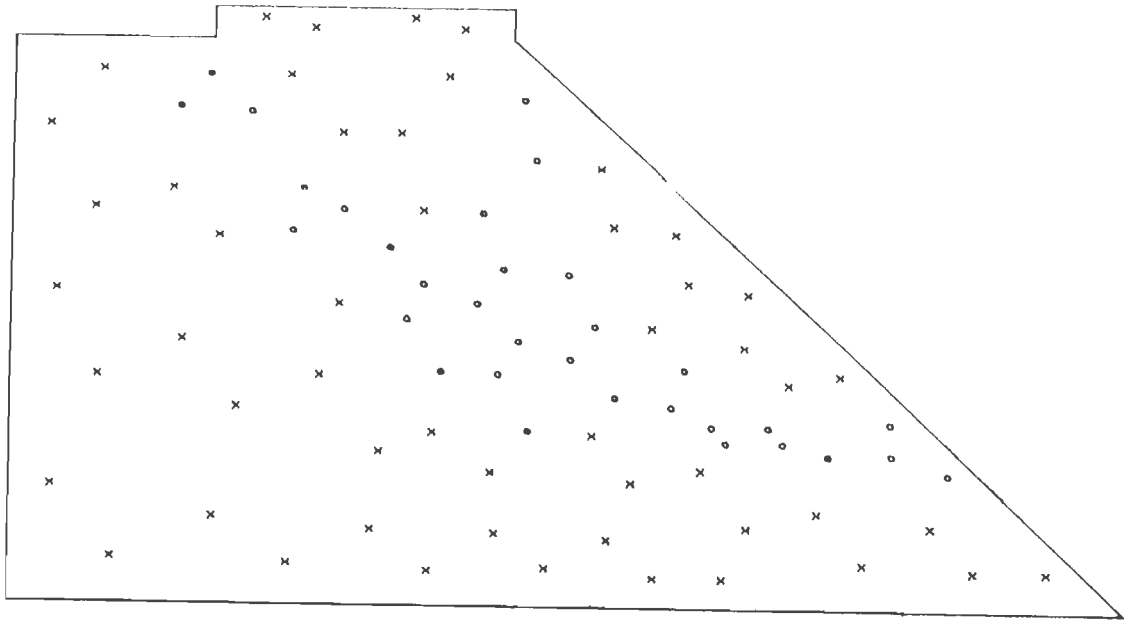

(a)

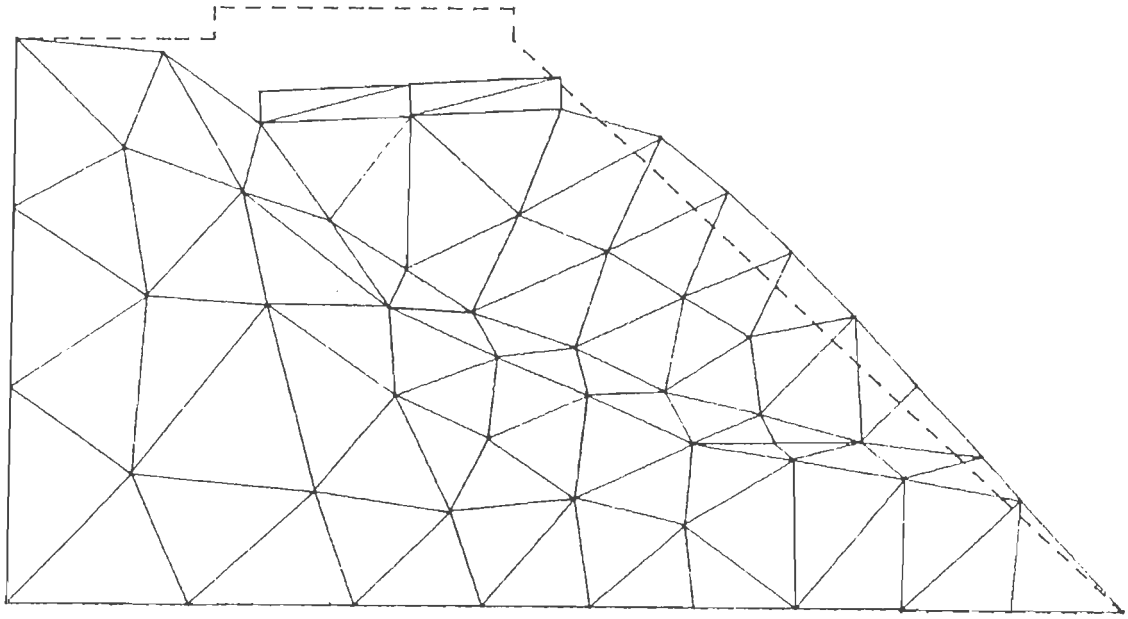

(b)

Fig. 8.27 Stability analysis using Hoffman plasticity ($f_{co} = 0.20, f_{to} = 0.05$) (a) Gauss point state plot and (b) deformed shape

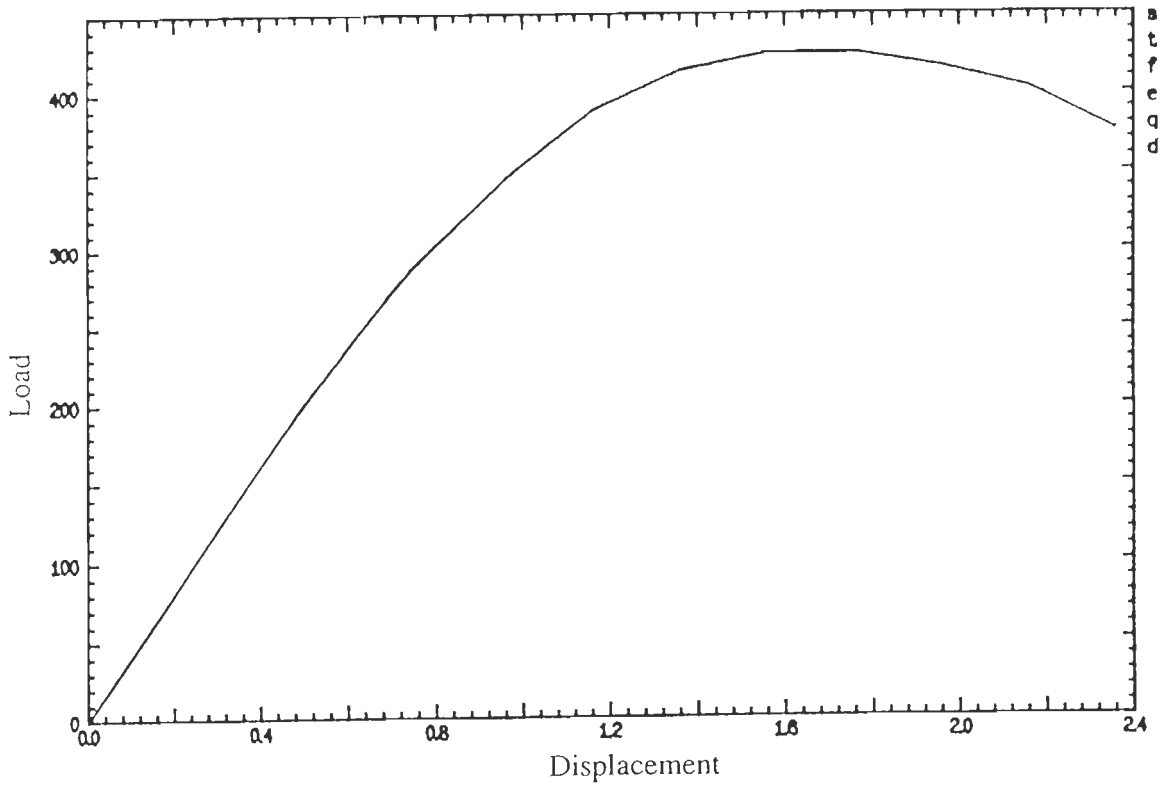

Fig. 8.28 Load deflection curve for stability problem using von Mises plasticity

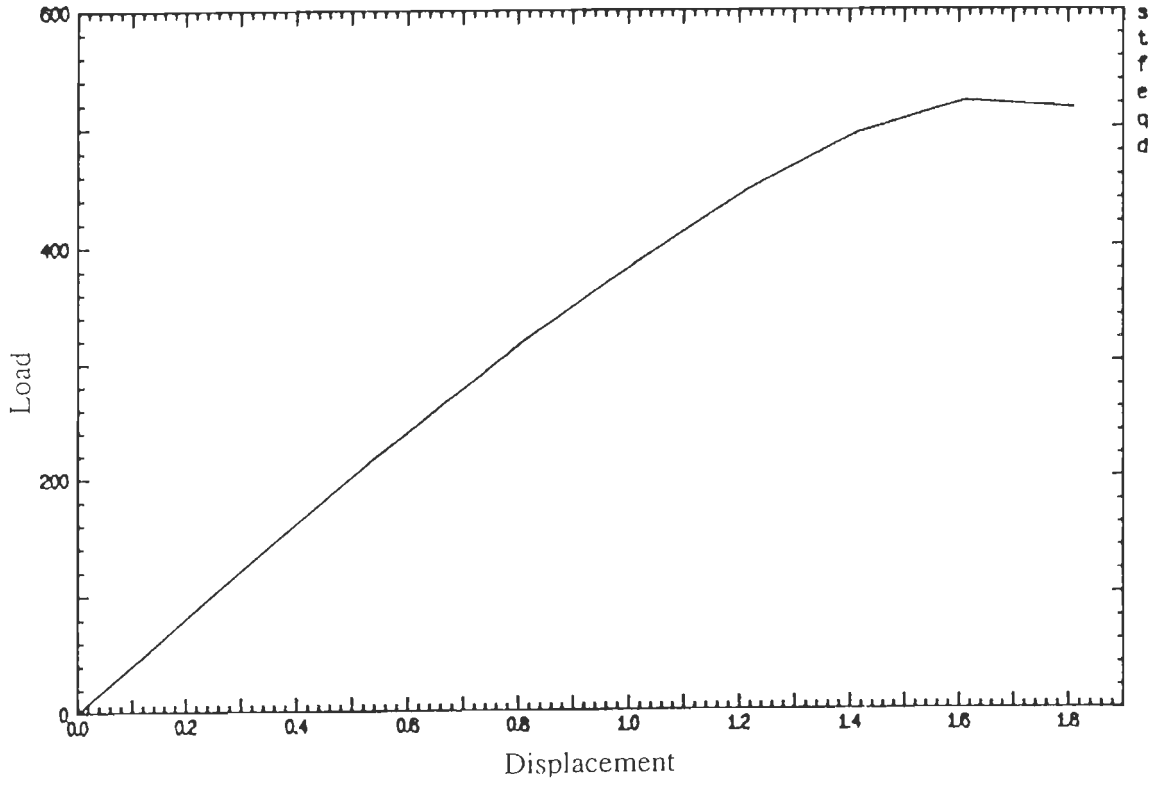

Fig. 8.29 Load deflection curve for stability problem using Hoffman plasticity $f_{co} = 0.20, f_{to} = 0.195$

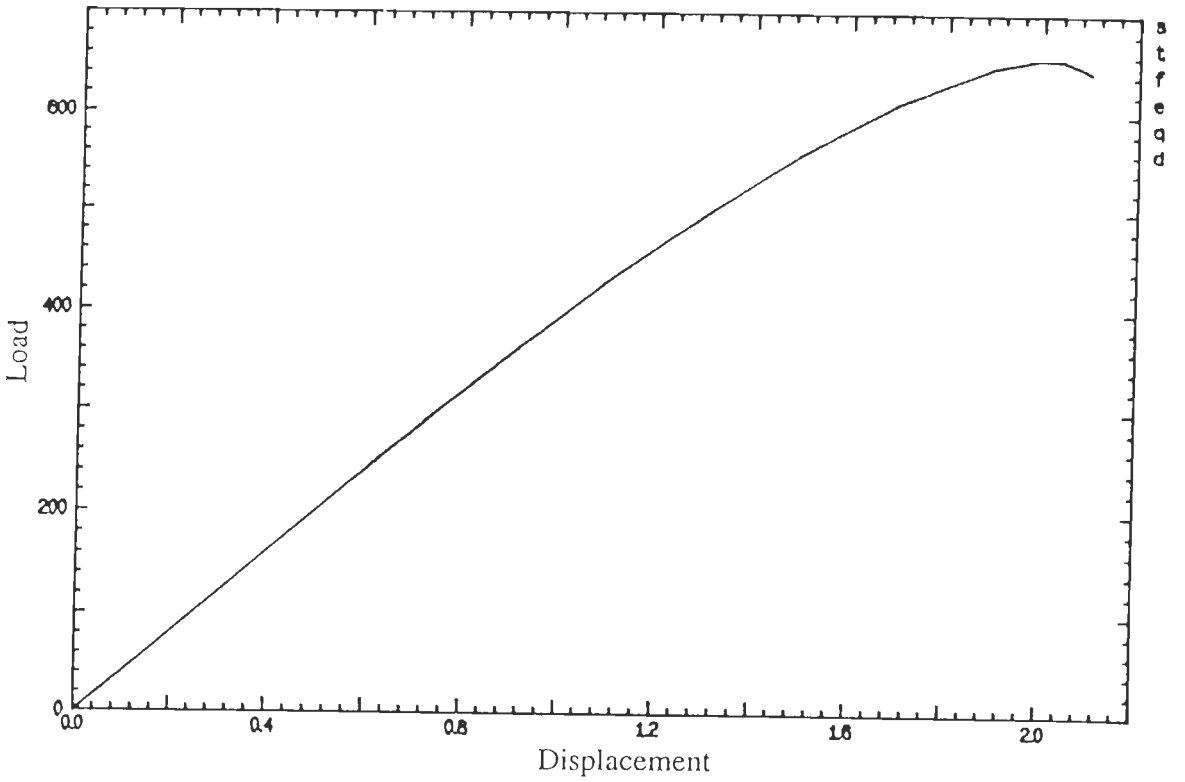

Fig. 8.30 Load deflection curve for stability problem using Hoffman plasticity $f_{co} = 0.20, f_{to} = 0.15$

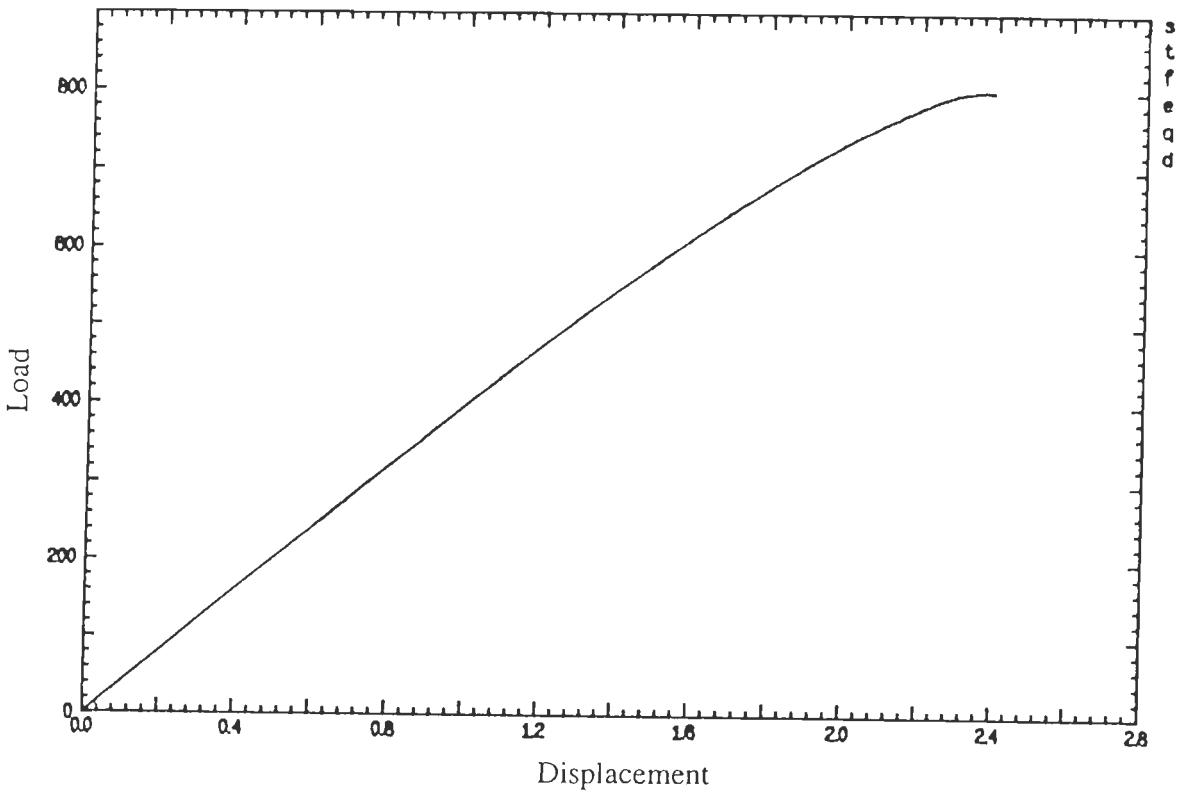

Fig. 8.31 Load deflection curve for stability problem using Hoffman plasticity $f_{co} = 0.20, f_{to} = 0.05$

8.6 Post-Peak Seismic Response of Koyna Dam

Strain softening has been utilised in static analysis for prediction of strain localization or cracking. In order to explore the possibility of using strain softening for prediction of cracking in a continuum under dynamic loads, the non overflow section of the Koyna dam (Fig. 8.32), which experienced an earthquake on Dec. 11, 1967 was analysed (Pankaj and Moin, 1996). The structure was idealized using 136 eight noded isoparametric elements as shown in Fig. 8.33. The dam section was assumed to be homogeneous with

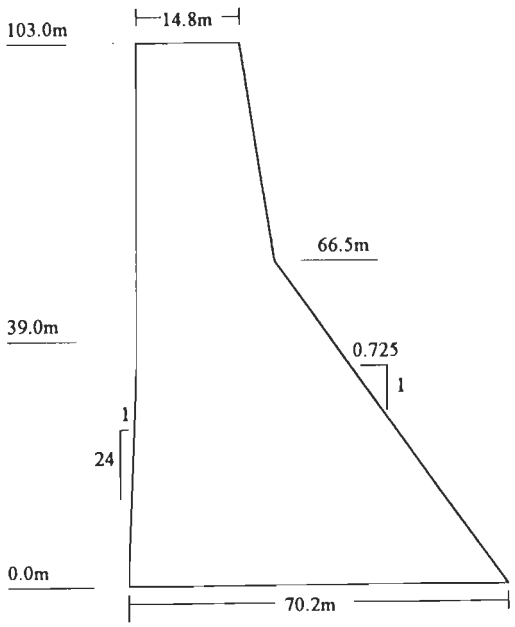

Fig. 8.32 Geometry of the non-overflow section of the Koyna dam

$E = 31.005 \times 10^6\, KN/m^2$, unit weight $\rho = 2.442\, KN\ \sec^2/m^4$ and Poisson's ratio $\nu = 0.2$ (Chopra and Chakrabarty, 1971). Damping was assumed to be 5% of critical. Isotropic strain softening plasticity using Mohr Coulomb yield function was employed to represent post-yield material behaviour. The cohesion $c = 7071\, KN/m^2$ and friction $\phi = 62.73^\circ$ were adopted from Owen and Hinton (1980). A linear post-yield softening modulus of 10% of E was also assumed. The dam was subjected to the horizontal component of Koyna earthquake (Krishna et al., 1969). The accelerograph of the longitudinal component of the Koyna earthquake is shown in Fig. 8.34. The principal strain plot at an instant when maximum principal strain (anywhere in the dam) is observed, is shown in

Fig. 8.35. Tensile strains are shown using double lines and compressive strains using single lines. Large strains can be seen to be confined to a localized region. Figure 8.36 shows the regions that have undergone some amount of permanent plastic strain at the end of the excitation. Localization is seen to be confined to small regions on upstream and downstream faces. These simulations match well with the actual cracks that were observed after the earthquake (Chopra and Chakrabarty, 1971). It is interesting to observe that similar localization pattern was illustrated for the Koyna dam by Batta and Pekau (1996), in which they used the discrete crack approach and the boundary element method. Hence it can be concluded that strain softening in the context of elastoplasticity appears to have the potential for predicting strain localization or cracking in seismic problems.

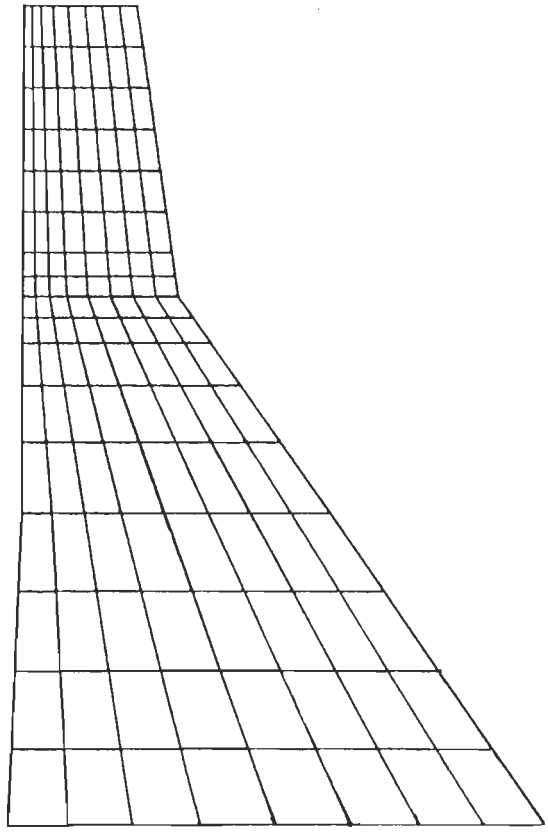

Fig. 8.33 Finite element discretisation of the Koyna dam

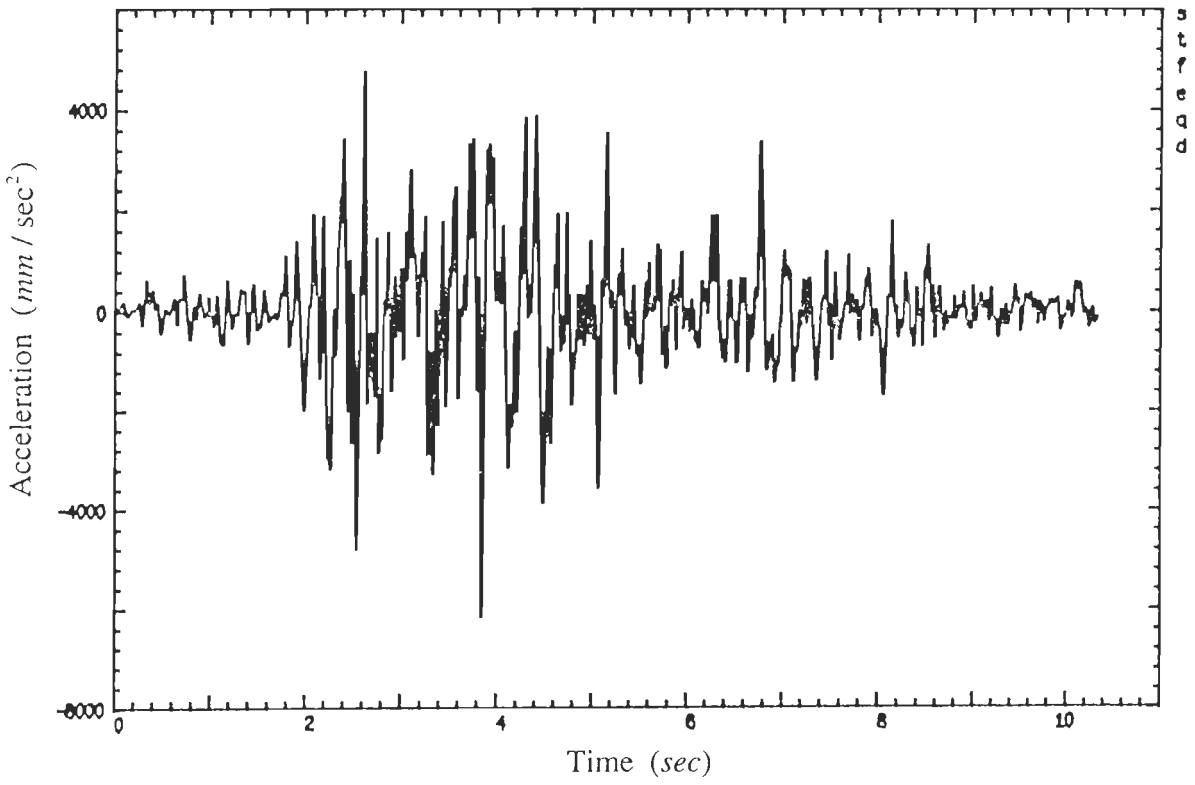

Fig. 8.34 Koyna accelerogram – longitudinal component

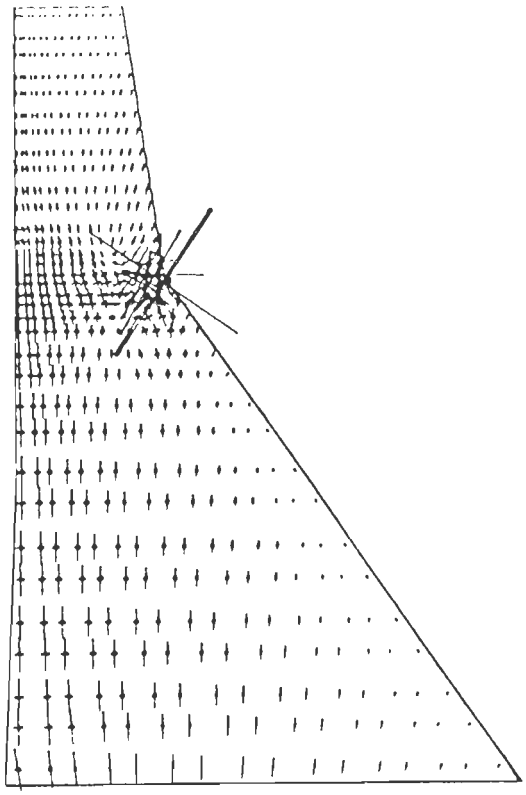

Fig. 8.35 Principal strain plot of Koyna dam

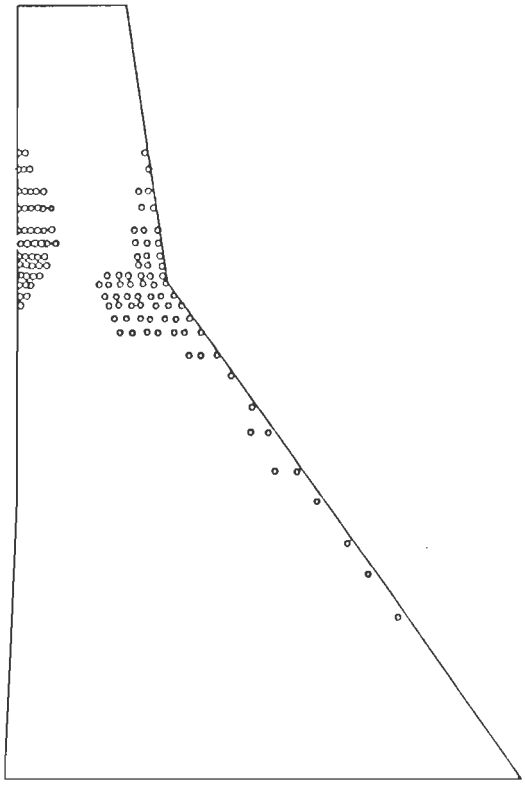

Fig. 8.36 Yielded Gauss points of the Koyna dam

References

Arrea, M. and Ingraffea, A.R. (1982) – Mixed mode crack propagation in mortar and concrete. *Report No. 81-13, Department of Structural Engineering*, Cornell University, Ithaka, New York.

Batta, V. and Pekau, O.A. (1996) – Seismic cracking analysis of pine flat dam: Case study, *Proceedings of Eleventh World Conference on Earthquake Engineering*, Mexico, June 23-28, Paper No. 1705.

Bicanic, N. Selman, A., Xie, Y.-M., Pankaj and Zienkiewicz, O. (1991) – On mesh dependence of failure mode predictions for dams, *Proceedings Int. Conf. on Dam Fracture*, Boulder, Colorado, 5-19.

Chopra, A.K. and Chakrabarti, P. (1971) – Koyna earthquake and the performance of Koyna dam, *Report No. EERC -71-1*, University of California, Berkeley, USA.

Krishna, J., Chandrasekaran, A.R. and Saini, S.S. (1969) – Analysis of Koyna accelerogram of December 11, 1967, *Bull. Seism. Soc. Am.*, **59**, 1719-1732.

Larrson, R., Runesson, K. and Ottosen, N.S. (1993) – Discontinuous displacement approximation for capturing plastic localization, *IJNME*, **36**, 2087-2105.

Moin, K. and Pankaj (1996) – Post-peak response analysis of structures using finite element method, *Proceedings International Conference on New Challenges for Civil Engineers of Developing Countries in the 21st Century* (NCCDC-96), New Delhi, Venus Publishers, 135-138.

Moran, B., Ortiz, M. and Shih, C.F. (1987) – Computation methods in finite deformation plasticity, *Int. J. Solids Structures*.

Ortiz, M. (1987) – Some computational aspects of finite deformation plasticity, *Computational Plasticity; Models, Software and Applications* (Eds. Owen, D.R.J., Hinton, E. and Onate, E.), 1717-1755.

Owen, D.R.J. and Hinton, E. (1980). Finite Elements in Plasticity: Theory and Practice, Pineridge Press Limited, Swansea, U.K.

Pankaj (1990) – Finite element analysis in strain softening and localization problems, *Ph.D. Thesis*, University College of Swansea, University of Wales.

Pankaj and Moin, K. (1996) – On the use of strain softening prediction of post-peak seismic response of structures, *Proceedings of Eleventh World Conference on Earthquake Engineering*, Mexico, June 23-28, Paper No. 1288.

Conclusions and Recommendations for Further Research

9.1 Concluding Remarks

The thesis was aimed at studying post-peak behaviour using strain softening elastoplasticity in conjunction with the finite element method. The objective has been to make a contribution in some areas which are less clearly understood and highlight some problems where the emphasis has been lacking. The significant conclusions are summarised as follows:

- The pressure sensitive Hoffman yield criterion, which appears to be an appropriate and simple choice for quasi-brittle materials was examined. Two forms of post yield softening were considered. First in which the softening is confined to the uniaxial tensile strength f_t and the second in which both f_t and uniaxial compressive strength f_c decline. It is seen that the former implies a decrease in cohesion and an increase in the frictional characteristics of the material. Integrations of the rate equations using Hoffman plasticity were discussed and a computational algorithm for this purpose was developed. Simple expression that can be used for the evaluation of exact contact stress state (stress state at the onset of yielding) has been derived. The determination of this state is essential when using semi implicit and explicit algorithms.

- Computational issues in strain softening plasticity in static and dynamic problems were discussed using one dimensional models. It is seen that the use of incremental strain procedure wherein the stress and strain states are updated only upon convergence, should be employed to avoid the development of spurious plastic strain. The strategy

prevents the accumulation of spurious plastic strains that may otherwise accumulate, even for single degree freedom dynamic problems.

- A computational algorithm using the generalised Newmark procedure was discussed. Simple tests using elastoplastic single degree freedom system indicate the superiority of the unconditionally stable Newmark algorithms. Comparisons were made with an exact solution developed for this purpose.

- It is seen that strain softening can be successfully used in dynamics without it leading to unbounded response. In general, strain softening introduces a zero frequency component in the response and does not alter other predominant frequency component significantly.

- Exact solution, for some specific cases, for von Mises and Mohr Coulomb plasticity were derived using prescribed displacement field format. These solutions include linear hardening/softening. The Mohr Coulomb criterion has similar (non smooth) regions. The possibility of stress state being in such regions was incorporated in the solutions. A number of benchmark tests were developed for the two criteria. It is felt that these tests can help in checking the validity of the computer codes.

- A number of illustrative tests for Hoffman criterion were evolved. It is seen that the Hoffman criterion exhibits considerable dilatancy when uniaxial compressive and tensile strengths are far apart. In fact, the direction of stress movement in the principal stress space is strongly influenced by the difference/ratio of the two uniaxial strengths.

- Uniaxial compression tests on single element under mixed (displacement and stress) boundary conditions were conducted. For von Mises plasticity it is seen that the localisation condition may not always be satisfied immediately after yield even under strain softening conditions. Correspondingly, the load deflection response may indicate increased load carrying capacity. softening parameters can however, be evolved such that the localisation condition is satisfied immediately after yield which results in a post-peak behaviour. Increasing the magnitude of the softening parameter beyond a certain level may lead to instability. This limit may be more stringent than the local uniqueness requirements.

- For Mohr Coulomb elastoplasticity, satisfaction of localisation condition leads to a post-peak response for simple single element uniaxial tests.

- For Hoffman criterion, the post-peak response is aided when both f_c and f_t are assumed to decline. For the uniaxial compression test conducted, a mere softening of f_t does not lead to a post peak response. The localisation conditions are also not satisfied. This is obviously because reduction in f_t only leads to the contraction of yield surface in some regions and expansion in other regions.

- Element size sensitivity study shows that mesh inobjective results may be obtained, if some form of non-local material laws are employed. Moreover, it appears that yield criterion has an important role to play in deciding if strain localisation would occur.

- Study of some engineering problems indicates that the von Mises criterion leads to fine localization zones as compared to the Hoffman criterion. The directions of the localisation bands are strongly influenced by the structural boundary conditions. For the notched shear beam analysed, it is seen that the boundary conditions lead to similar localization regions for both von Mises and Hoffman yield criteria. On the other hand the localisation patterns of a slope which has less stringent boundary conditions are influenced by the yield criterion being employed.

9.1 Suggestions for Further Research

Prediction of post-peak behaviour and strain localization are complex phenomena. Its numerical modelling involves various problems such as mesh sensitivity, load step sensitivity, stability, convergence and simulation of localization bands. For complex materials like reinforced concrete, failure may be caused due to several mechanisms such as mortar cracking, reinforcement yield, bond slip, concrete crushing and interface sliding. Further, for pressure sensitive quasi-brittle materials like concrete, additional problems like pressure dependent nonlinear hardening/softening moduli, choice of damage parameters and stiffness degradation further complicates the mathematical modelling. Hence it can be suggested that a wide range of problems in the field of post-peak nonlinear analysis are lying for further research. The suggestions which are considered to be more relevant are as follows:

- Similar studies using other failure criteria specially those that have emerged from experimental tests should be conducted.

- The effect of non-associated flow rule and 'non-isotropic' hardening models on post-peak problems should be studied. It should be noted that a large number of civil engineering materials are not isotropic.

- Mesh sensitivity issues, especially those related to mesh design need to be explored. Recent advances in adaptive meshing may be employed for this purpose.

- Strain softening plasticity can be used for dynamic problems. Its efficacy, however, needs to be further explored.